



# **Development of a seaweed-based fixed-bed sorption column for the removal of metals in a waste stream**

Adil Bakir M.Sc.

**Under the supervision of**

Dr. Eddy Fitzgerald

Submitted in partial fulfilment of the requirements for the degree of Doctor of Philosophy

Submitted to Waterford Institute of Technology

May 2010

## **Declaration**

---

No element of the work described in this Ph.D. thesis, except where otherwise acknowledged, has been previously submitted for a degree at this or any other institution. The work in this thesis has been performed entirely by the author.

Signature: \_\_\_\_\_

Adil Bakir

Date: \_\_\_\_\_

## Acknowledgements

---

I would like to sincerely thank my supervisor Dr. Eddy Fitzgerald for his invaluable support and guidance throughout this research. His patience, encouragement and enthusiasm were invaluable throughout my work.

A special thanks to my colleagues in the Estuarine Research Group (ERG), in particular Richard Walsh, Catherine Murphy and Siobhan Ryan for making me feel so welcome at WIT. Also, a sincere thanks to Dr. Brian Murphy for his valuable assistance and always being available for sampling when required.

I would also like to thank all my fellow postgraduates for their friendship and support.

I would like to thank all the staff of the WIT Science Department for their help, especially Dr. Jim Stack for the statistical analysis and Dr. Kieran Murphy for his mathematical expertise with the COMSOL modelling software.

I wish to thank Dr. Syed Tofail from the Materials and Surface Science Institute (MSSI), University of Limerick for his technical help and expertise with the X-Ray Photoelectron Spectroscopy (XPS) analysis.

The Irish Environmental Protection Agency, without whose generous funding this research would not have taken place.

Finally, I would like to thank all my family and friends, with a special mention of my parents, Sadia and Djellali, for their love and constant encouragement.

## Publications

---

1. A. Bakir, P. McLoughlin, S.A.M. Tofail, E. Fitzgerald, “Competitive sorption of antimony with zinc, nickel and aluminium in a seaweed-based fixed-bed sorption column”, *CLEAN* 37 (9) (2009) 712-719
2. A. Bakir, P. McLoughlin, E. Fitzgerald, “Regeneration and reuse of a seaweed-based biosorbent in single and multi-metal systems”, *CLEAN* 38 (3) (2010) 257-262

## Abstract

---

*Fucus vesiculosus*, *Polysiphonia lanosa*, *Ulva lactuca* and a seaweed waste material resulting from the industrial processing of *Ascophyllum nodosum* were screened for Zn(II), Ni(II), Al(III) and Sb(III) removal in dried form, in both single and multi-metal systems. The *Ascophyllum* waste material, which is referred to as Waste *Ascophyllum* Product (WAP), was also screened in wet form. WAP was shown to be efficient at removing Zn(II), Ni(II) and Al(III) in both single and multi-metal systems. Removal efficiencies (RE) for dried WAP were 93, 96 and 68% for Zn(II), Ni(II) and Al(III) respectively in single metal systems. *Polysiphonia lanosa* was found to be more effective at removing Sb(III) than WAP with a RE of 86%. In multi-metal systems, Sb(III) was found to adversely affect the sorption of Zn(II), Ni(II) and Al(III) by WAP, while *P. lanosa* removed Sb(III) in multi-metal systems. The antagonistic effect of Sb(III) on the sorption of the other metals by WAP was investigated using FTIR, XPS and conductimetric titrations. The results demonstrated that Sb(III) was able to bind on a larger and more diversified number of binding sites, preventing the uptake of Zn(II), Ni(II) and Al(III) by both *P. lanosa* and WAP. Maximum uptake capacity values ( $q_{\max}$ ) were calculated using the Langmuir, Freundlich and the combined Langmuir-Freundlich sorption isotherms.  $Q_{\max}$  values were very high in the case of WAP for the sorption of Zn(II), Ni(II) and Al(III) at 134.05, 114.94 and 99.7 mg/g biosorbent. The respective  $q_{\max}$  value for *P. lanosa* and Sb(III) was lower at 47.44 mg/g biosorbent. Fixed-bed column studies using WAP and *P. lanosa* immobilised in agar resulted in high removal efficiencies (RE), with 90, 90, 74% for Zn(II), Ni(II) and Al(III) respectively for WAP/agar and 67% for Sb(III) for *P. lanosa*/agar removal over 3 hours. Agar was found to contribute to the RE. The regeneration and reuse of the biosorbents was achieved using 0.1M HCl with very little loss in metal reuptake efficiency over five sorption cycles. Scale-up of the laboratory column was carried out, with a high RE observed for all metals under investigation. Mathematical and COMSOL modelling were effective tools for representing experimental data and predicting concentration breakthroughs over time.

## Table of contents

---

Declaration	I
Acknowledgements	II
Publications	III
Abstract	IV
Table of contents	V
List of abbreviations	XVII
List of figures	XX
List of tables	XXXII

### Chapter 1: General Introduction

1.1	Use of seaweeds in metal biosorption	2
1.2	Biosorbents of study-related importance	2
1.2.1	<i>Polysiphonia lanosa</i>	2
1.2.1.1	Origin and phylogeny	2
1.2.1.2	Geographical distribution	3
1.2.1.3	Morphology	4
1.2.2	<i>Ulva lactuca</i>	4
1.2.2.1	Origin and phylogeny	4
1.2.2.2	Geographical distribution	5
1.2.2.3	Morphology	5
1.2.3	<i>Fucus vesiculosus</i>	6
1.2.3.1	Origin and phylogeny	6
1.2.3.2	Geographical distribution	6
1.2.3.3	Morphology	7
1.2.4	Waste <i>Ascophyllum</i> Product (WAP)	7
1.3	Heavy metals	10
1.3.1	Sources of heavy metal pollution	10
1.3.2	Metals investigated in this research	11
1.3.2.1	Antimony	11

	1.3.2.2	Zinc	12
	1.3.2.3	Aluminium	13
	1.3.2.4	Nickel	15
1.4	Biosorption of metals by seaweed biomass		17
	1.4.1	Seaweed cell wall components and biomolecules involved in metal binding	17
	1.4.1.1	Seaweed cell wall	17
	1.4.2	Mechanisms of biosorption	22
	1.4.2.1	Physical adsorption	23
	1.4.2.2	Chemisorption	23
	1.4.2.3	Factors influencing biosorption	25
		<i>Binding sites</i>	25
		<i>Influence of pH</i>	27
		<i>Effect of temperature</i>	27
		<i>Effect of ion competition</i>	27
1.5	Heavy metal removal processes		28
	1.5.1	Ion exchange	28
	1.5.2	Precipitation/flocculation	28
	1.5.3	Other processes	29
	1.5.3.1	The fixed-bed sorption system	29
	1.5.3.2	The fluidised bed column sorption system	30
	1.5.3.3	The completely mixed sorption system	31
	1.5.4	Current heavy metal removal processes using biosorption	32
	1.5.4.1	AlgaSORB© Biological Sorption	32
	1.5.4.2	Bio-fix	33
	1.5.4.3	SORBEX™	34
1.6	Background		35
1.7	Aim		35
1.8	Objectives		35

**Chapter 2: Batch tests for the removal of zinc, nickel, aluminium and antimony(III) by dried biomass of *Fucus vesiculosus*, *Ulva lactuca*, *Polysiphonia lanosa* and Waste *Ascophyllum* Product.**

2.1	Introduction	38
2.2	Aims	39
2.3	Method	39
2.4	Statistical analysis	43
2.5	Results and discussion	43
	<i>Single metal sorption tests</i>	
2.5.1	Removal of Nickel by dried WAP, wet WAP, <i>Polysiphonia lanosa</i> , <i>Ulva lactuca</i> and <i>Fucus vesiculosus</i>	43
2.5.2	Removal of Zinc by dried WAP, wet WAP, <i>Polysiphonia lanosa</i> , <i>Ulva lactuca</i> and <i>Fucus vesiculosus</i>	45
2.5.3	Removal of Aluminium by dried WAP, wet WAP, <i>Polysiphonia lanosa</i> , <i>Ulva lactuca</i> and <i>Fucus vesiculosus</i>	46
2.5.4	Removal of Antimony by dried WAP, wet WAP, <i>Polysiphonia lanosa</i> , <i>Ulva lactuca</i> and <i>Fucus vesiculosus</i>	48
	<i>Combined metal sorption tests</i>	
2.5.5	Removal of Zinc and Nickel in a combined aqueous solution by dried WAP, wet WAP, <i>Polysiphonia lanosa</i> , <i>Ulva lactuca</i> and <i>Fucus vesiculosus</i>	49
2.5.6	Removal of Nickel and Antimony in a combined aqueous solution by dried WAP, wet WAP, <i>Polysiphonia lanosa</i> , <i>Ulva lactuca</i> and <i>Fucus vesiculosus</i>	51

2.5.7	Removal of Zinc and Antimony in a combined aqueous solution by dried WAP, wet WAP, <i>Polysiphonia lanosa</i> , <i>Ulva lactuca</i> and <i>Fucus vesiculosus</i>	53
2.5.8	Removal of Aluminium and Antimony in a combined aqueous solution by dried WAP, wet WAP, <i>Polysiphonia lanosa</i> , <i>Ulva lactuca</i> and <i>Fucus vesiculosus</i>	55
2.5.9	Removal of Zinc, Nickel, Aluminium and Antimony in a combined aqueous solution by dried WAP, wet WAP, <i>Polysiphonia lanosa</i> , <i>Ulva lactuca</i> and <i>Fucus vesiculosus</i>	57
2.6	Conclusions	64

### **Chapter 3: Maximum metal uptake capacity ( $q_{max}$ ) and adsorption isotherms**

3.1	Introduction	67
3.1.1	Biosorption equilibrium	67
3.1.2	Adsorption isotherms	68
	<i>Discrete distribution models: Langmuir isotherms</i>	68
	<i>Continuous distribution models: Freundlich isotherms</i>	69
	<i>Hybrid models: Langmuir-Freundlich model</i>	70
3.2	Aims	70
3.3	Methods	71
3.4	Results and discussion	72
3.4.1	Biosorption equilibrium isotherm for Zn(II) and WAP	73
3.4.2	Biosorption equilibrium isotherm for Ni(II) and WAP	74
3.4.3	Biosorption equilibrium isotherm for Al(III) and WAP	75
3.4.4	Biosorption equilibrium isotherm for Sb(III) and WAP	76
3.4.5	Biosorption equilibrium isotherm for Sb(III) and <i>P. lanosa</i>	77
3.4.6	Biosorption equilibrium isotherm for Zn(II)/Ni(II)/Al(III) and WAP	78

3.4.7	Biosorption equilibrium isotherm for Zn(II)/Ni(II)/Al(III)/Sb(III) and WAP	79
3.5	Conclusions	83

**Chapter 4: Fixed-bed column sorption system for the removal of Nickel, Aluminium, Zinc and Antimony(III) by Waste *Ascophyllum* Product (WAP) and *Polysiphonia lanosa* immobilised in agar**

4.1	Introduction	86
4.1.1	Fixed-bed column sorption system	86
4.2	Aims	87
4.3	Methods	87
4.4	Statistical analysis	92
4.5	Results and discussion	92
4.5.1	Fixed bed sorption column studies using agar-only blocks	92
4.5.1.1	3 hour study of zinc removal by agar blocks in a fixed bed sorption column	92
4.5.1.2	3 hour study of nickel removal by agar blocks in a fixed bed sorption column	93
4.5.1.3	3 hour study of aluminium removal by agar blocks in a fixed bed sorption column	94
4.5.1.4	3 hour study of antimony removal by agar blocks in a fixed bed sorption column	95
4.5.1.5	3 hour study on mixed metals (Zn(II), Ni(II) and Al(III)) removal by agar blocks in a fixed bed sorption column	96
4.5.2	Fixed bed sorption column studies using WAP/agar blocks and <i>P. lanosa</i> /agar blocks	99

4.5.2.1	3 hour study on nickel removal by WAP/agar blocks in a fixed bed sorption column	99
4.5.2.2	3 hour study on zinc removal by WAP/agar blocks in a fixed bed sorption column	100
4.5.2.3	3 hour study on aluminium removal by WAP/agar blocks in a fixed bed sorption column	101
4.5.2.4	3 hour study on antimony removal by WAP/agar blocks in a fixed bed sorption column	102
4.5.2.5	3 hour study on antimony removal by <i>P. lanosa</i> /agar blocks in a fixed bed sorption column	103
4.5.2.6	3 hour study on mixed metals (Zn(II), Ni(II) and Al(III)) removal by WAP/agar blocks in a fixed bed sorption column	104
4.5.2.7	3 hour study on mixed metals (Zn(II), Sb(III), Ni(II) and Al(III)) removal by WAP/agar blocks in a fixed bed sorption column	107
4.6	Conclusions	113

## **Chapter 5: Investigation into ion exchange mechanism**

5.1	Introduction	115
	5.1.1 Ion exchange mechanism	115
5.2	Aims	115
5.3	Methods	115
5.4	Results and discussion	116

5.4.1	Trace elements analysis during the removal of zinc by WAP/agar blocks in a fixed bed sorption column	116
5.4.2	Trace elements analysis during the removal of nickel by WAP/agar blocks in a fixed bed sorption column	117
5.4.3	Trace elements analysis during the removal of aluminium by WAP/agar blocks in a fixed bed sorption column	118
5.4.4	Trace elements analysis during the removal of antimony by <i>P. lanosa</i> /agar blocks in a fixed bed sorption column	119
5.4.5	Trace element analysis during the removal of a Zinc, Nickel, Aluminium and Antimony in a combined aqueous solution by WAP/agar blocks in a fixed bed sorption column	120
5.5	Conclusions	121

**Chapter 6: Column capacity (W) and operating time of the WAP/agar and *Polysiphonia lanosa*/agar biosorbents for nickel, zinc, aluminium and antimony**

6.1	Introduction	123
6.1.1	Explanation of column terms	123
6.2	Aims	124
6.3	Methods	124
6.3.1	Dynamic flow tests	124
6.3.2	Column calculations	125
6.4	Results and discussion	128
6.4.1	Overall column capacity (W) for Zn(II) removal by WAP/agar blocks	128
6.4.2	Overall column capacity (W) for Ni(II) removal by WAP/agar blocks	130

6.4.3	Overall column capacity (W) for Al(III) removal by WAP/agar blocks	133
6.4.4	Overall column capacity (W) for Sb(III) removal by WAP/agar blocks	136
6.4.5	Overall column capacity (W) for Sb(III) removal by <i>P. lanosa</i> /agar blocks	138
6.4.6	Comparison of the overall column capacities (W)	140
6.4.7	Comparison of the column characteristics	141
6.5	Conclusions	142

## **Chapter 7: Metal desorption and regeneration of biomass**

7.1	Introduction	145
7.1.1	Metal desorption	145
7.2	Aims	145
7.3	Methods	145
7.4	Results and discussion	147
7.4.1	Screening of potential desorbing solutions	147
7.4.2	Regeneration and re-use of the biomass	149
7.4.2.1	Regeneration of the WAP/agar blocks for the removal of Zn(II) dynamic flow tests using 0.1M HCl as the desorbing agent	149
7.4.2.2	Regeneration of the WAP/agar blocks for the removal of Ni(II) dynamic flow tests using 0.1M HCl as the desorbing agent	151
7.4.2.3	Regeneration of the WAP/agar blocks for the removal of Al(III) dynamic flow tests using 0.1M HCl as the desorbing agent	153

7.4.2.4	Regeneration of the <i>P. lanosa</i> /agar blocks for the removal of Sb(III) dynamic flow tests using 0.1M HCl as the desorbing agent	155
7.4.2.5	Regeneration of the WAP/agar blocks for the removal of Zn(II), Ni(II) and Al(III) in a multi-metal solution in dynamic flow tests using 0.1M HCl as the desorbing agent	157
7.5	Conclusions	163
<b>Chapter 8: Study of Sb(III) sorption by WAP and <i>Polysiphonia lanosa</i>: Antagonistic effects</b>		
8.1	Introduction	165
8.2	Aims	167
8.3	Methods	167
8.3.1	Potentiometric and conductimetric titrations	168
8.3.2	Fourier Transform Infra-red spectroscopy (FTIR)	169
8.3.3	X-Ray Photoelectron Spectroscopy (XPS)	170
8.4	Results and discussion	172
8.4.1	Potentiometric and conductimetric titrations	172
	8.4.1.1 Titration of biomass	172
	8.4.1.2 Titration of the metal bound biomass	174
8.4.2	Fourier Transform Infra-red spectroscopy (FTIR)	178
8.4.3	X-Ray Photoelectron Spectroscopy (XPS)	181
8.5	Conclusions	186

## **Chapter 9: Mathematical modelling of sorption in a fixed bed column**

9.1	Introduction	189
9.2	Aims	189
9.3	Methods	190
9.4	Results and discussion	190
9.4.1	Zn(II) removal by WAP/agar	190
9.4.2	Ni(II) removal by WAP/agar	191
9.4.3	Al(III) removal by WAP/agar	192
9.4.4	Sb(III) removal by WAP/agar	193
9.4.5	Sb(III) removal by <i>P. lanosa</i> /agar	194
9.4.6	Zn(II), Ni(II) and Al(III) removal by WAP/agar	195
9.4.7	Zn(II), Ni(II), Al(III) and Sb(III) removal by WAP/agar	196
9.4.8	Predictions	198
9.5	Conclusions	199

## **Chapter 10: COMSOL modelling**

10.1	Introduction	201
10.1.1	The Mass Transfer Column Model (MTCM)	202
10.2	Aims	206
10.3	Methods	206
10.3.1	Using COMSOL Multiphysics	206
10.3.2	Using COMSOL Script	210
10.4	Results and discussion	211
10.4.1	Time dependent analysis	211
10.4.2	Parametric analysis	213
10.4.3	COMSOL model for zinc removal by WAP/agar blocks	214
10.4.4	COMSOL model for nickel removal by WAP/agar blocks	216
10.4.5	COMSOL model for aluminium removal by WAP/agar blocks	217
10.4.6	COMSOL model for antimony removal by WAP/agar blocks	218
10.4.7	COMSOL model for antimony removal by <i>P. lanosa</i> /agar blocks	219

10.5 Conclusion	220
-----------------	-----

## **Chapter 11: Scale-up of fixed-bed sorption column**

11.1 Introduction	222
11.2 Aims	222
11.3 Methods	222
11.4 Results and discussion	231
11.4.1 Manufacture of the WAP/agar and <i>Polysiphonia lanosa</i> /agar blocks	231
11.4.2 Dynamic flow tests	231
11.4.2.1 Optimisation of the bed height	231
11.4.2.2 Dynamic flow test for Zn(II) removal in a single metal solution using WAP/agar blocks	232
11.4.2.3 Dynamic flow test for Ni(II) removal in a single metal solution using WAP/agar blocks	233
11.4.2.4 Dynamic flow test for Al(III) removal in a single metal solution using WAP/agar blocks	234
11.4.2.5 Dynamic flow test for Sb(III) removal in a single metal solution using <i>P. lanosa</i> /agar blocks	235
11.4.2.6 Dynamic flow test for Zn(II),Ni(II) and Al(III) removal in a multi metal solution using WAP/agar blocks	236
11.5 Conclusions	238

## Chapter 12: Summary and Future work

12.1 Summary	240
12.2 Future work	242
12.2.1 Further characterisation of WAP	242
12.2.2 Industrial-scale fixed bed sorption column	243
12.2.3 Further COMSOL modelling for multi-metal systems and for different operating settings	243
12.2.4 Market assessment	243
<b>References</b>	<b>244</b>

## Appendices

- Appendix A: A. Bakir, P. McLoughlin, S.A.M. Tofail, E. Fitzgerald, “Competitive sorption of antimony with zinc, nickel and aluminium in a seaweed-based fixed-bed sorption column”, *CLEAN* 37 (9) (2009) 712-719
- Appendix B: A. Bakir, P. McLoughlin, E. Fitzgerald, “Regeneration and reuse of a seaweed-based biosorbent in single and multi-metal systems”, *CLEAN* 38 (3) (2010) 257-262
- Appendix C: Langmuir and Freundlich binding isotherms
- Appendix D: COMSOL scripts

## List of abbreviations

---

Al = Aluminium

ANOVA = Analysis of variance

b = Langmuir affinity coefficient

Ca = Calcium

Cd = Cadmium

$C_i$  = Initial concentration

$C_f$  = Final concentration

CRM = Certified Reference Material

Cu = Copper

Dg = Solute distribution parameter

$D_Z$  = Axial dispersion coefficient

$F_0$  = Fluid-flow rate ( $\text{cm min}^{-1}$ )

FTIR = Fourier Transform Infrared Spectroscopy

*F. vesiculosus* = *Fucus vesiculosus*

g = Gram

ICP-OES = Inductively Coupled Plasma Optical Emission Spectroscopy

$K_f$  = Freundlich constant (L/g)

$K_{fM}$  = Overall mass transfer coefficient ( $\text{min}^{-1}$ )

Kg = Kilogram

$K_{N,M}$  = equilibrium binding constant

$Sh_M$  = Mass transfer/column length parameters for a species M

L = Litre

mg = Milligram

Mg = Magnesium

MTCM = Mass Transfer Column Model

MTZ = Mass Transfer Zone (hours)

$n$  = Binding isotherms Freundlich model exponent

Na = Sodium

Ni = Nickel

$p$  = Probability

Pe = Peclet number

*P. lanosa* = *Polysiphonia lanosa*

PTFE = Polytetrafluoroethylene (Teflon)

ppb = Part per billion

ppm = Part per million

$q_{\max}$  = Maximum uptake ( $\text{mg g}^{-1}$  or  $\text{mmol g}^{-1}$ )

Sb = Antimony

SD = Standard deviation

$t$  = Time (min or hours)

$T_B$  = Breakthrough point (hours)

$T_E$  = Exhaustion point (hours)

Tl = Tomato leaves

*U. lactuca* = *Ulva lactuca*

V = Volume solution (mL)

WAP = Waste Ascophyllum Product

wt = Weight

XPS = X-ray Photoelectron Spectroscopy

Zn = Zinc

$\mu$  = Micro

$\varepsilon$  = Column void fraction

$\rho_b$  = Packing density of dry biomass in the fixed-bed sorption column ( $\text{g L}^{-1}$ )

$v$  = Interstitial fluid velocity

## List of figures

---

Figure 1.1	Geographical distribution of <i>Polysiphonia lanosa</i> for United-Kingdom and Ireland	3
Figure 1.2	<i>Polysiphonia lanosa</i> as epiphyte of <i>Ascophyllum nodosum</i>	4
Figure 1.3	Geographical distribution of <i>Ulva lactuca</i> in Ireland and the United-Kingdom	5
Figure 1.4	<i>Ulva lactuca</i>	5
Figure 1.5	Geographical distribution of <i>Fucus vesiculosus</i> in Ireland and the United-Kingdom	6
Figure 1.6	<i>Fucus vesiculosus</i>	7
Figure 1.7	Processing of <i>Ascophyllum nodosum</i> and WAP production	9
Figure 1.8	Cell wall of brown algae	18
Figure 1.9	Structure of cellulose	19
Figure 1.10	basic molecule structure of agar	19
Figure 1.11	Structural characteristics of alginates	20
Figure 1.12	Schematic representation of carrageenan monomers	21
Figure 1.13	Schematic representation of fucoidan	22
Figure 1.14	Schematic representation of adsorption and ion exchange	23
Figure 1.15	Fixed bed column sorption system principle	30
Figure 1.16	Fluidised bed biosorption column	31
Figure 1.17	Mixed sorption system	32
Figure 1.18	AlgaSORB, portable effluent treatment equipment (PETE)	33
Figure 1.19	Biosorption process columns in operation	34
Figure 1.20	Different scales of sorption systems	35
Figure 2.1	Fethard-on-sea	40
Figure 2.2	Baginbun Bay	41
Figure 2.3	Mean nickel concentrations ( $\text{mg L}^{-1}$ ) from an initial aqueous Ni(II) solution ( $10 \text{ mg L}^{-1}$ ) after 12 hours exposure to dried WAP, wet WAP, <i>P. lanosa</i> , <i>U. lactuca</i> and <i>F. vesiculosus</i>	43

Figure 2.4	Mean zinc concentrations ( $\text{mg L}^{-1}$ ) from an initial aqueous Zn(II) solution ( $10 \text{ mg L}^{-1}$ ) after 12 hours exposure to dried WAP, wet WAP, <i>P. lanosa</i> , <i>U. lactuca</i> and <i>F. vesiculosus</i>	45
Figure 2.5	Mean aluminium concentrations ( $\text{mg L}^{-1}$ ) from an initial aqueous Al(III) solution ( $10 \text{ mg L}^{-1}$ ) after 12 hours exposure to dried WAP, wet WAP, <i>P. lanosa</i> , <i>U. lactuca</i> and <i>F. vesiculosus</i>	46
Figure 2.6	Mean antimony concentrations ( $\text{mg L}^{-1}$ ) from an initial aqueous Sb(III) solution ( $10 \text{ mg L}^{-1}$ ) after 12 hours exposure to dried WAP, wet WAP, <i>P. lanosa</i> , <i>U. lactuca</i> and <i>F. vesiculosus</i>	48
Figure 2.7	Mean zinc and nickel concentrations ( $\text{mg L}^{-1}$ ) from an initial combined aqueous solution of Zn(II) and Ni(II) ( $10 \text{ mg L}^{-1}$ ) after 12 hours exposure to dried WAP, wet WAP, <i>P. lanosa</i> , <i>U. lactuca</i> and <i>F. vesiculosus</i>	49
Figure 2.8	Mean nickel and antimony concentrations ( $\text{mg L}^{-1}$ ) from an initial combined aqueous solution of Ni(II) and Sb(III) ( $10 \text{ mg L}^{-1}$ ) after 12 hours exposure to dried WAP, wet WAP, <i>P. lanosa</i> , <i>U. lactuca</i> and <i>F. vesiculosus</i>	51
Figure 2.9	Mean zinc and antimony concentrations ( $\text{mg L}^{-1}$ ) from an initial combined aqueous solution of Zn(II) and Sb(III) ( $10 \text{ mg L}^{-1}$ ) after 12 hours exposure to dried WAP, wet WAP, <i>P. lanosa</i> , <i>U. lactuca</i> and <i>F. vesiculosus</i>	53
Figure 2.10	Mean aluminium and antimony concentrations ( $\text{mg L}^{-1}$ ) from an initial combined aqueous solution of Al(III) and Sb(III) ( $10 \text{ mg L}^{-1}$ ) after 12 hours exposure to dried WAP, wet WAP, <i>P. lanosa</i> , <i>U. lactuca</i> and <i>F. vesiculosus</i>	55

Figure 2.11	Mean zinc, nickel, aluminium and antimony concentrations ( $\text{mg L}^{-1}$ ) from an initial combined aqueous solution of Zn(II), Ni(II), Al(III) and Sb(III) ( $10 \text{ mg L}^{-1}$ ) after 12 hours exposure to dried WAP, wet WAP, <i>P. lanosa</i> , <i>U. lactuca</i> and <i>F. vesiculosus</i>	57
Figure 3.1	Example of a sorption isotherm	67
Figure 3.2	Relationship between Langmuirian $b$ and the equilibrium affinity $K$	69
Figure 3.3	Biosorption equilibrium isotherm ( $q$ vs. $C_f$ ) for 100 mg of WAP exposed to Zn(II) concentrations $5\text{-}350 \text{ mg L}^{-1}$	73
Figure 3.4	Linearised plot of the Langmuir relationship ( $1/q$ vs. $1/C_f$ ) between $q$ and $C_f$ of WAP biosorption isotherm	73
Figure 3.5	Biosorption equilibrium isotherm ( $q$ vs. $C_f$ ) for 100 mg of WAP exposed to Ni(II) concentrations $5\text{-}350 \text{ mg L}^{-1}$	74
Figure 3.6	Linearised plot of the Langmuir relationship ( $1/q$ vs. $1/C_f$ ) between $q$ and $C_f$ of WAP biosorption isotherm	74
Figure 3.7	Biosorption equilibrium isotherm ( $q$ vs. $C_f$ ) for 100 mg of WAP exposed to Al(III) concentrations $5\text{-}350 \text{ mg L}^{-1}$	75
Figure 3.8	Linearised plot of the Langmuir relationship ( $1/q$ vs. $1/C_f$ ) between $q$ and $C_f$ of WAP biosorption isotherm	75
Figure 3.9	Biosorption equilibrium isotherm ( $q$ vs. $C_f$ ) for 100 mg of WAP exposed to Sb(III) concentrations $5\text{-}350 \text{ mg L}^{-1}$	76
Figure 3.10	Linearised plot of the Langmuir relationship ( $1/q$ vs. $1/C_f$ ) between $q$ and $C_f$ of WAP biosorption isotherm	76
Figure 3.11	Biosorption equilibrium isotherm ( $q$ vs. $C_f$ ) for 100 mg of <i>P. lanosa</i> exposed to Sb(III) concentrations $5\text{-}350 \text{ mg L}^{-1}$	77
Figure 3.12	Linearised plot of the Langmuir relationship ( $1/q$ vs. $1/C_f$ ) between $q$ and $C_f$ of <i>P. lanosa</i> biosorption isotherm	77

Figure 3.13	Biosorption equilibrium isotherm ( $q$ vs. $C_f$ ) of 100 mg of WAP exposed to a combined solution of Ni(II), Zn(II) and Al(III) with concentrations 5-350 mg L <sup>-1</sup>	78
Figure 3.14	Linearised plot of the Langmuir relationship ( $1/q$ vs. $1/C_f$ ) between $q$ and $C_f$ of WAP biosorption isotherm	78
Figure 3.15	Biosorption equilibrium isotherm ( $q$ vs. $C_f$ ) of 100 mg of WAP exposed to a combined solution of Ni(II), Zn(II), Al(III) and Sb(III) with concentrations 5-350 mg L <sup>-1</sup>	79
Figure 3.16	Linearised plot of the Langmuir relationship ( $1/q$ vs. $1/C_f$ ) between $q$ and $C_f$ of WAP biosorption isotherm	79
Figure 4.1	Fixed bed column sorption system principle	87
Figure 4.2	Image of dried blocks of WAP immobilised in agar	89
Figure 4.3	Image of the fixed bed sorption columns	89
Figure 4.4	Schematic representation of the fixed bed sorption columns	90
Figure 4.5	CAD drawings of the sorption columns	91
Figure 4.6	Zinc removal in a single metal system (10 mg L <sup>-1</sup> ) by agar blocks	92
Figure 4.7	Nickel removal in a single metal system (10 mg L <sup>-1</sup> ) by agar blocks	93
Figure 4.8	Aluminium removal in a single metal system (10 mg L <sup>-1</sup> ) by agar blocks	94
Figure 4.9	Antimony removal in a single metal system (10 mg L <sup>-1</sup> ) by agar blocks	95
Figure 4.10	Zinc, Nickel and Aluminium removal in a multi-metal system (10 mg L <sup>-1</sup> each) by agar blocks	96
Figure 4.11	Zinc removal in a single metal system (10 mg L <sup>-1</sup> ) by WAP (7.5%)/agar (5%) blocks	99
Figure 4.12	Nickel removal in a single metal system (10 mg L <sup>-1</sup> ) by WAP (7.5%)/agar (5%) blocks	100
Figure 4.13	Aluminium removal in a single metal system (10 mg L <sup>-1</sup> ) by WAP (7.5%)/agar (5%) blocks	101

Figure 4.14	Antimony removal in a single metal system (10 mg L <sup>-1</sup> ) by WAP (7.5%)/agar (5%) blocks	102
Figure 4.15	Antimony removal in a single metal system (10 mg L <sup>-1</sup> ) by <i>P. lanosa</i> (7.5%)/agar (5%) blocks	102
Figure 4.16	Zinc, Nickel and Aluminium removal in a multi-metal system (10 mg L <sup>-1</sup> each) by WAP (7.5%)/agar (5%) blocks	104
Figure 4.17	Zinc, Nickel, Aluminium and Antimony removal in a multi-metal system (10 mg L <sup>-1</sup> each) by WAP (7.5%)/agar (5%) blocks	107
Figure 5.1	Trace element analysis from fixed bed column studies with WAP/agar blocks from a 10 mg L <sup>-1</sup> Zn(II) solution	116
Figure 5.2	Trace element analysis from fixed bed column studies with WAP/agar blocks from a 10 mg L <sup>-1</sup> Ni(II) solution	117
Figure 5.3	Trace element analysis from fixed bed column studies with WAP/agar blocks from a 10 mg L <sup>-1</sup> Al(III) solution	118
Figure 5.4	Trace element analysis from fixed bed column studies with <i>P. lanosa</i> /agar blocks from a 10 mg L <sup>-1</sup> Sb(III) solution	119
Figure 5.5	Trace element analysis from fixed bed column studies with WAP/agar blocks from a 10 mg L <sup>-1</sup> Zn(II), Ni(II), Al(III) and Sb(III) solution	120
Figure 6.1	Zn(II) remaining in effluent treated with 5% agar/7.5% WAP (water soaked) from a 10 mg L <sup>-1</sup> influent stream at 25 mL min <sup>-1</sup> for 44 hours	128
Figure 6.2	Removal efficiency in % for Zn(II) by 5% agar/7.5% WAP (water soaked) from a 10 mg L <sup>-1</sup> influent stream at 25 mL min <sup>-1</sup> for 44 hours	128
Figure 6.3	Ni(II) remaining in effluent treated with 5% agar/7.5% WAP (water soaked) from a 10 mg L <sup>-1</sup> influent stream at 25 mL min <sup>-1</sup> for 175 hours	130

Figure 6.4	Removal efficiency in % for Ni(II) by 5% agar/7.5% WAP (water soaked) from a 10 mg L <sup>-1</sup> influent stream at 25 mL min <sup>-1</sup> for 175 hours	131
Figure 6.5	Al(III) remaining in effluent treated with 5% agar/7.5% WAP (water soaked) from a 10 mg L <sup>-1</sup> influent stream at 25 mL min <sup>-1</sup> for 45 hours	133
Figure 6.6	Removal efficiency in % for Al(III) by 5% agar/7.5% WAP (water soaked) from a 10 mg L <sup>-1</sup> influent stream at 25 mL min <sup>-1</sup> for 45 hours	134
Figure 6.7	Sb(III) remaining in effluent treated with 5% agar/7.5% WAP (water soaked) from a 10 mg L <sup>-1</sup> influent stream at 25 mL min <sup>-1</sup> for 35 hours	136
Figure 6.8	Removal efficiency in % for Sb(III) by 5% agar/7.5% WAP (water soaked) from a 10 mg L <sup>-1</sup> influent stream at 25 mL min <sup>-1</sup> for 35 hours	136
Figure 6.9	Sb(III) remaining in effluent treated with 5% agar/7.5% <i>P. lanosa</i> (water soaked) from a 10 mg L <sup>-1</sup> influent stream at 25 mL min <sup>-1</sup> for 35 hours	138
Figure 6.10	Removal efficiency in % for Sb(III) by 5% agar/7.5% <i>P. lanosa</i> (water soaked) from a 10 mg L <sup>-1</sup> influent stream at 25 mL min <sup>-1</sup> for 35 hours	138
Figure 6.11	Comparison of dynamic flow tests for Zn(II), Al(III) and Sb(III) treated with 5% agar/7.5% WAP (water soaked) and Sb(III) treated with 5% agar/7.5% <i>P. lanosa</i> from single metal influents of 10 mg L <sup>-1</sup>	140
Figure 6.12	Comparison of dynamic flow tests for Zn(II), Ni(II), Al(III) and Sb(III) treated with 5% agar/7.5% WAP (water soaked) and Sb(III) treated with 5% agar/7.5% <i>P. lanosa</i> from single metal influents of 10 mg L <sup>-1</sup>	141
Figure 7.1	Ni(II) recovery from WAP/agar using various desorbing agents in batch tests	147

Figure 7.2	Zn(II) recovery from WAP/agar using various desorbing agents in batch tests	147
Figure 7.3	Desorption of Zn(II) from WAP/agar using 0.1M and 0.5M CaCl <sub>2</sub> at different pH values	148
Figure 7.4	Removal efficiency of Zn(II) from WAP/agar blocks in 5 successive regeneration and re-use cycles using 0.1M HCl as the desorbing solution	149
Figure 7.5	Mean removal efficiency of Zn(II) over 3 hours from 5 successive regeneration and re-use cycles using 0.1M HCl as the desorbing solution	150
Figure 7.6	Zn(II) concentrations in the effluent after 4 desorption cycles	150
Figure 7.7	Removal efficiency of Ni(II) from 5 successive regeneration and re-use cycles using 0.1M HCl as the desorbing solution	151
Figure 7.8	Mean removal efficiency of Ni(II) over 3 hours from 5 successive regeneration and re-use cycles using 0.1M HCl as the desorbing solution	152
Figure 7.9	Ni(II) concentrations in the effluent after 4 desorption cycles	152
Figure 7.10	Removal efficiency of Al(III) from 5 successive regeneration and re-use cycles using 0.1M HCl as the desorbing solution	153
Figure 7.11	Mean removal efficiency of Al(III) over 3 hours from 5 successive regeneration and re-use cycles using 0.1M HCl as the desorbing solution	154
Figure 7.12	Al(III) concentrations in the effluent after 4 desorption cycles	154
Figure 7.13	Removal efficiency of Sb(III) from 5 successive regeneration and re-use cycles using 0.1M HCl as the desorbing solution	155

Figure 7.14	Mean removal efficiency of Sb(III) over 3 hours from 5 successive regeneration and re-use cycles using 0.1M HCl as the desorbing solution	156
Figure 7.15	Sb(III) concentrations in the effluent after 4 desorption cycles	156
Figure 7.16	Mean removal efficiency of Ni(II), Zn(II) and Al(III) over 3 hours from 5 successive regeneration and re-use cycles using 0.1M HCl as the desorbing solution	157
Figure 7.17	Removal efficiency of Ni(II) from 5 successive regeneration and re-use cycles using 0.1M HCl as the desorbing solution	158
Figure 7.18	Ni(II) concentrations in the effluent after 4 desorption cycles	158
Figure 7.19	Removal efficiency of Zn(II) from 5 successive regeneration and re-use cycles using 0.1M HCl as the desorbing solution	159
Figure 7.20	Zn(II) concentrations in the effluent after 4 desorption cycles	160
Figure 7.21	Removal efficiency of Al(III) from 5 successive regeneration and re-use cycles using 0.1M HCl as the desorbing solution	160
Figure 7.22	Al(II) concentrations in the effluent after 4 desorption cycles	161
Figure 8.1	(a) Digilab Scimitar Series Infrared Spectrometer (b) MIRacle™ Single Reflection HATR accessory	170
Figure 8.2	Kratos AXIS 165 X-ray photoelectron spectrometer	171
Figure 8.3	Stretching frequencies observed for (a) protonated and (b) Sb(III) loaded <i>Polysiphonia lanosa</i> , (c) protonated and (d) Sb(III)-loaded Waste <i>Ascophyllum</i> Product	172
Figure 8.4	Potentiometric titration curves obtained for protonated WAP and protonated <i>P. lanosa</i>	173

Figure 8.5	Conductimetric titration for protonated WAP and protonated <i>P. lanosa</i>	173
Figure 8.6	Potentiometric titration for protonated biomass of WAP and protonated <i>P. lanosa</i>	174
Figure 8.7	Potentiometric titration curves obtained for Sb(III) exposed WAP and <i>P. lanosa</i>	175
Figure 8.8	Conductimetric titration curves obtained for Sb(III) exposed WAP and <i>P. lanosa</i>	175
Figure 8.9	Potentiometric titration of protonated biomass of WAP and <i>P. lanosa</i>	179
Figure 8.10	XPS Sb spectra (binding energy against intensity) for raw (PL raw), 1000 mg L <sup>-1</sup> (PL Sb1) and 2000 mg L <sup>-1</sup> (PL Sb2) Sb(III)-loaded <i>P. lanosa</i>	181
Figure 8.11	XPS N spectra (binding energy against intensity) for raw (PL raw), 1000 (PL Sb1) and 2000 mg L <sup>-1</sup> Sb(III)-loaded <i>P. lanosa</i>	182
Figure 8.12	XPS C1s spectra (binding energy against intensity) (a) Raw <i>P. lanosa</i> , 1000 mg L <sup>-1</sup> (PL Sb1) and 2000 mg L <sup>-1</sup> (PL Sb2) Sb(III)-loaded <i>P. lanosa</i> , (b) Raw WAP, 1000 (WAP Sb1) and 2000 mg L <sup>-1</sup> (WAP Sb2) Sb(III)-loaded WAP	183
Figure 9.1	Linear plot of the Yoon-Nelson model for Zn(II) removal by WAP/agar	190
Figure 9.2	Model fitting to the experimental data for Zn(II) removal by WAP/agar	191
Figure 9.3	Linear plot of the Yoon-Nelson model for Ni(II) removal by WAP/agar	191
Figure 9.4	Model fitting to the experimental data for Ni(II) removal by WAP/agar	192
Figure 9.5	Linear plot of the Yoon-Nelson model for Al(III) removal by WAP/agar	192

Figure 9.6	Model fitting to the experimental data for Al(III) removal by WAP/agar	193
Figure 9.7	Linear plot of the Yoon-Nelson model for Sb(III) removal by WAP/agar	193
Figure 9.8	Model fitting to the experimental data for Sb(III) removal by WAP/agar	194
Figure 9.9	Linear plot of the Yoon-Nelson model for Sb(III) removal by <i>P. lanosa</i> /agar	194
Figure 9.10	Model fitting to the experimental data	195
Figure 9.11	Linear plot of the Yoon-Nelson model for Zn(II), Ni(II), Al(III) removal by WAP/agar	195
Figure 9.12	Model fitting to the experimental data	196
Figure 9.13	Linear plot of the Yoon-Nelson model for Zn(II), Ni(II), Al(III) and Sb(III) removal by WAP/agar	196
Figure 9.14	Model fitting to the experimental data	197
Figure 9.15	Breakthrough curve predictions using Yoon-Nelson model for metals in single component solutions with WAP/agar	198
Figure 9.16	Breakthrough curve predictions using Yoon-Nelson model for Zn(II), Ni(II) and Al(III) in a combined metal solution with WAP/agar	198
Figure 9.17	Breakthrough curve predictions using Yoon-Nelson model for Zn(II), Ni(II), Al(III) and Sb(III) in a combined metal solution with WAP/agar	199
Figure 10.1	Mesh representation in COMSOL	207
Figure 10.2	Constant values in COMSOL	208
Figure 10.3	Breakthrough concentrations curves against time in min	212
Figure 10.4	Breakthrough concentrations curves for different mass transfer coefficients	213
Figure 10.5	Breakthrough concentrations curves for dispersion coefficients	213
Figure 10.6	Breakthrough concentrations curves for void fractions	214

Figure 10.7	Model generated from COMSOL script for Zn(II) removal by WAP/agar	215
Figure 10.8	Model generated from COMSOL script for Ni(II) removal by WAP/agar	216
Figure 10.9	Model generated from COMSOL script for Al(III) removal by WAP/agar	217
Figure 10.10	Model generated from COMSOL script for Sb(III) removal by WAP/agar	218
Figure 10.11	Model generated from COMSOL script for Sb(III) removal by <i>P. lanosa</i> /agar	219
Figure 11.1	Production line for the processing of 5% agar/7.5% WAP or <i>P. lanosa</i> blocks	224
Figure 11.2	Schematic representation of the scaled-up fixed bed sorption column	226
Figure 11.3	Laboratory configuration and set-up of the scaled-up fixed bed sorption column	227
Figure 11.4	Spray system for the introduction of the metal bearing solution	228
Figure 11.5	WAP/agar blocks packed into the scaled-up fixed bed column	229
Figure 11.6	Zn(II) RE (%) by 7.5% WAP/5% agar blocks over 15 min for different bed heights	231
Figure 11.7	RE in % for Zn(II) by 7.5% WAP/5% agar blocks in a single metal system	232
Figure 11.8	RE in % for Ni(II) by 7.5% WAP/5% agar blocks in a single metal system	233
Figure 11.9	RE in % for Al(III) by 7.5% WAP/5% agar blocks in a single metal system	234
Figure 11.10	RE in % for Sb(III) by 7.5% <i>P. lanosa</i> /5% agar blocks in a single metal system	235
Figure 11.11	RE in % for Zn(II), Ni(II) and Al(II) by 7.5% WAP/5% agar blocks in a multi metal system	236

## List of tables

---

Table 1.1	Standards for metals (dissolved and colloidal/suspended solids)	10
Table 1.2	Ranking of metal interest priorities	11
Table 1.3	Reported primary aluminium production in the world for the period 2003-2007	14
Table 1.4	Binding groups for metal biosorption	26
Table 2.1	One-way ANOVA analysis for Ni(II) sorption by dried WAP, wet WAP, <i>P. lanosa</i> , <i>U. lactuca</i> and <i>F. vesiculosus</i>	44
Table 2.2	Tukey test for Ni(II) sorption by dried WAP, wet WAP, <i>P. lanosa</i> , <i>U. lactuca</i> and <i>F. vesiculosus</i>	44
Table 2.3	One-way ANOVA analysis for Zn(II) sorption by dried WAP, wet WAP, <i>P. lanosa</i> , <i>U. lactuca</i> and <i>F. vesiculosus</i>	45
Table 2.4	Tukey test for Zn(II) sorption by dried WAP, wet WAP, <i>P. lanosa</i> , <i>U. lactuca</i> and <i>F. vesiculosus</i>	46
Table 2.5	One-way ANOVA analysis for Al(III) sorption by dried WAP, wet WAP, <i>P. lanosa</i> , <i>U. lactuca</i> and <i>F. vesiculosus</i>	47
Table 2.6	Tukey test for Al(III) sorption by dried WAP, wet WAP, <i>P. lanosa</i> , <i>U. lactuca</i> and <i>F. vesiculosus</i>	47
Table 2.7	One-way ANOVA analysis for Sb(III) sorption by dried WAP, wet WAP, <i>P. lanosa</i> , <i>U. lactuca</i> and <i>F. vesiculosus</i>	48
Table 2.8	Tukey test for Sb(III) sorption by dried WAP, wet WAP, <i>P. lanosa</i> , <i>U. lactuca</i> and <i>F. vesiculosus</i>	49
Table 2.9	Two-way ANOVA analysis for Ni(II)/Zn(II) sorption by dried WAP, wet WAP, <i>P. lanosa</i> , <i>U. lactuca</i> and <i>F. vesiculosus</i>	50

Table 2.10	Tukey test for Ni(II)/Zn(II) sorption by dried WAP, wet WAP, <i>P. lanosa</i> , <i>U. lactuca</i> and <i>F. vesiculosus</i>	51
Table 2.11	Two-way ANOVA for Ni(II)/Sb(III) sorption by dried WAP, wet WAP, <i>P. lanosa</i> , <i>U. lactuca</i> and <i>F. vesiculosus</i>	52
Table 2.12	Tukey test for Ni(II)/Sb(III) sorption by dried WAP, wet WAP, <i>P. lanosa</i> , <i>U. lactuca</i> and <i>F. vesiculosus</i>	53
Table 2.13	Two-way ANOVA for Zn(II)/Sb(III) sorption by dried WAP, wet WAP, <i>P. lanosa</i> , <i>U. lactuca</i> and <i>F. vesiculosus</i>	54
Table 2.14	Tukey test for Zn(II)/Sb(III) sorption by dried WAP, wet WAP, <i>P. lanosa</i> , <i>U. lactuca</i> and <i>F. vesiculosus</i>	55
Table 2.15	Two-way ANOVA for Al(III)/Sb(III) sorption by dried WAP, wet WAP, <i>P. lanosa</i> , <i>U. lactuca</i> and <i>F. vesiculosus</i>	56
Table 2.16	Tukey test for Al(III)/Sb(III) sorption by dried WAP, wet WAP, <i>P. lanosa</i> , <i>U. lactuca</i> and <i>F. vesiculosus</i>	57
Table 2.17	Two-way ANOVA for Zn(II)/Ni(II)/Al(III)/Sb(III) sorption by dried WAP, wet WAP, <i>P. lanosa</i> , <i>U. lactuca</i> and <i>F. vesiculosus</i>	58
Table 2.18	Tukey test (biosorbents) for Zn(II)/Ni(II)/Al(III)/Sb(III) sorption by dried WAP, wet WAP, <i>P. lanosa</i> , <i>U. lactuca</i> and <i>F. vesiculosus</i>	59
Table 2.19	Tukey test (metals) for Zn(II)/Ni(II)/Al(III)/Sb(III) sorption by dried WAP, wet WAP, <i>P. lanosa</i> , <i>U. lactuca</i> and <i>F. vesiculosus</i>	59
Table 2.20	Removal efficiencies in % for different biosorbents (batch tests)	60
Table 2.21	Uptake capacities (q) in mg g <sup>-1</sup> for different biosorbents for single metal solutions	61
Table 2.22	Uptake capacities (q) in mg g <sup>-1</sup> for <i>F. vesiculosus</i> , <i>U. lactuca</i> and <i>P. lanosa</i> for combined metal solutions	61

Table 2.23	Uptake capacities (q) in mg g <sup>-1</sup> for <i>F. vesiculosus</i> , <i>U. lactuca</i> and <i>P. lanosa</i> for combined metal solutions	62
Table 3.1	Comparison of the correlation coefficients between the Langmuir, Freundlich and the combined Langmuir-Freundlich biosorption models	72
Table 3.2	Langmuir parameters and maximum adsorption values (q <sub>max</sub> )	80
Table 3.3a	Comparison of maximum uptake capacity values (q <sub>max</sub> ) for WAP and <i>P. lanosa</i> for Zn(II), Ni(II), Al(III) and Sb(III) derived from the Langmuir isotherms in this research	81
Table 3.3b	Comparison of maximum uptake capacity values (q <sub>max</sub> ) for other biosorbents in different reactors	82
Table 4.1	One-Way ANOVA analysis for Zn(II) removal using a fixed bed sorption column with agar alone	93
Table 4.2	One-Way ANOVA analysis for Ni(II) removal using a fixed bed sorption column with agar alone	94
Table 4.3	One-Way ANOVA analysis for Al(III) removal using a fixed bed sorption column with agar alone	95
Table 4.4	One-Way ANOVA analysis for Sb(III) removal using a fixed bed sorption column with agar alone	96
Table 4.5	Multivariate tests from the general linear model	97
Table 4.6	Mauchly's test of sphericity from the general linear model	98
Table 4.7a	Tests of within-subjects effects	98
Table 4.7b	Tests of between-subjects effects	99
Table 4.8	One-Way ANOVA analysis for Ni(II) removal using a fixed bed sorption column with 5%agar/7.5% WAP sorbents	100
Table 4.9	One-Way ANOVA analysis for Zn(II) removal using a fixed bed sorption column with 5%agar/7.5% WAP sorbents	101

Table 4.10	One-Way ANOVA analysis for Al(III) removal using a fixed bed sorption column with 5%agar/7.5% WAP sorbents	102
Table 4.11	One-Way ANOVA analysis for Sb(III) removal using a fixed bed sorption column with 5%agar/7.5% WAP sorbents	103
Table 4.12	One-Way ANOVA analysis for Sb(III) removal using a fixed bed sorption column with 5%agar/7.5% <i>P. lanosa</i> sorbents	104
Table 4.13	Multivariate tests from the general linear model	105
Table 4.14	Mauchly's test of sphericity from the general linear model	106
Table 4.15a	Tests of within-subjects effects	106
Table 4.15b	Tests of between-subjects effects	107
Table 4.16	Multivariate tests from the general linear model	108
Table 4.17	Mauchly's test of sphericity from the general linear model	109
Table 4.18a	Tests of within-subjects effects	109
Table 4.18b	Tests of between-subjects effects	110
Table 4.19	Mean removal efficiencies over 3 hours in % for WAP and <i>P. lanosa</i> blocks (fixed bed columns) immobilised in agar (7.5%:5% WAP:agar)	111
Table 6.1	Column characteristics for Zn(II) dynamic flow test with 5% agar/7.5% WAP	129
Table 6.2	Column characteristics for Ni(II) dynamic flow test with 5% agar/7.5% WAP	132
Table 6.3	Column characteristics for Al(III) dynamic flow test with 5% agar/7.5% WAP	135
Table 6.4	Column characteristics for Sb(III) dynamic flow test with 5% agar/7.5% WAP	137
Table 6.5	Column characteristics for Sb(III) dynamic flow test with 5% agar/7.5% <i>P. lanosa</i>	139
Table 8.1	Stretching frequencies for Sb(III)-loaded WAP and <i>P. lanosa</i> .	176

Table 8.2	pK <sub>a</sub> values and quantity of acidic groups	180
Table 8.3	XPS atomic concentration (in percentage) of the relevant chemical elements in WAP and <i>P. lanosa</i> before and after exposure to Sb(III) and ions at two different concentrations (1000 and 2000 mg L <sup>-1</sup> )	184
Table 8.4	Carbon 1s binding energies and peak ratios for <i>Polysiphonia lanosa</i> and WAP	184
Table 9.1	Summary of parameters and correlation coefficients	197
Table 10.1	Operational settings for Zn(II) removal by WAP/agar blocks	215
Table 10.2	Operational settings for Ni(II) removal by WAP/agar blocks	216
Table 10.3	Operational settings for Al(III) removal by WAP/agar blocks	217
Table 10.4	Operational settings for Sb(III) removal by WAP/agar blocks	218
Table 10.5	Operational settings for Sb(III) removal by <i>P. lanosa</i> /agar blocks	219
Table 11.1	Operational settings for Zn(II) dynamic flow test	232
Table 11.2	Operational settings for Ni(II) dynamic flow test	233
Table 11.3	Operational settings for Al(II) dynamic flow test	234
Table 11.4	Operational settings for Sb(III) dynamic flow test	235
Table 11.5	Operational settings for Zn(II), Ni(II) and Al(III) dynamic flow test	236
Table 11.6	Mean RE (%) over 60 min for Zn(II), Ni(II), Al(III) in single and multi-metal systems by WAP/agar, and Sb(III) removal by <i>P. lanosa</i> /agar	237

# **Chapter 1**

## **General Introduction**

## **1.1 Use of seaweeds in metal biosorption**

Marine algae, commonly known as seaweeds, are abundant along the coasts of Ireland. Seaweeds are very efficient in binding a variety of metals in either living (bioaccumulation) or non-viable form (biosorption) (Volesky, 1990). Biosorption is a property of certain types of inactive, dead biomasses to bind and concentrate heavy metals from even very dilute aqueous solutions (BV Sorbex, 2008b).

Ion exchange is recognized as the principal mechanism in metal binding by seaweeds, involving carboxyl, hydroxyl and sulphonate groups present on their surfaces (Fourest et al., 1996; Fourest and Volesky, 1996; Volesky, 2004).

## **1.2 Biosorbents of study-related importance**

In this research, four different species of seaweeds were investigated. They were *Polysiphonia lanosa* (Red), *Ulva lactuca* (Green), *Fucus vesiculosus* (Brown) and a seaweed waste product derived from *Ascophyllum nodosum* (referred to as WAP).

### **1.2.1 *Polysiphonia lanosa***

#### **1.2.1.1 Origin and phylogeny**

*Polysiphonia lanosa* is a Rhodophyte (red seaweed), and is found growing mostly on the Phaeophyte *Ascophyllum nodosum* (Fig. 1.2) and more rarely on other fucoids, such as *Fucus vesiculosus*, in the form of small tufts. The red colour is due to the pigment phycobilin, masking the green colour of chlorophyll. Production of a red pigment is an adaptative strategy to absorb the green and blue-green light in deeper sea waters. *P. lanosa* is found growing on rocks from the mid-shore to at least 27 m depth and many species are abundant in rock pools (Parmentier, 1999).

- Kingdom: *Protista*
- Phylum: *Rhodophycota*
- Class: *Florideophyceae*
- Order: *Ceramiales*
- Family: *Rhodomelaceae*
- Genus: *Polysiphonia*
- Species: *P. lanosa*

### 1.2.1.2 Geographical distribution



*Polysiphonia lanosa* is found associated with *Ascophyllum nodosum* as an epiphyte and is relatively common on the mid-littoral rocky shores all over Ireland and Britain. Species are also found from Europe to Asia, Australia to New Zealand and is widely spread from North America to South America. The species is also found in the Pacific Ocean, South Africa, Greenland and Antarctica.

Fig. 1.1 Geographical distribution of *Polysiphonia lanosa* about the United-Kingdom and Ireland (MarLIN, 2008a).

### 1.2.1.3 Morphology



Fig. 1.2 *Polysiphonia lanosa* as an epiphyte of *Ascophyllum nodosum* (Algaebase, 2008b).

## 1.2.2 *Ulva lactuca*

### 1.2.2.1 Origin and phylogeny

*Ulva lactuca*, also commonly known as Sea lettuce (Fig. 1.4), is part of a small genus found in marine and brackish water.

- Kingdom: *Plantae*
- Phylum: *Chlorophyta*
- Class: *Ulvophyceae*
- Order: *Ulvales*
- Family: *Ulvaceae*
- Genus: *Ulva*
- Species: *U. lactuca*

### 1.2.2.2 Geographical distribution



*Ulva lactuca* is very common along Irish shores all year around. *Ulva* species may be heavily dense in areas such as quiet bays and salt marshes. The shape is quite variable; plants may be circular, quite narrow or elongated (Lee, 1977).

Fig. 1.3 Geographical distribution of *Ulva lactuca* about Ireland and the United-Kingdom Note: recorded (dark blue)/expected (light blue) (MarLIN, 2008b).

### 1.2.2.3 Morphology



Fig. 1.4 *Ulva lactuca* (MarLIN, 2008b).

### 1.2.3 *Fucus vesiculosus*

#### 1.2.3.1 Origin and phylogeny

*Fucus* is a small genus of macroscopic marine seaweeds. *Fucus vesiculosus*, commonly known as “bladder wrack”, is found mainly on rocky shores in a wide range of locations. It is also common on the mid-shore, often associated with *Ascophyllum nodosum*.

- Kingdom: *Protista*
- Phylum: *Phaeophyta*
- Class: *Phaeophyceae*
- Order: *Fucales*
- Family: *Fucaceae*
- Genus: *Fucus*
- Species: *F. vesiculosus*

#### 1.2.3.2 Geographical distribution



*Fucus vesiculosus* is found in the Baltic Sea, Faroes, Norway (including Spitsbergen), Sweden, Britain, Ireland, the Atlantic coast of France, Spain and Morocco, Madeira, the Azores, Portugal, the North Sea coast of Denmark, Germany, the Netherlands and Belgium and along the eastern shores of United States and Canada (MarLIN, 2008c).

Fig. 1.5 Geographical distribution of *Fucus vesiculosus* about Ireland and the United Kingdom. Note: recorded (dark blue)/expected (light blue) (MarLIN, 2008c).

### 1.2.3.3 Morphology

The plant morphology (Fig. 1.6) can vary according to local conditions.



Fig. 1.6 *Fucus vesiculosus* (Algaebase, 2008a).

The plants consist of a flattened, dichotomously-branched thallus which has a small stipe and a holdfast. The blade usually has a locally-thickened area which is centrally placed and which is called a midrib. Air bladders are frequently present and these help to keep the seaweed afloat when submerged (Guiry, 2008).

### 1.2.4 Waste *Ascophyllum* Product (WAP)

A seaweed waste product, resulting from the industrial processing of *Ascophyllum nodosum* (referred to as Waste *Ascophyllum* Product or WAP), was also selected for investigation. WAP was supplied by Oilean Glas Teo (OGT) (Ballymoon Industrial Estate, Kilcar, Co. Donegal, Ireland). OGT uses *Ascophyllum nodosum* for the manufacture of a liquid extract used as a natural fertiliser and pesticide in agriculture and horticulture. It can also be used as a basis for cosmetics and Thallasso therapies. The *Ascophyllum nodosum* was harvested from Kilcar, Co. Donegal by OGT. Polysaccharides, polyphenols, plant hormones, vitamins and proteins are removed by

grinding and cold extraction procedures (no steps higher than 30°C) (Fig. 1.7). The waste is mainly composed of cellulose and alginate and has the appearance of a thick paste containing 89% water.

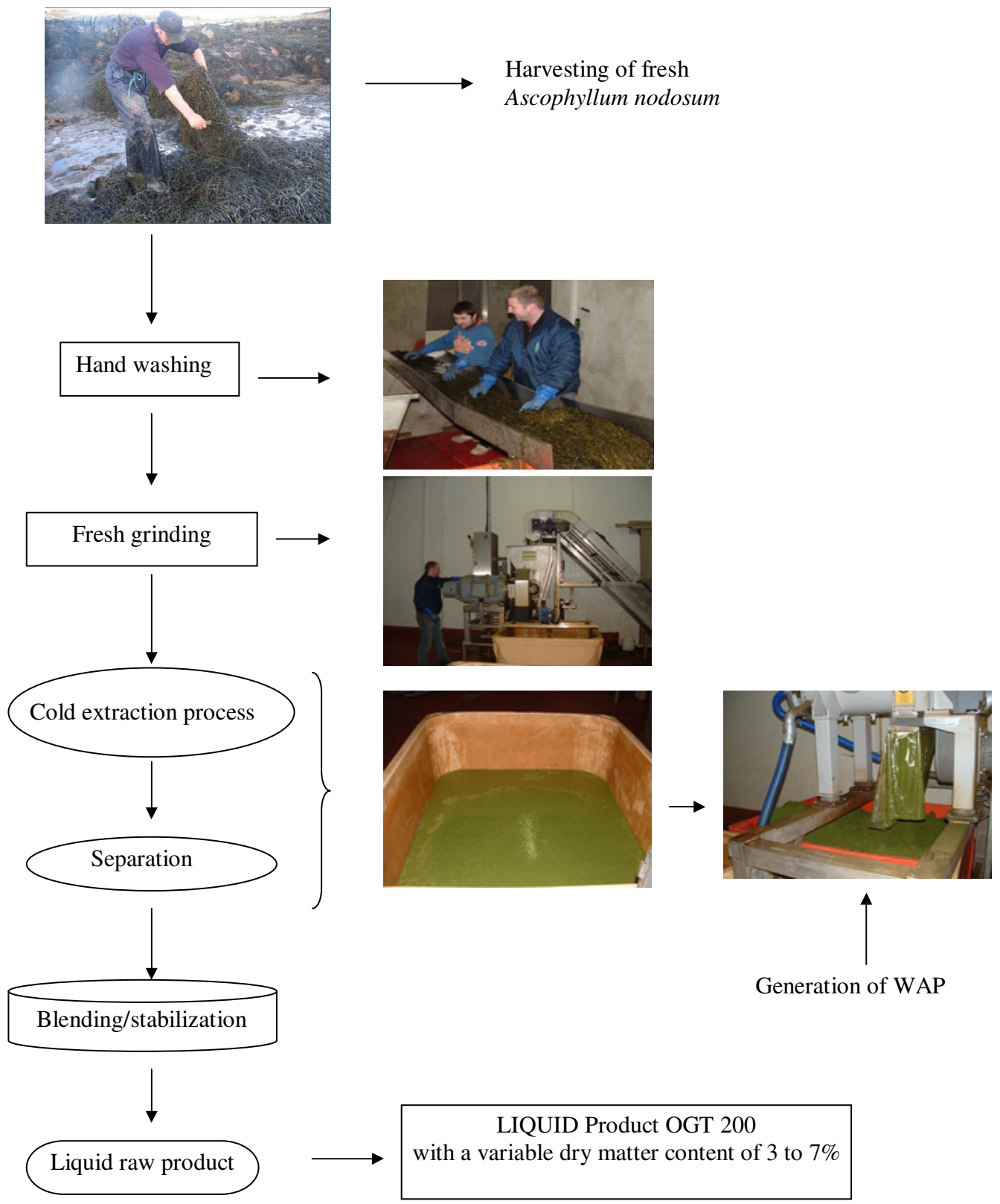


Fig. 1.7 Processing of *Ascophyllum nodosum* and WAP production (Oilean Glas Teo, 2008).

## 1.3 Heavy metals

### 1.3.1 Sources of heavy metal pollution

Metals with high atomic weight, known as heavy metals, have a wide spectrum of industrial uses.

The Water Quality (Dangerous substances) Regulations (S.I. No. 12 of 2001) (Clenaghan et al., 2005) was introduced to implement the Council Directive 76/464/EEC on pollution caused by a list of dangerous substances discharged into the aquatic environment and to ensure the compliance to the Water Framework Directive (2000/60/EC).

The directive specifies water quality standards for a list of substances including certain metals as shown in Table 1.1.

Table 1.1 Standards for metals (dissolved and colloidal/suspended solids) (Clenaghan et al., 2005).

Metal	Standard ( $\mu\text{g/L}$ ) for Fresh Waters		Standard ( $\mu\text{g/L}$ ) for Tidal Waters
	Hardness of water measured in $\text{mg/L CaCO}_3$		
	$\leq 100$	$\geq 100$	
Copper	5	30	5
Chromium	5	30	15
Lead	5	10	5
Nickel	8	50	25
Zinc	*	100	40

\* in the case of Zinc, the standard is  $8 \mu\text{g/L}$  for water hardness less than or equal to  $10 \text{ mg/L CaCO}_3$  or  $50 \mu\text{g/L}$  for water hardness greater than  $10 \text{ mg/L CaCO}_3$  and less than or equal to  $100 \text{ mg/L CaCO}_3$ .

### 1.3.2 Metals investigated during this study

For this study, four different metals were selected: Zinc (Zn(II)), Nickel ((Ni(II)), Aluminium (Al(III)) and Antimony (Sb(III)). Zn(II), Ni(II) and Al(III) are metals of environmental importance (Table 1.2) and are included in the 2005 Irish EPA dangerous substances national implementation report (Clenaghan et al., 2005).

Table 1.2 Ranking of metal interest priorities (Volesky, 2001b)

Relative priority	Environmental risk	Combined factors
High	Cd	Cd
	Pb	Pb
	Hg	Hg
	-	<b>Zn</b>
Medium	-	<b>Zn</b>
	Cr	-
	Co	Co
	Cu	Cu
	<b>Ni</b>	<b>Ni</b>
	<b>Zn</b>	<b>Ni</b>
	<b>Al</b>	<b>Al</b>
	-	Cr
Fe	Fe	

#### 1.3.2.1 Antimony

Antimony (Sb) is a silvery-white metal found in the earth's crust. Stibnite ( $Sb_2S_3$ ) is the most important ore of antimony. Other sulphide ores include ullmanite (NiSbS), livingstonite ( $HgSb_4S_8$ ), tetrahedrite ( $Cu_3SbS_3$ ), wolfsbergite ( $CuSbS_2$ ) and jamesonite ( $FePb_4Sb_6S_{14}$ ) (Greenwood and Earnshaw, 1994).

### *Application*

The most important use of antimony metal is as a hardener in lead for storage batteries. The metal also finds applications in solders and other alloys. Antimony trioxide is the most important of the antimony compounds and is primarily used in flame-retardant formulations. These flame-retardant properties are utilized in such sectors as children's clothing, toys, aircraft and automobile seat covers.

### *Antimony toxicity*

Industrial and terrestrial activities are the main source of antimony in the human environment. Sb toxicity depends on its oxidation state in compounds, with the trivalent compounds more toxic than the pentavalent compounds (Hou and Narasaki, 1998). Exposure to high levels of Sb can result in a variety of adverse health effects. For example, the breathing of high levels of Sb, for a long time, can irritate eyes and lungs and can cause heart and lung problems, stomach pain, diarrhoea, vomiting, and stomach ulcers. Sb can also irritate the skin on prolonged contact (Department of the Environment and Water Resources, 2008).

### **1.3.2.2 Zinc**

Zinc (Zn) is a silvery solid with a bluish lustre when freshly formed. Zinc is one of the most important metals in terms of biological requirements and is necessary to all forms of life. It is also the second most common trace metal, after iron, naturally found in the human body.

The major ores of Zn are ZnS and ZnCO<sub>3</sub>. Less important ores include hemimorphite [Zn<sub>4</sub>Si<sub>2</sub>O<sub>7</sub>(OH)<sub>2</sub>·H<sub>2</sub>O] and franklinite (Zn,Fe)O·Fe<sub>2</sub>O<sub>3</sub> (Greenwood and Earnshaw, 1994).

### *Application*

Zinc uses range from metal products to rubber and medicines. About three-quarters of the amount of zinc used is utilised as a coating to protect iron and steel from corrosion (galvanised metal), as an alloying metal to make bronze and brass, as zinc-based die casting alloy, or as rolled zinc. The remaining one-fourth is used as zinc compounds mainly by the rubber, chemical, paint, and agricultural industries (US Geological Surveys, 2008).

### *Zinc toxicity*

Zn is an essential trace element that is required in both humans and animals for a variety of physiological functions including immune and antioxidant function, growth and reproduction (Shay and Mangian, 2000). Zn has been shown to interfere with the utilisation of other nutrients, particularly copper, to impair immune functions and to adversely affect lipoprotein profiles (Fosmire, 2008). In aquatic systems,  $[\text{Zn}(\text{H}_2\text{O})_6]^{2+}$  is the predominant form. Aquatic systems are at risk downstream of industry, landfills, contaminated lands, ports, urban stormwater overflows and runoff, and waste water treatment plants (Clenaghan et al., 2005).

### **1.3.2.3 Aluminium**

Aluminium is a silvery-white, ductile and malleable metal. It is highly concentrated in soil-derived dusts from such activities as mining and agriculture, and in particulate matter from coal combustion. It occurs ubiquitously in the environment in the form of silicates, oxides and hydroxides, combined with other elements such as sodium and fluorine and as complexes with organic matter (Birchall and Chappel, 1998). It is not found as free metal because of its reactivity. Natural processes far outweigh direct anthropogenic contributions to the environment. Furthermore, mobilisation of aluminium through human actions is mostly direct and occurs as a result of emission of acidifying substances (United nations Environmental Programme, 1997a).

Large world-wide consumption, more than 22 million tonnes in 1986, has led to increased discharge into the environment (Duffield and Williams, 1998). More recent figures, published by the International Aluminium Institute website (2005), estimated the 2006 global aluminium production to be 60.4 million tonnes, including 34 million tonnes primary metal and 16.4 million tonnes recycled metal. Primary aluminium production for different geographical areas is shown in Table 1.3.

Table 1.3 Reported primary aluminium production in the world for the period 2003-2007 (International Aluminium Institute, 2008)

Period		Reported Primary Aluminium Production							
		(Thousands of Metric Tons)							
		Area 1:	Area 2:	Area 3:	Area 4/5:	Area 6A:	Area 6B:	Area 7:	Total
		Africa	North America	Latin America	Asia	West Europe	East/Central Europe	Oceania	
Year	2003	1,428	5,495	2,275	2,475	4,068	3,996	2,198	21,935
Year	2004	1,711	5,110	2,356	2,735	4,295	4,139	2,246	22,592
Year	2005	1,753	5,382	2,391	3,139	4,352	4,194	2,252	23,463
Year	2006	1,864	5,333	2,493	3,493	4,182	4,230	2,274	23,869
Jan-Oct	2007	1,511	4,672	2,122	3,083	3,556	3,691	1,928	20,563

The different areas are divided as following:

Area 1: Africa: Cameron, Mozambique, Nigeria, South-Africa

Area 2: North America: Canada, United States of America

Area 3: Latin America: Argentina, Brazil, Mexico, Suriname, Venezuela

Area 4: East Asia: China, Japan, North Mexico, South Korea, Tadjikistan

Area 5: South Asia: Azerbaijan, Bahrain, India, Indonesia, Iran, Turkey, United Arab Emirates

Area 6a: West Europe: France, Germany, Iceland, Italy, Netherlands, Norway, Spain, Sweden, Switzerland, United Kingdom

Area 6b: East/Central Europe: Bosnia and Herzegovina, Croatia, Hungary, Poland, Romania, Russian Federation, Serbia and Montenegro

Area 7: Oceania: Australia, New-Zealand

### *Application*

As shown in Table 1.3, primary aluminium production increased through to 2006. Increased production results from the fact that aluminium metal has a wide variety of uses, including as structural materials in construction, automobiles and aircraft, and in the production of metal alloys. Aluminium compounds and materials also have a wide variety of uses, including the production of glass, ceramics, rubber, wood preservatives, pharmaceuticals and waterproofing textiles. Natural aluminium minerals, especially bentonite and zeolite, are used in water purification, sugar refining, brewing and paper industries (United Nations Environmental Programme, 1997b).

### *Aluminium toxicity*

In animals and humans, toxicity from aluminium is generally due to a slow accumulation and was believed to be linked with senile dementia and Alzheimer disease (Lewis, 1990). However, a direct causal role for aluminium has not been demonstrated (Campbell, 2002). Aluminium has been shown to accumulate in freshwater organisms which can lead to fish contamination that can later be consumed by humans (Alexopoulos et al., 2004).

#### **1.3.2.4 Nickel**

In industry, two nickel ores are of commercial interest (Greenwood and Earnshaw, 1994):

- Laterites, referring to oxide/silicate ores such as garnierite,  $(\text{Ni,Mg})_6\text{Si}_4\text{O}_{10}(\text{OH})_8$ , and nickeliferous limonite,  $(\text{Fe,Ni})\text{O}(\text{OH}) \cdot n\text{H}_2\text{O}$ .
- Sulfides, such as pentlandite,  $(\text{Ni,Fe})_9\text{S}_8$ , associated with copper, cobalt and precious metals forming ores containing typically 1 ½% Ni.

### *Application*

Anthropogenic sources of nickel in the environment result from diverse industrial processes, including (Clenaghan et al., 2005):

- Electroplating waste;
- Manufacturing of alloys;
- Landfill sites;
- Protective and ornamental coating for metals;
- Nickel steel is used in automobile parts such as axles, crankshafts, gears, valves and rods, in machine parts and in armour plate;
- Nickel-containing alloys such as German silver, Invar, Monel metal, Nichrome and Permalloy;
- Scrap yards;
- Nickel-cadmium batteries.

### *Nickel toxicity in the environment*

Nickel has been classified as a dangerous substance, according to the 2005 Irish EPA report “Dangerous substances regulations, National Implementation Report” (Clenaghan et al., 2005). Waters at risk include those downstream of industry, contaminated lands, ports, landfills, urban stormwater overflows and runoff and waste water treatment plants.

Nickel has been also classified as a possible carcinogen (Group 2B) by the International Agency for Research on Cancer (IARC, 2009). Nickel is also toxic to plants and has been shown to be hazardous to fish (Clenaghan et al., 2005).

## **1.4 Biosorption of metals by seaweed biomass**

### **1.4.1 Seaweed cell wall components and biomolecules involved in metal binding**

The main biomolecules present in seaweeds include cellulose, agar, alginic acid (alginate), carrageenan and fucoidan. The amount of each present is variable, depending on seaweed divisions and species (Davis et al., 2003).

#### **1.4.1.1 Seaweed cell wall**

The structure of the cell wall is an important feature in metal binding as most trace elements enter biological systems through the cell wall (Ray et al., 1981). The seaweed cell wall is composed of a multilayered microfibrillar framework, usually consisting of cellulose interspersed with amorphous material (Fig. 1.8). Silica or carbonate often encrusts the cell wall (Volesky, 1990). Amino, carboxyl groups, and sulfate can be provided by the polysaccharides of the cell wall. The amino and carboxyl groups, the imidazole of histidine, and the nitrogen and oxygen of the peptide bond can be available for metal binding through coordination. Furthermore, such bond formation can be coupled by displacement of protons, dependent in part on the extent of protonation, as determined by the pH. Electrostatic binding of metallic ions can also occur with unprotonated carboxyl oxygen and sulphate (Ray et al., 1981). Consequently, the cell wall can be regarded as a complex ion exchanger similar to commercial resin (Volesky, 1990).

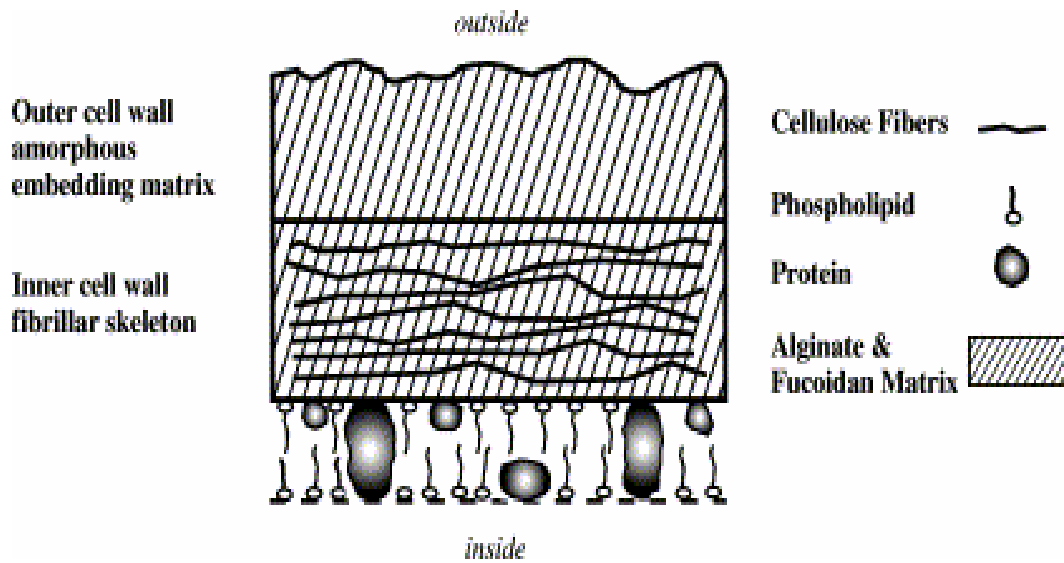


Fig. 1.8 Cell wall of brown algae (Davis et al., 2003).

The cell walls of brown seaweeds are composed of two key constituents, cellulose and alginic acid. Alginate (Fig. 1.11) is an important component of the cell wall of the brown seaweeds, and constitutes between 10% and 40% of their dried weight. Their composition varies according to the season and to the depth at which the algae are developing (Andresen et al., 1977; Davis et al., 2003). In the same way as cellulose in terrestrial plants, the biological function of alginate is to give the plant both mechanical strength and flexibility (Andresen et al., 1977).

## Cellulose

Cellulose is the most abundant component in plants. It is a polymer composed of  $\beta$ -1,4-D glucose (Fig. 1.9). As cellulose only contains hydroxyl groups that become charged at  $\text{pH} > 10$ , at lower pH they show negligible metal sorption (Volesky, 2004).

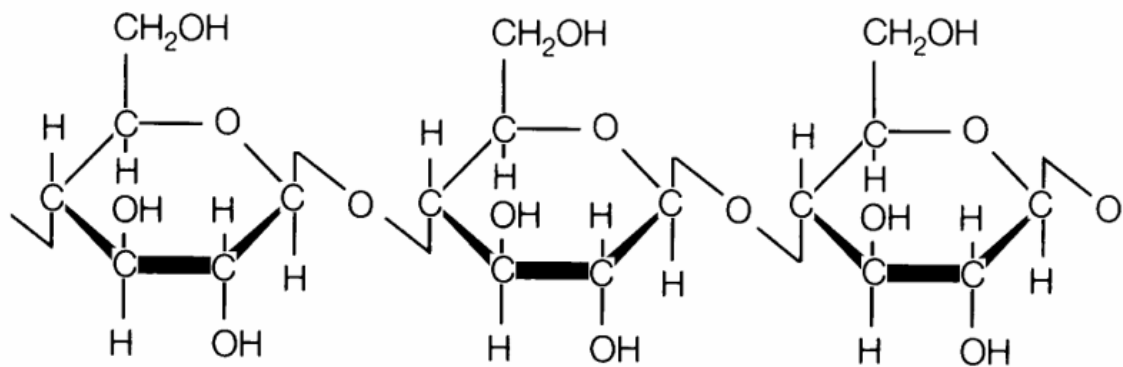


Fig. 1.9 Structure of cellulose (Cybercolloids, 2004).

### Agar

Agar is a sulphated polysaccharide (SPS) that can occur both in the cell wall and the intracellular region of the agarophytes including *Gelidium*, *Gracilaria*, *Acanthopeltis*, *Ahnfeltia*, *Ceranium*, *Campylaephora*, *Phyllophora* and *Pterocladia* (Volesky, 2004). It is comprised of two types of polysaccharides, agarose and agaropectin (Fig. 1.10).

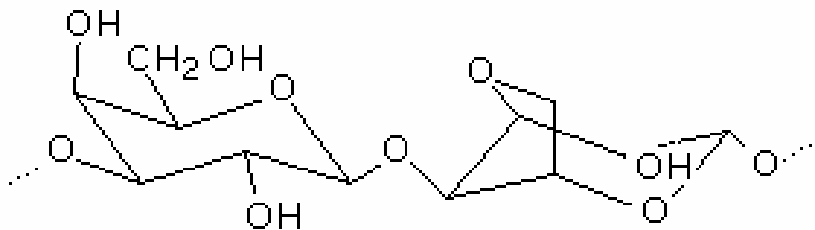


Fig.1.10 Basic molecular structure of agar (Cybercolloids, 2004).

## Alginic acid (alginate)

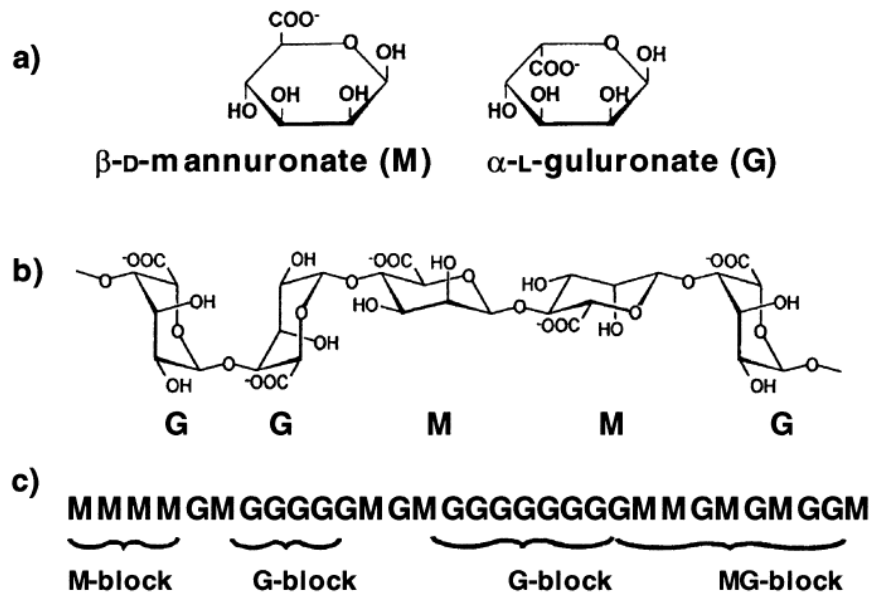


Fig. 1.11 Structural characteristics of alginates (a) alginate monomers, (b) chain conformation, (c) block distribution (Draget et al., 2005).

Fig. 1.11 shows that M- and G- sequences vary in their constitution and it is the proportion that determinates the physical properties and reactivity of the alginate (Haug et al., 1967; Davis et al., 2003)

Alginate can be used as an immobilising agent due to its gelling properties. Indeed, alginate is capable of the selective binding of multivalent cations and is the basis for gel formation. In industry, alginates are found in a wide spectrum of applications including the textile and pharmaceutical industries. Commercial alginates are mainly extracted and produced from *Laminaria digitata*, *Macrocystis pyrifera*, *Ascophyllum nodosum*, *Laminaria japonica*, *Ecklonia maxima*, *Lessonia nigrescens*, *Durvillea Antarctica* and *Sargassum* sp. (Draget et al., 2005).

## Carrageenan

Carrageenan is found in *Chondrus*, *Gigartina*, *Furcellaria*, *Euchema*, *Hypnea*, *Iridaea* and *Polyides* (Volesky, 2004). There are a variety of carrageenans, differing in their chemical structure and properties (Fig. 1.12).

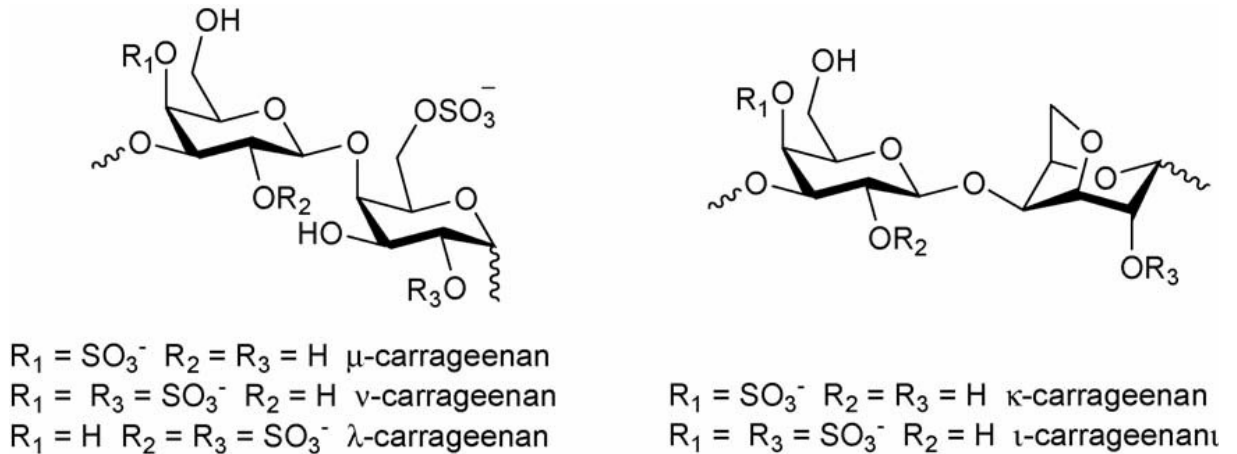


Fig. 1.12 Schematic representation of carrageenan monomers (Hilliou et al., 2006)

The carrageenans of commercial interest are called iota, kappa and lambda. However, it is known that kappa- and lambda-carrageenan do not occur together in the same plant, but are elaborated at different stages of the reproductive cycle. Indeed, kappa-carrageenan occurs in the haploid gametophytes and lambda in the diploid tetrasporophytes (Chen et al., 1973; Stanley, 2006). Different carrageenan-types possess the following properties (Stanley, 2006):

- **Kappa and Iota:** strong, rigid gel, formed with potassium salts. Brittle gel forms with calcium salts. Slightly opaque gel becomes clear with sugar addition.
- **Lambda:** No gel formation, forms high viscous solutions.

Most of the commercial carrageenan is extracted from commercial seaweed species including, *Kappaphycus alvarezzi* and *Euchema denticulum*.

## Fucoidan

Fucoidan is an extracellular sulphated polysaccharide of brown macroalgae (Fig. 1.13). It is a branched polysaccharide sulfate ester with 1-fucose 4-sulfate building blocks as the major component (Davis et al., 2003).

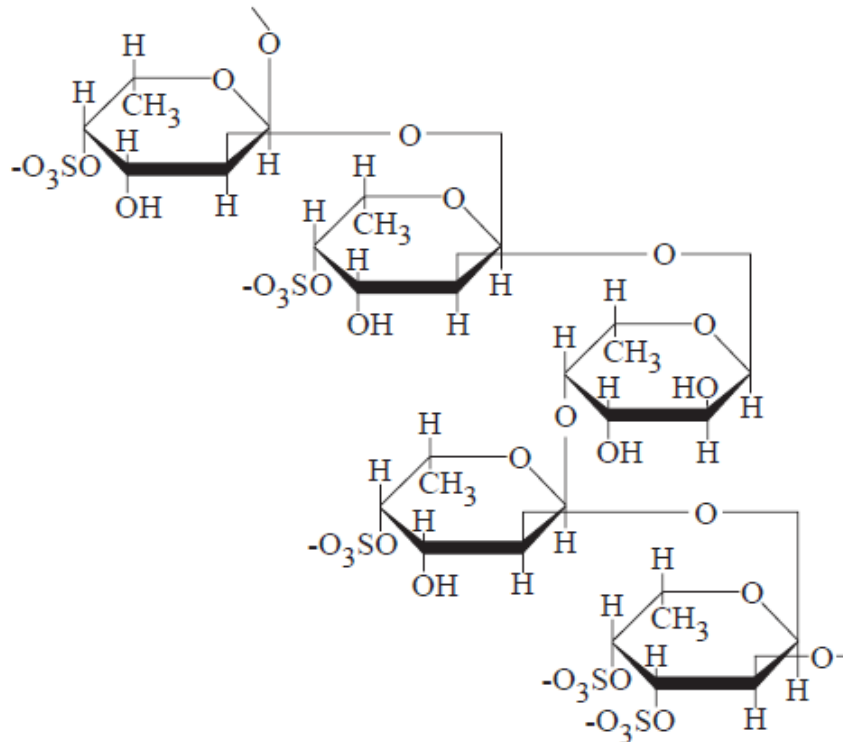


Fig. 1.13 Schematic representation of fucoidan (Davis et al., 2003).

### 1.4.2 Mechanisms of biosorption

Biosorption can be defined as the passive sequestering of metal ions by metabolic inactive biomass (Volesky, 2004). Several mechanisms exist in metal-binding by macro-algal biomass, probably acting simultaneously, including:

- Physical adsorption
- Chemisorption:
  - complexation
  - coordination

- chelation
- ion exchange

#### 1.4.2.1 Physical adsorption

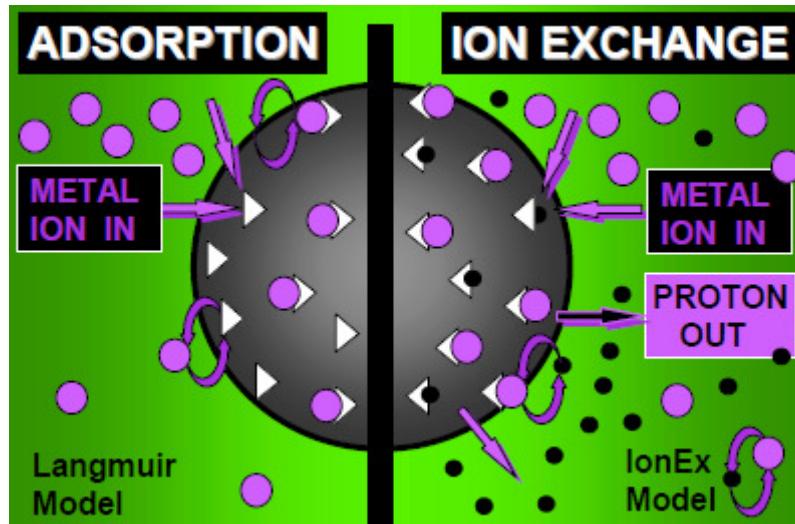


Fig. 1.14 Schematic representation of adsorption and ion exchange (Volesky, 2004).

#### *Adsorption*

Adsorption is the process by which molecules adhere to solid surfaces (Volesky, 2004). Metallic cations are attracted to negatively charged sites at the surface of the cell. The list of anionic ligands involved in the metal binding mechanism includes phosphoryl, carboxyl, sulfhydryl and hydroxyl groups of the membrane proteins (Volesky, 1990). However, different parts of the seaweed can show varying biosorbent abilities (Nigro et al., 2002).

#### 1.4.2.2 Chemisorption

#### *Complexation*

Complexation is a term used to describe the mechanism resulting in the production of molecules or compounds formed by the combination of ligands and metal ions. For

example, in algae, phytochelatins are the main metal binding peptides produced enzymatically in response to many metals (Ahner et al., 1995; Pawlik-Skowronska, 2001).

### *Coordination*

In coordination compounds, metals are surrounded by groups known as ligands (Cotton et al., 1995). The central metal atom is bound to its immediate neighbours by covalent bonds formed as the result of the metal atom accepting an electron pair from each non-metal atom, the latter is known as the donor and the former as the acceptor atom (Volesky, 2004).

### *Chelation*

Chelation is the binding or complexation of a bi- or multidentate ligand. Thus, metal chelates are metal complexes where there is an organic compound bound to the metal by at least two available sites (Volesky, 2004).

### *Ion exchange*

Ion exchange is the predominant mechanism in metal biosorption. It can be defined as the reversible interchange of ions between a solid phase (the ion exchanger) and a solution phase, the ion exchanger being insoluble in the medium in which the exchange mechanism is carried out (Harland, 1994). Studies have showed that ion exchange is the main mechanism in metal binding by inactive algal biomass (Crist et al., 1990; Crist et al., 1994; Davis et al., 2000).

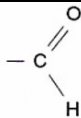
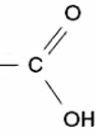
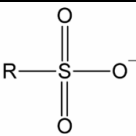
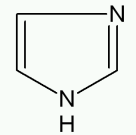
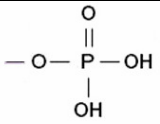
### **1.4.2.3 Factors influencing biosorption**

#### *Binding sites*

Several functional groups were shown to be involved in metal binding by algal biomass, including carboxyl, hydroxyl and sulfhydryl groups (Table 1.4) (Fourest et al., 1996; Fourest and Volesky, 1996; Davis et al., 2003). The involvement of the functional groups in metal binding depends on various factors (Volesky, 2004):

- quantity of sites in the biosorbent material
- accessibility of the sites
- chemical state of the site
- affinity between site and metal

Table 1.4 Binding groups for metal biosorption (Volesky, 2004).

Binding group	Structural formula	Acid dissociation constant (pKa)	HSAB classification	Ligand atom	Occurrence in selected biomolecules
Hydroxyl	-OH	9.5-13	hard	O	PS, UA, SPS, AA
Carbonyl (ketone)		-	hard	O	Peptide bond
Carboxyl		1.7-4.7	hard	O	UA, AA
Sulfhydryl (thiol)	-SH	8.3-10.8	soft	S	AA
Sulphonate		1.3	hard	O	SPS
Thioether	>S	-	soft	S	AA
Amine	-NH <sub>2</sub>	8-11	intermed.	N	Cto, AA
Secondary amine	>NH	13	intermed.	N	PG, peptide bond
Amide		-	intermed.	N	AA
Imine	=NH	11.6-12.6	intermed.	N	AA
Imidazole		6.0	soft	N	AA
phosphonate		0.9-2.1 6.1-6.8	hard	O	PL

HSAB=hard soft acid base classifications; PS=polysaccharides; UA=uronic acids; SPS=sulfated PS; Cto=chitosan; PG=peptidoglycan; AA=amino acids; TA=teichoic acid; PL=phospholipids; LPS=lipoPS

### *Influence of pH*

Metal biosorption by specific seaweed species has been found to be highly pH-dependent (Volesky, 1990). Indeed, pH can affect biosorption not only by influencing the chemical state of the binding sites on the surface of the biomass and speciation/solubility of the metal in solution but also by affecting the integrity of the biosorbent.

### *Effect of temperature*

A change in temperature will influence a series of factors, occurring individually or simultaneously, affecting biosorption (Volesky, 1990). These factors include:

- the stability of the metal ion species present in the initial metal bearing solution
- the presence of competing ligands
- the stability the complex between the seaweed and the metal (depending on the biosorption sites)
- the change in algal cell wall configuration
- the ionisation of chemical moieties on the cell wall

Volesky (2004) reported that the binding of Co by the brown algae *Ascophyllum nodosum* increased by 50-70% when the temperature was raised from 4 to 23°C. Also extreme temperatures, such as 60°C, caused a loss in the sorption capacity due to deterioration of the sorbent material.

### *Effect of ion competition*

The presence of competing ions can also interfere in the efficiency of metal uptake by a biosorbent. According to Volesky (1990), assuming temperature is held constant, the pH is the predominant factor influencing metal binding, followed by the presence of competing ions. A good example of such competition can be found in the work of Sag & Kutsal (1998), with the simultaneous biosorption of Cr(VI), Fe(III) and Cu(II) on the fungus *Rhizopus arrhizus* (Sag and Kutsal, 1998). This study showed different sorption rates depending on the particular metal elements present in a same aqueous solution.

Indeed, the inhibitory effects of Cu(II) ions on the competitive biosorption of Cr(VI) ions were higher than those of Fe(III) ions.

## **1.5 Heavy metal removal processes**

### **1.5.1 Ion exchange**

Ion exchangers can be defined as insoluble solid materials (e.g. resins) which carry exchangeable cations or anions. These ions can be exchanged for a stoichiometrically equivalent amount of other ions of the same charge when the ion exchanger is in contact with an electrolyte solution (Helfferich, 1995). Such ion exchange resins are commercially available and can be regenerated repeatedly using calcium chloride or by acidic treatments. However, such systems are expensive to install and operate (Brower et al., 1997).

### **1.5.2 Precipitation/flocculation**

Precipitation has long been the main method of treating metal-laden industrial wastewater. Metal precipitation from contaminated water involves the conversion of soluble heavy metal salts to insoluble salts that will precipitate out. The precipitate can then be removed from the treated wastewater by physical methods such as settling or filtration (Naja and Volesky, 2006a). Precipitation is usually achieved by adjusting the pH or by flocculation, relying on the addition of a chemical precipitant such as calcium chloride (lime), potassium or sodium hydroxide. More environmental-friendly flocculating agents have been developed recently such as chitosan (Renault et al., 2008). However, this metal removal process presents several limitations as listed below (Naja and Volesky, 2006a):

- the addition of the precipitant must be carefully controlled to avoid any excess concentrations in the effluent
- the process may generate toxic sludge requiring a specific disposal
- the process may be costly depending on the type of precipitant used
- a polymer may be needed to achieve adequate settling of solids

- the efficacy of the system highly depends on adequate solids separation techniques e.g. filtration

The high operating cost and the negative environmental impact of the flocculation process has led researchers to investigate novel, environmental friendly methods to remove metals from industrial wastewaters.

### **1.5.3 Other processes**

Other, less frequently used, methods include activated carbon adsorption, electro dialysis and reverse osmosis. However, these techniques are often ineffective or very expensive when used to remove heavy metal ions at very low concentrations (Olguin et al., 2000). As a result, new low-cost technologies are required to reduce metal concentrations to environmentally acceptable levels. Biosorption has been widely researched over the last decade due to its efficacy, sustainability and low operation costs and was found to outperform conventional metal processes in several cases (Brower et al., 1997; Volesky, 2004). There are three basic types of sorption systems (Volesky, 2004):

- the fixed bed or packed-bed column
- the fluidised-bed system
- the completely mixed system

#### **1.5.3.1 The fixed bed sorption system**

The immobilised sorbent is tightly packed into a column where a metal-bearing feed is fed through and dissolved metal ions are gradually removed from the solution (Fig. 1.15). As the sorbent becomes saturated with the metal, the column can be regenerated using a desorbing solution (e.g. any acid or alkali), leading to the release of the metal ions in solution. The metal can then be recycled and reused.

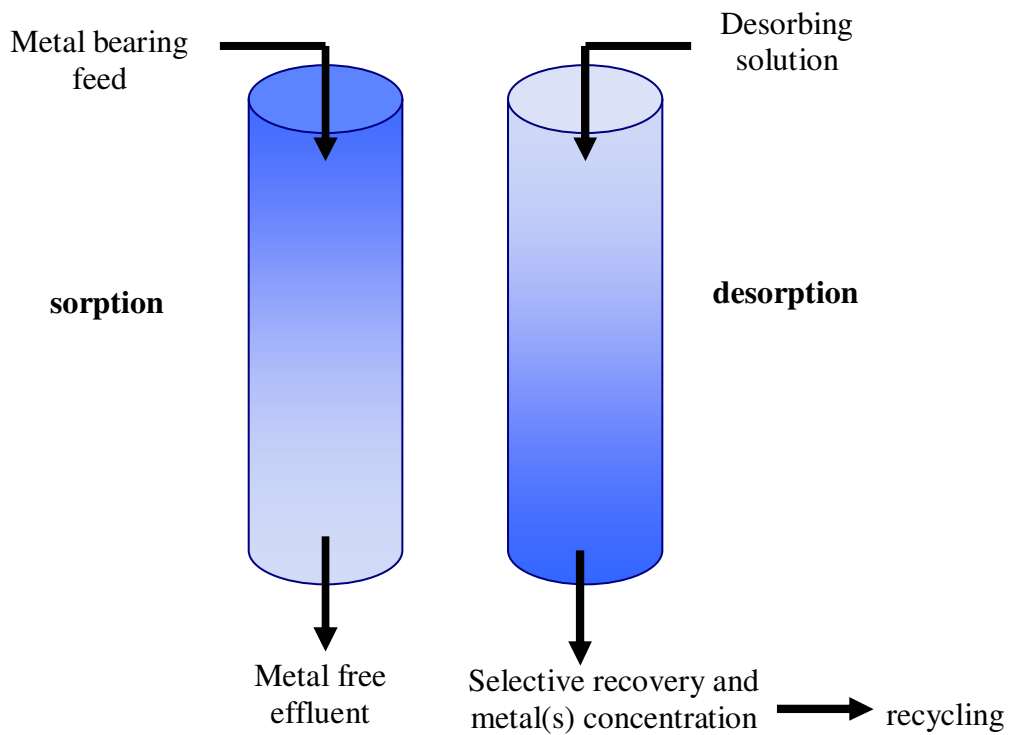


Fig. 1.15 Fixed bed column sorption system principle (biosorption and desorption).

### 1.5.3.2 The fluidised bed column sorption system

The particles of biosorbents are fluidised in the column bed by upward flowing liquid (Fig. 1.16). The main advantage of this design is that the metal bearing feed does not need to be particle-free, as in the case of the fixed-bed column, and so could act as a filter for suspended particles. The main disadvantage is that power is required for fluidisation (Volesky, 2004).

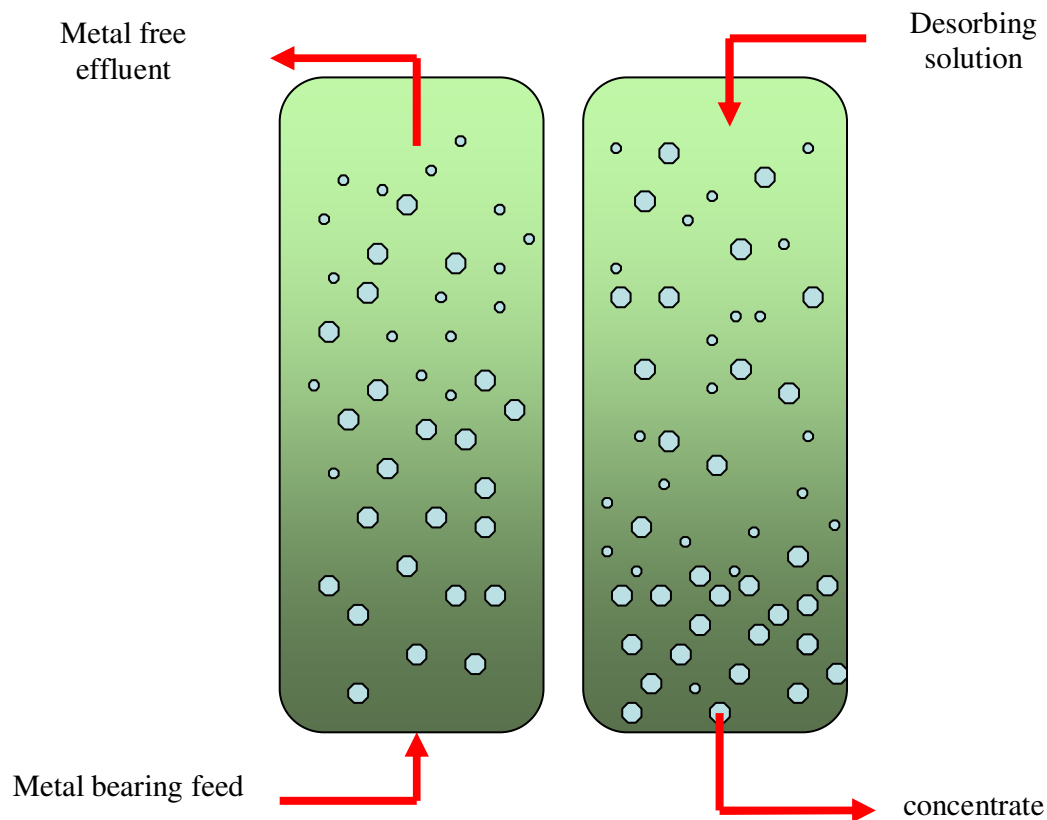


Fig. 1.16 Fluidised bed biosorption system.

### 1.5.3.3 The completely mixed sorption system

This type of sorption system (Fig. 1.17) may be useful if working with the following conditions (Volesky, 2004):

- the effluent concentration is not of concern
- the biosorbent is in a powder form
- there is a solid/liquid separation step (e.g. filtration)

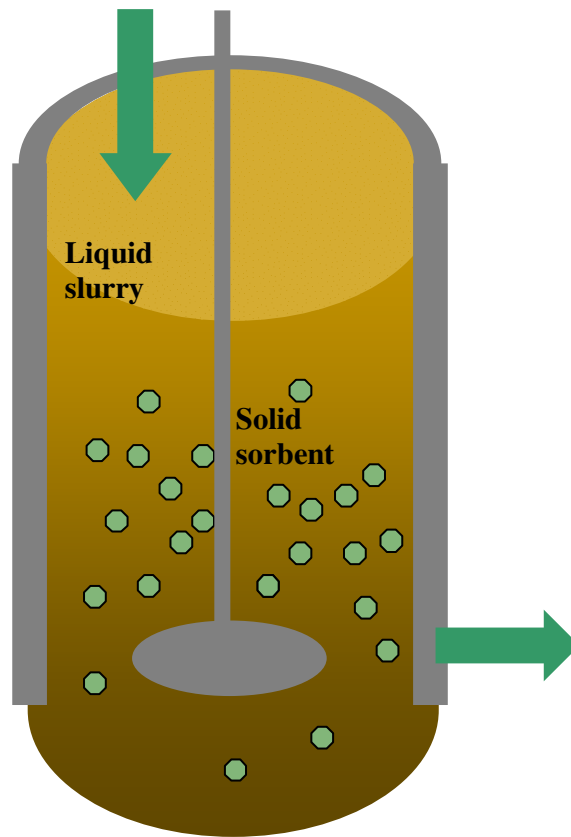


Fig. 1.17 Mixed sorption system

#### **1.5.4 Current heavy metal removal processes using biosorption**

##### **1.5.4.1 AlgaSORB© Biological Sorption**

The AlgaSORB© sorption process technology, produced by Bio-recovery Systems Inc., is based on the use of seaweeds to remove heavy metal ions from aqueous solutions (Wase and Forster, 1997). The portable effluent treatment equipment (PETE) unit, (Fig. 1.18), consists of two columns operating either in series or in parallel (Darnall and Hosea, 1990).

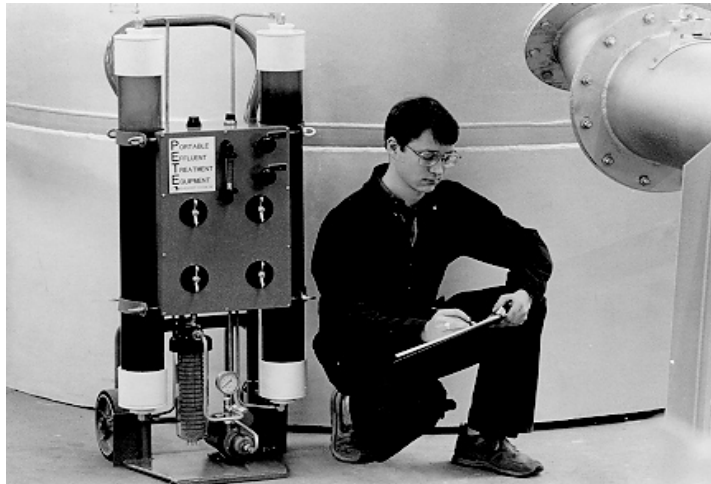


Fig. 1.18 AlgaSorb©, portable effluent treatment equipment (PETE) unit (Darnall and Hosea, 1990)

This AlgaSorb© technology is based on a seaweed ion-exchange resin to bind both metallic cations and metallic oxoanions. Anions such as chlorides or sulfates are only weakly bound or not bound at all. Divalent cations, typical of hard water, such as calcium ( $\text{Ca}^{2+}$ ) and magnesium ( $\text{Mg}^{2+}$ ), or monovalent cations, such as sodium ( $\text{Na}^+$ ) and potassium ( $\text{K}^+$ ), do not significantly interfere with the binding of toxic heavy metal ions to the algae-silica matrix (United States Environmental Protection Agency, 2008). AlgaSorb© has been shown to be efficient in the removal of a wide spectrum of metals from effluents, including aluminium, cadmium, chromium, cobalt, copper, gold, iron, lead, manganese, mercury, molybdenum, nickel, platinum, selenium, silver, uranium, vanadium, and zinc (Darnall and Hosea, 1990).

The main advantage of the AlgaSorb© technology is the regenerative properties of the biomass, which can be re-used for further sorption cycles. Regeneration can be accomplished using acids, alkaline solutions or other suitable reagents.

#### **1.5.4.2 Bio-fix**

Bio-fix is a granular biosorbent produced by the U.S. Bureau of Mines (Wase and Forster, 1997). It consists of a variety of biomasses, including macro-algae immobilised in porous polypropylene beads, for the removal of arsenic, cadmium, copper, lead, manganese and zinc (Jeffers et al., 1991). The resulting beads are chemically and

mechanically resistant, with rapid extraction kinetics. Elution and regeneration of the beads is accomplished using dilute mineral acids and caustic solutions. Bio-fix was found to outperform ion-exchange resins when the initial metal concentration is less than 20 ppm (Brower et al., 1997).

#### **1.5.4.3 SORBEX™**

Sorbex™ (Figs. 1.19-1.20) is the most recent technology for the removal of metals from effluents using biosorption. This technology, developed by a Canadian company (BV SORBEX, Inc.), has been shown to successfully remove a wide spectrum of metals including Cd, Cr, Cu, Zn, Pb, U, Hg and Au.

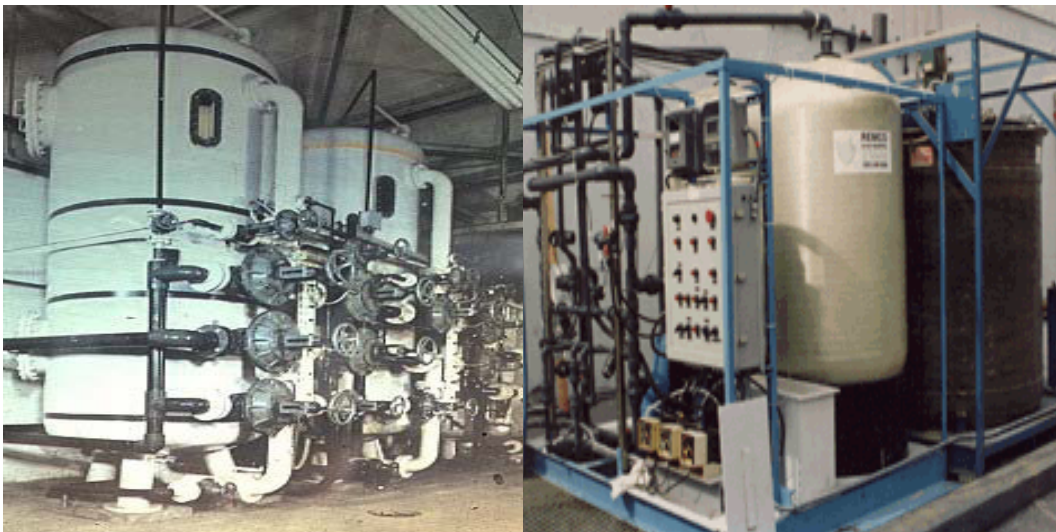


Fig. 1.19 Biosorption process columns in operation (BV Sorbex, 2008a).

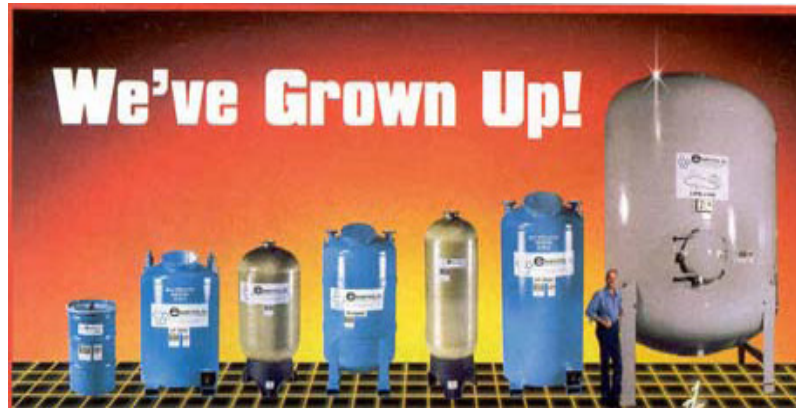


Fig. 1.20 Different scales of sorption systems are available, ranging from a small “canister” size to larger ones up to 2m in diameter and 5m high (BV Sorbex, 2008a)

## 1.6 Background

Following on from research by Fitzgerald (2002), the Estuarine Research Group (ERG) was set-up in 2004 at WIT to investigate the metal uptake properties of seaweeds. The ERG examines the potential of seaweeds as biosorbents (Walsh, 2008) and has developed a laboratory-scale biosorption system.

## 1.7 Aim

The primary aim is to develop a modified seaweed biosorption column, using a waste product from the industrial processing of *Ascophyllum nodosum* (referred to as WAP) and biomasses from *Ulva lactuca*, *Fucus vesiculosus* and *Polysiphonia lanosa*, for the remediation and recovery of metal(s) in industrial waste streams.

## 1.8 Objectives

- 1) To evaluate a laboratory scale fixed-bed sorption column with regard to removal efficiency for selected heavy metals from an aqueous solution.
- 2) To investigate the regeneration properties of the biosorbents.

- 3) To investigate desorption techniques and the selective recovery of metals from multi-component solutions.
- 4) To investigate the longevity and robustness of the seaweed materials
- 5) To study related chemical and physical properties, such as interactions between different metals present in the same effluent (antagonistic/synergistic effects)
- 6) To develop mathematical modelling to validate and predict experimental data.
- 7) To develop a novel large scale, yet portable, fixed bed sorption column

## **Chapter 2**

**Batch tests for the removal of Zinc, Nickel, Aluminium and Antimony(III) by dried biomass of *Fucus vesiculosus*, *Ulva lactuca*, *Polysiphonia lanosa* and Waste *Ascophyllum* Product.**

## 2.1 Introduction

Heavy metals, such as nickel and zinc, are amongst the most toxic pollutants present in marine, ground and industrial wastewaters (Al-Rub et al., 2006). Other elements, such as aluminium and antimony, present a lesser environmental risk but are also commonly found in industrial effluents and need to be removed.

The removal of heavy metals using biosorption has been widely reported in literature (Volesky, 1990; Volesky, 2004). A biosorbent used for the removal and recovery of metals from industrial effluents should achieve the following objectives (Volesky, 1990):

- the sorbent should have a high affinity for the metal(s) selected
- the mechanism of metal uptake and release should be rapid and efficient
- the manufacturing and re-use of the biosorbent should be achieved at the lowest cost possible
- the particle size of the biosorbent should be suitable for use in a continuous-flow reactor systems such as fixed-bed, mixed or fluidised sorption columns
- the removal of the biosorbent from the solution should be practical, cost-effective, rapid and efficient
- metal desorption from the biosorbent should be practical, selective and cost-effective without any deterioration of the biosorbent itself

Past research (Aderhold et al., 1996; Stirk and Van Staden, 2000; Feng and Aldrich, 2004; Al-Rub et al., 2006) has shown that the use of seaweeds as a sorbent agent meets all the requirements listed above, making them an excellent choice for metal sorption.

Screening of seaweed species is necessary to identify the most promising types of biomass. This is done primarily by batch equilibrium sorption tests (Volesky, 2001a).

This chapter presents the results of the screening of three seaweed species (*Fucus vesiculosus*, *Ulva lactuca* and *Polysiphonia lanosa*) and a seaweed waste product resulting from the processing of *Ascophyllum nodosum*. The seaweed species and WAP were investigated for the removal of Zn(II), Ni(II), Al(III) and Sb(III) from aqueous

solution. As most industrial effluents may contain a number of metals, the sorption studies were carried out for both single and combined metal aqueous solutions.

## 2.2 Aims

- To study the metal biosorption properties of the three seaweed species in stirred batch reactors for Zn(II), Ni(II), Al(III) and Sb(III) in single and combined metal aqueous solutions
- To study the metal biosorption properties of a Waste Ascophyllum Product (WAP) in wet and dried form in stirred batch reactors for Zn(II), Ni(II), Al(III) and Sb(III) in single and combined metal aqueous solutions
- To identify seaweed biomasses with high sorption capability for Zn(II), Ni(II), Al(III) and Sb(III) in single and combined metal aqueous solutions
- To investigate interactions (i.e. synergistic/antagonistic effects) when combining different metals in a single metal aqueous solution
- To evaluate the most suitable sorbents for use in an existing fixed-bed sorption column

## 2.3 Method

### Seaweed collection and preparation

Fresh samples of *Polysiphonia lanosa*, *Ulva lactuca* and *Fucus vesiculosus* were harvested from Fethard-on-Sea, Co. Wexford (52° 11'53.68'' N 6° 49' 34.64''W) (Fig. 2.1) and Baginbun Bay, Co. Wexford (52° 10'30.63'' N 6° 49'42.28'' W) (Fig. 2.2), both located in the south-east of Ireland. The sampling sites were considered to be low pollution sites according to the EPA water quality ENVision map (EPA, 2008). Collected seaweed samples were washed with tap water to remove sand and epiphytes and then rinsed thoroughly in deionised water. The samples were dried at 60°C for 12 hours and then ground to a powder form and sieved to obtain a fine particle size of  $\leq 850 \mu\text{m}$ .

The Waste *Ascophyllum* Product (or WAP) was supplied by “Oilean Glas Teo” (OGT) (Ballymoon Industrial Estate, Kilcar, Co. Donegal, Ireland), who manufacture solid and liquid extracts from *Ascophyllum nodosum* for use as a natural fertilizer and pesticide in agriculture and horticulture. The extracts can also be used as a basis for cosmetics and Thallasso therapies (Oilean Glas Teo, 2008). The WAP was received in large sealed plastic containers in the form of a green, dense paste. The WAP was dried overnight at 60°C and then ground to a powder form and sieved to obtain a fine particle size of  $\leq 850 \mu\text{m}$ .



Fig. 2.1 Fethard-on-sea. Source: Google Earth



Fig. 2.2 Baginbun Bay. Source: Google Earth

### **Prevention of aluminium contamination**

Due to the abundance of aluminium in the environment, the background aluminium content had to be minimised. Plastic-ware was used, when possible, throughout the aluminium-related studies as aluminium is a constituent of glass in the form of aluminosilicate. Prior to use, the plastic-ware was soaked in 10% nitric acid ( $\text{HNO}_3$ ) for 24 hours. The plastic-ware was then rinsed in double distilled water for a further 24 hours, dried in an oven at  $70^\circ\text{C}$ , and sealed in plastic bags until required.

## **Validation of Certified Reference Material (CRM)**

In order to validate the results obtained throughout the experiment, 3 different Certified Reference Materials or CRMs were used: Tomato leaves, Sea lettuce (*Ulva lactuca*) and BCR 060 Aquatic plant (*Lagarosiphon major*).

## **Chemicals**

- 1000mg L<sup>-1</sup> Sb(III) as Sb<sub>2</sub>O<sub>3</sub> (analytical grade), Cu, Zn and Al - Sigma-Aldrich Ltd., Dublin, Ireland.
- Nitric Acid (69%) – Sigma-Aldrich Ltd, Dublin, Ireland.
- Hydrogen peroxide – Sigma-Aldrich Ltd, Dublin, Ireland.

## **Instrumentation**

Metal analysis was carried out using a Varian 710-ES Inductively Coupled Plasma Optical Emission Spectrometer (ICP-OES) with auto-sampler.

## **Screening in batch tests**

Batch tests were carried out by exposing 1g of dried biomass or 1g of wet WAP (non-dried WAP) in 200 mL of aqueous solution containing the metal to be tested in single or mixed metal solutions at a 10 mg L<sup>-1</sup> concentration. For a multi-metal solution, 10 mg L<sup>-1</sup> of each metal under investigation was added. The initial pH of the metal solutions was recorded and was 3.24. Prior to metal exposure, dried, grounded and sieved seaweed biomass (to a particle size of  $\leq 850 \mu\text{m}$ ) was placed in an oven at 60°C overnight to dehydrate further.

The metal bearing solution at a concentration of 10 mg L<sup>-1</sup>, containing the selected biomass, was placed on a rotary shaker at 180 rpm at room temperature (22°C) for 12 hours. Afterwards, the biomass was removed by vacuum filtration and the filtrate analysed using a Varian 710-ES ICP Optical Emission Spectrometer with auto-sampler.

## 2.4 Statistical analysis

For the batch tests, single metal experiments were analysed using a one-way ANOVA with replication. A succession of one-way ANOVA with replication was carried-out for multi-metal experiments. In all of the ANOVA statistical tests, the level of significance used was  $p < 0.05$ . The null hypothesis ( $H_0$ ) was that there were no significant differences ( $p < 0.05$ ) between the different biomasses for metal uptake. Four replicates were used in all experiments. Calculations were carried-out using SPSS 15 (SPSS Inc., 2008). Tukey tests were also performed.

## 2.5 Results and discussion

### Comparison of seaweed biosorbents in batch tests for metal sorption

#### Single metal sorption tests

##### 2.5.1 Removal of Nickel by dried WAP, wet WAP, *Polysiphonia lanosa*, *Ulva lactuca* and *Fucus vesiculosus*.

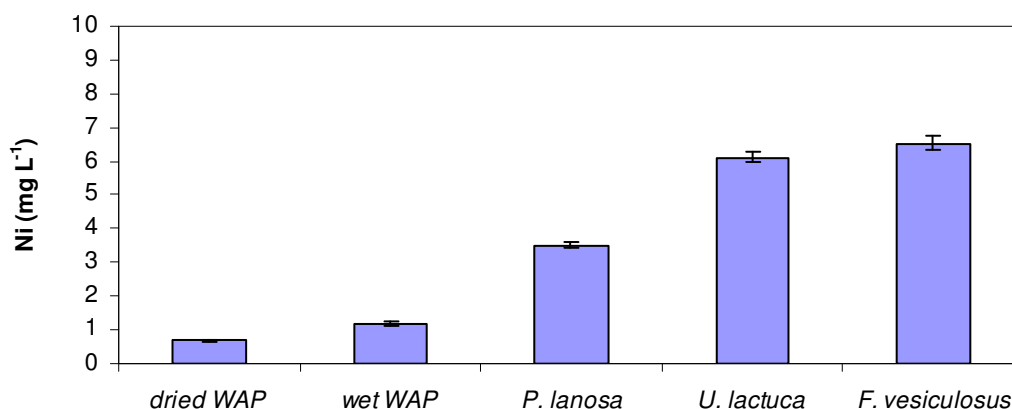


Fig. 2.3 Mean nickel concentration ( $\text{mg L}^{-1}$ ) from an initial aqueous Ni(II) solution ( $10 \text{ mg L}^{-1}$ ) after 12 hours exposure to dried WAP, wet WAP, *P. lanosa*, *U. lactuca* and *F. vesiculosus* ( $\pm 95\%$  confidence intervals,  $n = 4$ ).

Fig. 2.3 shows that 9.3 mg L<sup>-1</sup> of the Ni(II) was removed by dried WAP and 8.8 mg L<sup>-1</sup> by wet WAP. The lowest concentrations of Ni(II) were removed by *F. vesiculosus* and *U. lactuca*.

*Statistical analysis:*

Table 2.1: One-Way ANOVA analysis for Ni(II) sorption by dried WAP, wet WAP, *P. lanosa*, *U. lactuca* and *F. vesiculosus*.

**ANOVA**

concentrations

	Sum of Squares	df	Mean Square	F	Sig.
Between Groups	116,772	4	29,193	1286,476	,000
Within Groups	,340	15	,023		
Total	117,112	19			

There were significant differences ( $p < 0.05$ ) between the biosorbents for Ni(II) uptake. The Tukey test was applied to characterise the level of differentiation between the biomasses (Table 2.2).

Table 2.2: Tukey test for Ni(II) sorption by dried WAP, wet WAP, *P. lanosa*, *U. lactuca* and *F. vesiculosus*.

**concentrations**

Tukey HSD<sup>a</sup>

biosorbents	N	Subset for alpha = .05				
		1	2	3	4	5
dried WAP	4	,68212				
wet WAP	4		1,19027			
<i>P. lanosa</i>	4			3,50970		
<i>U. lactuca</i>	4				6,11919	
<i>F. vesiculosus</i>	4					6,51852
Sig.		1,000	1,000	1,000	1,000	1,000

Means for groups in homogeneous subsets are displayed.

a. Uses Harmonic Mean Sample Size = 4,000.

All biomasses were significantly different ( $p < 0.05$ ) for Ni(II) sorption.

**2.5.2 Removal of Zinc by dried WAP, wet WAP, *Polysiphonia lanosa*, *Ulva lactuca* and *Fucus vesiculosus*.**

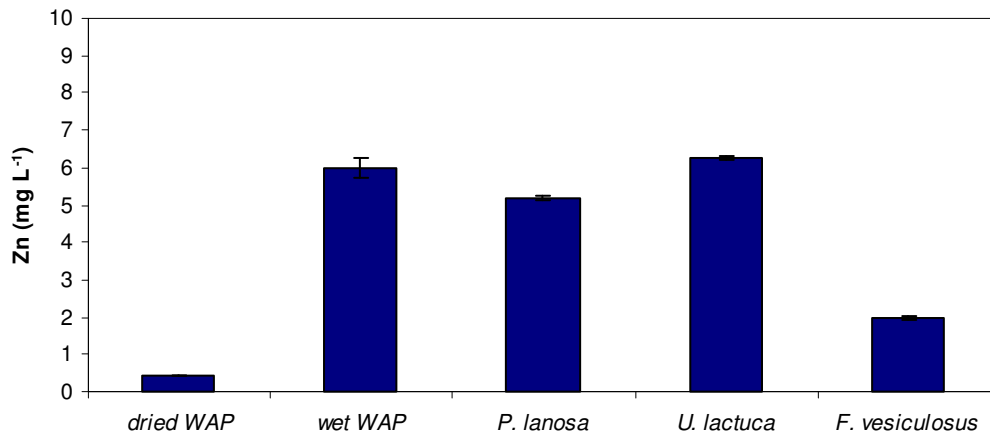


Fig. 2.4 Mean zinc concentrations (mg L<sup>-1</sup>) from an initial aqueous Zn(II) solution (10 mg L<sup>-1</sup>) after 12 hours exposure to dried WAP, wet WAP, *P. lanosa*, *U. lactuca* and *F. vesiculosus* ( $\pm$  95% confidence intervals, n = 4).

Fig. 2.4 shows that 9.6 mg L<sup>-1</sup> of the Zn(II) was removed by dried WAP and 8 mg L<sup>-1</sup> by *F. vesiculosus*.

Statistical analysis:

Table 2.3: One-Way ANOVA analysis for Zn(II) sorption by dried WAP, wet WAP, *P. lanosa*, *U. lactuca* and *F. vesiculosus*.

ANOVA					
concentration					
	Sum of Squares	df	Mean Square	F	Sig.
Between Groups	108,835	4	27,209	1210,952	,000
Within Groups	,337	15	,022		
Total	109,172	19			

There were significant differences ( $p < 0.05$ ) between the biosorbents for Zn(II) uptake. The Tukey test was applied to characterise the level of differentiation between the biomasses (Table 2.4).

Table 2.4: Tukey test for Zn(II) sorption by dried WAP, wet WAP, *P. lanosa*, *U. lactuca* and *F. vesiculosus*.

**concentration**

Tukey HSD<sup>a</sup>

biosorbent	N	Subset for alpha = .05			
		1	2	3	4
dried WAP	4	,4180			
F. vesiculosus	4		1,9845		
<i>P. lanosa</i>	4			5,1932	
wet WAP	4				5,9721
<i>U. lactuca</i>	4				6,2385
Sig.		1,000	1,000	1,000	,140

Means for groups in homogeneous subsets are displayed.

a. Uses Harmonic Mean Sample Size = 4,000.

*U. lactuca* and wet WAP were significantly similar ( $p < 0.05$ ) in terms of Zn(II) uptake. The other biomasses, however, differed significantly for Zn(II) uptake.

### 2.5.3 Removal of Aluminium by dried WAP, wet WAP, *Polysiphonia lanosa*, *Ulva lactuca* and *Fucus vesiculosus*.

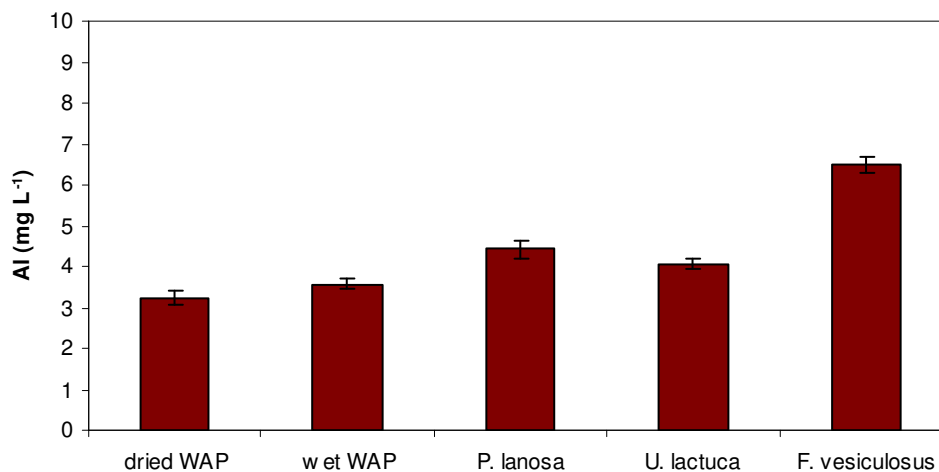


Fig. 2.5 Mean aluminium concentrations ( $\text{mg L}^{-1}$ ) from an initial aqueous Al(III) solution ( $10 \text{ mg L}^{-1}$ ) after 12 hours exposure to dried WAP, wet WAP, *P. lanosa*, *U. lactuca* and *F. vesiculosus* ( $\pm 95\%$  confidence intervals,  $n = 4$ ).

Fig. 2.5 shows that dried WAP was the most efficient at removing Al(III). However, only 6.8 mg L<sup>-1</sup> of Al(III) was removed using the biosorbent.

Statistical analysis:

Table 2.5: One-Way ANOVA analysis for Al(III) sorption dried WAP, wet WAP, *P. lanosa*, *U. lactuca* and *F. vesiculosus*.

**ANOVA**

concentrations

	Sum of Squares	df	Mean Square	F	Sig.
Between Groups	25,948	4	6,487	159,418	,000
Within Groups	,610	15	,041		
Total	26,559	19			

There were significant differences ( $p < 0.05$ ) between the biosorbents for Al(III) uptake. The Tukey test was applied to characterise the level of differentiation between the biomasses (Table 2.6).

Table 2.6: Tukey test for Al(III) sorption by dried WAP, wet WAP, *P. lanosa*, *U. lactuca* and *F. vesiculosus*.

**concentrations**

Tukey HSD<sup>a</sup>

biosorbent	N	Subset for alpha = .05		
		1	2	3
wet WAP	4	3,23		
dried WAP	4	3,57		
<i>U. lactuca</i>	4		4,06	
<i>P. lanosa</i>	4		4,43	
<i>F. vesiculosus</i>	4			6,48
Sig.		,179	,118	1,000

Means for groups in homogeneous subsets are displayed.

a. Uses Harmonic Mean Sample Size = 4,000.

*U. lactuca* and *P. lanosa* were similar ( $p < 0.05$ ) in terms of Al(III) uptake. Dried WAP and wet WAP were also similar.

**2.5.4 Removal of Antimony by dried WAP, wet WAP, *Polysiphonia lanosa*, *Ulva lactuca* and *Fucus vesiculosus*.**

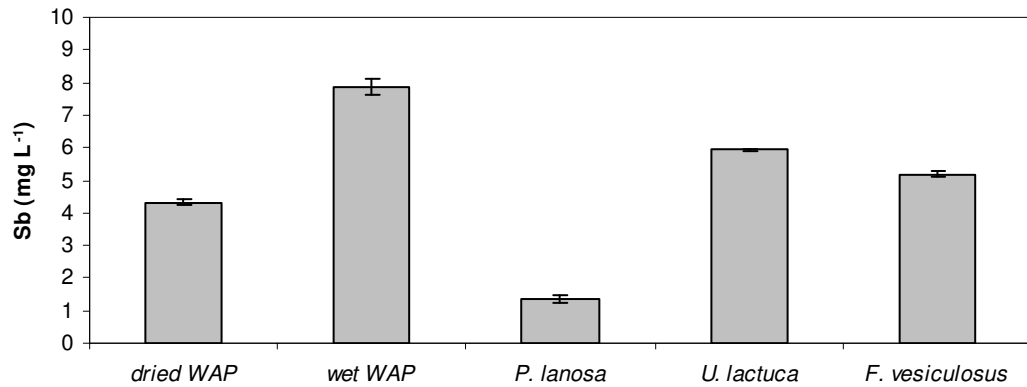


Fig. 2.6 Mean antimony concentrations (mg L<sup>-1</sup>) from an initial aqueous Sb(III) solution (10 mg L<sup>-1</sup>) after 12 hours exposure to dried WAP, wet WAP, *P. lanosa*, *U. lactuca* and *F. vesiculosus* ( $\pm$  95% confidence intervals, n = 4).

Fig. 2.6 shows that 8.6 mg L<sup>-1</sup> of the Sb(III) was removed by *P. lanosa*. The other biomasses were far less effective at removing Sb(III).

Statistical analysis:

Table 2.7: One-Way ANOVA analysis for Sb(III) sorption by dried WAP, wet WAP, *P. lanosa*, *U. lactuca* and *F. vesiculosus*.

ANOVA					
concentrations					
	Sum of Squares	df	Mean Square	F	Sig.
Between Groups	91,203	4	22,801	908,958	,000
Within Groups	,376	15	,025		
Total	91,580	19			

There were significant differences (p < 0.05) between the biomasses for Sb(III) uptake. The Tukey test was applied to characterise the level of differentiation between the biomasses (Table 2.8).

Table 2.8: Tukey test for Sb(III) sorption by dried WAP, wet WAP, *P. lanosa*, *U. lactuca* and *F. vesiculosus*.

		concentrations				
Tukey HSD <sup>a</sup>		Subset for alpha = .05				
biosorbent	N	1	2	3	4	5
<i>P. lanosa</i>	4	1,35				
dried WAP	4		4,31			
<i>F. vesiculosus</i>	4			5,18		
<i>U. lactuca</i>	4				5,92	
wet WAP	4					7,86
Sig.		1,000	1,000	1,000	1,000	1,000

Means for groups in homogeneous subsets are displayed.

a. Uses Harmonic Mean Sample Size = 4,000.

All biomasses were significantly different (95% significance) for Sb(III) uptake.

### Multi-metal sorption tests

#### 2.5.5 Removal of Zinc and Nickel in a combined aqueous solution by dried WAP, wet WAP, *Polysiphonia lanosa*, *Ulva lactuca* and *Fucus vesiculosus*.

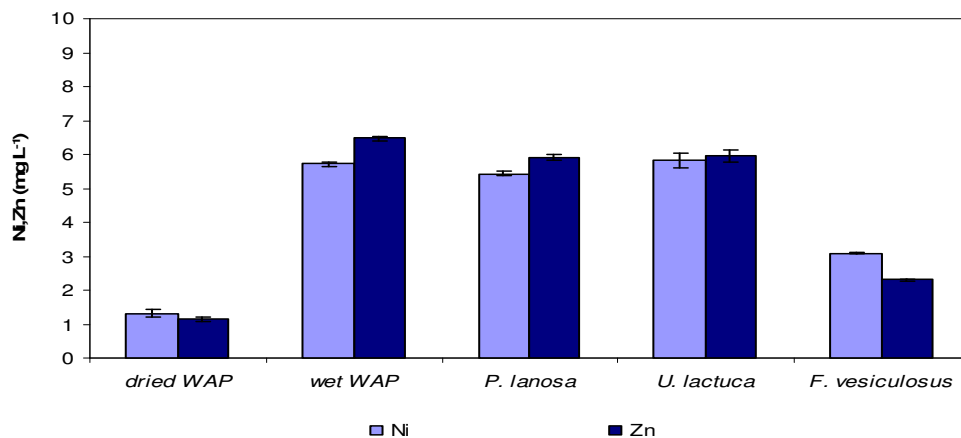


Fig. 2.7 Mean zinc and nickel concentrations ( $\text{mg L}^{-1}$ ), from an initial combined aqueous solution of Zn(II) and Ni(II) ( $10 \text{ mg L}^{-1}$  each), after 12 hours exposure to dried WAP, wet WAP, *P. lanosa*, *U. lactuca* and *F. vesiculosus* ( $\pm 95\%$  confidence intervals,  $n = 4$ ).

Fig. 2.7 shows that the best removal of Zn(II) and Ni(II) from a combined solution was by dried WAP, with  $8.9 \text{ mg L}^{-1}$  and  $8.7 \text{ mg L}^{-1}$  removed respectively. This was followed by *F. vesiculosus* ( $7.7 \text{ mg L}^{-1}$  for Zn(II) and  $6.9 \text{ mg L}^{-1}$  for Ni(II)). The remaining

species *P. lanosa* and *U. lactuca* were much less efficient at removing the combined metals.

Statistical analysis:

Table 2.9: Two-Way ANOVA analysis for Ni(II)/Zn(II) sorption by dried WAP, wet WAP, *P. lanosa*, *U. lactuca* and *F. vesiculosus*.

**Tests of Between-Subjects Effects**

Dependent Variable: concentration

Source	Type III Sum of Squares	df	Mean Square	F	Sig.
Corrected Model	168,070 <sup>a</sup>	9	18,674	1069,162	,000
Intercept	765,318	1	765,318	43816,512	,000
biosorbents	166,272	4	41,568	2379,880	,000
metal	,011	1	,011	,657	,424
biosorbents * metal	1,787	4	,447	25,571	,000
Error	,524	30	,017		
Total	933,912	40			
Corrected Total	168,594	39			

a. R Squared = ,997 (Adjusted R Squared = ,996)

There were no significant differences ( $p > 0.05$ ) between Ni(II) and Zn(II), suggesting no synergistic/antagonistic interactions between the metals.

There were significant differences (95% significance) between the biosorbents for Ni(II) and Zn(II) uptake. The Tukey test was applied to characterise the level of differentiation between the biomasses (Table 2.10). No post hoc tests could be applied for the metals as there are fewer than 3 groups.

Table 2.10: Tukey test for Ni(II)/Zn(II) sorption by dried WAP, wet WAP, *P. lanosa*, *U. lactuca* and *F. vesiculosus*.

concentration

Tukey HSD<sup>a,b</sup>

biosorbents	N	Subset				
		1	2	3	4	5
dried WAP	8	1,22468				
F. vesiculosus	8		2,69505			
P. lanosa	8			5,66957		
U. lactuca	8				5,88941	
wet WAP	8					6,39189
Sig.		1,000	1,000	1,000	1,000	1,000

Means for groups in homogeneous subsets are displayed.  
Based on Type III Sum of Squares  
The error term is Mean Square(Error) = ,017.

a. Uses Harmonic Mean Sample Size = 8,000.

b. Alpha = ,05.

All the biosorbents were significantly different ( $p < 0.05$ ) for Ni(II) and Zn(II) uptake.

### 2.5.6 Removal of Nickel and Antimony in combined aqueous solution by dried WAP, wet WAP, *Polysiphonia lanosa*, *Ulva lactuca* and *Fucus vesiculosus*.

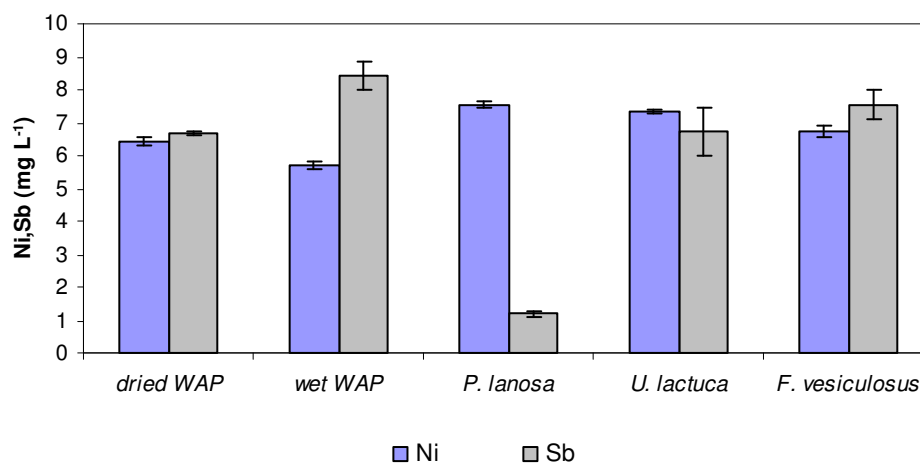


Fig. 2.8 Mean nickel and antimony concentrations ( $\text{mg L}^{-1}$ ), from an initial combined aqueous solution of Ni(II) and Sb(III) ( $10 \text{ mg L}^{-1}$  each), after 12 hours exposure to dried WAP, wet WAP, *P. lanosa*, *U. lactuca* and *F. vesiculosus* ( $\pm 95\%$  confidence intervals,  $n = 4$ ).

Fig. 2.8 shows that most of the Sb(III) present in a combined Sb(III) and Ni(II) solution was removed by *P. lanosa* (8.8 mg L<sup>-1</sup>). Only 1.60 mg L<sup>-1</sup> of Sb(III) was removed by wet WAP and 3.3mg L<sup>-1</sup> by dried WAP.

Statistical analysis:

Table 2.11: Two-Way ANOVA analysis for Ni(II)/Sb(III) sorption by dried WAP, wet WAP, *P. lanosa*, *U. lactuca* and *F. vesiculosus*.

**Tests of Between-Subjects Effects**

Dependent Variable: concentrations

Source	Type III Sum of Squares	df	Mean Square	F	Sig.
Corrected Model	146,420 <sup>a</sup>	9	16,269	120,806	,000
Intercept	1674,117	1	1674,117	12431,295	,000
biosorbents	62,580	4	15,645	116,174	,000
metal	21,594	1	21,594	160,350	,000
biosorbents * metal	62,245	4	15,561	115,552	,000
Error	4,040	30	,135		
Total	1824,577	40			
Corrected Total	150,460	39			

a. R Squared = ,973 (Adjusted R Squared = ,965)

There were significant differences ( $p < 0.05$ ) between Ni(II) and Sb(III), suggesting an synergistic/antagonistic effect between the metals.

There were significant differences ( $p < 0.05$ ) between the biosorbents for Ni(II) and Sb(III) uptake. The Tukey test was applied to characterise the level of differentiation between the biomasses (Table 2.12). No post hoc tests could be applied for the metals as there are fewer than 3 groups.

Table 2.12: Tukey test for Ni(II)/Sb(III) sorption by dried WAP, wet WAP, *P. lanosa*, *U. lactuca* and *F. vesiculosus*.

**concentrations**

Tukey HSD <sup>a,b</sup>

biosorbents	N	Subset			
		1	2	3	4
<i>P. lanosa</i>	8	4,3691			
<i>F. vesiculosus</i>	8		6,1856		
dried WAP	8		6,5533	6,5533	
<i>U. lactuca</i>	8			7,0370	
wet WAP	8				8,2019
Sig.		1,000	,288	,089	1,000

Means for groups in homogeneous subsets are displayed.

Based on Type III Sum of Squares

The error term is Mean Square(Error) = ,135.

a. Uses Harmonic Mean Sample Size = 8,000.

b. Alpha = ,05.

All biomasses were significantly different for Ni(II) and Sb(III) sorption, except for *F. vesiculosus* with dried WAP, and *U. lactuca* with dried WAP. However, *F. vesiculosus* and *U. lactuca* were significantly (95%) different.

### 2.5.7 Removal of Zinc and Antimony in a combined aqueous solution by dried WAP, wet WAP, *Polysiphonia lanosa*, *Ulva lactuca* and *Fucus vesiculosus*.

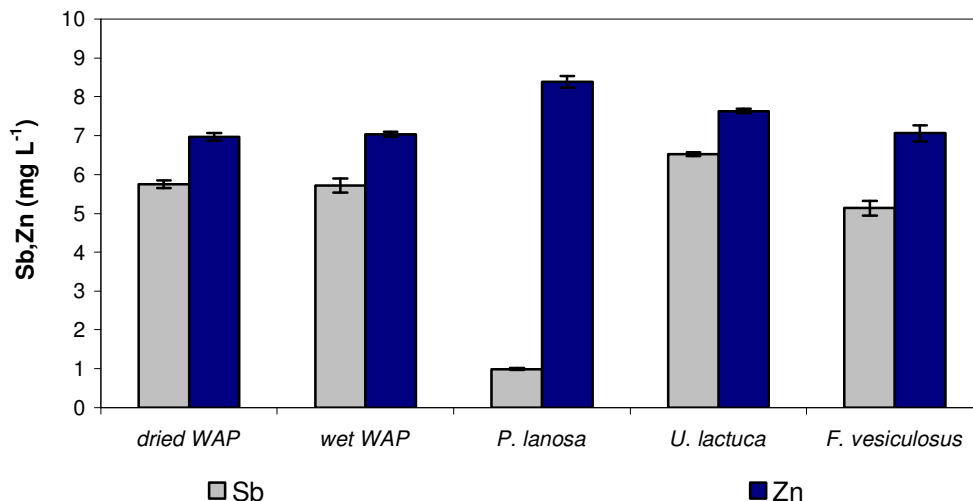


Fig. 2.9 Mean zinc and antimony concentrations (mg L<sup>-1</sup>), from an initial combined aqueous solution of Zn(II) and Sb(III) (10 mg L<sup>-1</sup> each), after 12 hours exposure to dried WAP, wet WAP, *P. lanosa*, *U. lactuca* and *F. vesiculosus* ( $\pm$  95% confidence intervals, n = 4).

Fig. 2.9 shows that 9.0 mg L<sup>-1</sup> of the Sb(III) present in a combined solution of Sb(III) and Zn(II) was removed by *P. lanosa*, but only 1.6 mg L<sup>-1</sup> of Zn(II) was removed. The Sb(III) and Zn(II) removals by the other seaweed species and WAP were low.

Statistical analysis:

Table 2.13: Two-Way ANOVA analysis for Zn(II)/Sb(III) sorption by dried WAP, wet WAP, *P. lanosa*, *U. lactuca* and *F. vesiculosus*.

**Tests of Between-Subjects Effects**

Dependent Variable: concentration

Source	Type III Sum of Squares	df	Mean Square	F	Sig.
Corrected Model	5,995 <sup>a</sup>	9	,666	715,727	,000
Intercept	23,829	1	23,829	25604,009	,000
biosorbent	1,008	4	,252	270,812	,000
metal	2,605	1	2,605	2798,565	,000
biosorbent * metal	2,382	4	,596	639,931	,000
Error	,028	30	,001		
Total	29,852	40			
Corrected Total	6,023	39			

a. R Squared = ,995 (Adjusted R Squared = ,994)

There were significant differences ( $p < 0.05$ ) between Sb(III) and Zn(II), suggesting an interaction between the metals.

There were significant differences ( $p < 0.05$ ) between the biosorbents for Zn(II) and Sb(III) uptake. The Tukey test was applied to characterise the level of differentiation between the biomasses (Table 2.14). No post hoc tests could be applied for the metals as there are fewer than 3 groups.

Table 2.14: Tukey test for Zn(II)/Sb(III) sorption by dried WAP, wet WAP, *P. lanosa*, *U. lactuca* and *F. vesiculosus*.

		concentration			
Tukey HSD <sup>a,b</sup>		Subset			
biosorbent	N	1	2	3	4
<i>U. lactuca</i>	8	,5848			
wet WAP	8		,7039		
dried WAP	8		,7278		
<i>F. vesiculosus</i>	8			,7802	
<i>P. lanosa</i>	8				1,0624
Sig.		1,000	,528	1,000	1,000

Means for groups in homogeneous subsets are displayed.

Based on Type III Sum of Squares

The error term is Mean Square(Error) = ,001.

a. Uses Harmonic Mean Sample Size = 8,000.

b. Alpha = ,05.

Dried and wet WAP were similar ( $p < 0.05$ ). The other biomasses, however, differed significantly.

### 2.5.8 Removal of Aluminium and Antimony in a combined aqueous solution by dried WAP, wet WAP, *Polysiphonia lanosa*, *Ulva lactuca* and *Fucus vesiculosus*.

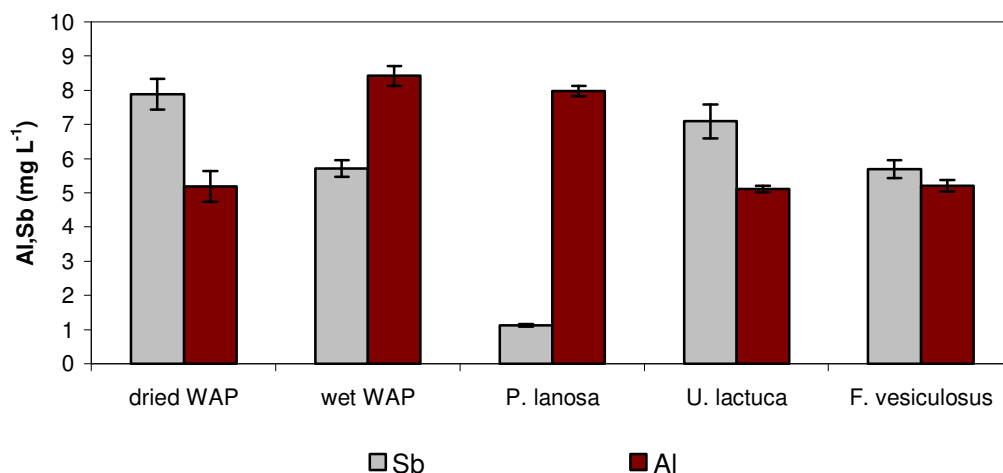


Fig. 2.10 Mean aluminium and antimony concentrations ( $\text{mg L}^{-1}$ ), from an initial mixed combined aqueous solution of Al(III) and Sb(III) ( $10 \text{ mg L}^{-1}$  each), after 12 hours exposure to dried WAP, wet WAP, *P. lanosa*, *U. lactuca* and *F. vesiculosus* ( $\pm 95\%$  confidence intervals,  $n = 4$ ).

Fig. 2.10 shows that 5.8 mg L<sup>-1</sup> of the Al(III), present in a combined Al(III) and Sb(III) solution, was removed by *U. lactuca*, followed by dried WAP (5.7 mg L<sup>-1</sup>). Removal of Sb(III) was poor with wet WAP which only removed 5.3 mg L<sup>-1</sup> of the Sb(III) present. *P. lanosa* was the most efficient at removing Sb(III) with a removal of 8.9 mg L<sup>-1</sup>.

Statistical analysis:

Table 2.15: Two-Way ANOVA analysis for Al(III)/Sb(III) sorption by dried WAP, wet WAP, *P. lanosa*, *U. lactuca* and *F. vesiculosus*.

**Tests of Between-Subjects Effects**

Dependent Variable: concentrations

Source	Type III Sum of Squares	df	Mean Square	F	Sig.
Corrected Model	198,892 <sup>a</sup>	9	22,099	172,650	,000
Intercept	1581,989	1	1581,989	12359,299	,000
biosorbents	81,101	4	20,275	158,400	,000
metal	,349	1	,349	2,723	,109
biosorbents * metal	117,443	4	29,361	229,381	,000
Error	3,840	30	,128		
Total	1784,721	40			
Corrected Total	202,732	39			

a. R Squared = ,981 (Adjusted R Squared = ,975)

There were significant differences ( $p < 0.05$ ) between Al(III) and Sb(III), suggesting an interaction between the metals.

They were significant differences (95% significance) between the biosorbents for Al(III) and Sb(III) sorption in a combined metal solution. The Tukey test was applied to characterise the level of differentiation between the biomasses (Table 2.16). No post hoc tests could be applied for the metals as there are fewer than 3 groups.

Table 2.16: Tukey test for Al(III)/Sb(III) sorption by dried WAP, wet WAP, *P. lanosa*, *U. lactuca* and *F. vesiculosus*.

		concentrations			
Tukey HSD <sup>a,b</sup>		Subset			
biosorbents	N	1	2	3	4
<i>P. lanosa</i>	8	4,5525			
<i>F. vesiculosus</i>	8		5,4513		
<i>U. lactuca</i>	8			6,1030	
dried WAP	8			6,5334	
wet WAP	8				8,8042
Sig.		1,000	1,000	,141	1,000

Means for groups in homogeneous subsets are displayed.

Based on Type III Sum of Squares

The error term is Mean Square(Error) = ,128.

a. Uses Harmonic Mean Sample Size = 8,000.

b. Alpha = ,05.

*U. lactuca* and dried WAP were similar ( $p < 0.05$ ) for Sb(III) and Al(III) uptake. Wet WAP was significantly different ( $p < 0.05$ ) to *U. lactuca* and dried WAP for the uptake of these metals.

### 2.5.9 Removal of Zinc, Nickel, Aluminium and Antimony in a combined aqueous solution by dried WAP, wet WAP *Polysiphonia lanosa*, *Ulva lactuca* and *Fucus vesiculosus*.

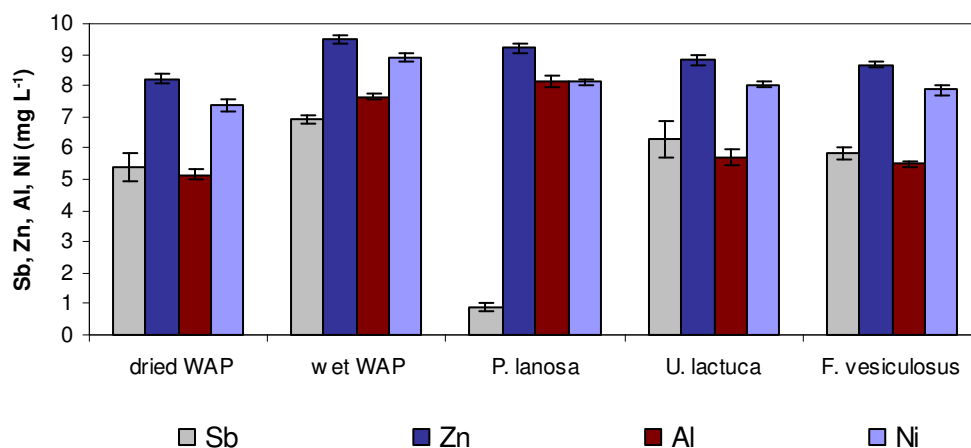


Fig. 2.11 Mean zinc, nickel, aluminium and antimony concentrations, from an initial combined aqueous solution of Zn(II), Ni(II), Al(III) and Sb(III) (10 mg L<sup>-1</sup> each), after 12 hours exposure to dried WAP, wet WAP, *P. lanosa*, *U. lactuca* and *F. vesiculosus* ( $\pm$  95% confidence intervals, n = 4).

Fig. 2.11 shows that in a combined solution of Sb(III), Zn(II), Al(III) and Ni(II), 8.4 mg L<sup>-1</sup> of the Sb(III) was removed by *P. lanosa*. The removal capacities of the other metals by the remaining seaweed species were low by comparison.

Statistical analysis:

Table 2.17: Two-Way ANOVA analysis for Zn(II)/Ni(II)/Al(III)/Sb(III) sorption by dried WAP, wet WAP, *P. lanosa*, *U. lactuca* and *F. vesiculosus*.

**Tests of Between-Subjects Effects**

Dependent Variable: concentrations

Source	Type III Sum of Squares	df	Mean Square	F	Sig.
Corrected Model	1036,436 <sup>a</sup>	19	54,549	898,192	,000
Intercept	1515,381	1	1515,381	24951,833	,000
biosorbents	818,172	4	204,543	3367,945	,000
metals	76,390	3	25,463	419,271	,000
biosorbents * metals	141,874	12	11,823	194,672	,000
Error	3,644	60	,061		
Total	2555,461	80			
Corrected Total	1040,080	79			

a. R Squared = ,996 (Adjusted R Squared = ,995)

All the biosorbents were significantly different ( $p < 0.05$ ) for Ni(II), Sb(III), Al(III) and Zn(II) sorption in a combined metal solution.

The metals were significantly different ( $p < 0.05$ ), suggesting an interaction between the different metals. Significant differences ( $p < 0.05$ ) between the biosorbents for Al(III) and Sb(III) uptake. The Tukey test was applied to characterise the level of differentiation between the biomasses and between the different metals (Tables 2.18 & 2.19).

Table 2.18 Tukey test (biosorbents) for Zn(II)/Ni(II)/Al(III)/Sb(III) sorption by dried WAP, wet WAP, *P. lanosa*, *U. lactuca* and *F. vesiculosus*.

**concentrations**

Tukey HSD <sup>a,b</sup>

biosorbents	N	Subset		
		1	2	3
wet WAP	16	,3613		
<i>F. vesiculosus</i>	16	,5781		
dried WAP	16		6,5269	
<i>P. lanosa</i>	16		6,5965	
<i>U. lactuca</i>	16			7,6986
Sig.		,107	,930	1,000

Means for groups in homogeneous subsets are displayed.

Based on Type III Sum of Squares

The error term is Mean Square(Error) = ,061.

a. Uses Harmonic Mean Sample Size = 16,000.

b. Alpha = ,05.

Dried WAP with *P. lanosa* and wet WAP with *F. vesiculosus* were not significantly different ( $p < 0.05$ ) to each other. *U. lactuca* was significantly different to the other biosorbents.

Table 2.19 Tukey test (metals) for Zn(II)/Ni(II)/Al(III)/Sb(III) sorption by dried WAP, wet WAP, *P. lanosa*, *U. lactuca* and *F. vesiculosus*.

**concentrations**

Tukey HSD <sup>a,b</sup>

metals	N	Subset			
		1	2	3	4
Sb	20	2,7437			
Al	20		4,4928		
Ni	20			4,8269	
Zn	20				5,3457
Sig.		1,000	1,000	1,000	1,000

Means for groups in homogeneous subsets are displayed.

Based on Type III Sum of Squares

The error term is Mean Square(Error) = ,061.

a. Uses Harmonic Mean Sample Size = 20,000.

b. Alpha = ,05.

All the metals were significantly different ( $p < 0.05$ ).

### Summary of the results

Table 2.20 shows the Removal Efficiencies (RE) in % obtained from the screening of different sorbents (seaweeds and WAP).

Table 2.20 Removal efficiencies in % for different biosorbents (batch tests)

Metal	Removal efficiency in %				
	Dried WAP	Wet WAP	<i>Polysiphonia lanosa</i>	<i>Ulva lactuca</i>	<i>Fucus vesiculosus</i>
Ni	93	88	65	39	35
Zn	96	40	48	38	80
Al	68	64	56	59	35
Sb	57	21	86	41	48
Zn/Ni	89/87	35/43	41/46	40/42	77/69
Zn/Sb	30/42	30/43	16/90	24/35	29/49
Ni/Sb	36/33	43/16	25/88	27/33	33/43
Al/Sb	48/21	16/43	29/89	49/29	57/53
Ni/Zn/Al/Sb	25/20/50/38	11/9/26/22	17/10/20/83	18/14/44/29	19/16/47/37

Dried WAP displayed high RE values for the uptake of Ni(II), Zn(II) and Al(III), but a much lower level for Sb(III). In contrast, *P. lanosa* displayed a high RE for Sb(III) in both single and combined metal solutions.

Tables 2.21-2.23 show the corresponding uptake capacities ( $q$ ) in  $\text{mg g}^{-1}$ . Uptake capacities are calculated using the following equation (Eq.[1]) (Volesky, 2004). The higher the value of  $q$ , the greater the uptake capacity of the biosorbent for the metal.

$$q = \frac{V(C_f - C_i)}{S} \quad \text{Eq.[1]}$$

where  $V$  is the volume in L,  $C_f$  and  $C_i$  are the final and initial metal concentrations in  $\text{mg L}^{-1}$ , and  $S$  is the weight of the biosorbent in g. The  $q$  values for wet WAP are expressed per g of dried biomass for comparison purposes with the other biomasses.

Table 2.21 Uptake capacities ( $q$ ) in  $\text{mg g}^{-1}$  for different biosorbents for single metal solutions.

Metals	$q$ ( $\text{mg g}^{-1}$ )				
	Dried WAP	Wet WAP*	<i>Polysiphonia lanosa</i>	<i>Ulva lactuca</i>	<i>Fucus vesiculosus</i>
Zn	$1.92 \pm 0.01$	$0.94 \pm 0.06$	$0.96 \pm 0.01$	$0.75 \pm 0.01$	$1.60 \pm 0.01$
Ni	$1.86 \pm 0.01$	$2.05 \pm 0.01$	$1.30 \pm 0.02$	$0.78 \pm 0.03$	$0.70 \pm 0.04$
Al	$1.35 \pm 0.03$	$1.45 \pm 0.03$	$1.11 \pm 0.04$	$1.19 \pm 0.03$	$0.70 \pm 0.04$
Sb	$1.14 \pm 0.02$	$0.50 \pm 0.05$	$1.73 \pm 0.01$	$0.82 \pm 0.02$	$0.96 \pm 0.02$

\* dried weight

Table 2.22 Uptake capacities ( $q$ ) in  $\text{mg g}^{-1}$  for *F. vesiculosus*, *U. lactuca* and *P. lanosa* for combined metal solutions.

Metals	$q$ ( $\text{mg g}^{-1}$ )											
	<i>Polysiphonia lanosa</i>				<i>Ulva Lactuca</i>				<i>Fucus vesiculosus</i>			
Zn/Ni	0.82 $\pm 0.02$	0.91 $\pm 0.01$	1.54 $\pm 0.01$	1.38 $\pm 0.02$	1.54 $\pm 0.01$	1.38 $\pm 0.02$	1.54 $\pm 0.01$	1.38 $\pm 0.02$	1.54 $\pm 0.01$	1.38 $\pm 0.02$	1.54 $\pm 0.01$	1.38 $\pm 0.02$
Zn/Sb	0.32 $\pm 0.03$	1.80 $\pm 0.01$	0.59 $\pm 0.04$	0.97 $\pm 0.04$	0.59 $\pm 0.04$	0.97 $\pm 0.04$	0.59 $\pm 0.04$	0.97 $\pm 0.04$	0.59 $\pm 0.04$	0.97 $\pm 0.04$	0.59 $\pm 0.04$	0.97 $\pm 0.04$
Ni/Sb	0.49 $\pm 0.02$	1.76 $\pm 0.02$	0.66 $\pm 0.04$	0.87 $\pm 0.09$	0.66 $\pm 0.04$	0.87 $\pm 0.09$	0.66 $\pm 0.04$	0.87 $\pm 0.09$	0.66 $\pm 0.04$	0.87 $\pm 0.09$	0.66 $\pm 0.04$	0.87 $\pm 0.09$
Al/Sb	0.58 $\pm 0.2$	1.77 $\pm 0.05$	0.98 $\pm 0.02$	0.58 $\pm 0.10$	0.98 $\pm 0.02$	0.58 $\pm 0.10$	0.98 $\pm 0.02$	0.58 $\pm 0.10$	0.98 $\pm 0.02$	0.58 $\pm 0.10$	0.98 $\pm 0.02$	0.58 $\pm 0.10$
Ni/Zn/Al/Sb	0.37 $\pm 0.02$	0.16 $\pm 0.04$	0.40 $\pm 0.02$	0.31 $\pm 0.02$	0.93 $\pm 0.02$	0.67 $\pm 0.05$	0.47 $\pm 0.05$	0.75 $\pm 0.12$	0.40 $\pm 0.02$	0.31 $\pm 0.02$	0.93 $\pm 0.02$	0.67 $\pm 0.05$

Table 2.23 Uptake capacities (q) in mg g<sup>-1</sup> for dried and wet WAP for combined metal solutions.

Metals	q (mg g <sup>-1</sup> )							
	Dried WAP				Wet WAP*			
Zn/Ni	1.77 ± 0.04		1.74 ± 0.004		0.82 ± 0.05		0.86 ± 0.05	
Zn/Sb	0.61 ± 0.02		0.85 ± 0.02		0.69 ± 0.02		0.95 ± 0.04	
Ni/Sb	0.71 ± 0.02		0.67 ± 0.01		0.47 ± 0.03		0.37 ± 0.1	
Al/Sb	0.96 ± 0.09		0.42 ± 0.09		0.37 ± 0.07		0.19 ± 0.06	
Ni/Zn/Al/Sb	0.53 ± 0.04	0.35 ± 0.03	0.97 ± 0.03	0.92 ± 0.09	0.50 ± 0.03	0.17 ± 0.05	0.56 ± 0.05	0.22 ± 0.07

\* dried weight

Tables 2.21-2.23 show that in general, dried WAP displayed higher uptake capacities (q values) than the other sorbents. Dried WAP, however, displayed a lower uptake capacity for Sb(III) compared to *P. lanosa*.

Screening of seaweeds for metal sorption has been carried-out by many authors (Holan and Volesky, 1994; Yu et al., 1999; Hamdy, 2000; Lau et al., 2003; Senthilkumar et al., 2006; Murphy et al., 2007). Most studies have focused on the use of *Sargassum* species for the uptake of a variety of heavy metals, including Cu(II), Zn(II), Ni(II), Cd(II) and Fe(III) (Kratochvil and Volesky, 2000; De França et al., 2002; Cossich, 2004; Vijayaraghavan et al., 2005a; Lodeiro et al., 2006; Naja and Volesky, 2006a).

However, only a few studies have investigated the potential of seaweed derivatives and by-products for metal sorption (Aderhold et al., 1996; Stirk and Van Staden, 2000; Feng and Aldrich, 2004). The early work of Aderhold et al (1996), investigated the capacity of two seaweed waste products for the sorption of Cu(II), Ni(II), Zn(II), Pb(II) and

Cd(II) in single or combined metals aqueous solutions. The seaweeds derivatives were defined as alginated fibres and dealginated seaweed waste, both resulting from the processing of seaweeds. The results showed that the alginate compound was effective for the removal of Ni(II), Zn(II) and Cd(II), with a RE of approximately 95%. The dealginated material also showed a relatively high RE, with an average of 90% RE for the metals. Dried WAP in our study showed very high RE for Ni(II) and Zn(II) at 93% and 96% respectively (Table 2.20).

It was reported by Holan & Volesky (1994) that the difference in morphological structure existing between seaweed species, especially the structure of their cell walls, even within the same order, can influence the sorption process. The cell walls of brown algae generally contain three components: cellulose, alginic acid, sulphated polysaccharides with the presence of different salts such as calcium, magnesium, sodium and potassium. As a consequence, carboxyl and sulphate are the predominant active groups in this kind of algae (Romera et al., 2007). Red algae also contain cellulose but the main groups involved in metal sorption result in the presence of sulphated polysaccharides made of galactanes (agar and carrageenan). Green algae are mainly constituted of cellulose. A high proportion of the cell wall of the different algae are proteins bonded to polysaccharides to form glycoproteins and these compounds contain several functional groups (amino, carboxyl, sulphate, hydroxyl,...) which could be heavily involved in the metal binding process (Romera et al., 2007).

Alginates are suspected to play a large part in this metal binding as WAP is processed from the brown seaweed *Ascophyllum nodosum*, which contains a high level of alginate. Haug (1961) showed that alginates displayed an affinity for divalent cations such as Pb(II), Cu(II), Cd(II), Zn(II) and Ca(II). This could explain the high REs obtained for both Zn(II) and Ni(II) by WAP and less for Al(III) and Sb(III). However, *Fucus vesiculosus*, a brown seaweed, displayed a low affinity for Ni(II) and Al(III) while removing most of the Zn(II) present in the aqueous solution. Morphological differences existing within the same order could explain this difference in affinity for the same metals and also the structure and amount of alginates, involved in metal binding, differs between young and old tissues and also according to the different parts of the plants utilised (Holan and Volesky, 1994). Figueira et al. (1999) postulated that seaweed sulphonate groups are responsible for the uptake of trivalent metal cations. This could

explain the high RE of Sb(III) by *P. lanosa* as sulphonate groups are present as sulphonic acids of polysaccharides, abundant in this particular seaweed.

Further research is recommended into the mechanisms involved and the chemical composition of the different seaweed species. Furthermore, dried WAP showed higher REs than the wet form, indicating that the dried form of the waste product is more efficient in metal binding. This may be due to the ability of the dried biomass to adsorb and retain more liquid by capillarity than the wet biomass.

Lau *et al* (2003), investigated the capacity of three *Ulva* species for the uptake of Cu(II), Ni(II) and Zn(II). The maximum RE was observed for *U. lactuca* for the three metals at pH5. In our study, the initial pH of 3.24 was not changed due to the high REs obtained, but *Ulva lactuca* was much less efficient in the removal of Ni and Zn compared with dried WAP, *P. lanosa* and *F. vesiculosus*.

The same study showed that the presence of other metals in a combined metal aqueous solution slightly affected the RE by the three *Ulva species*. In our study, WAP showed high RE for both Ni(II) and Zn(II) in single metals solutions, at 93% and 96%, respectively (Table 2.20). However, when Ni(II) and Zn(II) were combined, the REs reduced to 87% and 89%, respectively. This may indicate competition between different metal ions for the binding sites at the surface of the sorbent resulting in a loss of removal efficiency for both metals. The same trend was observed for *P. lanosa* which showed a relatively high RE for Ni(II) at 65%, but when combined with Sb(III) the RE was reduced to 46%. There was no observed change in RE when Ni(II) was combined with Zn(II). A similar trend was observed for the biosorption of cadmium-zinc ions by *Sargassum filipendula*. It was reported that the quantity of zinc removed by the seaweed decreased with increasing concentration of cadmium ions in a binary system (Fagundes-Klen *et al.*, 2007).

*P. lanosa* was observed to be very effective at removing Sb(III) in both single and multi-metal solutions. In contrast, dried WAP, which was very effective at removing Ni(II), Zn(II) and Al(III), displayed a very low affinity for Sb(III). Table 2.20 shows that Sb(III), when combined with Ni(II), Zn(II) and Al(III), reduced the capacity of WAP for binding the other metals. This suggests an antagonistic effect of Sb(III) on the sorption of Ni(II), Zn(II) and Al(III) by WAP biomass. The antagonistic effects of

Sb(III) on the sorption of the other metals by WAP is discussed in more detail in Chapter 8.

## 2.6 Conclusions

The screening of three seaweed species, *F. vesiculosus*, *U. lactuca* and *P. lanosa*, and a waste product resulting from the processing of *Ascophyllum nodosum* (WAP) showed that WAP in dried form was the most efficient biosorbent for the removal of Ni(II), Zn(II) and Al(III) from both single and combined metal solutions. WAP, however, demonstrated poor removal efficiencies for Sb(III) in both single and combined metal solutions. *P. lanosa* showed a high affinity for Sb(III) and was very efficient in the removal of Sb(III) from both single and combined metal solutions. Consequently, the most promising sorbents were identified as dried WAP for Ni(II), Zn(II) and Al(III) and *P. lanosa* for Sb(III). An antagonistic effect of Sb(III) on the sorption of the other metals by WAP was also observed.

## **Chapter 3**

**Maximum metal uptake capacity ( $q_{\max}$ ) and adsorption isotherms.**

### 3.1 Introduction

#### 3.1.1 Biosorption equilibrium

Metal uptake behaviour can be determined quantitatively from experimental biosorption equilibrium isotherms. According to research by Volesky (1990), following contact between a biosorbent and the solution containing the metal species, an equilibrium is established at a given temperature. Consequently, a certain amount of the sorbed metal sequestered by the sorbent is in equilibrium with the metal left free in the solution.

Fig. 3.1 is a plot of metal uptake by the biosorbent against the residual metal concentration in solution.

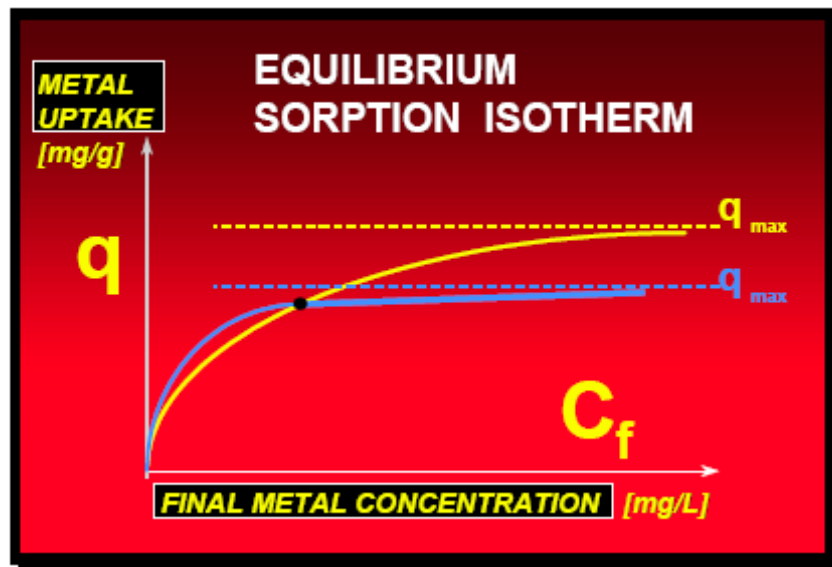


Fig. 3.1 Example of a sorption isotherm (Volesky, 2001a).

The maximum sorption uptake ( $q_{\max}$ ) is commonly used to characterise the efficiency of a sorbent for metal sorption, especially for comparative studies (Volesky, 1990).

### 3.1.2 Adsorption Isotherms

An adsorption isotherm is a measure of the relationship between the equilibrium concentrations of bound and free metal over a certain concentration range and is generally generated from equilibrium batch binding studies. Binding properties can be calculated by fitting the adsorption isotherm to specific binding models (Umpleby et al., 2001). Two models are commonly used, and are known as discrete and continuous distribution models (García-Calzón and Díaz-García, 2007).

#### *Discrete distribution models: Langmuir isotherms*

This isotherm (Eq. [2]) is based on three assumptions (García-Calzón and Díaz-García, 2007):

- adsorption cannot proceed beyond monolayer coverage
- all surface binding sites are equivalent
- the ability of a metal ion to bind at a given site does not depend on the occupation of neighbouring sites.

To summarise, a basic assumption of the Langmuir theory is that sorption takes place at specific homogenous sites within the adsorbent. It is then assumed that once a metal ion occupies a site, no further adsorption can take place (García-Calzón and Díaz-García, 2007).

$$q = \frac{q_{\max} C_f}{b^{-1} + C_f} \quad \text{Eq. [2]}$$

The Langmuir constant,  $b = 1/K$  (Fig. 3.2), is related to the energy of adsorption. The higher the value of  $b$ , the smaller the value of  $K$  is going to be. The affinity of the sorbent for the sorbate,  $q_{\max}$ , can also be interpreted as the total number of binding sites that are available for biosorption, and  $q$  as the number of binding sites that are in fact occupied by the sorbate at the final concentration  $C_f$  (Volesky, 2004).

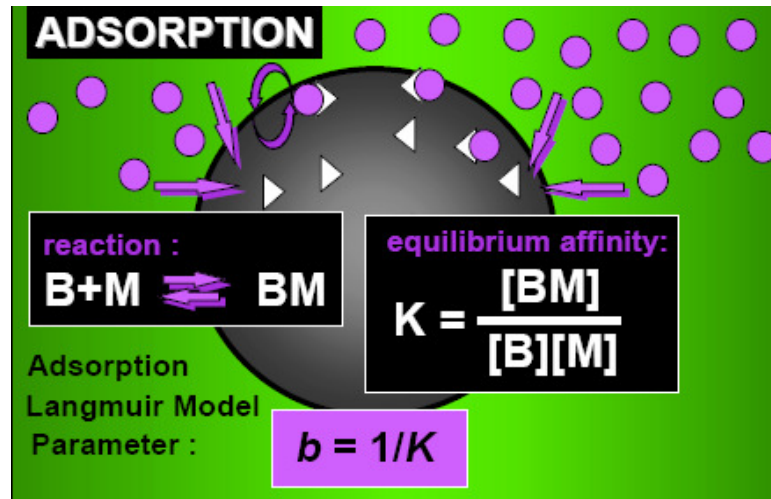


Fig. 3.2: Relationship between Langmuirian  $b$  and the equilibrium affinity constant  $K$ , where  $B$  represents the free binding sites,  $M$  is the metal in the solution and  $BM$  represents the adsorbed metal bound on  $B$ .  $[ ]$  denotes the concentrations of  $B$ ,  $M$  and  $BM$  (Volesky, 2004).

*Continuous distribution models: Freundlich isotherms*

Like the Langmuir isotherm, the extent of adsorption/sorption is determined as a function of the equilibrium concentration of the metal in solution, without reference to pH or other ions in the same aqueous system. The Freundlich isotherm assumes that the stronger binding sites are occupied first and that the binding strength decreases with increasing degree of site occupation (Davis et al., 2003). The Freundlich isotherm is defined by the following equation:

$$q = kC_f^{(1/n)} \quad \text{Eq. [3]}$$

where  $k$  and  $n$  are Freundlich constants

Both the Langmuir and Freundlich adsorption isotherm models have been modified to represent multi-component isotherms (Sheindorf and Rebhun, 1980). There is also the concept of competitive and non-competitive Langmuir and Freundlich adsorption

models for both single and combined metal solutions with or without the presence of competing ions (Aksu et al., 1997).

#### *Hybrid models: Langmuir-Freundlich model*

The Langmuir-Freundlich (L-F) isotherm is a function that describes a specific relationship between the equilibrium concentration of bound (B) and free (F) metal ions in heterogeneous systems with three coefficients:  $N_t$ ,  $a$  and  $m$  (Umpleby et al., 2001):

$$B = \frac{N_t a F^m}{1 + a F^m} \quad \text{Eq. [4]}$$

where  $N_t$  is the total number of binding sites,  $a$  is related to the median binding affinity ( $K_0$ ) via  $K_0 = a^{1/m}$ , and  $m$  is the heterogeneity index, which varies from 0 to 1. For a homogeneous material  $m = 1$ . When  $m < 1$  the material is heterogeneous.

As stated by Umpleby et al (2001), when  $m = 1$ , the L-F isotherm (Eq.[4]) reduces to the Langmuir isotherm (Eq.[2]), in which  $a$  corresponds directly to binding affinity ( $K$ ). On the other hand, as either  $a$  or  $F$  approaches 0, the L-F isotherm reduces to the Freundlich isotherm (Eq.[3]).

### **3.2 Aims**

- To compare the Langmuir, Freundlich and combined Langmuir-Freundlich sorption isotherms as models for the experimental data.
- To determine  $q_{\max}$  (overall capacity for sorption) and affinity coefficients for *P. lanosa* and WAP for Zn(II), Ni(II), Al(III) and Sb(III) sorption in both single and combined solutions.

### 3.3 Methods

#### Biosorption equilibrium isotherm

100 mg of WAP (dried and  $\leq 850 \mu\text{m}$  particle size) was exposed to 50 mL of increasing concentrations of Zn(II), Ni(II), Al(III) and Sb(III) (5, 10, 50, 100, 200, 300 and 350 mg L<sup>-1</sup>) for 12 hours on a rotary shaker at 180 rpm. The same protocol was followed for *P. lanosa* exposure to Sb(III). Four replicates of each metal concentration were examined. Samples of biosorbent and solution were taken after 12 hours and acidified with nitric acid. Biosorbents in distilled water and metal free solutions were prepared as controls. Analysis was carried out as in Section 2.3.

#### Chemicals

- 1000mg L<sup>-1</sup> Sb(III) as Sb<sub>2</sub>O<sub>3</sub> (analytical grade), Zn(II), Ni(II) and Al(III) - Sigma-Aldrich Ltd., Dublin, Ireland.

### 3.4 Results and discussion

Table 3.1 Comparison of correlation coefficients for Langmuir, Freundlich and combined Langmuir-Freundlich biosorption models.

biomass	metals	$r^2$		
		Langmuir	Freundlich	Langmuir-Freundlich
WAP	Zn	0.996	0.888	0.995
WAP	Ni	0.842	0.905	0.905
WAP	Al	0.931	0.936	0.936
WAP	Sb	0.978	0.908	0.911
<i>P. lanosa</i>	Sb	0.879	0.907	0.903
WAP (metal mixture)	Zn	0.895	0.949	0.865
	Ni	0.699	0.654	0.276
	Al	0.867	0.675	0.573
WAP (metal mixture)	Zn	0.908	0.891	0.891
	Ni	0.924	0.949	0.946
	Al	0.250	0.406	0.510
	Sb	0.657	0.427	0.879

Table 3.1 shows that, in general, higher correlation coefficients were obtained for the Langmuir sorption model compared to the Freundlich and the Langmuir-Freundlich adsorption isotherms. As a result, the Langmuir binding isotherms are examined in this chapter. The Freundlich and Langmuir-Freundlich isotherms can be found in Appendix C.

### 3.4.1 Biosorption equilibrium isotherm for Zn(II) and WAP

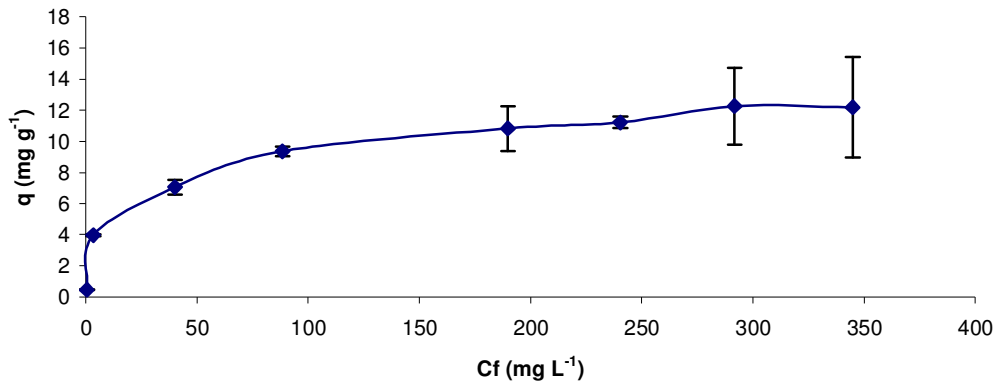


Fig. 3.3 Biosorption equilibrium isotherm ( $q$  vs.  $C_f$ ) for 100 mg of WAP exposed to Zn(II) concentrations 5-350 mg L<sup>-1</sup> ( $\pm$  95% confidence intervals,  $n = 4$ ).

In Fig. 3.3 that the steep initial slope represents the high affinity of Zn(II) for WAP. The isotherm plateau denotes the maximum uptake value possible by 100 mg of WAP.

The linearised plot of the Langmuir model for Zn(II) ( $1/q$  vs.  $1/C_f$ ) is shown in Fig. 3.4. The correlation coefficient was 0.9958.

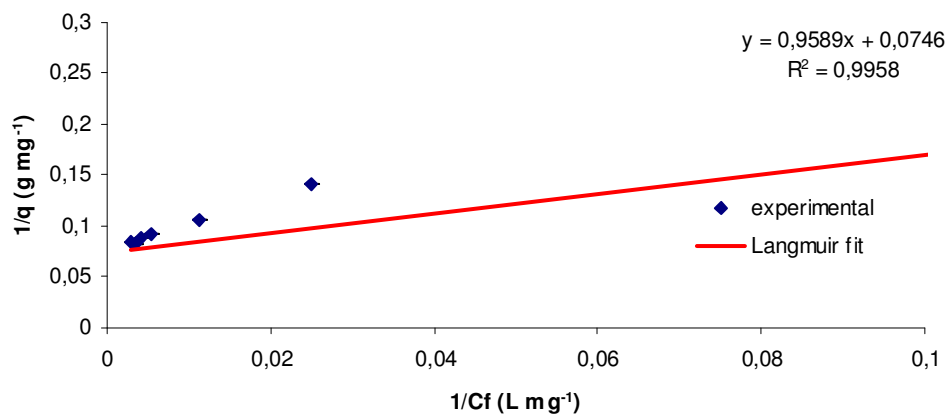


Fig. 3.4 Linearised plot of the Langmuir relationship ( $1/q$  vs.  $1/C_f$ ) between  $q$  and  $C_f$  of WAP biosorption isotherm. Equation of the line and regression value displayed ( $\pm$  95% confidence intervals,  $n = 4$ ).

### 3.4.2 Biosorption equilibrium isotherm for Ni(II) and WAP

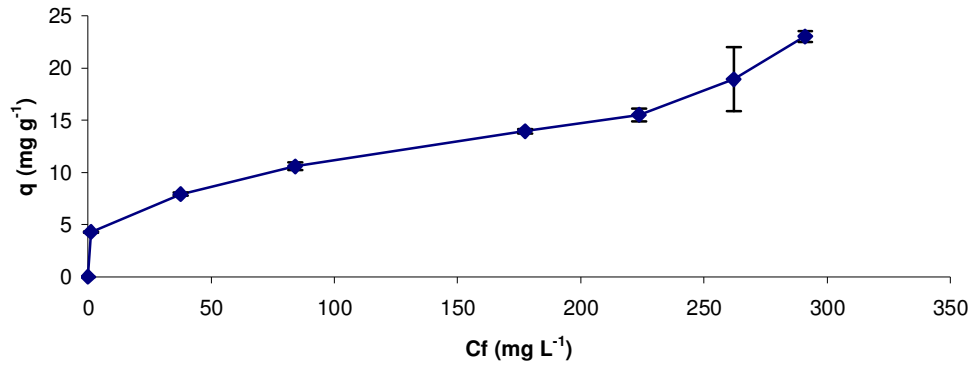


Fig. 3.5 Biosorption equilibrium isotherm ( $q$  vs.  $C_f$ ) for 100 mg of WAP exposed to Ni(II) concentrations 5-300 mg L<sup>-1</sup> ( $\pm$  95% confidence intervals,  $n = 4$ ).

In Fig. 3.5 the steep initial slope represents the high affinity of Ni(II) for WAP.

The linearised plot of the Langmuir model for Ni(II) ( $1/q$  vs.  $1/C_f$ ) is shown in Fig. 3.6. The correlation coefficient was 0.8419.

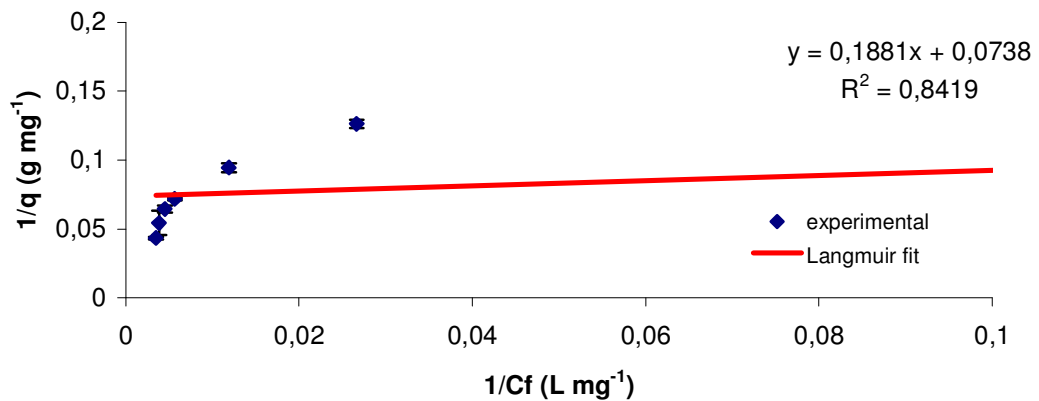


Fig. 3.6 Linearised plot of the Langmuir relationship ( $1/q$  vs.  $1/C_f$ ) between  $q$  and  $C_f$  of WAP biosorption isotherm. Equation of the line and regression value displayed ( $\pm$  95% confidence intervals,  $n = 4$ ).

### 3.4.3 Biosorption equilibrium isotherm for Al(III) and WAP

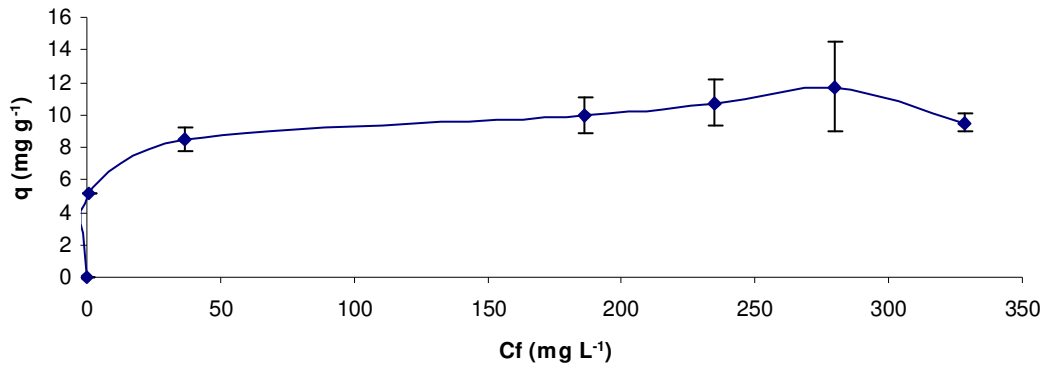


Fig. 3.7 Biosorption equilibrium isotherm ( $q$  vs.  $C_f$ ) for 100 mg of WAP exposed to Al(III) concentrations 5-350 mg L<sup>-1</sup> ( $\pm$  95% confidence intervals,  $n = 4$ ).

In Fig. 3.7 the steep initial slope represents the high affinity of Al(III) for WAP. The isotherm plateau denotes the maximum uptake value possible by 100 mg of WAP.

The linearised plot of the Langmuir model for Al(III) ( $1/q$  vs.  $\ln C_f$ ) is shown in Fig. 3.8. The correlation coefficient was 0.931.

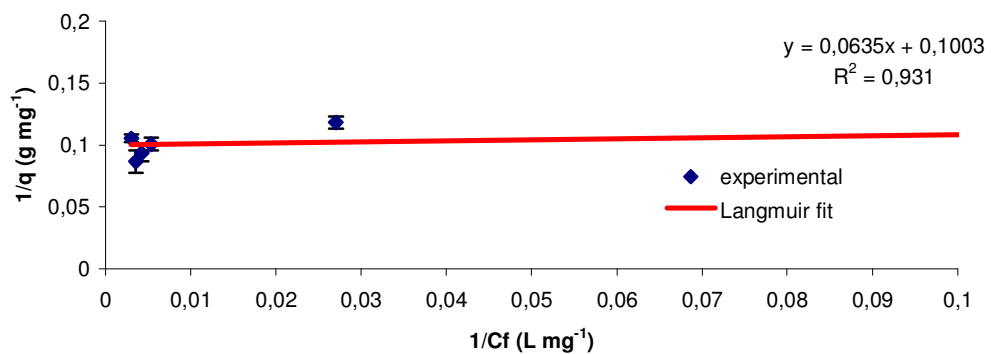


Fig. 3.8 Linearised plot of the Langmuir relationship ( $1/q$  vs.  $1/C_f$ ) between  $q$  and  $C_f$  of WAP biosorption isotherm. Equation of the line and regression value displayed ( $\pm$  95% confidence intervals,  $n = 4$ ).

### 3.4.4 Biosorption equilibrium isotherm for Sb(III) and WAP

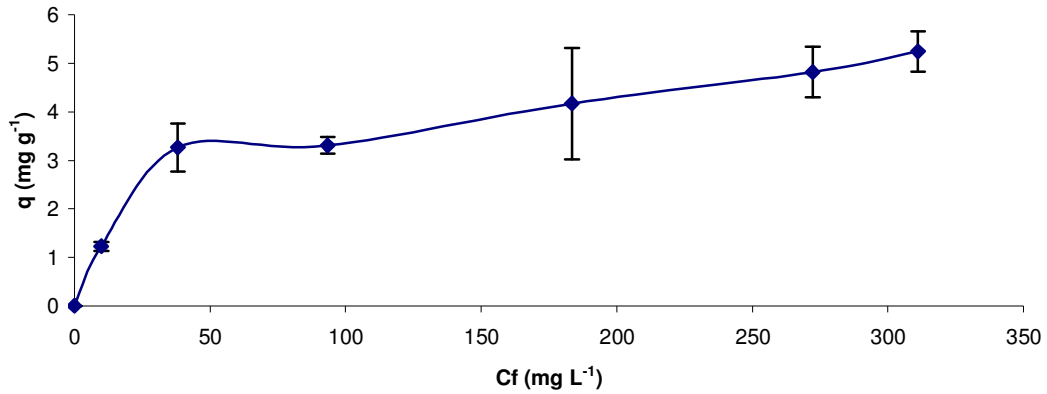


Fig. 3.9 Biosorption equilibrium isotherm ( $q$  vs.  $C_f$ ) for 100 mg of WAP exposed to Sb(III) concentrations 5-350 mg L<sup>-1</sup> ( $\pm$  95% confidence intervals,  $n = 4$ ).

In Fig. 3.9 the steep initial slope represents the affinity of Sb(III) for WAP. The isotherm plateau denotes the maximum uptake value possible by 100 mg of WAP.

The linearised plot of the Langmuir model for Sb(III) ( $1/q$  vs.  $1/C_f$ ) is shown in Fig. 3.10. The correlation coefficient was 0.9797.

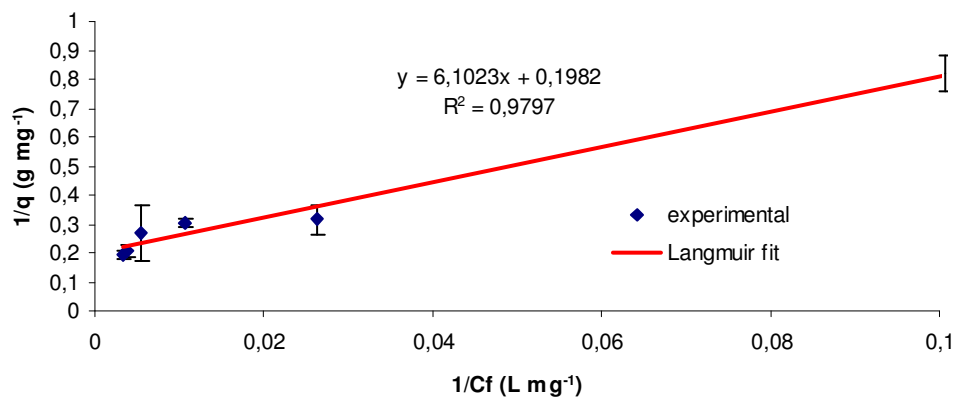


Fig. 3.10 Linearised plot of the Langmuir relationship ( $1/q$  vs.  $1/C_f$ ) between  $q$  and  $C_f$  of WAP biosorption isotherm. Equation of the line and regression value displayed ( $\pm$  95% confidence intervals,  $n = 4$ ).

### 3.4.5 Biosorption equilibrium isotherm for Sb(III) and *P. lanosa*

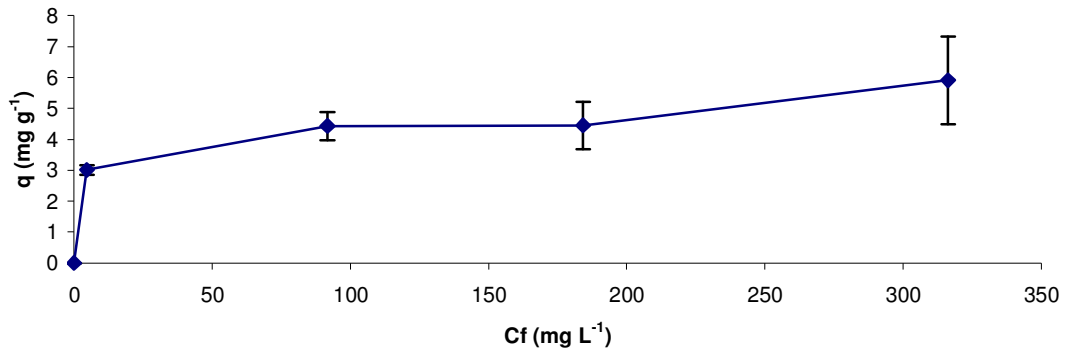


Fig. 3.11 Biosorption equilibrium isotherm ( $q$  vs.  $C_f$ ) for 100 mg of *P. lanosa* exposed to Sb(III) concentrations 5-350 mg L<sup>-1</sup> ( $\pm$  95% confidence intervals,  $n = 4$ ).

In Fig. 3.11 the steep initial slope represents the high affinity of Sb(III) for *P. lanosa*. The isotherm plateau denotes the maximum uptake value possible by 100 mg of *P. lanosa*.

The linearised plot of the Langmuir model for Sb(III) ( $1/q$  vs.  $1/C_f$ ) is shown in Fig. 3.12. The correlation coefficient was 0.8787.

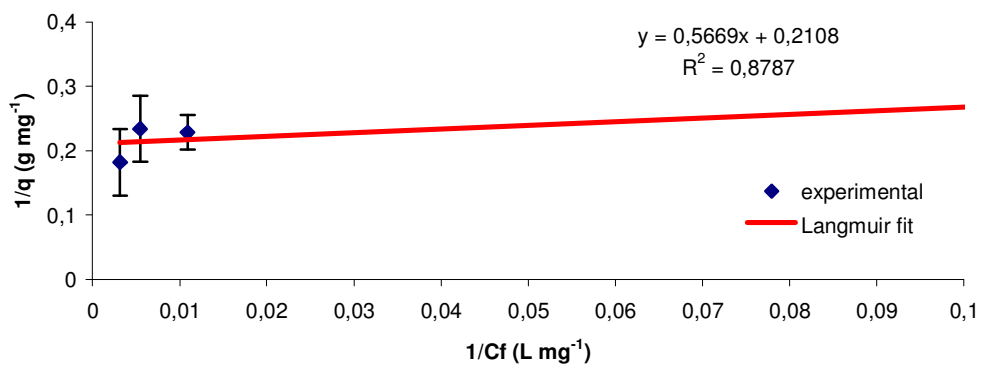


Fig. 3.12 Linearised plot of the Langmuir relationship ( $1/q$  vs.  $1/C_f$ ) between  $q$  and  $C_f$  of *P. lanosa* biosorption isotherm. Equation of the line and regression value displayed ( $\pm$  95% confidence intervals,  $n = 4$ ).

### 3.4.6 Biosorption equilibrium isotherm for Zn(II)/Ni(II)/Al(III) and WAP

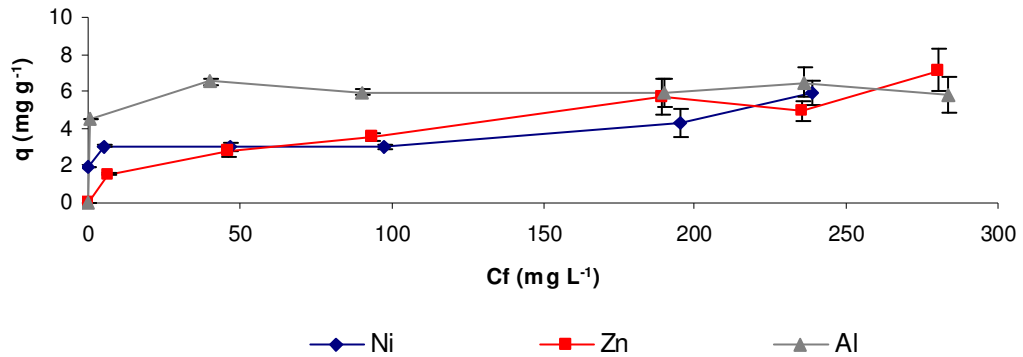


Fig. 3.13 Biosorption equilibrium isotherm ( $q$  vs.  $C_f$ ) of 100 mg for WAP exposed to a combined solution of Ni(II), Zn(II) and Al(III) with concentrations 5-300 mg L<sup>-1</sup> ( $\pm$  95% confidence intervals,  $n = 4$ ).

In Fig. 3.13 the steep initial slopes represent the high affinity of Zn(II), Ni(II) and Al(III) for WAP.

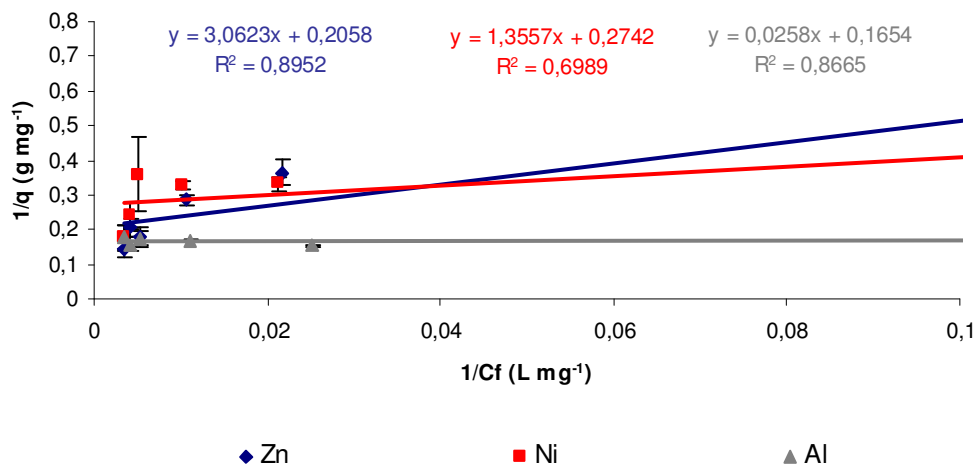


Fig. 3.14 Linearised plot of the Langmuir relationship ( $1/q$  vs.  $1/C_f$ ) between  $q$  and  $C_f$  of WAP biosorption isotherm. Equation of the lines and regression values displayed ( $\pm$  95% confidence intervals,  $n = 4$ ).

### 3.4.7 Biosorption equilibrium isotherm for Zn(II)/Ni(II)/Al(III)/Sb(III) and WAP

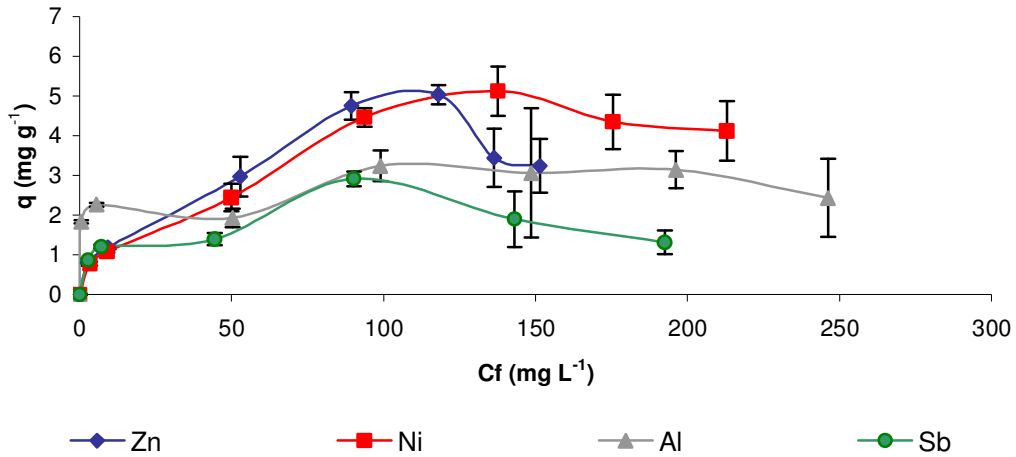


Fig. 3.15 Biosorption equilibrium isotherm ( $q$  vs.  $C_f$ ) for 100 mg of WAP exposed to a combined solution of Zn(II), Ni(II), Al(III) and Sb(III) with concentrations 5-300  $\text{mg L}^{-1}$  ( $\pm 95\%$  confidence intervals,  $n = 4$ ).

In Fig. 3.15 the steep initial slopes represents the high affinity of Zn(II), Ni(II), Al(III) for WAP. The isotherm plateaus denote the maximum uptake values possible by 100 mg of WAP.

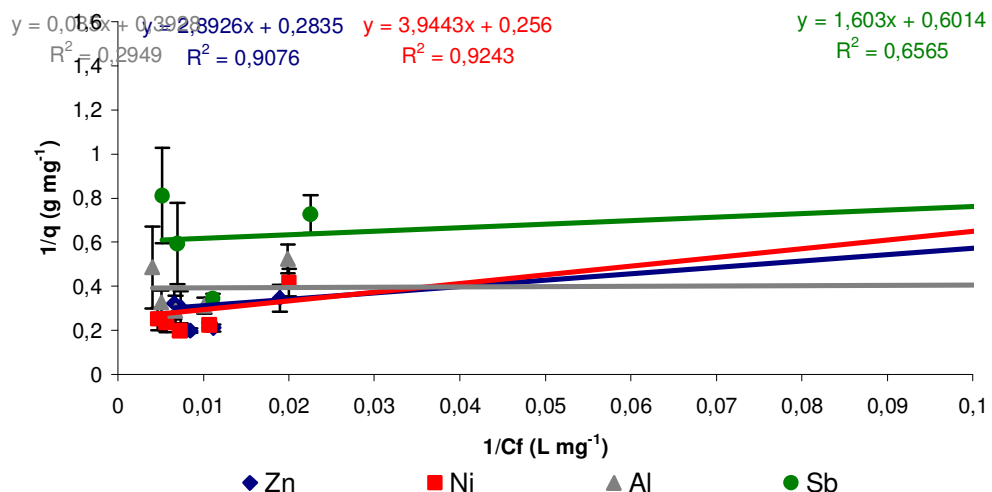


Fig. 3.16 Linearised plot of the Langmuir relationship ( $1/q$  vs.  $1/C_f$ ) between  $q$  and  $C_f$  of WAP biosorption isotherm. Equation of the lines and regression values displayed ( $\pm 95\%$  confidence intervals,  $n = 4$ ).

Table 3.2 Langmuir parameters and maximum adsorption values ( $q_{max}$ )

biomass	metals	$q_{max}$ (mmol/g)	$q_{max}$ (mg/g)	b (L/mg)	$r^2$
WAP	Zn	2.05 $\pm 0.10$	134.05 $\pm 6.47$	0.78 $\pm 0.04$	0.996
WAP	Ni	2.31 $\pm 0.08$	114.94 $\pm 4.85$	3.92 $\pm 0.80$	0.842
WAP	Al	3.69 $\pm 0.09$	99.7 $\pm 2.51$	15.79 $\pm 0.09$	0.931
WAP	Sb	0.41 $\pm 0.04$	50.45 $\pm 5.29$	0.32 $\pm 0.04$	0.980
<i>P. lanosa</i>	Sb	0.39 $\pm 0.06$	47.44 $\pm 3.75$	3.72 $\pm 0.08$	0.879
WAP	Zn	0.74 $\pm 0.05$	48.59 $\pm 3.52$	0.67 $\pm 0.08$	0.895
	Ni	0.62 $\pm 0.01$	36.47 $\pm 4.33$	2.02 $\pm 0.38$	0.699
	Al	2.24 $\pm 0.18$	60.46 $\pm 2.98$	64.11 $\pm 11.76$	0.867
WAP	Zn	0.54 $\pm 0.05$	35.27 $\pm 3.08$	0.98 $\pm 0.18$	0.908
	Ni	0.66 $\pm 0.04$	39.06 $\pm 2.32$	0.65 $\pm 0.06$	0.924
	Al	0.94 $\pm 0.08$	25.46 $\pm 2.17$	46.21 $\pm 12.63$	0.295
	Sb	0.14 $\pm 0.01$	16.63 $\pm 1.65$	3.75 $\pm 0.97$	0.657

The b values displayed in Table 3.2 indicate the affinity of the biomass for a given metal and the equilibrium constant of the reaction between active sites of the cell wall and the metal in solution (Romera et al., 2006). A biosorbent with a lower  $q_{max}$  and a

higher  $b$  should display superior performance over a biosorbent with a higher  $q_{max}$  and a lower  $b$ , especially in cases where the metal ion to be removed is at trace levels.

The Langmuir metal sorption capacity ( $q_{max}$ ) decreased in the following order: Zn(II)/WAP > Ni(II)/WAP > Al(III)/WAP > Sb(III)/WAP > Sb(III)/*P. lanosa*. Sorption intensity ( $b$ ) decreased in the order: Al(III)/WAP > Ni(II)/WAP > Sb(III)/*P. lanosa* > Zn(II)/WAP > Sb(III)/WAP. Sb(III) sorption by WAP and *P. lanosa* showed similar sorption capacity, however the sorption intensity was greater for *P. lanosa* ( $3.72 \pm 0.08$  L/mg) than for WAP ( $0.32 \pm 0.04$  L/mg), highlighting a greater affinity for the seaweed.

Table 3.3a Comparison of maximum observed uptake capacity values ( $q_{max}$ ) for WAP and *P. lanosa* for Zn(II), Ni(II), Al(III) and Sb(III), derived from Langmuir isotherms (BSR: Batch Stirred Reactor).

(a)

Adsorbent	Metals	$q_{max}$ (mmol/g)	Type of reactor
WAP	Ni	2.31	BSR
WAP	Zn	2.05	BSR
WAP	Al	3.69	BSR
WAP	Sb	0.41	BSR
<i>P. lanosa</i>		0.39	BSR

Table 3.3b Comparison of maximum uptake capacity values ( $q_{\max}$ ) for other biosorbents in different reactors (BSR: Batch Stirred Reactor, PBR: Packed Bed Reactor) (Lesmana et al., 2008).

(b)

Adsorbent	Metals	$q_{\max}$ values (mmol/g)	Type of reactor	References	
<i>Cassia fistula</i> biomass: - leaves - stems bark - pods bark	Ni	2.793	BSR	(Hanif et al., 2007)	
		2.937			
		3.341			
<i>Sargassum</i> sp.		0.61	BSR	(Sheng et al., 2004)	
<i>Ulva</i> sp.		0.47	BSR	(Lau et al., 2003; Sheng et al., 2004)	
<i>Gracilaria</i> sp.		0.28	BSR	(Lee and Suh, 2001)	
Formaldehyde reinforced <i>S. fluitans</i>		1.99	BSR	(Leusch et al., 1995)	
Glutaraldehyde reinforced <i>A. nodosum</i>		1.96	BSR	(Leusch et al., 1995)	
<i>Bacillus subtilis</i>		Zn	2.09	BSR	(Brierley et al., 1986)
Fungal biomass			1.50	BSR	(Brierley et al., 1986)
Palm tree leaves	0.225		BSR	(Al-Rub, 2006)	
Rice Bran	0.279		BSR	(Wang et al., 2006)	
Rice husk	0.211		PBR	(Mohan and Sreelakshmi, 2008)	
Wheat bran	0.239		BSR and PBR	(Dupont et al., 2005)	
<i>Sargassum</i> sp.	0.50		BSR	(Sheng et al., 2004)	
<i>Ulva</i> sp.	0.76		BSR	(Lau et al., 2003; Sheng et al., 2004)	
<i>Gracilaria</i> sp.	0.40		BSR	(Lee and Suh, 2001)	
Formaldehyde reinforced <i>S. fluitans</i>	1.36		BSR	(Leusch et al., 1995)	
Ca-loaded <i>S. fluitans</i>	Al	2.95	BSR	(Lee and Suh, 2001)	
NaOH-treated <i>S. fluitans</i>		3.740	BSR	(Lee and Volesky, 1999)	

Tables 3.3a and 3.3b show that  $q_{max}$  values for WAP were greater, in general, than conventional seaweeds for Zn(II), Ni(II) and Al(III). However,  $q_{max}$  values for chemically modified *S. fluitans* were found to be higher or similar to WAP for Al(III) uptake (Lee and Volesky, 1999). The microorganism *Bacillus subtilis* was also shown to be very efficient for Zn(II) uptake, with a  $q_{max}$  value of 2.09 (Brierley et al., 1986) comparable to the uptake capacity of WAP. The same trend was observed with the utilisation of *Cassia fistula* biomass for Ni(II) uptake which showed similar  $q_{max}$  values to WAP (Hanif et al., 2007).

Maximum uptake capacity values for Sb(III) sorption by both WAP and *P. lanosa* were very similar (0.41 and 0.39 mmol g<sup>-1</sup> respectively). However, as shown in Table 3.2, the sorption intensity (b) was very low for WAP (0.32 ± 0.04 L mg<sup>-1</sup>) as opposed to *P. lanosa* (3.72 ± 0.08 L mg<sup>-1</sup>). No comparison was possible for  $q_{max}$  values for Sb(III) with other biosorbents due to the lack of the data in the literature.

The differences in metal sorption by different species of macroalgae may be due to the difference in composition, as well as the involvement of different functional groups (Sheng et al., 2004). For example the cell wall of brown algae contains alginate, fucoidan and cellulose. This mixture of polysaccharides in brown algae was shown to be very effective in metal binding (Fourest et al., 1996; Fourest and Volesky, 1996). In contrast, the red and green algae contain only pectic substances and cellulose. The high  $q_{max}$  values observed for WAP may result from the processing of the waste. The *Ascophyllum nodosum* is put through a series of cold extraction processes (see Section 1.2.4) which may lead to the purification and concentration of binding sites at the surface of the biomass.

### 3.5 Conclusions

The Langmuir, Freundlich and combined Langmuir-Freundlich binding isotherms were compared for Ni(II), Zn(II), Al(III) and Sb(III) removal by WAP and Sb(III) removal by *P. lanosa*, in single and in multi-metal solutions. The Langmuir isotherm was shown to model the experimental data very closely, with correlation coefficients greater than 0.9. High  $q_{max}$  values were obtained for Zn(II) and Ni(II) sorption by WAP, with 134.05 ± 6.47 and 114.94 ± 4.85 mg g<sup>-1</sup> respectively. Lower  $q_{max}$  values were obtained for Al(III)

and Sb(III), with  $99.7 \pm 2.51$  and  $50.45 \text{ mg g}^{-1}$  respectively. *P. lanosa* displayed a maximum sorption capacity of  $47.44 \pm 3.75 \text{ mg g}^{-1}$  for Sb(III). However, the affinity coefficient (b) was much higher for *P. lanosa* than WAP indicating that *P. lanosa* is far more efficient at Sb(III) removal than WAP. When using multi-element solutions, the  $q_{\text{max}}$  values decreased dramatically, indicating competition among the combined metal ions for the binding sites.

Finally, comparing WAP sorption capacities with other research showed that WAP displayed higher  $q_{\text{max}}$  values than conventional seaweeds and was comparable to chemically-reinforced biomasses.

## **Chapter 4**

**Fixed bed sorption column for the removal of  
Nickel, Aluminium, Zinc and Antimony(III) by Waste  
*Ascophyllum* Product (WAP) and *Polysiphonia lanosa*  
immobilised with Agar.**

## 4.1 Introduction

As outlined in Chapter 2, dried biomass of seaweed can be used as a sustainable, low-cost and reusable biosorbent for a range of metals. The screening of various seaweed species and a waste product resulting from the processing of *Ascophyllum nodosum* (WAP) (Chapter 2) led to the selection of dried biomass of WAP and *Polysiphonia lanosa* for the fixed-bed column studies.

Immobilisation of the biomass is necessary in this study in order to produce a biosorbent that is stable and suited for use in the column. When reduced to a powder form and entrapped in an immobilising agent (agar or carrageenan), a porous sorbent is produced that can be used in a continuous flow column. Investigations into the immobilisation of WAP and *P. lanosa* particles ( $\leq 850 \mu\text{m}$ ) using different immobilising agents (e.g. agar, alginate and carrageenan) have been carried-out at the Estuarine Research Group (ERG) (Walsh, 2008). The most efficient metal removals were obtained using blocks composed of the following proportions: 7.5%:5% WAP:agar. The same ratio was used for the manufacture of WAP and *Polysiphonia lanosa* blocks with agar in this study.

### 4.1.1 Fixed bed column sorption system

A fixed bed sorption column system was used in this research. Fig. 4.1 presents the principle of the fixed-bed sorption column for both sorption and desorption.

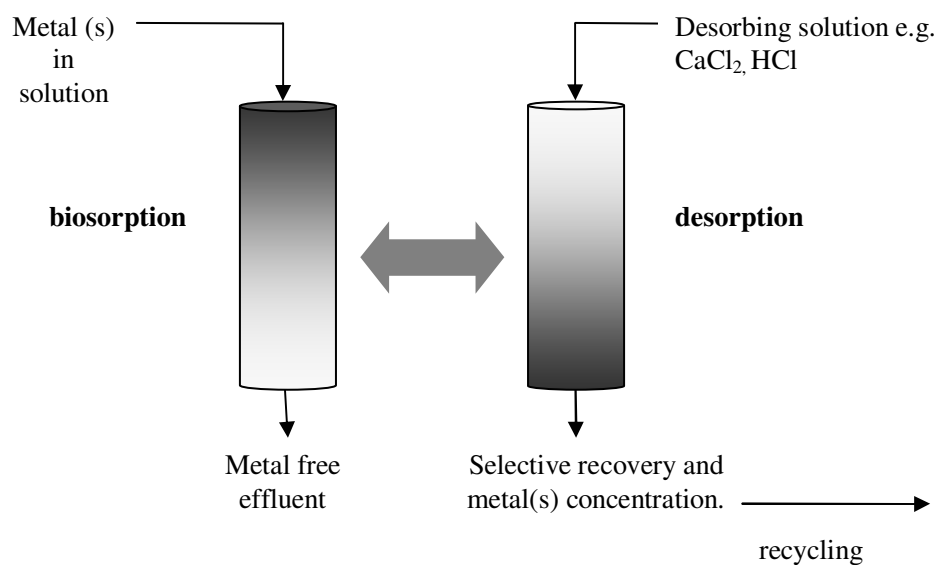


Fig. 4.1 Fixed bed column sorption system principle (biosorption and desorption) (Volesky, 2004)

## 4.2 Aims

- To investigate the efficiency of a laboratory fixed-bed sorption column for the removal of Zn(II), Ni(II), Al(III) and Sb(III) in single and combined metal aqueous solutions.
- To investigate any interactions (i.e. synergistic/antagonistic effects) when combining different metals in the same metal aqueous solution.
- To compare the efficiency of 5% agar/7.5% WAP and 5% agar/7.5% *P. lanosa* for the removal of Sb(III).

## 4.3 Methods

### Seaweed collection and preparation

Fresh samples of *Polysiphonia lanosa* were harvested from Fethard-on-Sea, Co. Wexford (Section 2.3), located in the south-east of Ireland, and were prepared as in Section 2.3.

The Waste *Ascophyllum* Product (or WAP) was supplied by “Oilean Glas Teo” (OGT) (Ballymoon Industrial Estate, Kilcar, Co. Donegal, Ireland), and was prepared as in Section 2.3.

## Chemicals

- 1000mg L<sup>-1</sup> Sb(III) as Sb<sub>2</sub>O<sub>3</sub> (analytical grade), Cu(II), Zn(II) and Al(III) - Sigma-Aldrich Ltd., Dublin, Ireland.
- Sodium Hydroxide (solid) - Ridel de Haën, Germany.
- Sodium Chloride (solid) - Ridel de Haën, Germany.
- Hydrochloric Acid (37%) - LabScan Ltd., Dublin, Ireland.
- Nitric Acid (69%) – Sigma-Aldrich Ltd, Dublin, Ireland.
- Agar (OXOID LP0011 agar bacteriological No. 1).

## Instrumentation

- Varian 710-ES ICP Optical Emission Spectrometer with auto-sampler

## Immobilised biosorbent preparation

The method used for biomass preparation was as follows: 15 g of dried WAP ( $\leq 850 \mu\text{m}$  in size) was weighed into a 250 mL conical flask. 10 g of agar was added and mixed with the WAP. 200 mL of distilled water was added to the flask and the WAP/agar solution carefully mixed to obtain a homogenous solution. The solution was autoclaved, poured into small plastic trays and allowed to dry in a cold chamber at 4°C for 20 min. Once solidified, the blocks were cut to equal sizes (6 x 10x 15mm) and dried at 60°C for 24 hours (Fig. 4.2).

The same protocol was used to produce *Polysiphonia lanosa* and agar blocks (7.5%:5% *P. lanosa*:agar).

Controls, using agar only, were prepared in the same manner to investigate metal removal by the agar.



Fig. 4.2 Image of dried blocks of WAP immobilised in agar.

### Sorption column studies

A laboratory scale fixed-bed sorption column was previously developed by the ERG and tested for the removal of Cu, Pb and Cr(III) (Fig. 4.3) (Walsh, 2008).

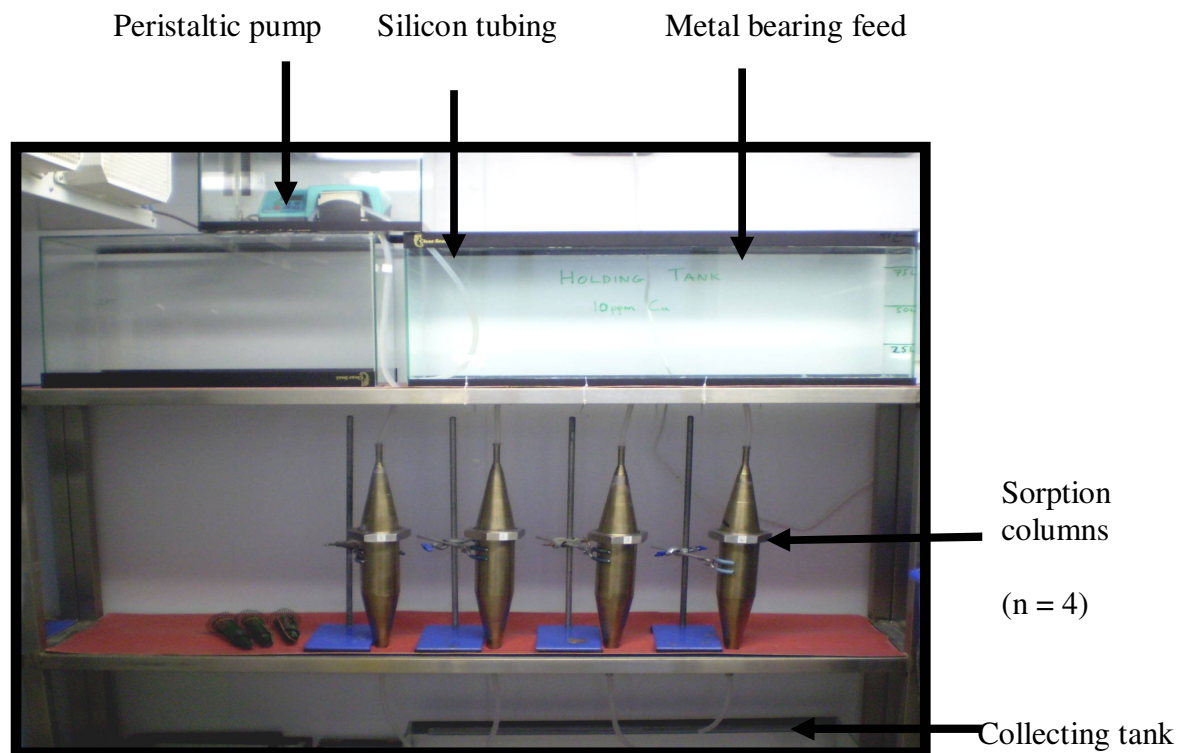


Fig. 4.3 Image of the fixed bed sorption columns. The columns are connected in parallel.

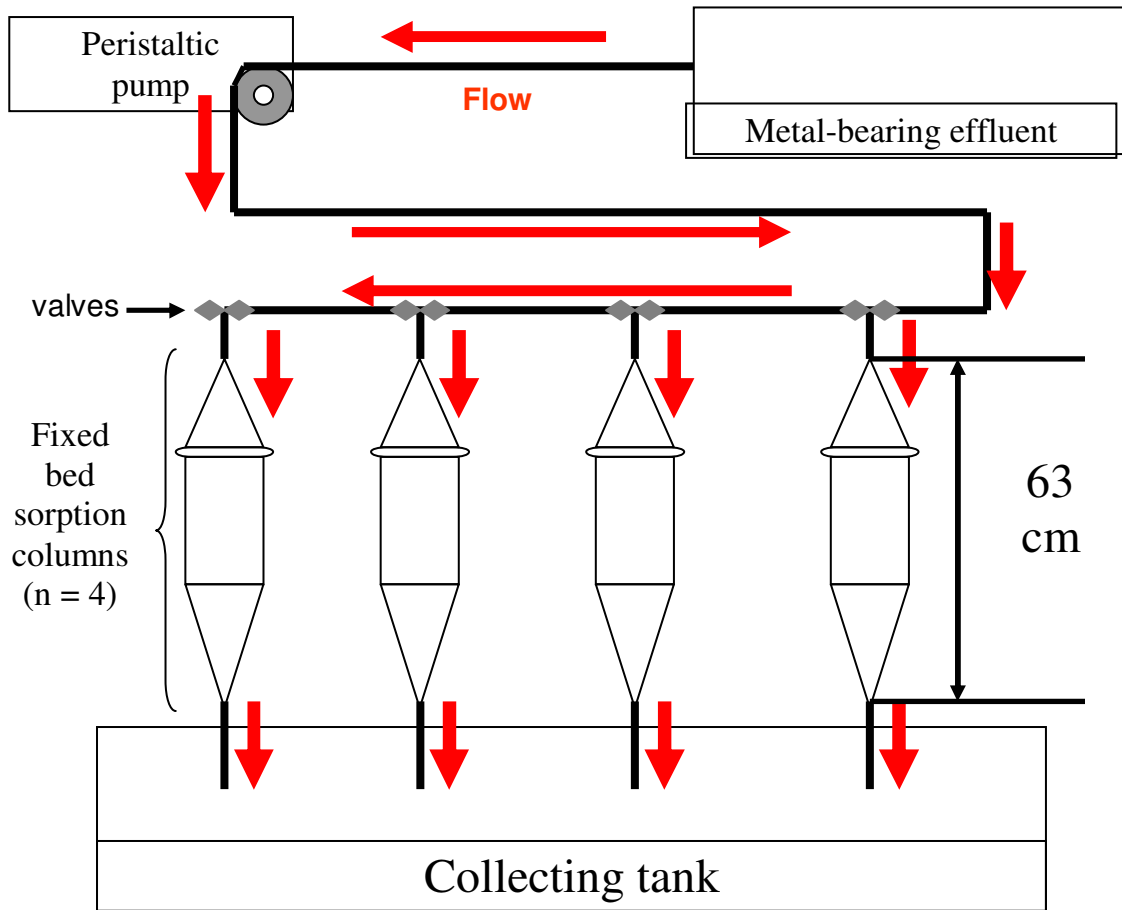


Fig. 4.4 Schematic representation of the fixed bed sorption columns.

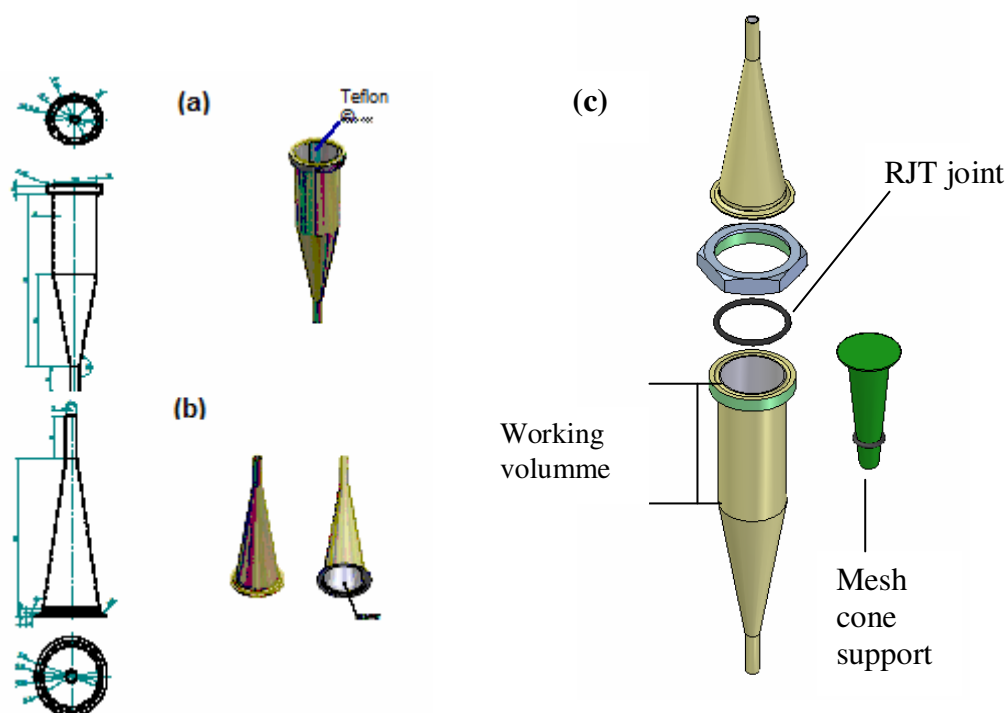


Fig. 4.5 CAD drawings of the sorption columns (a) Bottom section, (b) Top Section and (c) Exploded view of the completed column (Walsh, 2008).

The bisorption column design was as follows (Figs. 4.4-4.5):

- Stainless steel column with PTFE (Teflon) coated interior.
- Two sections coupled by RJT joint.
- Total height of 63cm.
- Cylinder diameter of 7.2cm.
- Working height of 16cm
- Working volume of 638 cm<sup>3</sup>.

Prior to utilisation, the biosorbents blocks were soaked in distilled water for 2 hours to allow expansion. The blocks were filled into the column up to the top of the working volume, supported on a plastic mesh cone in order to avoid any blockage of the column. A flow rate of 25mL min<sup>-1</sup> of 10 mg L<sup>-1</sup> metal bearing feed for 3 hours was employed. Samples of effluent were taken every 2 minutes for the first 10 minutes and then every 15 minutes until the end of the experiment (3 hours). Single and combined metal solution of Zn(II), Al(III), Ni(II) and Sb(III) were examined. Control runs, using blocks containing only agar, were also performed.

## 4.4 Statistical analysis

The statistical analysis included an investigation of time/treatment interaction effects. One-way ANOVA was carried out for single metal solutions and two-way mixed ANOVA (general linear model) was carried out for the treatment of multi-metal solutions. In all the ANOVA statistical tests, the level of significance was  $p < 0.05$ . Four replicates were run for all the experiments. Calculations were carried-out using SPSS 15 (SPSS, Inc). The null hypothesis ( $H_0$ ) for the one-way ANOVA was that there were no significant differences ( $p < 0.05$ ) between the metal concentrations at the different time intervals. For the two-way mixed ANOVA the null hypothesis ( $H_0$ ) was that the error covariance matrix of the orthonormalised transformed dependent variables was proportional to an identity matrix. Sig.  $> 0.05$  and sphericity can be assumed.

## 4.5 Results and Discussion

### 4.5.1 Fixed bed sorption studies using agar-only blocks – Control runs

#### 4.5.1.1 3 hour study of zinc removal by agar blocks in a fixed bed sorption column

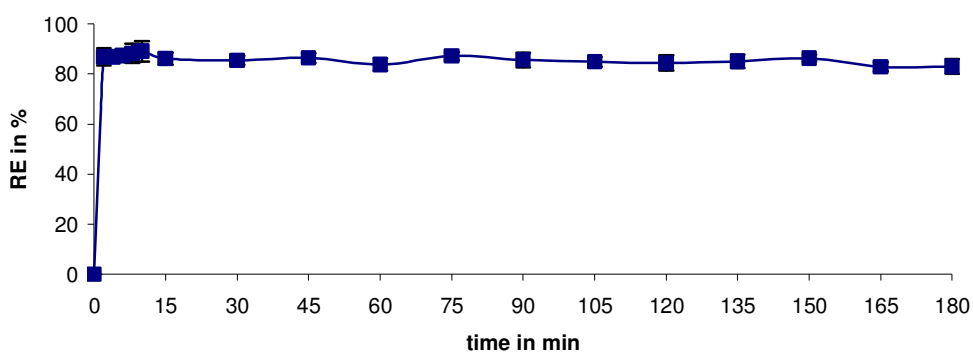


Fig. 4.6 Zinc removal in a single metal system ( $10 \text{ mg L}^{-1}$ ) by agar blocks. ( $\pm 95\%$  confidence intervals,  $n = 4$ ).

Fig. 4.6 shows that agar removed most of the Zn(II), with a maximum RE of 89% within 10 min. The removal of Zn(II) decreased slowly over the subsequent 3 hours to reach an RE of 83% at the end of the experiment.

Statistical analysis:

Table 4.1 One-Way ANOVA analysis for Zn(II) removal using a fixed bed sorption column with agar blocks.

**ANOVA**

Zinc

	Sum of Squares	df	Mean Square	F	Sig.
Between Groups	28032,000	17	1648,941	189,655	,000
Within Groups	469,500	54	8,694		
Total	28501,500	71			

There were significant differences ( $p < 0.05$ ) between Zn(II) REs at the different time intervals.

**4.5.1.2 3 hour study of nickel removal by agar blocks in a fixed bed sorption column**

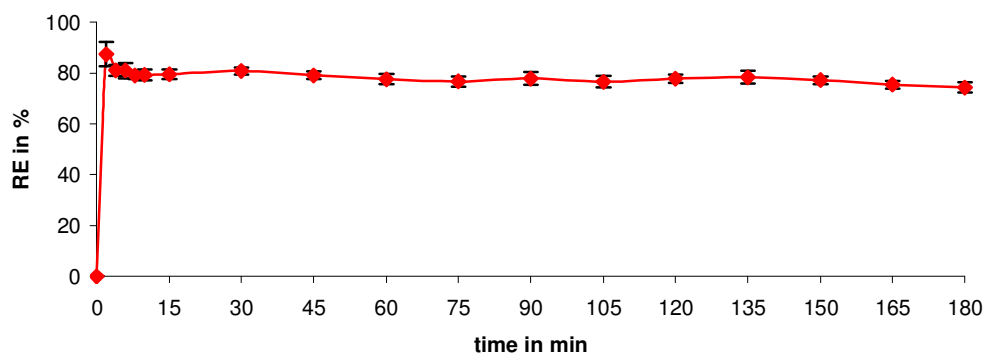


Fig. 4.7 Nickel removal in a single metal system ( $10 \text{ mg L}^{-1}$ ) by agar blocks. ( $\pm 95\%$  confidence intervals,  $n = 4$ ).

Fig. 4.7 shows that agar removed most of the Ni(II), with a maximum RE of 87% within 2 min. The removal of Ni(II) decreased slowly over the subsequent 3 hours to reach an RE of 74% at the end of the experiment.

Statistical analysis:

Table 4.2 One-Way ANOVA analysis for Ni(II) removal using a fixed bed sorption column with agar blocks.

**ANOVA**

Nickel

	Sum of Squares	df	Mean Square	F	Sig.
Between Groups	24007,403	17	1412,200	191,485	,000
Within Groups	398,250	54	7,375		
Total	24405,653	71			

There were significant differences ( $p < 0.05$ ) between Ni(II) REs at the different time intervals.

**4.5.1.3 3 hour study of aluminium removal by agar blocks in a fixed bed sorption column**

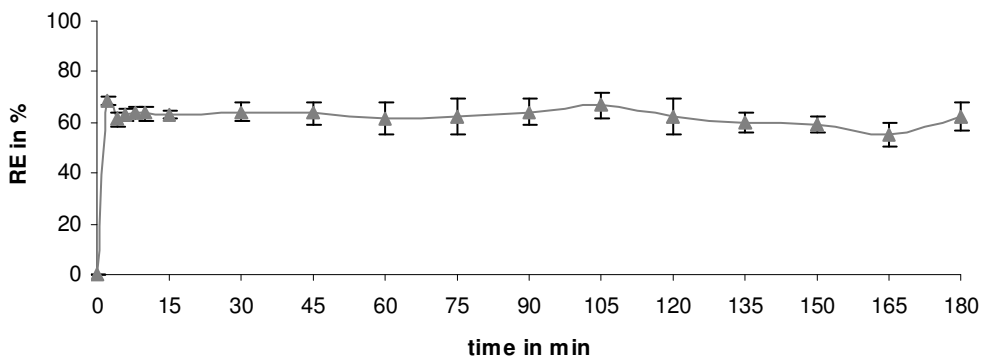


Fig. 4.8 Aluminium removal in a single metal system ( $10 \text{ mg L}^{-1}$ ) by agar blocks. ( $\pm$  95% confidence intervals,  $n = 4$ ).

Fig. 4.8 shows that agar removed Al(III), with a maximum RE of 68% within 2 min. The removal of Al(III) decreased slowly over the subsequent 3 hours to reach an RE of 55% at the end of the experiment.

Statistical analysis:

Table 4.3 One-Way ANOVA analysis for Al(III) removal using a fixed bed sorption column with agar blocks.

**ANOVA**

Aluminium

	Sum of Squares	df	Mean Square	F	Sig.
Between Groups	15312,625	17	900,743	34,248	,000
Within Groups	1420,250	54	26,301		
Total	16732,875	71			

There were significant differences ( $p < 0.05$ ) between Al(III) REs at the different time intervals.

**4.5.1.4 3 hour study of antimony removal by agar blocks in a fixed bed sorption column**

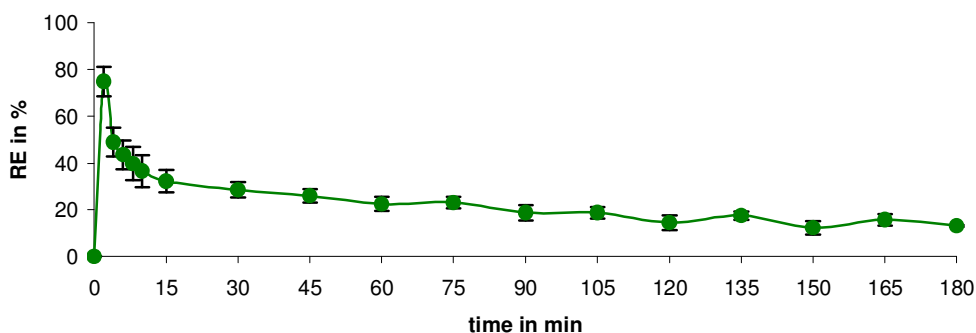


Fig. 4.9 Antimony removal in a single metal system ( $10 \text{ mg L}^{-1}$ ) by agar blocks. ( $\pm 95\%$  confidence intervals,  $n = 4$ ).

Fig. 4.9 shows that agar removed Sb(III), with a maximum RE of 75% within 2 min. The removal of Al(III) decreased sharply over the subsequent 3 hours to reach an RE of 13% at the end of the experiment.

Statistical analysis:

Table 4.4 One-Way ANOVA analysis for Sb(III) removal using a fixed bed sorption column with agar blocks.

**ANOVA**

Antimony

	Sum of Squares	df	Mean Square	F	Sig.
Between Groups	20168,000	17	1186,353	48,997	,000
Within Groups	1307,500	54	24,213		
Total	21475,500	71			

There were significant differences ( $p < 0.05$ ) between Sb(III) REs at the different time intervals.

**4.5.1.5 3 hour study of zinc, nickel and aluminium removal in a multi-metal system by agar blocks in a fixed bed sorption column**

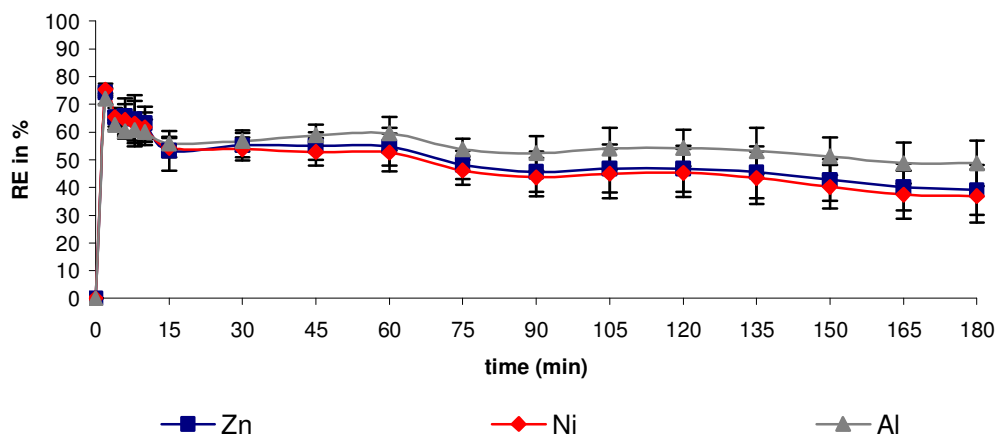


Fig. 4.10 Zinc, Nickel and Aluminium removal in a multi-metal system ( $10 \text{ mg L}^{-1}$  each) by agar blocks. ( $\pm 95\%$  confidence intervals,  $n = 4$ ).

Fig. 4.10 shows that agar was able to remove 72, 74 and 75% of Al(III), Zn(II) and Ni(II), respectively, in a multi-metal system within 2 min. RE decreased rapidly to reach minimum values of 49, 39 and 37% at the end of the experiment.

*Statistical analysis: (Two-Way Mixed ANOVA)*

Table 4.5 Multivariate tests from the general linear model

Multivariate Tests <sup>c</sup>						
Effect		Value	F	Hypothesis df	Error df	Sig.
Time	Pillai's Trace	. <sup>a</sup>	.	.	.	.
	Wilks' Lambda	. <sup>a</sup>	.	.	.	.
	Hotelling's Trace	. <sup>a</sup>	.	.	.	.
	Roy's Largest Root	. <sup>a</sup>	.	.	.	.
Metals	Pillai's Trace	,996	241,430 <sup>b</sup>	2,000	2,000	,004
	Wilks' Lambda	,004	241,430 <sup>b</sup>	2,000	2,000	,004
	Hotelling's Trace	241,430	241,430 <sup>b</sup>	2,000	2,000	,004
	Roy's Largest Root	241,430	241,430 <sup>b</sup>	2,000	2,000	,004
Time * Metals	Pillai's Trace	. <sup>a</sup>	.	.	.	.
	Wilks' Lambda	. <sup>a</sup>	.	.	.	.
	Hotelling's Trace	. <sup>a</sup>	.	.	.	.
	Roy's Largest Root	. <sup>a</sup>	.	.	.	.

a. Cannot produce multivariate test statistics because of insufficient residual degrees of freedom.

b. Exact statistic

c.

Design: Intercept

Within Subjects Design: Time+Metals+Time\*Metals

Table 4.5 displays four multivariate tests of significance of each effect in the model. No multivariate tests were calculated for time alone or for time\*metals due to insufficient residual degrees of freedom. The following tests will, however, bring more solid statistical conclusions (SPSS, 1999).

All multivariate tests for metals alone showed that there was a significant effect ( $p < 0.05$ ) of combining Zn(II), Ni(II) and Al(III) on their sorption by agar.

Table 4.6 Mauchly's test of sphericity from the general linear model

**Mauchly's Test of Sphericity<sup>b</sup>**

Measure: MEASURE\_1

Within Subjects Effect	Mauchly's W	Approx. Chi-Square	df	Sig.	Epsilon <sup>a</sup>		
					Greenhouse-Geisser	Huynh-Feldt	Lower-bound
Time	,000	.	152	.	,164	1,000	,059
Metals	,111	4,400	2	,111	,529	,576	,500
Time * Metals	,000	.	594	.	,065	,259	,029

Tests the null hypothesis that the error covariance matrix of the orthonormalized transformed dependent variables is proportional to an identity matrix.

a. May be used to adjust the degrees of freedom for the averaged tests of significance. Corrected tests are displayed in the Tests of Within-Subjects Effects table.

b.

Design: Intercept

Within Subjects Design: Time+Metals+Time\*Metals

Table 4.7 Test (a) within-subjects and (b) between-subjects effects.

**Tests of Within-Subjects Effects**

Measure: MEASURE\_1

Source		Type III Sum of Squares	df	Mean Square	F	Sig.
Time	Sphericity Assumed	48256,667	17	2838,627	18,700	,000
	Greenhouse-Geisser	48256,667	2,792	17283,070	18,700	,001
	Huynh-Feldt	48256,667	17,000	2838,627	18,700	,000
	Lower-bound	48256,667	1,000	48256,667	18,700	,023
Error(Time)	Sphericity Assumed	7741,519	51	151,794		
	Greenhouse-Geisser	7741,519	8,376	924,205		
	Huynh-Feldt	7741,519	51,000	151,794		
	Lower-bound	7741,519	3,000	2580,506		
Metals	Sphericity Assumed	742,583	2	371,292	122,691	,000
	Greenhouse-Geisser	742,583	1,059	701,436	122,691	,001
	Huynh-Feldt	742,583	1,151	645,116	122,691	,001
	Lower-bound	742,583	1,000	742,583	122,691	,002
Error(Metals)	Sphericity Assumed	18,157	6	3,026		
	Greenhouse-Geisser	18,157	3,176	5,717		
	Huynh-Feldt	18,157	3,453	5,258		
	Lower-bound	18,157	3,000	6,052		
Time * Metals	Sphericity Assumed	1351,083	34	39,738	13,096	,000
	Greenhouse-Geisser	1351,083	2,220	608,601	13,096	,004
	Huynh-Feldt	1351,083	8,820	153,181	13,096	,000
	Lower-bound	1351,083	1,000	1351,083	13,096	,036
Error(Time*Metals)	Sphericity Assumed	309,509	102	3,034		
	Greenhouse-Geisser	309,509	6,660	46,473		
	Huynh-Feldt	309,509	26,461	11,697		
	Lower-bound	309,509	3,000	103,170		

As the sphericity was assumed, only the “sphericity assumed” line was considered. As  $p < 0.05$  for time\*metals, it can be concluded that there was a significant effect of both time and combining Zn(II), Ni(II) and Al(III) in the same solution on their sorption by agar.

(b)

**Tests of Between-Subjects Effects**

Measure: MEASURE\_1

Transformed Variable: Average

Source	Type III Sum of Squares	df	Mean Square	F	Sig.
Intercept	560592,667	1	560592,667	2416,991	,000
Error	695,815	3	231,938		

The intercept represents the interaction of both time and metals alone and time\*metals. All the factors had a significant effect between them ( $p < 0.05$ ).

**4.5.2 Fixed bed sorption column studies using WAP/agar blocks and *P. lanosa*/agar blocks**

**4.5.2.1 3 hour study of zinc removal by WAP/agar blocks in a fixed bed sorption column**

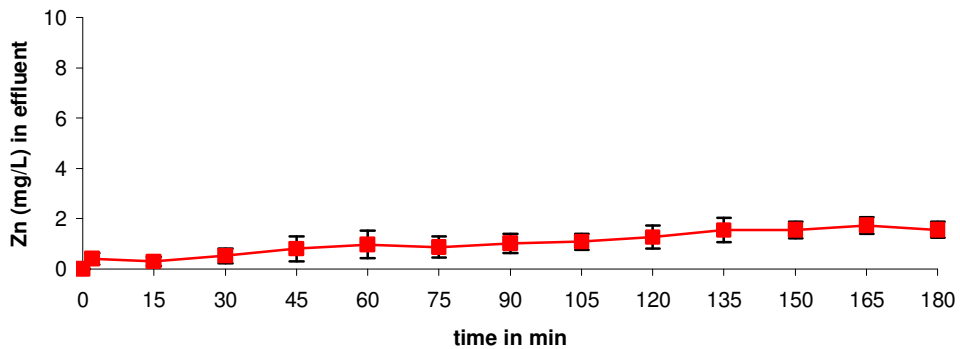


Fig. 4.11 Zinc removal in a single metal system ( $10 \text{ mg L}^{-1}$ ) by WAP (7.5%)/agar (5%) blocks ( $\pm 95\%$  confidence intervals,  $n = 4$ ).

Fig. 4.11 shows that  $9.6 \text{ mg L}^{-1}$  of Zn(II) was removed within 2 min. After 15 min, the Zn(II) concentration in the effluent started to increase slightly, reaching the final concentration of  $1.56 \text{ mg L}^{-1}$  after 3 hours.

Statistical analysis:

Table 4.8 One-Way ANOVA analysis for Zn(II) removal using a fixed bed sorption column with 5% agar/7.5% WAP sorbent.

ANOVA					
conc	Sum of Squares	df	Mean Square	F	Sig.
Between Groups	14,656	13	1,127	5,956	,000
Within Groups	7,949	42	,189		
Total	22,605	55			

There were significant differences ( $p < 0.05$ ) between Zn(II) concentrations at the different time intervals.

**4.5.2.2 3 hour study of nickel removal by WAP/agar blocks in a fixed bed sorption column**

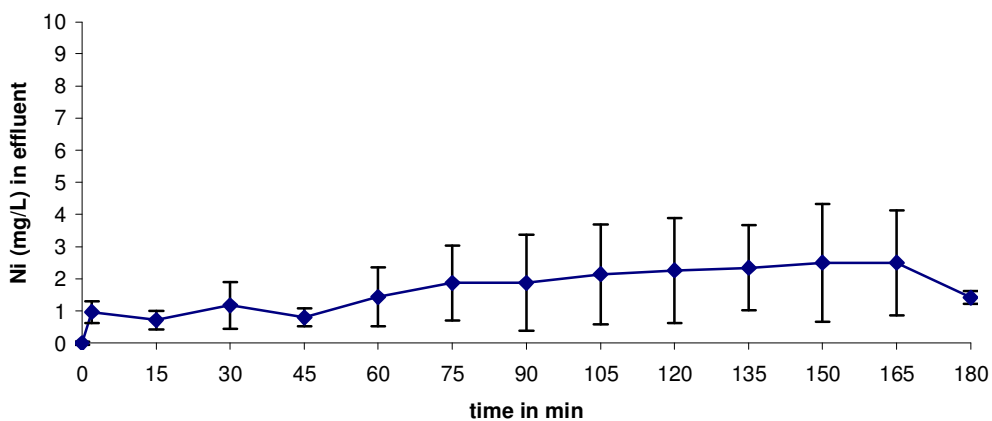


Fig. 4.12 Nickel removal in a single metal system ( $10 \text{ mg L}^{-1}$ ) by WAP (7.5%)/agar (5%) blocks ( $\pm 95\%$  confidence intervals,  $n = 4$ ).

Fig. 4.12 shows that  $9.8 \text{ mg L}^{-1}$  of the Ni(II) was removed in the first 2 min. The Ni(II) concentration in the effluent was then relatively stable until the 45 min time point, before starting to increase gradually to reach a Ni(II) removal concentration of  $8.2 \text{ mg L}^{-1}$  after 165 min.

Statistical analysis:

Table 4.9 One-Way ANOVA analysis for Ni(II) removal using a fixed bed sorption column with 5% agar/7.5% WAP sorbent.

**ANOVA**

concentrations

	Sum of Squares	df	Mean Square	F	Sig.
Between Groups	30,648	13	2,358	1,307	,247
Within Groups	75,749	42	1,804		
Total	106,397	55			

There were no significant differences ( $p > 0.05$ ) for Ni(II) concentrations at the different time intervals.

**4.5.2.3 3 hour study of aluminium removal by WAP/agar blocks in a fixed bed sorption column**

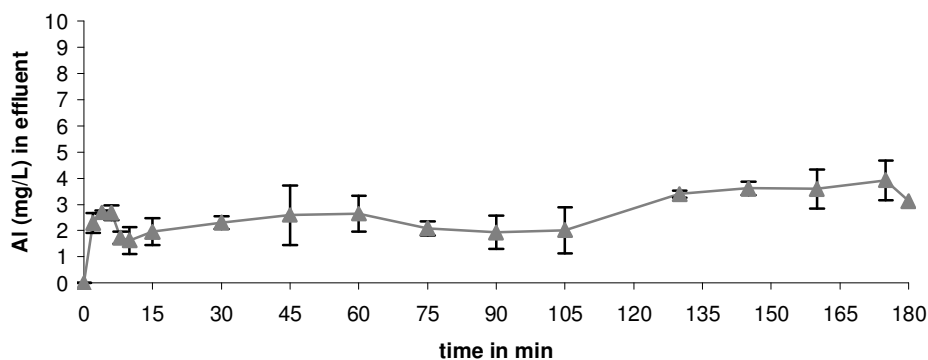


Fig. 4.13 Aluminium removal in a single metal system ( $10 \text{ mg L}^{-1}$ ) by WAP (7.5%)/agar (5%) blocks ( $\pm 95\%$  confidence intervals,  $n = 4$ ).

Fig. 4.13 shows that  $7.7 \text{ mg L}^{-1}$  of the Al(III) was removed in the first 2 min. Al(III) concentration fluctuated over the 3 hour experiment to reach a final concentration of  $3.94 \text{ mg L}^{-1}$  after 3 hours.

Statistical analysis:

Table 4.10 One-Way ANOVA analysis for Al(III) concentrations removal using a fixed bed sorption column with 5% agar/7.5% WAP sorbents.

**ANOVA**

concentration	Sum of Squares	df	Mean Square	F	Sig.
Between Groups	58,299	17	3,429	8,317	,000
Within Groups	22,266	54	,412		
Total	80,564	71			

There were significant differences ( $p < 0.05$ ) between Al(III) at the different time intervals.

**4.5.2.4 3 hour study of antimony removal by WAP/agar blocks in a fixed bed sorption column**

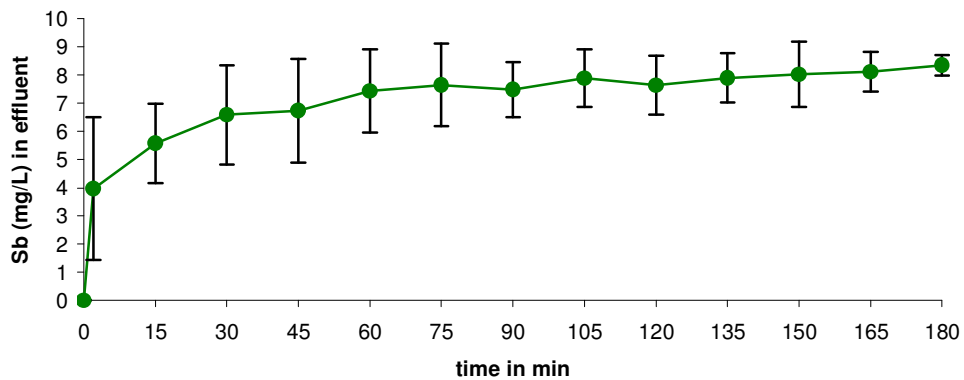


Fig. 4.14 Antimony removal in a single metal system ( $10 \text{ mg L}^{-1}$ ) by WAP (7.5%)/agar (5%) blocks ( $\pm 95\%$  confidence intervals,  $n = 4$ ).

Fig. 4.14 shows that only  $6 \text{ mg L}^{-1}$  of Sb(III) was removed in the first 2 min. Sb(III) concentration in the effluent fluctuated over the 3 hour experiment to reach a final concentration of  $8.35 \text{ mg L}^{-1}$ .

Statistical analysis:

Table 4.11 One-Way ANOVA analysis for Sb(III) removal using a fixed bed sorption column with 5% agar/7.5% WAP sorbent.

ANOVA					
concentrations					
	Sum of Squares	df	Mean Square	F	Sig.
Between Groups	263,680	13	20,283	8,163	,000
Within Groups	104,364	42	2,485		
Total	368,044	55			

There were significant differences ( $p < 0.05$ ) between Sb(III) concentrations for the different time intervals.

**4.5.2.5 3 hour study of antimony removal by *P. lanosa*/agar blocks in a fixed bed sorption column**

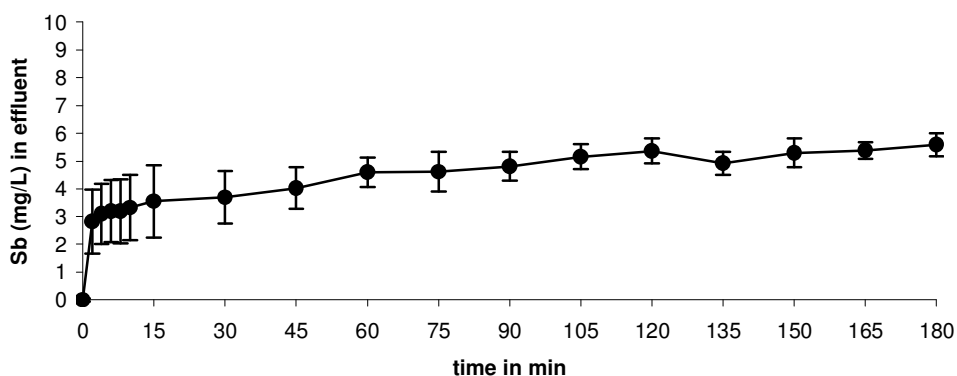


Fig. 4.15 Antimony removal in a single metal system ( $10 \text{ mg L}^{-1}$ ) by *P. lanosa* (7.5%)/agar (5%) blocks ( $\pm 95\%$  confidence intervals,  $n = 4$ ).

Fig. 4.15 shows that  $8.2 \text{ mg L}^{-1}$  of the Sb(III) was removed in the first 2 min. Sb concentration in the effluent fluctuated over the experiment to reach a final concentration of  $5.59 \text{ mg L}^{-1}$  after 3 hours.

Statistical analysis:

Table 4.12 One-Way ANOVA analysis for Sb(III) removal using a fixed bed sorption column with 5% agar/7.5% *P. lanosa* sorbent.

**ANOVA**

concentrations

	Sum of Squares	df	Mean Square	F	Sig.
Between Groups	127,314	17	7,489	8,184	,000
Within Groups	49,412	54	,915		
Total	176,726	71			

There were significant differences ( $p < 0.05$ ) between Sb(III) concentrations for the different time intervals.

**4.5.2.6 3 hour study of mixed metals (Zn(II), Ni(II) and Al(III)) removal by WAP/agar blocks in a fixed bed sorption column**

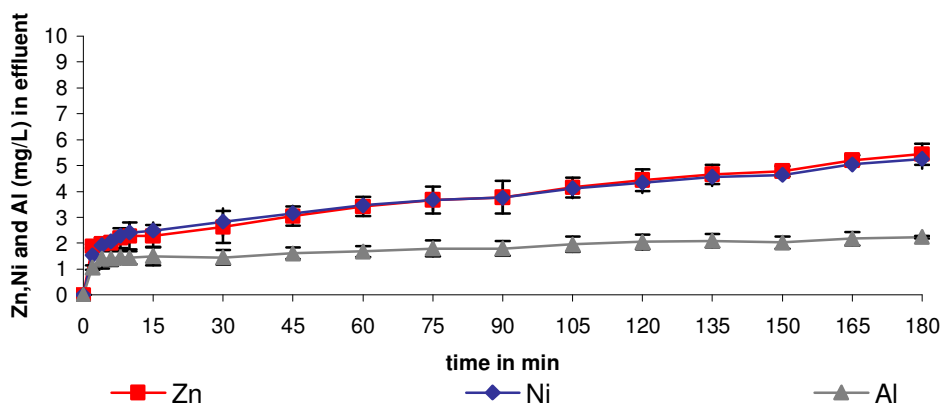


Fig. 4.16 Zinc, Nickel and Aluminium removal in a multi-metal system ( $10 \text{ mg L}^{-1}$  each) by WAP (7.5%)/agar (5%) blocks ( $\pm 95\%$  confidence intervals,  $n = 4$ ).

Fig. 4.16 shows that most of the Zn(II), Al(III) and Ni(II) was removed in the first 2 min, with concentrations of  $9.0 \text{ mg L}^{-1}$ ,  $9.3 \text{ mg L}^{-1}$  and  $9.1 \text{ mg L}^{-1}$  removed respectively for Zn(II), Ni(II) and Al(III). After 2 minutes, metals concentrations increased slowly in the effluent to reach final concentrations of  $5.44 \text{ mg L}^{-1}$  for Zn(II),  $2.24 \text{ mg L}^{-1}$  for Al(III) and  $5.26 \text{ mg L}^{-1}$  for Ni(II) after 3 hours.

*Statistical analysis: (Two-Way Mixed ANOVA)*

Table 4.13 Multivariate tests from the general linear model

Multivariate Tests <sup>c</sup>						
Effect		Value	F	Hypothesis df	Error df	Sig.
time	Pillai's Trace	. <sup>a</sup>	.	.	.	.
	Wilks' Lambda	. <sup>a</sup>	.	.	.	.
	Hotelling's Trace	. <sup>a</sup>	.	.	.	.
	Roy's Largest Root	. <sup>a</sup>	.	.	.	.
metals	Pillai's Trace	,999	755,223 <sup>b</sup>	2,000	2,000	,001
	Wilks' Lambda	,001	755,223 <sup>b</sup>	2,000	2,000	,001
	Hotelling's Trace	755,223	755,223 <sup>b</sup>	2,000	2,000	,001
	Roy's Largest Root	755,223	755,223 <sup>b</sup>	2,000	2,000	,001
time * metals	Pillai's Trace	. <sup>a</sup>	.	.	.	.
	Wilks' Lambda	. <sup>a</sup>	.	.	.	.
	Hotelling's Trace	. <sup>a</sup>	.	.	.	.
	Roy's Largest Root	. <sup>a</sup>	.	.	.	.

a. Cannot produce multivariate test statistics because of insufficient residual degrees of freedom.

b. Exact statistic

c.

Design: Intercept

Within Subjects Design: time+metals+time\*metals

Table 4.13 displays four multivariate tests of significance of each effect in the model. No multivariate tests were calculated for time alone or for time\*metals due to insufficient residual degrees of freedom. The following tests will, however, bring more solid statistical conclusions.

All multivariate tests for metals alone showed that there was a significant effect ( $p < 0.05$ ) of combining Zn(II), Ni(II) and Al(III) on their sorption by 5% agar/7.5% WAP.

Table 4.14 Mauchly's test of sphericity from the general linear model.

**Mauchly's Test of Sphericity<sup>b</sup>**

Measure: conc

Within Subjects Effect	Mauchly's W	Approx. Chi-Square	df	Sig.	Epsilon <sup>a</sup>		
					Greenhouse-Geisser	Huynh-Feldt	Lower-bound
time	,000	.	152	.	,143	,813	,059
metals	,421	1,730	2	,421	,633	,885	,500
time * metals	,000	.	594	.	,078	,741	,029

Tests the null hypothesis that the error covariance matrix of the orthonormalized transformed dependent variables is proportional to an identity matrix.

a. May be used to adjust the degrees of freedom for the averaged tests of significance. Corrected tests are displayed in the Tests of Within-Subjects Effects table.

b.  
Design: Intercept  
Within Subjects Design: time+metals+time\*metals

Table 4.15 Tests of (a) within-subjects effects and (b) between-subjects effects.

**(a) Tests of Within-Subjects Effects**

Measure: conc

Source		Type III Sum of Squares	df	Mean Square	F	Sig.
time	Sphericity Assumed	247,756	17	14,574	43,046	,000
	Greenhouse-Geisser	247,756	2,439	101,597	43,046	,000
	Huynh-Feldt	247,756	13,813	17,936	43,046	,000
	Lower-bound	247,756	1,000	247,756	43,046	,007
Error(time)	Sphericity Assumed	17,267	51	,339		
	Greenhouse-Geisser	17,267	7,316	2,360		
	Huynh-Feldt	17,267	41,439	,417		
	Lower-bound	17,267	3,000	5,756		
metals	Sphericity Assumed	121,587	2	60,793	1964,478	,000
	Greenhouse-Geisser	121,587	1,267	95,967	1964,478	,000
	Huynh-Feldt	121,587	1,769	68,719	1964,478	,000
	Lower-bound	121,587	1,000	121,587	1964,478	,000
Error(metals)	Sphericity Assumed	,186	6	,031		
	Greenhouse-Geisser	,186	3,800	,049		
	Huynh-Feldt	,186	5,308	,035		
	Lower-bound	,186	3,000	,062		
time * metals	Sphericity Assumed	39,783	34	1,170	17,135	,000
	Greenhouse-Geisser	39,783	2,657	14,970	17,135	,001
	Huynh-Feldt	39,783	25,190	1,579	17,135	,000
	Lower-bound	39,783	1,000	39,783	17,135	,026
Error(time*metals)	Sphericity Assumed	6,965	102	,068		
	Greenhouse-Geisser	6,965	7,972	,874		
	Huynh-Feldt	6,965	75,570	,092		
	Lower-bound	6,965	3,000	2,322		

As the sphericity was assumed, only the "sphericity assumed" line was considered. As  $p < 0.05$  for time\*metals, it can be concluded that there was a significant effect of both

time and combining Zn(II), Ni(II) and Al(III) in the same solution on their sorption by 5% agar/7.5% WAP.

(b) **Tests of Between-Subjects Effects**

Measure: conc

Transformed Variable: Average

Source	Type III Sum of Squares	df	Mean Square	F	Sig.
Intercept	1547,614	1	1547,614	14042,530	,000
Error	,331	3	,110		

The intercept represents the interaction of both time and metals alone and time\*metals. All the factors had a significant effect between them ( $p < 0.05$ ).

**4.5.2.7 3 hour study of mixed metals (Zn(II), Ni(II), Al(III) and Sb(III)) removal by WAP/agar blocks in a fixed bed sorption column**

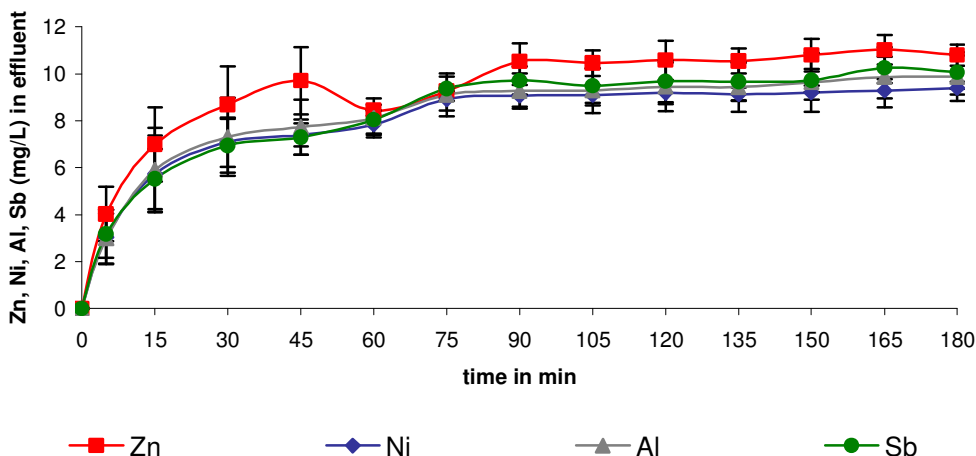


Fig. 4.17 Zinc, Nickel, Aluminium and Antimony removal in a multi-metal system ( $10 \text{ mg L}^{-1}$  each) by WAP (7.5%)/agar (5%) blocks ( $\pm 95\%$  confidence intervals,  $n = 4$ ).

Fig. 4.17 shows that most of the Zn(II), Ni(II), Al(III) and Sb(III) was removed in the first 2 min with concentrations of  $7.7 \text{ mg L}^{-1}$ ,  $7.7 \text{ mg L}^{-1}$ ,  $7.1 \text{ mg L}^{-1}$  and  $6.4 \text{ mg L}^{-1}$  removed for Zn(II), Ni(II), Al(III) and Sb(III) respectively. Thereafter metal

concentrations increased sharply in the effluent to reach final concentrations of 10.80 mg L<sup>-1</sup> for Zn(II), 9.39 mg L<sup>-1</sup> for Ni(II), 9.87 mg L<sup>-1</sup> for Al(III) and 10.07 mg L<sup>-1</sup> for Sb(III) and after 3 hours.

*Statistical analysis (General Linear Model):*

Table 4.16 Multivariate tests from the general linear model.

Multivariate Tests <sup>c</sup>						
Effect		Value	F	Hypothesis df	Error df	Sig.
time	Pillai's Trace	. <sup>a</sup>	.	.	.	.
	Wilks' Lambda	. <sup>a</sup>	.	.	.	.
	Hotelling's Trace	. <sup>a</sup>	.	.	.	.
	Roy's Largest Root	. <sup>a</sup>	.	.	.	.
metals	Pillai's Trace	,993	47,175 <sup>b</sup>	3,000	1,000	,107
	Wilks' Lambda	,007	47,175 <sup>b</sup>	3,000	1,000	,107
	Hotelling's Trace	141,526	47,175 <sup>b</sup>	3,000	1,000	,107
	Roy's Largest Root	141,526	47,175 <sup>b</sup>	3,000	1,000	,107
time * metals	Pillai's Trace	. <sup>a</sup>	.	.	.	.
	Wilks' Lambda	. <sup>a</sup>	.	.	.	.
	Hotelling's Trace	. <sup>a</sup>	.	.	.	.
	Roy's Largest Root	. <sup>a</sup>	.	.	.	.

a. Cannot produce multivariate test statistics because of insufficient residual degrees of freedom

b. Exact statistic

c.

Design: Intercept

Within Subjects Design: time+metals+time\*metals

Table 4.16 displays four multivariate tests of significance of each effect in the model. No multivariate tests were calculated for time alone or for time\*metals due to insufficient residual degrees of freedom. The following tests will, however, bring more solid statistical conclusions.

All multivariate tests for metals alone showed that Sig. < 0.05, suggesting a significant effect of combining Zn(II), Ni(II), Al(III) and Sb(III) on their sorption by 5% agar/7.5% WAP.

Table 4.17 Mauchly's test of sphericity from the general linear model.

**Mauchly's Test of Sphericity<sup>b</sup>**

Measure: conc

Within Subjects Effect	Mauchly's W	Approx. Chi-Square	df	Sig.	Epsilon <sup>a</sup>		
					Greenhouse-Geisser	Huynh-Feldt	Lower-bound
time	,000	.	90	.	,191	1,000	,077
metals	,016	7,073	5	,279	,370	,431	,333
time * metals	,000	.	779	.	,066	,510	,026

Tests the null hypothesis that the error covariance matrix of the orthonormalized transformed dependent variables is proportional to an identity matrix.

a. May be used to adjust the degrees of freedom for the averaged tests of significance. Corrected tests are displayed in the Tests of Within-Subjects Effects table.

b.

Design: Intercept  
 Within Subjects Design: time+metals+time\*metals

Table 4.18 Tests of (a) within-subjects effects and (b) between-subjects effects.

**(a) Tests of Within-Subjects Effects**

Measure: conc

Source		Type III Sum of Squares	df	Mean Square	F	Sig.
time	Sphericity Assumed	1826,048	13	140,465	103,744	,000
	Greenhouse-Geisser	1826,048	2,477	737,298	103,744	,000
	Huynh-Feldt	1826,048	13,000	140,465	103,744	,000
	Lower-bound	1826,048	1,000	1826,048	103,744	,002
Error(time)	Sphericity Assumed	52,805	39	1,354		
	Greenhouse-Geisser	52,805	7,430	7,107		
	Huynh-Feldt	52,805	39,000	1,354		
	Lower-bound	52,805	3,000	17,602		
metals	Sphericity Assumed	48,006	3	16,002	11,910	,002
	Greenhouse-Geisser	48,006	1,111	43,211	11,910	,034
	Huynh-Feldt	48,006	1,294	37,107	11,910	,025
	Lower-bound	48,006	1,000	48,006	11,910	,041
Error(metals)	Sphericity Assumed	12,092	9	1,344		
	Greenhouse-Geisser	12,092	3,333	3,628		
	Huynh-Feldt	12,092	3,881	3,116		
	Lower-bound	12,092	3,000	4,031		
time * metals	Sphericity Assumed	16,686	39	,428	1,623	,025
	Greenhouse-Geisser	16,686	2,582	6,464	1,623	,261
	Huynh-Feldt	16,686	19,900	,839	1,623	,077
	Lower-bound	16,686	1,000	16,686	1,623	,292
Error(time*metals)	Sphericity Assumed	30,836	117	,264		
	Greenhouse-Geisser	30,836	7,745	3,982		
	Huynh-Feldt	30,836	59,699	,517		
	Lower-bound	30,836	3,000	10,279		

As the sphericity was assumed, only the "sphericity assumed" line was considered. As Sig. < 0.05 for time\*metals, it can be concluded that there was a significant effect of

both time and combining Zn(II), Ni(II), Al(III) and Sb(III) in the same solution on their sorption by 5% agar/7.5% WAP.

(b)

**Tests of Between-Subjects Effects**

Measure: conc

Transformed Variable: Average

Source	Type III Sum of Squares	df	Mean Square	F	Sig.
Intercept	14011,032	1	14011,032	464,489	,000
Error	90,493	3	30,164		

The intercept represents the interaction of both time and metals alone and time\*metals. All the factors had a significant effect ( $p < 0.05$ ) between them.

***Summary of results***

Table 4.19 shows the RE in % for the removal of Zn(II), Ni(II), Al(III) and Sb(III) by the fixed-bed sorption column using WAP/agar blocks, *P. lanosa*/agar blocks and agar only blocks. The results show the mean removal efficiencies over the 3 hour experimental period.

Table 4.19 Mean removal efficiencies (%) over 3 hours for WAP/agar, *P. lanosa*/agar and agar only blocks (fixed bed columns, n = 4).

Metal	Mean RE in %						
	WAP/agar			<i>P. lanosa</i> /agar	agar		
Ni	90 ± 3			*	79 ± 2.13		
Zn	90 ± 2			*	86 ± 0.80		
Al	74 ± 3			*	63 ± 4.13		
Sb	28 ± 6			67 ± 4	29 ± 4		
Zn/Ni/Al	75 ± 6	72 ± 5	87 ± 2	*	53 ± 7	52 ± 6	57 ± 5
Zn/Ni/Al/Sb	28 ± 10	17 ± 10	24 ± 10	16 ± 11	*	*	

\* not assessed.

Metal biosorption using fixed bed columns has been carried-out by various researchers, commonly using *Sargassum sp.* as the biosorbent (Kratochvil and Volesky, 2000; De França et al., 2002; Cossich, 2004; Vijayaraghavan et al., 2005a; Lodeiro et al., 2006; Naja and Volesky, 2006a).

Table 4.19 shows the mean removal efficiencies obtained for single and combined metals in aqueous solution. Batch tests carried out previously in the research (Section 2.5) demonstrated that *P. lanosa* had poor sorptive properties for Ni(II), Zn(II) and Al(III). This seaweed species however demonstrated good sorptive properties for Sb(III). For this reason the *P. lanosa*/agar blocks were tested only for Sb(III) sorption in the fixed bed sorption columns. High removal efficiencies were obtained with the 7.5%WAP/5% agar blocks for all metals, with the following order observed: Ni(II) > Zn(II) > Al(III) > Sb(III). However, blocks made from 7.5% *P. lanosa*/5% agar showed a far higher affinity for Sb(III), with an RE of 67%, as compared with only 28% for WAP/agar blocks, over the 3 hours.

When treating combined metal solutions containing Sb(III), removal efficiencies were severely reduced and the order was altered as follows: Ni(II) > Al(III) > Zn(II) > Sb(III). However, treating a combined metal solution composed of Ni(II), Zn(II) and Al(III), with no Sb(III), led to higher REs of 72%, 75% and 87%, respectively. In this case, the ranking from the highest RE to the lowest was as following: Al(III) > Zn(II) > Ni(II). Sb(III), when combined with other metals in the same aqueous solution, appears to reduce the RE of the other metals. This indicates an antagonistic effect, and such an effect has been referred to by a number of authors for other metals (Kratochvil and Volesky, 2000; Andrade et al., 2006). The possible mechanisms of Sb(III) antagonism are discussed in more detail in Chapter 8.

Lee & Suh (2001) demonstrated that Al(III) interfered with the sorption of Zn(II). They found that Al(III) reduced the uptake of Pb(II), Cu(II), Zn(II) and Cd(II) by *Sargassum fluitans*. They hypothesised that the reduction in uptake results from the sequestration of Al in the biomass in the form of polynuclear aluminium species such as  $\{Al_6(OH)_{12}(H_2O)_{12}\}^{6+}$  and  $Al_{13}(OH)_{32}^{7+}$  and that these polymerised aluminium ions prevented other heavy metals from accessing the binding sites. However, aluminium antagonism was not observed in our study, and Al(III) showed a higher RE when combined with Ni(II) and Zn(II). This may indicate differences in the binding sites available within different seaweed species or seaweed by-products.

In all the sorption column studies, the maximum sorption of metals was achieved within the first 2 min. Thereafter uptake proceeded at a slower rate, corresponding to a gradual saturation of the sorbent. However, no final saturation was observed over the 3 hour period. The higher sorption rate at the beginning is probably due to the large availability of binding sites at the initial stage, which become progressively less available during the later stages of the sorption process (Senthilkumar et al., 2006).

Table 4.19 shows that agar alone had relatively high REs, with the following order: Zn(II) > Ni(II) > Al(III) > Sb(III). REs were however lower than when using WAP with agar as the immobilising agent. Agar was particularly poor at removing Sb(III), with a mean RE of only 29% as opposed to 67% with *P. lanosa* immobilised in agar. The

results show that agar plays a significant role in the high REs observed with WAP/agar blocks. However, such a role was not observed for the removal of Sb(III) by *P. lanosa*/agar blocks.

## 4.6 Conclusions

High removal efficiencies were observed for Ni(II), Zn(II) and Al(III) by WAP/agar in the fixed-bed sorption column studies. Metal sorption by agar was shown to play a significant role in these high REs. However, agar did not demonstrate any significant role in the high removal of Sb(III) by *P. lanosa*/agar blocks. Metal sorption was relatively fast and reached a maximum within 2 min for all biomasses examined. However, WAP/agar blocks did not effectively remove Sb(III) from single or combined aqueous solutions. *P. lanosa* displayed a relatively high removal efficiency for Sb(III) in a single Sb(III) aqueous solution. Sb(III) was shown to adversely affect the sorption of Ni(II), Zn(II) and Al(III) when combined in the same aqueous solution.

## **Chapter 5**

### **Investigation into ion exchange mechanism**

## **5.1 Introduction**

### **5.1.1 Ion exchange mechanism**

Many studies have been carried out into adsorption efficiencies or equilibrium uptake for biomasses (Holan and Volesky, 1994; Schiewer and Volesky, 1996; Da Costa and De Franca, 1997; Sag, 2001; Andrade et al., 2006; Al-Rub et al., 2006; Naja and Volesky, 2006a; Fagundes-Klen et al., 2007). However, little investigation has been carried out into the release of ions from biomass into solution (Crist et al., 1990; Crist et al., 1992; Crist et al., 1994; Lee and Volesky, 1997). In this chapter, the release of trace elements such as sodium, magnesium, calcium and potassium for a number of sorption studies was investigated.

## **5.2 Aims**

To investigate the ion exchange mechanism that occurs during metal uptake by seaweed biomass.

## **5.3 Methods**

During the metal sorption experiments carried out in Chapter 4, the effluent from each experiment was analysed using the ICP-OES for traces of  $\text{Ca}^{2+}$ ,  $\text{Mg}^{2+}$ ,  $\text{Na}^+$  and  $\text{K}^+$ .

### **Chemicals**

- 1000 mg L<sup>-1</sup> Ca as CaCO<sub>3</sub> (analytical grade) – Sigma-Aldrich Ltd, Dublin, Ireland
- 1000 mg L<sup>-1</sup> Mg (analytical grade) – Sigma-Aldrich Ltd, Dublin, Ireland
- 1000 mg L<sup>-1</sup> Na as NaNO<sub>3</sub> (analytical grade) – Sigma-Aldrich Ltd, Dublin, Ireland
- 1000 mg L<sup>-1</sup> K (analytical grade) – Sigma-Aldrich Ltd, Dublin, Ireland

## 5.4 Results and discussion

### 5.4.1 Trace element analysis during the removal of Zinc by WAP/agar blocks in a fixed bed sorption column

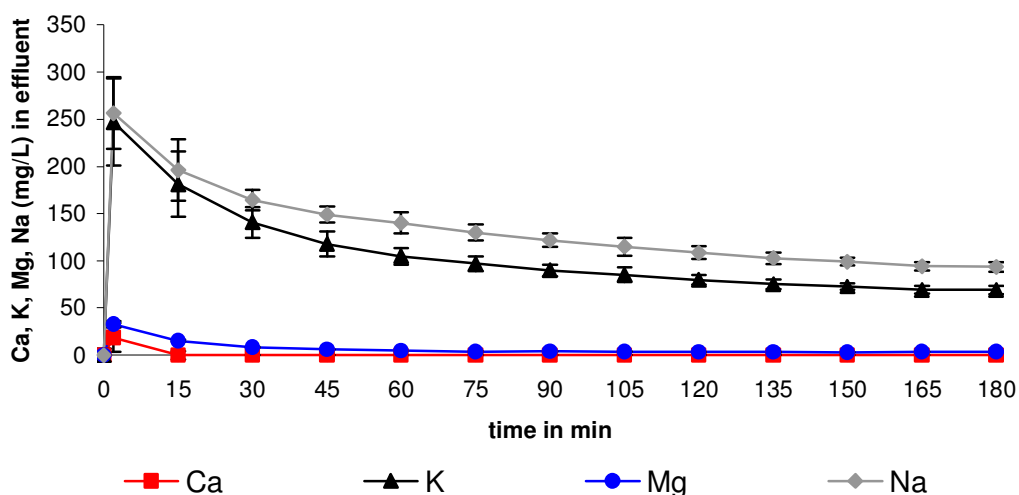


Fig. 5.1 Trace element analysis from fixed bed column studies with WAP/agar blocks. 10 mg L<sup>-1</sup> Zn(II) solution ( $\pm$  95% confidence intervals, n = 4).

Fig. 5.1 shows that a rapid release of Ca<sup>2+</sup>, Mg<sup>2+</sup>, Na<sup>+</sup> and K<sup>+</sup> occurred within 2 min, corresponding to the sorption of Zn(II) by the WAP/agar blocks. Na<sup>+</sup> and K<sup>+</sup> were the predominant elements, with respective concentrations of 256.63 mg L<sup>-1</sup> and 246.92 mg L<sup>-1</sup>. The release of Ca<sup>2+</sup> and Mg<sup>2+</sup> was lower, with respective concentrations of 18.76 mg L<sup>-1</sup> and 32.85 mg L<sup>-1</sup>. The concentration of all the trace elements in the effluent decreased quickly after 2 min to reach minimum values of 1.56 mg L<sup>-1</sup> for Ca<sup>2+</sup>, 3.62 mg L<sup>-1</sup> for Mg<sup>2+</sup>, 93.92 mg L<sup>-1</sup> for Na<sup>+</sup> and 68.97 mg L<sup>-1</sup> for K<sup>+</sup> after 3 hours.

#### 5.4.2 Trace element analysis during the removal of Nickel by WAP/agar blocks in a fixed bed sorption column

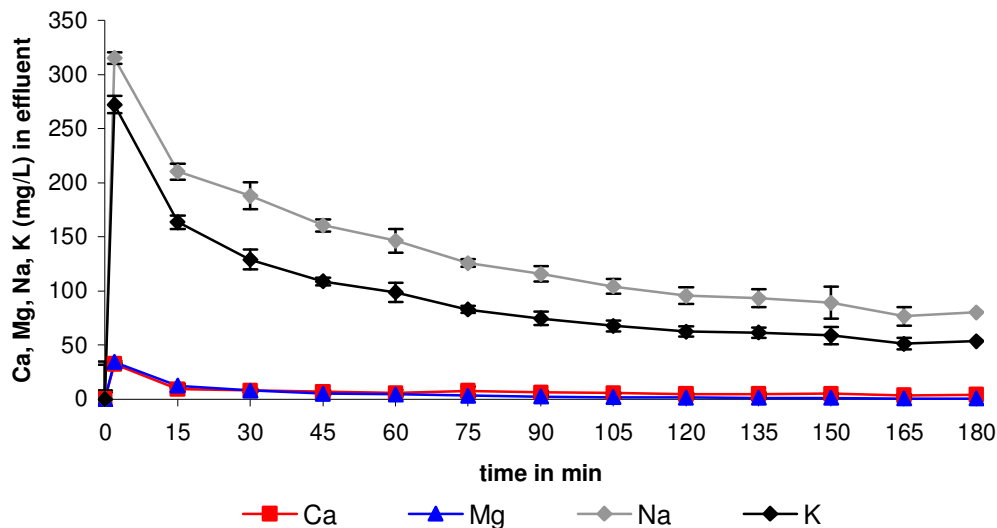


Fig. 5.2 Trace element analysis from fixed bed column studies with WAP/agar blocks. 10 mg L<sup>-1</sup> Ni(II) solution ( $\pm$  95% confidence intervals, n= 4).

Fig. 5.2 shows that a rapid release of Ca<sup>2+</sup>, Mg<sup>2+</sup>, Na<sup>+</sup> and K<sup>+</sup> occurred within 2 min, corresponding to the sorption of Ni(II) by the WAP/agar blocks. Na<sup>+</sup> and K<sup>+</sup> were the predominant elements, with respective concentrations of 315.41 mg L<sup>-1</sup> and 272.23 mg L<sup>-1</sup>. The release of Ca<sup>2+</sup> and Mg<sup>2+</sup> was lower, with respective concentrations of 32.50 mg L<sup>-1</sup> and 34.33 mg L<sup>-1</sup>. The concentration of all the trace elements in the effluent decreased quickly after 2 min, to reach minimum values of 4.05 mg L<sup>-1</sup> for Ca<sup>2+</sup>, 0.49 mg L<sup>-1</sup> for Mg<sup>2+</sup>, 80.14 mg L<sup>-1</sup> for Na<sup>+</sup> and 53.62 mg L<sup>-1</sup> for K<sup>+</sup> after 3 hours.

### 5.4.3 Trace element analysis during the removal of Aluminium by WAP/agar blocks in a fixed bed sorption column

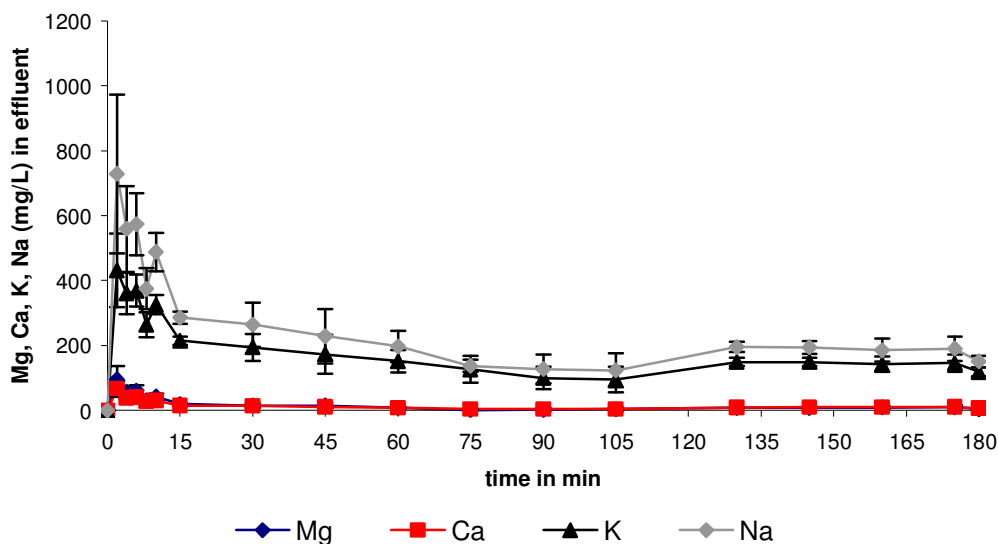


Fig. 5.3 Trace element analysis from fixed bed column studies with WAP/agar blocks. 10 mg L<sup>-1</sup> Al(III) solution ( $\pm$  95% confidence intervals, n= 4).

Fig. 5.3 shows that a rapid release of Ca<sup>2+</sup>, Mg<sup>2+</sup>, Na<sup>+</sup> and K<sup>+</sup> occurred within 2 min, corresponding to the sorption of Al(III) by the WAP/agar blocks. Na<sup>+</sup> and K<sup>+</sup> were the predominant elements, with respective concentrations of 728.67 mg L<sup>-1</sup> and 430.54 mg L<sup>-1</sup>. The release of Ca<sup>2+</sup> and Mg<sup>2+</sup> was lower, with respective concentrations of 66.68 mg L<sup>-1</sup> and 95.89 mg L<sup>-1</sup>. The concentration of all the trace elements in the effluent decreased quickly after 2 min, to reach minimum values of 6.50 mg L<sup>-1</sup> for Ca<sup>2+</sup>, 3.66 mg L<sup>-1</sup> for Mg<sup>2+</sup>, 150.93 mg L<sup>-1</sup> for Na<sup>+</sup> and 118.16 mg L<sup>-1</sup> for K<sup>+</sup> after 3 hours.

#### 5.4.4 Trace element analysis during the removal of Antimony by *P. lanosa*/agar blocks in a fixed-bed column

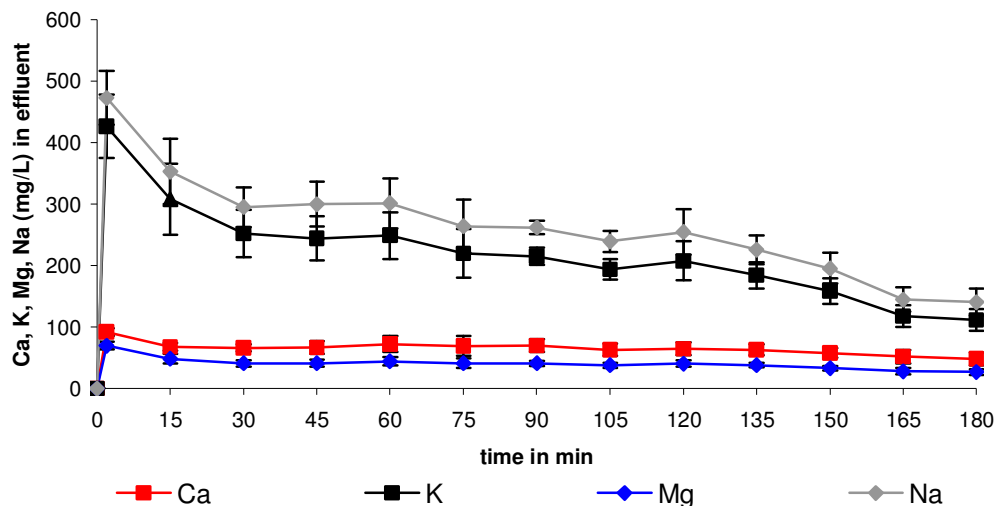


Fig. 5.4 Trace element analysis from fixed bed column studies with *P. lanosa*/agar blocks. 10 mg L<sup>-1</sup> Sb(III) solution ( $\pm$  95% confidence intervals, n= 4).

Fig. 5.4 shows that a rapid release of Ca<sup>2+</sup>, Mg<sup>2+</sup>, Na<sup>+</sup> and K<sup>+</sup> occurred within 2 min, corresponding to the sorption of Sb(III) by the *P. lanosa*/agar blocks. Na<sup>+</sup> and K<sup>+</sup> were the predominant elements, with respective concentrations of 472.74 mg L<sup>-1</sup> and 426.45 mg L<sup>-1</sup>. The release of Ca<sup>2+</sup> and Mg<sup>2+</sup> was lower, with respective concentrations of 91.99 mg L<sup>-1</sup> and 69.69 mg L<sup>-1</sup>. The concentration of all the trace elements decreased quickly after 2 min, to reach minimum values of 48.42 mg L<sup>-1</sup> for Ca<sup>2+</sup>, 27.09 mg L<sup>-1</sup> for Mg<sup>2+</sup>, 140.36 mg L<sup>-1</sup> for Na<sup>+</sup> and 111.42 mg L<sup>-1</sup> for K<sup>+</sup> after 3 hours.

#### 5.4.5 Trace element analysis during the removal of a Zinc, Nickel, Aluminium and Antimony in a combined aqueous solution by WAP/agar blocks in a fixed bed sorption column

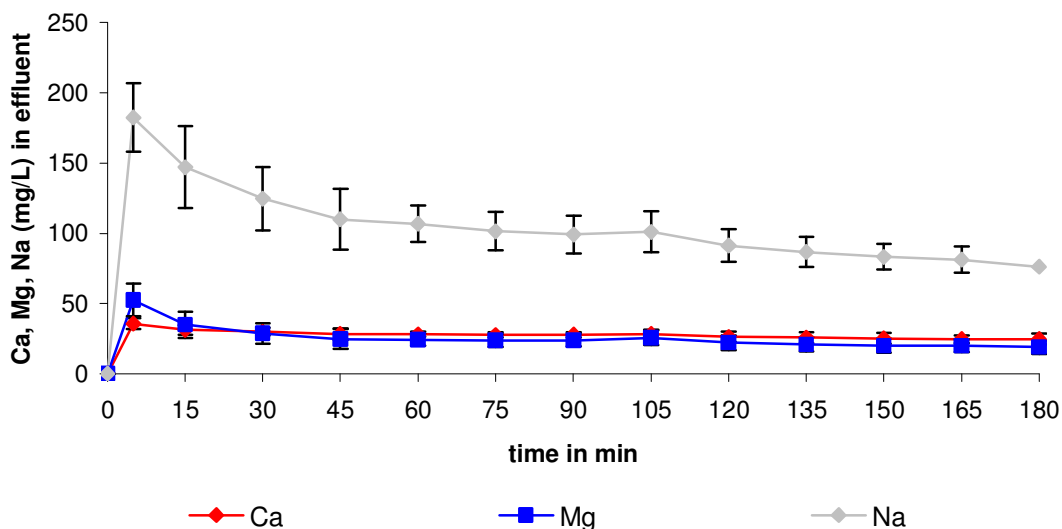


Fig. 5.5 Trace element analysis from fixed bed column studies with WAP/agar blocks. 10 mg L<sup>-1</sup> Zn(II), Ni(II), Al(III) and Sb(III) combined solution ( $\pm$  95% confidence intervals, n= 4).

Fig. 5.5 shows that a rapid release of Ca<sup>2+</sup>, Mg<sup>2+</sup>, Na<sup>+</sup> occurred within 2 min, corresponding to the sorption of Al(III), Ni(II), Zn(II) and Sb(III) by the WAP/agar blocks. Na<sup>+</sup> was the predominant element, with a concentration of 182.35 mg L<sup>-1</sup>. The release of Ca<sup>2+</sup> and Mg<sup>2+</sup> was lower, with respective concentrations of 35.82 mg L<sup>-1</sup> and 52.66 mg L<sup>-1</sup>. The concentration of all the trace elements decreased quickly after 2 min, to reach minimum values of 24.89 mg L<sup>-1</sup> for Ca<sup>2+</sup>, 18.94 mg L<sup>-1</sup> for Mg<sup>2+</sup> and 76.17 mg L<sup>-1</sup> for Na<sup>+</sup> after 3 hours.

As seen in Figures 5.1-5.5, the quantity of trace elements released was as follows: Na<sup>+</sup> > K<sup>+</sup> > Ca<sup>2+</sup> > Mg<sup>2+</sup>. The consistency of the ion exchange mechanism for all the metal sorption studies indicates that ion exchange is an integral process in the sorption of metals by the seaweed biomasses. Corresponding to the maximum sorption rate by the

biomass within the first 2 min, there was a concurrent maximum release of  $\text{Ca}^{2+}$ ,  $\text{Mg}^{2+}$ ,  $\text{K}^+$  and  $\text{Na}^+$ , also within the first 2 min. The gradual reduction of release in the later stages may also indicate a gradual saturation of the sorbent with less ion exchange occurring. Furthermore, the order of the trace elements released upon metal sorption was similar for both WAP/agar and *P. lanosa*/agar blocks.

The results also indicate that the biosorbents, before exposure to metal ions, were saturated with  $\text{Ca}^{2+}$ ,  $\text{Mg}^{2+}$ ,  $\text{K}^+$  and  $\text{Na}^+$  (Lee and Volesky, 1997). Davis et al (2003) reported that untreated algal biomass generally contains light metal ions such as  $\text{Ca}^{2+}$ ,  $\text{Mg}^{2+}$ ,  $\text{K}^+$  and  $\text{Na}^+$ , acquired from seawater and bound to acid functional groups present on their surface. The analysis of seawater sampled from Fethard-on-sea carried out by the ERG showed that the concentration of the different trace elements were 10,533.3 mg L<sup>-1</sup>, 389.3 mg L<sup>-1</sup>, 421.7 mg L<sup>-1</sup> and 1,283.3 mg L<sup>-1</sup> for  $\text{Na}^+$ ,  $\text{K}^+$ ,  $\text{Ca}^{2+}$  and  $\text{Mg}^{2+}$  respectively.

The relatively large scale release of  $\text{Na}^+$  and  $\text{K}^+$ , compared to  $\text{Ca}^{2+}$  and  $\text{Mg}^{2+}$ , may also indicate that the biomass more readily releases sodium and potassium ions. The calcium and magnesium ions may be more strongly bound to the functional groups present. Another reason could be that  $\text{Na}^+$  and  $\text{K}^+$  are more abundant than  $\text{Ca}^{2+}$  and  $\text{Mg}^{2+}$ , and therefore released in larger quantities. However this abundance did not follow the concentration of the different trace elements present in the seawater of the sampling site Fethard-on-sea.

## 5.5 Conclusions

Characterisation of column effluent showed that  $\text{Ca}^{2+}$ ,  $\text{Mg}^{2+}$ ,  $\text{Na}^+$  and  $\text{K}^+$  were released following metal sorption, in the following quantities  $\text{Na}^+ > \text{K}^+ > \text{Ca}^{2+} > \text{Mg}^{2+}$ .  $\text{Na}^+$  and  $\text{K}^+$  were released in greater quantities than  $\text{Ca}^{2+}$  and  $\text{Mg}^{2+}$ . Ion exchange is a key process in the sorption of metals by some seaweed biomasses.

## **Chapter 6**

**Column capacity (W) and operating time of the  
agar/WAP and agar/*Polysiphonia lanosa* biosorbents  
for nickel, zinc, aluminium and antimony**

## 6.1 Introduction

The dynamic flow tests carried out in Chapter 4 were limited to a 3 hour experimental period. During this time, the biosorbents did not reach saturation. Therefore, column overall capacity ( $W$  in  $\text{mg g}^{-1}$ ), over a longer period of time, was examined in order to assess saturation capacity of the biosorbents.

In order to test column overall capacity, 5% agar/7.5% WAP blocks were investigated for the treatment of Zn(II), Ni(II), Al(III) and Sb(III). In addition, 5% agar/7.5% *P. lanosa* blocks were also tested for the treatment of Sb(III).

### 6.1.1 Explanation of column terms

#### Breakthrough curves, breakthrough and exhaustion points

The breakthrough curve relates to the plot of effluent metal concentration ( $\text{mg L}^{-1}$ ) against time (hours).

The breakthrough point ( $T_B$ ) corresponds to the time (in hours) at which the metal effluent concentration reaches a predetermined level, after which the column is no longer efficient (Volesky et al., 2003). For this experiment, the  $T_B$  was determined when a concentration of  $2 \text{ mg L}^{-1}$  was detected in the effluent representing 80% removal efficiency. A predetermined concentration of  $2 \text{ mg L}^{-1}$  in the effluent was previously selected at the ERG (Walsh, 2008) for the treatment of Cu(II). This is the copper level permitted in drinking water under the EU Drinking Water Directive (Council Directive 98/83/EC). For comparison purposes, a same metal concentration value of  $2 \text{ mg L}^{-1}$  in the effluent was selected in this study.

The exhaustion point ( $T_E$ ) corresponds to the time (in hours) at which the biosorbent inside the column reaches saturation and is no longer efficient. For this experiment, the  $T_E$  was reached when a metal concentration in the effluent reaches  $8 \text{ mg L}^{-1}$ , which is the difference between the initial metal concentration ( $10 \text{ mg L}^{-1}$ ) and the breakthrough point value ( $2 \text{ mg L}^{-1}$ ).

## Mass Transfer Zone

The overall performance of a fixed-bed sorption column can be represented by the length and shape of the ion-exchange zone that develops during the metal solution exposure to the sorbent. This zone develops between the section of the column that gradually becomes saturated with the sorbate and the virgin biosorbent section (Naja and Volesky, 2006b). The time interval between the  $T_B$  and the  $T_E$  is the length of the Mass Transfer Zone (MTZ) and is measured in hours. MTZ appears as an S-shape on the breakthrough curve due to adsorption and mass transport conditions. The metric length of the MTZ is called the adsorption zone (also known as the critical or minimum bed length). This parameter is the shortest possible bed length required to obtain the breakthrough time at  $t = 0$  (Ruthven, 1984).

## 6.2 Aims

- Using dynamic flow conditions, to determine the overall metal removal capacity (W) of the 5% agar/7.5% WAP biosorbent for Zn(II), Ni(II), Al(III) and the 5% agar/7.5% *P. lanosa* for Sb(III).
- To determine the breakthrough point ( $T_B$ ), exhaustion point ( $T_E$ ) and corresponding mass transfer zone (MTZ) of the 5% agar/7.5% WAP biosorbents for Zn(II), Ni(II), Al(III) and Sb(III) and the 5% agar/7.5% *P. lanosa* biosorbents for Sb(III).
- To calculate the void fraction inside the column (%), the adsorption zone length (cm), the pre- and post-experiment swelling of the sorbents (% and  $\text{cm}^3$ ), and the total volume of influent treated (L).

## 6.3 Methods

### 6.3.1 Dynamic flow tests

The laboratory configuration of the fixed-bed sorption columns and the preparation of the 5% agar/7.5% WAP and 5% agar/7.5% *P. lanosa* were as outlined in Section 4.3.4.

The biosorbents were exposed to Zn(II), Ni(II), Al(III) and Sb(III) until the exhaustion point of the column was reached. The predetermined breakthrough point ( $T_B$ ) was 2 mg L<sup>-1</sup> for all metals tested. The influent was a 10 mg L<sup>-1</sup> solution of the metal being tested and prepared using Fluka atomic spectroscopy standard solutions. The flow rate of the solution was a continuous 25 mL min<sup>-1</sup> (measured at the outlet pipe) for the duration of the test. Tests were carried out in four replicates in a temperature controlled room at 12°C.

Samples of metal solution (effluent) were taken at the outlet pipe after 2 min, and then at intervals of 3 hours for the duration of the experiment. Samples were acidified using 0.5 mL of nitric acid (69%) and stored in HDPE bottles at 4°C. Analysis was carried out using an Inductively Coupled Plasma Optical Emission Spectroscopy with auto-sampler (Varian 710-ES ICP Optical Emission Spectrometer, ICP Expert II Software). Three certified reference materials (or CRMs) were used: Sea lettuce (*Ulva lactuca*), Tomato leaves and BCR 060 Aquatic plant (*Lagarosiphon major*). Control samples from the influent storage tank were also analysed.

### 6.3.2 Column calculations

The height of the biosorbent above the “working level” (Fig. 4.4) of the fixed-bed column was measured on each column at the beginning and at the end of the dynamic flow tests. This measurement enabled the calculation of the total bed length (cm), the total bed volume (cm<sup>3</sup>), the swelling of the biosorbent (cm<sup>3</sup>), the percentage swelling (%) and the packing density (g L<sup>-1</sup>). The volume of the biosorbent in the top section of the column (Fig. 4.4) was calculated using the formula:

$$1/3 \times \pi \times L (R^2 + Rr + r^2) \quad \text{Eq. [5]}$$

where L is the total bed length (cm) and R is the radius of circular face (cm).

### *Void fraction*

The void fraction, corresponding to the volume of biosorbent bed not occupied by the biosorbent, was calculated as a percentage of the total bed volume. To determine the void fraction, the columns were drained following completion of each dynamic flow test. The outlet pipe was plugged and water was added to the column containing the biosorbent through the inlet pipe. Once the water level had reached the top of the column, the outlet pipe was unplugged to drain the water. The quantity of water was measured and the volume of the biosorbent bed not occupied by the biosorbent was calculated.

### *Breakthrough and exhaustion points ( $T_B$ and $T_E$ )*

Using the graph of 'effluent metal concentration in  $\text{mg L}^{-1}$  vs. time in hours' the breakthrough ( $T_B$ ) and exhaustion ( $T_E$ ) points were determined. The breakthrough point ( $T_B$ ) was determined as the time at which the effluent concentration reached  $2 \text{ mg L}^{-1}$ . The exhaustion point ( $T_E$ ) was determined as the time at which the effluent concentration reached  $8 \text{ mg L}^{-1}$ .

### *Mass transfer zone (MTZ)*

The mass transfer zone (MTZ) (hours) was calculated using the following formula (Vijayaraghavan et al., 2005b):

$$\text{MTZ} = T_E - T_B \quad \text{Eq. [6]}$$

where  $T_E$  is the exhaustion time (hours) and  $T_B$  is the breakthrough time (hours)

### *Adsorption zone ( $L_m$ )*

The adsorption zone (also known as the critical or minimum bed length) was calculated using the following formula (Ruthven, 1984):

$$L_m = L \times (1 - T_B / T_E) \quad \text{Eq. [7]}$$

where:  $L_m$  is the adsorption zone (cm),  $L$  is the average total bed length (cm),  $T_E$  is the exhaustion time (hours) and  $T_B$  is the breakthrough time (hours).

#### *Capacity of the column (W)*

The overall uptake capacity ( $W$ ) of the biosorbent (also known as column capacity) was calculated using the following formula (Vijayaraghavan et al., 2005a; Vijayaraghavan et al., 2005b):

$$W = M_{AD} / M \quad \text{Eq. [8]}$$

where  $W$  is the overall uptake capacity of the biosorbent ( $\text{mg g}^{-1}$ ),  $M_{AD}$  is the total quantity of metal sorbed in the column (mg) and  $M$  is the mass the biosorbent, dry weight (g).

$M_{AD}$  was calculated from the area above the breakthrough curve of the “effluent metal concentration in  $\text{mg L}^{-1}$  vs. time in hours” plot multiplied by the flow rate ( $\text{ml min}^{-1}$ ). The area above the curve was determined by integration using Origin 8 software.

## 6.4 Results and discussion

### 6.4.1 Overall column capacity (W) for Zn(II) removal by WAP/agar blocks

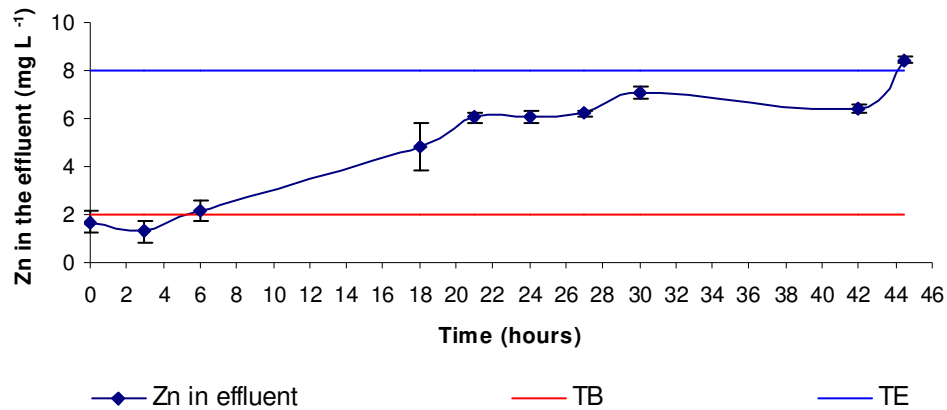


Fig. 6.1 Zn(II) remaining in effluent treated with 7.5% WAP/5% agar (water soaked) from a  $10 \text{ mg L}^{-1}$  influent stream at  $25 \text{ mL min}^{-1}$  for 44 hours ( $\pm 95\%$  confidence intervals,  $n = 4$ ).

From Fig. 6.1, the overall capacity (W) of the 7.5% WAP/5% agar biosorbent blocks for Zn(II) was calculated as  $46.2 \text{ mg g}^{-1}$ . The breakthrough point ( $T_B$ ) was reached after 5.5 hours while the exhaustion point ( $T_E$ ) was reached at 44 hours. This resulted in a mass transfer zone (MTZ) of 38.5 hours.

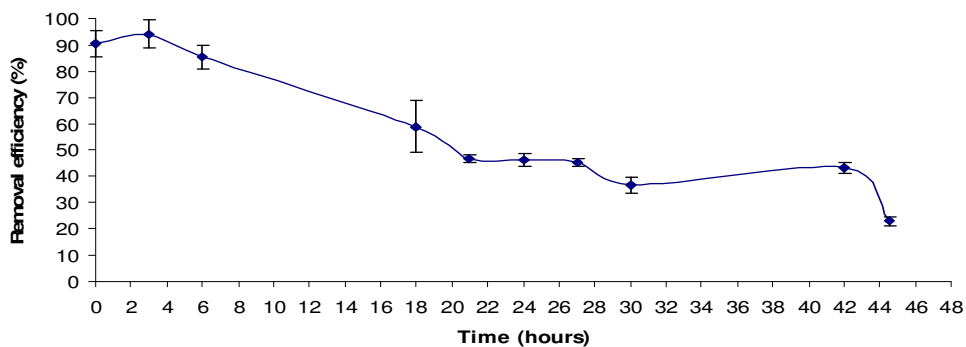


Fig. 6.2 Removal efficiency in % for Zn(II) by 7.5% WAP/5% agar (water soaked) from a  $10 \text{ mg L}^{-1}$  influent stream at  $25 \text{ mL min}^{-1}$  for 44 hours ( $\pm 95\%$  confidence intervals,  $n = 4$ ).

Fig. 6.2 shows that high removal efficiencies were maintained for 6 hours. After 6 hours the RE declined sharply to reach a minimum RE of 23% after 44 hours. The column characteristics are summarised in Table 6.1.

Table 6.1: Column characteristics for Zn(II) dynamic flow test with 5% agar/7.5% WAP ( $\pm 95\%$  confidence intervals,  $n = 4$ ).

<b>Total bed volume (average) cm<sup>3</sup></b>	<b>Swelling of biosorbent in column (average) cm<sup>3</sup></b>	<b>Swelling in column (average) %</b>	<b>Void fraction (average) %</b>
836.0 $\pm$ 6.6	100.2 $\pm$ 16.1	30.5 $\pm$ 1.5	4.6 $\pm$ 0.8
<b>Total bed length (average) cm</b>	<b>Breakthrough pt. (T<sub>B</sub>) hours</b>	<b>Exhaustion pt. (T<sub>E</sub>) hours</b>	<b>Mass transfer Zone (<math>\Delta T</math>)</b>
22.9 $\pm$ 0.3	5.5	44	38.5
<b>Adsorption zone (L<sub>m</sub>) cm</b>	<b>Pre-swelling density (av.) g L<sup>-1</sup></b>	<b>Post-swelling density (av.) g L<sup>-1</sup></b>	<b>Density decrease (av.) g L<sup>-1</sup></b>
20.04	213.9 $\pm$ 8.3	137.1 $\pm$ 10.3	76.8 $\pm$ 12.3
<b>Density decrease (av.) %</b>	<b>Total volume of influent treated (L)</b>	<b>Total Bed volumes treated</b>	<b>Capacity mg g<sup>-1</sup></b>
35.8 $\pm$ 5.1	66	78.9	46.2
<b>m<sub>ad</sub> (mg)</b>	<b>m<sub>total</sub> (mg)</b>	<b>Total metal removal (%)</b>	
633.3	7082	89.4	

Table 6.1 shows that swelling of the biosorbent occurred within the column (30.5  $\pm$  1.5%) despite the pre-soaking in deionised water prior to utilisation. The free area inside the column allows expansion to take place and this factor was taken into account when scaling up the column (see Chapter 11). After full expansion of the sorbent inside the column, the void fraction remained low at only 4.6  $\pm$  0.8%. Concurrently, a decrease in the density of the biosorbent was observed (35.8  $\pm$  5.1%). This would be a disadvantage

if the drop in density was not accompanied by the swelling of the sorbent (Walsh, 2008). A high total metal removal of 89 % was achieved.

#### 6.4.2 Overall column capacity (W) for Ni(II) removal by WAP/agar blocks

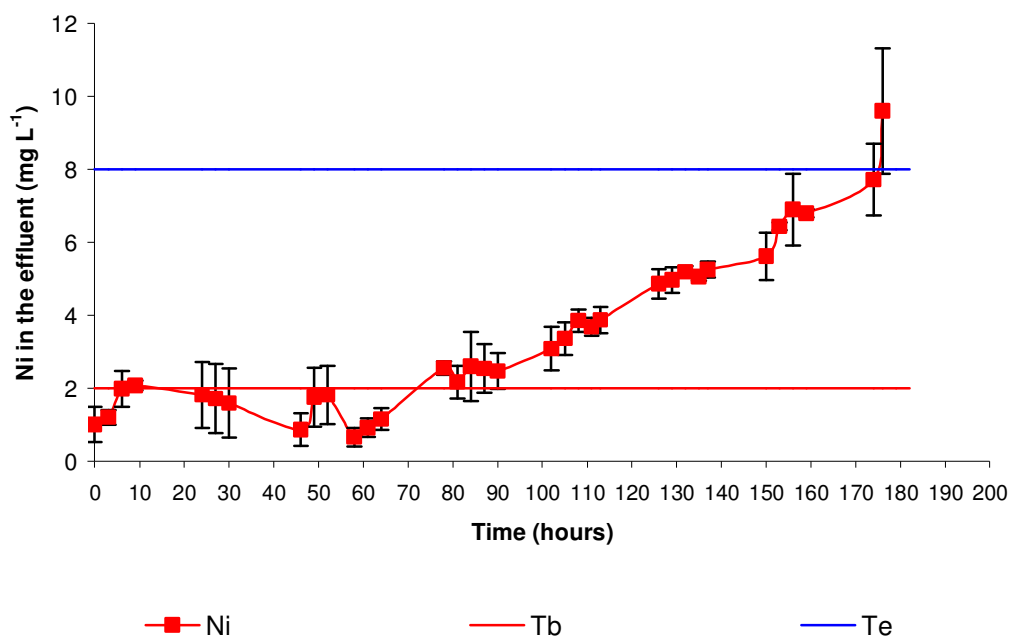


Fig. 6.3 Ni(II) remaining in effluent treated with 7.5% WAP/5% agar (water soaked) from a 10 mg L<sup>-1</sup> influent stream at 25 mL min<sup>-1</sup> for 175 hours ( $\pm$  95% confidence intervals, n = 4).

From Fig. 6.3, the overall capacity (W) of the 5% agar/7.5% WAP biosorbent for Ni(II) was calculated as 149.6 mg g<sup>-1</sup>. The breakthrough point (T<sub>B</sub>) was reached after 6 hours, while the exhaustion point (T<sub>E</sub>) was reached at 175 hours. This resulted in a mass transfer zone (MTZ) of 169 hours.

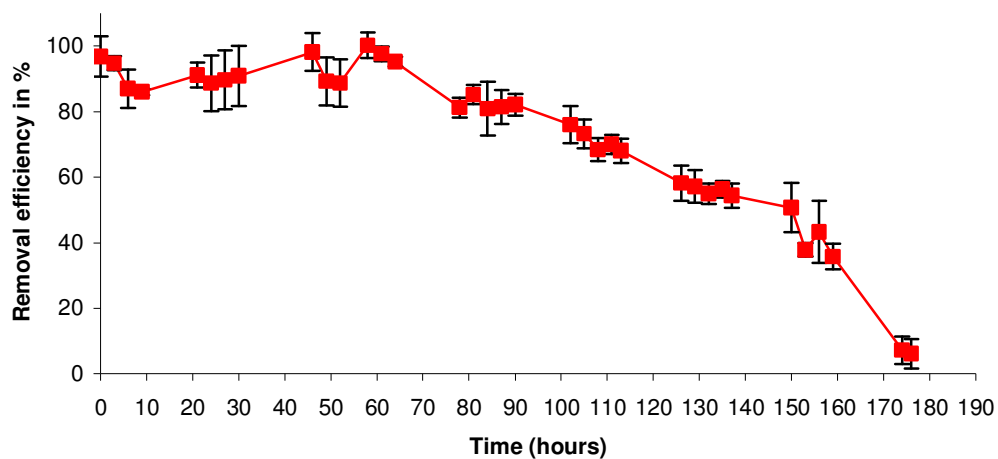


Fig. 6.4 Removal efficiency in % for Ni(II) by 7.5% WAP/5% agar (water soaked) from a 10 mg L<sup>-1</sup> influent stream at 25 mL min<sup>-1</sup> for 175 hours ( $\pm$  95% confidence intervals, n = 4).

Fig. 6.4 shows that high RE were obtained during the early stages of the dynamic flow test for Ni(II), with RE above 80%. The RE began to decline slowly after 60 hours to reach a minimum RE of 6% after 176 hours. The column characteristics are summarised in Table 6.2.

Table 6.2: Column characteristics for Ni(II) dynamic flow test with 5% agar/7.5% WAP ( $\pm$  95% confidence intervals, n = 4).

<b>Total bed volume (average) cm<sup>3</sup></b> 947.5 $\pm$ 46.7	<b>Swelling of biosorbent in column (average) cm<sup>3</sup></b> 176.6 $\pm$ 0.7	<b>Swelling in column (average) %</b> 33.9 $\pm$ 3.3	<b>Void fraction (average) %</b> 7.1 $\pm$ 0.5
<b>Total bed length (average) cm</b> 20 $\pm$ 0.3	<b>Breakthrough pt. (T<sub>B</sub>) hours</b> 6	<b>Exhaustion pt. (T<sub>E</sub>) hours</b> 175	<b>Mass transfer Zone (<math>\Delta</math>T)</b> 169
<b>Adsorption zone (Lm) cm</b> 19.6	<b>Pre-swelling density (av.) g L<sup>-1</sup></b> 296.4 $\pm$ 3.2	<b>Post-swelling density (av.) g L<sup>-1</sup></b> 125.5 $\pm$ 2.9	<b>Density decrease (av.) g L<sup>-1</sup></b> 170.9 $\pm$ 0.7
<b>Density decrease (av.) %</b> 57.7 $\pm$ 0.6	<b>Total volume of influent treated (L)</b> 262.5	<b>Total Bed volumes treated</b> 277	<b>Capacity mg g<sup>-1</sup></b> 149.6
<b>m<sub>ad</sub> (mg)</b> 1876.4	<b>m<sub>total</sub> (mg)</b> 2817	<b>Total metal removal (%)</b> 67	

A swelling of the biosorbent inside the column was observed (33.9  $\pm$  3.3%). The void fraction was slightly higher than for Zn with an average percentage of 7.1  $\pm$  0.5%. The large density decrease (57.7  $\pm$  0.6%) was also accompanied by the swelling inside the column. A total metal removal of 67% was achieved.

### 6.4.3 Overall column capacity (W) for Al(III) removal by WAP/agar blocks

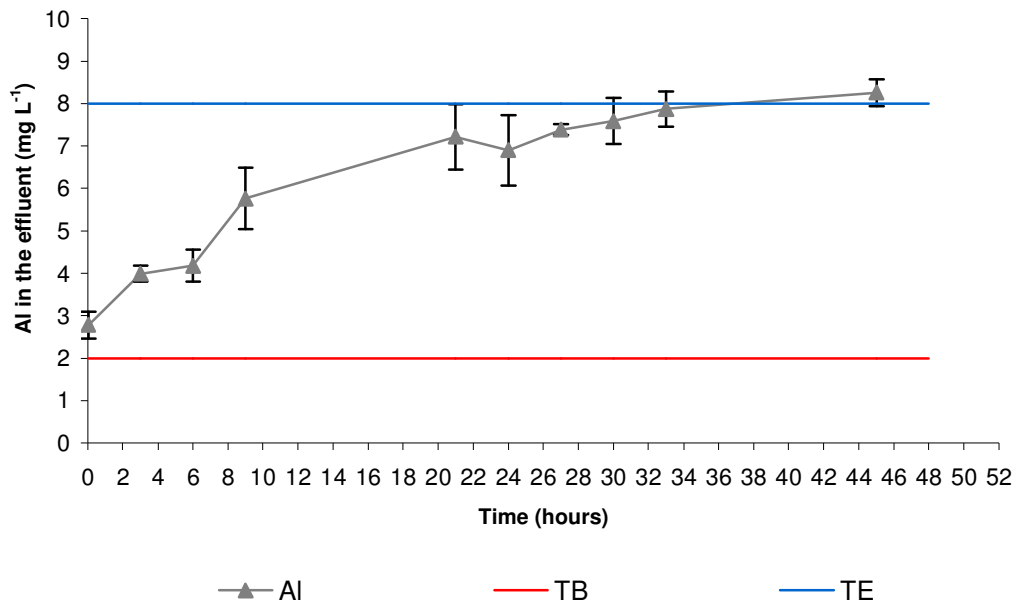


Fig. 6.5 Al(III) remaining in effluent treated with 7.5% WAP/5% agar (water soaked) from a 10 mg L<sup>-1</sup> influent stream at 25 mL min<sup>-1</sup> for 45 hours ( $\pm$  95% confidence intervals, n = 4).

From Fig. 6.5, the overall capacity, (W), of the 7.5% WAP/5% agar biosorbent for Al(III) was calculated as 39.5 mg g<sup>-1</sup>. The breakthrough point (T<sub>B</sub>) was reached after 0.03 hours, while the exhaustion point (T<sub>E</sub>) was at 36 hours. This resulted in a mass transfer zone (MTZ) of 35.97 hours.

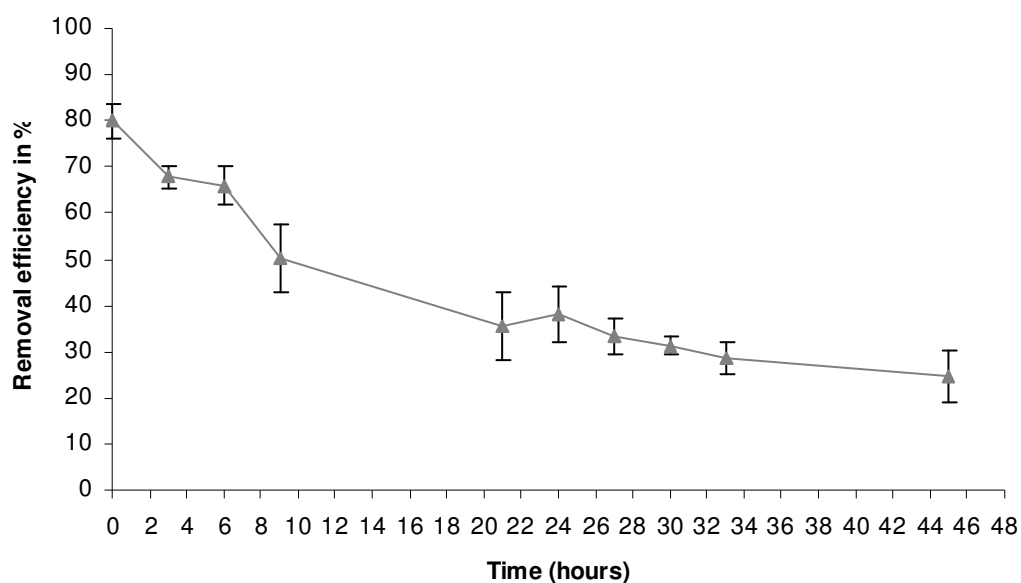


Fig. 6.6 Removal efficiency in % for Al(III) by 7.5% WAP/5% agar (water soaked) from a  $10 \text{ mg L}^{-1}$  influent stream at  $25 \text{ mL min}^{-1}$  for 45 hours ( $\pm 95\%$  confidence intervals,  $n = 4$ ).

Fig. 6.6 shows that the maximum RE was 80% at 0.03 hours, and that the RE decreased very rapidly to reach a minimum of 25% after 45 hours. The column characteristics are summarised in Table 6.3.

Table 6.3: Column characteristics for Al(III) dynamic flow test with 5% agar/7.5% WAP ( $\pm 95\%$  confidence intervals,  $n = 4$ ).

<b>Total bed volume (average) cm<sup>3</sup></b>	<b>Swelling of biosorbent in column (average) cm<sup>3</sup></b>	<b>Swelling in column (average) %</b>	<b>Void fraction (average) %</b>
862.5 $\pm$ 40.6	161.7 $\pm$ 7.9	32.2 $\pm$ 0.1	5.4 $\pm$ 1
<b>Total bed length (average) cm</b>	<b>Breakthrough pt. (T<sub>B</sub>) hours</b>	<b>Exhaustion pt. (T<sub>E</sub>) hours</b>	<b>Mass transfer Zone (<math>\Delta T</math>)</b>
20 $\pm$ 0.3	0.03	36	35.97
<b>Adsorption zone (L<sub>m</sub>) cm</b>	<b>Pre-swelling density (av.) g L<sup>-1</sup></b>	<b>Post-swelling density (av.) g L<sup>-1</sup></b>	<b>Density decrease (av.) g L<sup>-1</sup></b>
19.98	291.9 $\pm$ 8.1	130.3 $\pm$ 1.9	213.7 $\pm$ 10.5
<b>Density decrease (av.) %</b>	<b>Total volume of influent treated (L)</b>	<b>Total Bed volumes treated</b>	<b>Capacity mg g<sup>-1</sup></b>
55.3 $\pm$ 1.3	54	63	39.5
<b>m<sub>ad</sub> (mg)</b>	<b>m<sub>total</sub> (mg)</b>	<b>Total metal removal (%)</b>	
508.75	1018	72.4	

Table 6.3 shows a swelling average of  $32.2 \pm 0.1\%$ , with an average density decrease of  $55.3 \pm 1.3\%$ . The void fraction was also minimised ( $5.4 \pm 1\%$ ) due to the swelling of the blocks inside the column. Total metal removal was  $72.4\%$ .

#### 6.4.4 Overall column capacity (W) for Sb(III) removal by WAP/agar blocks

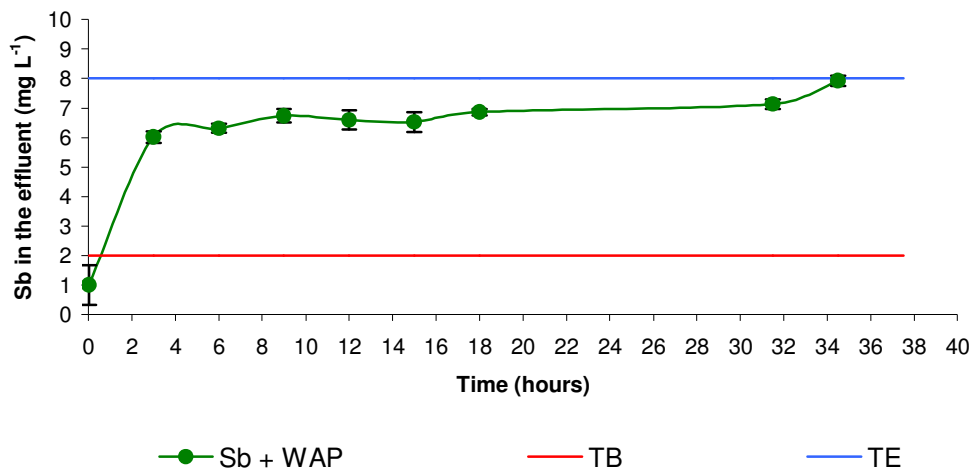


Fig. 6.7 Sb(III) remaining in effluent treated with 7.5% WAP/5% agar (water soaked) from a 10 mg L<sup>-1</sup> influent stream at 25 mL min<sup>-1</sup> for 35 hours ( $\pm$  95% confidence intervals, n = 4).

From Fig. 6.7, the overall capacity, (W), of the 7.5% WAP/5% agar biosorbent for Sb(III) was calculated as 18.7 mg g<sup>-1</sup>. The breakthrough point (T<sub>B</sub>) was reached after 0.6 hours, while the exhaustion point (T<sub>E</sub>) was at 34.5 hours. This resulted in a mass transfer zone (MTZ) of 33.9 hours.

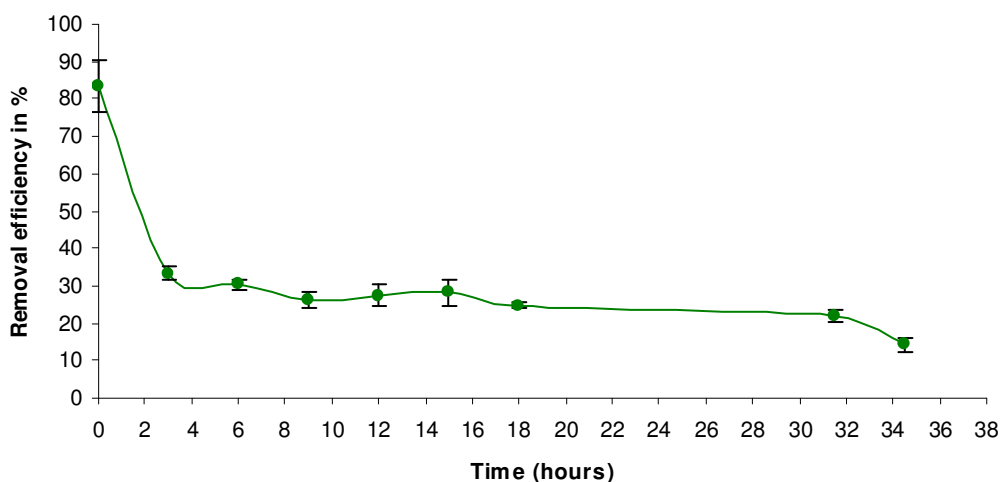


Fig. 6.8 Removal efficiency in % for Sb(III) by 7.5% WAP/5% agar (water soaked) from a 10 mg L<sup>-1</sup> influent stream at 25 mL min<sup>-1</sup> for 35 hours ( $\pm$  95% confidence intervals, n = 4).

Fig. 6.8 shows that the RE decreased rapidly after 2 min (maximum RE of 83%) reaching a minimum RE of 14% after 34.5 hours. The column characteristics are summarised in Table 6.4.

Table 6.4: Column characteristics for Sb(III) dynamic flow test with 5% agar/7.5% WAP ( $\pm 95\%$  confidence intervals,  $n = 4$ ).

<b>Total bed volume (average) cm<sup>3</sup></b> 996.3 $\pm$ 2.1	<b>Swelling of biosorbent in column (average) cm<sup>3</sup></b> 78.3 $\pm$ 4.4	<b>Swelling in column (average) %</b> 46.5 $\pm$ 2	<b>Void fraction (average) %</b> 9.7 $\pm$ 0.6
<b>Total bed length (average) cm</b> 21 $\pm$ 0.5	<b>Breakthrough pt. (T<sub>B</sub>) hours</b> 0.6	<b>Exhaustion pt. (T<sub>E</sub>) hours</b> 34.5	<b>Mass transfer Zone (<math>\Delta T</math>)</b> 33.9
<b>Adsorption zone (L<sub>m</sub>) cm</b> 20.63	<b>Pre-swelling density (av.) g L<sup>-1</sup></b> 183.4 $\pm$ 5.8	<b>Post-swelling density (av.) g L<sup>-1</sup></b> 129.9 $\pm$ 3.2	<b>Density decrease (av.) g L<sup>-1</sup></b> 53.5 $\pm$ 3
<b>Density decrease (av.) %</b> 29.1 $\pm$ 0.9	<b>Total volume of influent treated (L)</b> 51.75	<b>Total Bed volumes treated</b> 51.9	<b>Capacity mg g<sup>-1</sup></b> 18.7
<b>m<sub>ad</sub> (mg)</b> 242.8	<b>m<sub>total</sub> (mg)</b> 483.6	<b>Total metal removal (%)</b> 50.2	

Table 6.4 shows a very low column capacity of only 18.7 mg g<sup>-1</sup>, with a corresponding low metal removal of 50%. This highlights the previously observed low affinity between the sorbent (5% agar/7.5% WAP) and Sb(III).

#### 6.4.5 Overall column capacity (W) for Sb(III) removal by *P. lanosa*/agar blocks

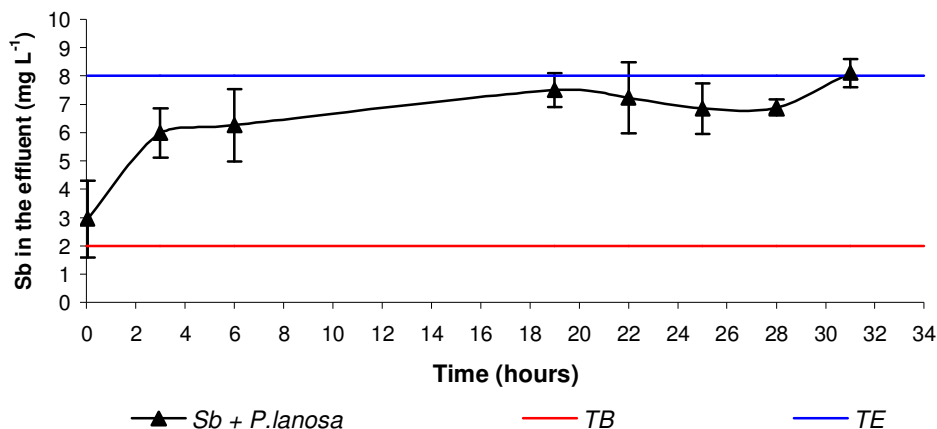


Fig. 6.9 Sb(III) remaining in effluent treated with 7.5% *P. lanosa*/5% agar (water soaked) from a 10 mg L<sup>-1</sup> influent stream at 25 mL min<sup>-1</sup> for 31 hours ( $\pm$  95% confidence intervals, n = 4).

From Fig. 6.9, the overall capacity, (W), of the 7.5% *P. lanosa*/5% agar biosorbent for Sb(III) was calculated as 27.9 mg g<sup>-1</sup>. The breakthrough point (T<sub>B</sub>) was reached after 0.03 hours, while the exhaustion point (T<sub>E</sub>) was reached at 31 hours. This resulted in a mass transfer zone (MTZ) of 30.97 hours.

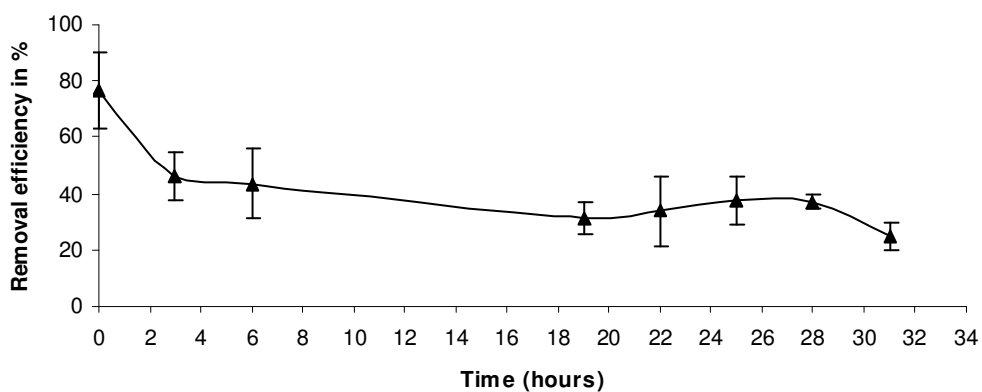


Fig. 6.10 Removal efficiency in % for Sb(III) by 7.5% *P. lanosa*/5% agar (water soaked) from a 10 mg L<sup>-1</sup> influent stream at 25 mL min<sup>-1</sup> for 31 hours ( $\pm$  95% confidence intervals, n = 4).

Fig. 6.10 shows that a maximum RE of 77% was reached after 2 min, followed by a sharp decrease to reach a minimum of 25% after 31 hours. The column characteristics are summarised in Table 6.5.

Table 6.5: Column characteristics for Sb(III) dynamic flow test with 5% agar/7.5% *P. lanosa* ( $\pm$  95% confidence intervals, n = 4).

<b>Total bed volume (average) cm<sup>3</sup></b>	<b>Swelling of biosorbent in column (average) cm<sup>3</sup></b>	<b>Swelling in column (average) %</b>	<b>Void fraction (average) %</b>
840 $\pm$ 63.1	53.2 $\pm$ 4.2	46.9 $\pm$ 0.4	6.7 $\pm$ 0.4
<b>Total bed length (average) cm</b>	<b>Breakthrough pt. (T<sub>B</sub>) hours</b>	<b>Exhaustion pt. (T<sub>E</sub>) hours</b>	<b>Mass transfer Zone (<math>\Delta</math>T)</b>
17.8 $\pm$ 1.1	0,03	31	30.97
<b>Adsorption zone (Lm) cm</b>	<b>Pre-swelling density (av.) g L<sup>-1</sup></b>	<b>Post-swelling density (av.) g L<sup>-1</sup></b>	<b>Density decrease (av.) g L<sup>-1</sup></b>
17.8	145.2 $\pm$ 11.2	109 $\pm$ 8.4	36.2 $\pm$ 2.8
<b>Density decrease (av.) %</b>	<b>Total volume of influent treated (L)</b>	<b>Total Bed volumes treated</b>	<b>Capacity mg g<sup>-1</sup></b>
24.9 $\pm$ 0.5	46.5	55.4	27.9
<b>m<sub>ad</sub> (mg)</b>	<b>m<sub>total</sub> (mg)</b>	<b>Total metal removal (%)</b>	
304.3	494	61.7	

Utilising 5% Agar/7.5% *P. lanosa* blocks, instead of 7.5% WAP, revealed little difference in the physical properties of the blocks. As seen in Table 6.5, a similar swelling of the blocks inside the column was observed, with an average value of 46.9  $\pm$

0.4 %. The decrease in density was also low ( $24.9 \pm 0.5$  %), leading to a small void fraction ( $6.7 \pm 0.4$  %). The column capacity ( $27.9 \text{ mg g}^{-1}$ ) is higher than the 5% Agar/7.5% WAP blocks ( $18.7 \text{ mg g}^{-1}$ ) highlighting that *P. lanosa*/agar is more suitable for Sb(III) removal. Total metal removal was 61.7% compared to 50.2% for WAP/agar. The adsorption zone was 17.8 cm, which was exactly the length of the bed ( $17.8 \pm 1.1$ ), showing that the column was operating under optimum conditions.

#### 6.4.6 Comparison of overall column capacities (W)

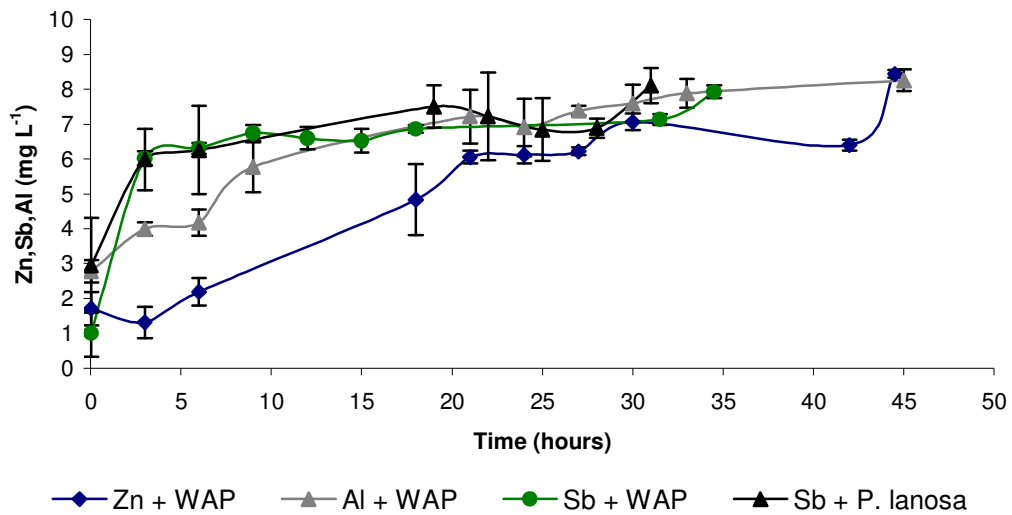


Fig. 6.11 Comparison of dynamic flow tests for Zn(II), Al(III) and Sb(III) treated with 7.5% WAP/5% agar (water soaked), and Sb(III) treated with 7.5% *P. lanosa*/5% agar from single metal influents of  $10 \text{ mg L}^{-1}$  ( $\pm 95\%$  confidence intervals,  $n = 4$ ).

Fig. 6.11 shows that longer operation times were achieved for Zn and Al. The curve for Sb treated with *P. lanosa*/agar also showed that the exhaustion point was reached rapidly, indicating a quicker saturation of the seaweed biomass compared to WAP.

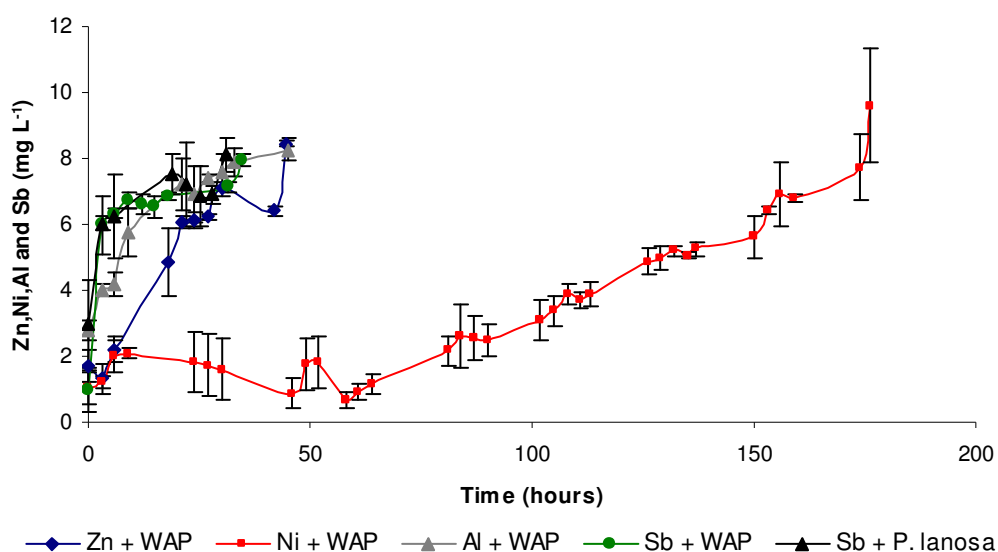


Fig. 6.12 Comparison of dynamic flow tests for Zn(II), Ni(II), Al(III) and Sb(III) treated with 7.5% WAP/5% agar (water soaked), and Sb(III) treated with 7.5% *P. lanosa*/5% agar from single metal influents of 10 mg L<sup>-1</sup> ( $\pm$  95% confidence intervals, n = 4).

Fig. 6.12 shows that the dynamic flow test for Ni(II) was performed over a far longer time period compared with the other metals. The shape of the curve for Ni(II) also highlights a slow increase compared to the other metals.

#### 6.4.7 Comparison of the column characteristics

The majority of the column characteristics, such as the total bed volume, void fraction and the swelling of the biosorbent, were similar for the different studies, indicating a consistency in the configuration and packing of the columns. Therefore, direct comparison for the different metals is feasible.

Large differences in capacities (W) were observed for the different metals and for the two biomasses. For Zn(II), Ni(II), Al(III) and Sb(III) with 7.5% WAP/5% agar biosorbent, the metal removal capacities (W) were 46.2 mg g<sup>-1</sup>, 149.6 mg g<sup>-1</sup>, 35.97 mg g<sup>-1</sup> and 18.7 mg g<sup>-1</sup>, respectively. Utilizing 7.5% *P. lanosa*/5% agar biosorbent increased the W value to 27.9 mg g<sup>-1</sup> for Sb(III).

A broad MZT indicates that the biosorbent is not being efficiently utilised, and comparing the different MZT values obtained for the different metals gives a good indication of how efficient the column will be in industrial trials. Narrow MZTs were obtained for all metals, except for Ni(II) which displayed a very broad MZT of 169 hours. A higher column capacity can however be obtained by reducing the flow rate or increasing the total bed height, allowing a longer residence time as reported by Vijayaraghavan et al (2004). Increasing the bed height would increase the number of available binding sites for sorption and thus increase the overall column capacity. However, decreasing the flow rate may not increase overall column capacity, as reported for Zn(II) sorption by *Azolla filiculoides* (Zhao et al., 1999). On the other hand, increases in flow rate have been shown to decrease both breakthrough and exhaustion time due to an insufficient residence time of the solute within the column and the diffusion limitations of the solute into the pores of the sorbent at higher flow rates (Ko et al., 2000; Senthilkumar et al., 2006).

Each column examined treated a large quantity of influent, especially in the case of Ni(II) with more than 260 litres of Ni(II) solution treated during the 175 hours of the experiment. Lower volumes were treated for of Zn(II), Al(III), Sb(III) with 7.5% WAP/5% agar, with 66 L, 54 L and 51.75 L, respectively. 46.5 L of Sb(III) solution was treated with 7.5% *P. lanosa*/5% agar.

In terms of overall column performance, as defined by column operating time and overall column capacity (W), the biosorbents may be ranked in the following:

$$\text{Ni(II)/WAP} > \text{Zn(II)/WAP} > \text{Al(III)/WAP} > \text{Sb(III)/P. lanosa} > \text{Sb(III)/WAP}$$

## 6.5 Conclusions

The overall metal removal capacities (W) of the 7.5% WAP/5% agar biosorbent for Zn(II), Ni(II), Al(III) and Sb(III) were 46.2 mg L<sup>-1</sup>, 149.6 mg L<sup>-1</sup>, 39.5 mg L<sup>-1</sup> and 18.7 mg L<sup>-1</sup> respectively. For Sb(III) treated with 7.5 % *P. lanosa*/5% agar the W was 27.9 mg L<sup>-1</sup>.

The highest level of metal removal was achieved in the case of Ni(II) with a breakthrough point ( $T_B$ ) of 6 hours. The lowest was achieved in the case of Sb(III), although the *P. lanosa*/agar blocks gave a higher Sb(III) removal than the WAP/agar blocks. The broad MZT observed for Ni(II) indicated that the biosorbent was not efficiently utilised, thereby suggesting better removal may be achieved by reducing the flow rate and/or increasing the sorbent bed height.

## **Chapter 7**

### **Metal desorption and regeneration of biomass.**

## **7.1 Introduction**

### **7.1.1 Metal desorption**

Metal desorption and regeneration of the biomass is an important factor in developing a viable biosorbent. A number of authors have investigated the desorption properties of eluting agents for a diverse range of biomasses (Zhao et al., 1999; Zeroval et al., 2003; Volesky, 2004; Vijayaraghavan et al., 2006). Acidic solutions were found to be the most effective. However, if not recycled, the utilisation of acids may be expensive and pose an environmental threat. The utilisation of mineral acids was also reported to cause a loss in biomass. Acid solutions may dissolve some types of polysaccharides that contain metal binding sites, as well as the mineral contents of the biosorbent (Vijayaraghavan et al., 2006).

Desorption using calcium chloride was shown to be highly pH dependent, with an optimum pH range of 2-3 (Vijayaraghavan et al., 2006). In the case of CaCl<sub>2</sub> elution, no significant biomass loss was observed down to pH 2.5. However, a further decrease in pH resulted in appreciable biomass loss (Vijayaraghavan et al., 2006).

## **7.2 Aims**

- To identify suitable desorbing agents for Zn(II), Ni(II), Al(III) and Sb(III) in both single and multi-metal systems.
- To investigate successive sorption and desorption cycles (regeneration and reuse of the biosorbent) in both single and multi-metal systems.

## **7.3 Method**

### **Metal exposure**

2 g of dried WAP (size  $\leq 850 \mu\text{m}$ ) was exposed to 400 mL of 10 mg L<sup>-1</sup> metal solution for 12 hours on a rotary shaker at 180 rpm. The biomass was then removed by vacuum filtration. Metal analysis was carried out as in Section 2.3.

## Screening of desorbing solutions

400 mg of metal-laden biomass was exposed to 200 mL of a number of desorbing agents (0.1 M H<sub>2</sub>SO<sub>4</sub>, 0.1 M HCl, 0.1 M HNO<sub>3</sub>, 0.1 M KCl, 0.1 M EDTA, 0.1 M CaCl<sub>2</sub> and 0.1 M NaOH) for 12 hours on a rotary shaker at 180 rpm. The control was distilled water. The biomass was removed by vacuum filtration and the filtrate solution analysed as in Section 2.3.

For pH studies, 1 g of metal-laden biomass was exposed to 50 mL of CaCl<sub>2</sub> solution, at two concentrations (0.1 and 0.5 M), adjusted to pH 1, 2, 3, 4 and 5 using 0.1 M NaOH and HCl. The control was CaCl<sub>2</sub> solution with no adjustment of pH. The initial pH was 5.46.

## Dynamic flow tests

7.5% WAP/5% agar and 7.5%P. lanosa/5% agar blocks were prepared as in Section 4.3 and exposed to 10 mg L<sup>-1</sup> of the metal solutions over 3 hours and initial samples of effluents were taken after 2 min and then every 15 min until the end of the experiment.

A flow rate of 25 mL min<sup>-1</sup> of the desorbing solution over 3 hours was employed for both sorption and desorption studies. The initial samples of effluent were taken after 2 min and then every 15 min until the end of the experiment (3 hours). Single and combined metals solution of Zn(II), Al(III), Ni(II) and Sb(III) were examined, using 0.1M HCl as the desorption agent. To investigate desorption and subsequent regeneration of the biomass, 5 successive metal exposure/desorption cycles were examined (Hashim et al., 2000; Vijayaraghavan et al., 2005a; Gupta and Rastogi, 2008).

## Chemicals

- 1000mg L<sup>-1</sup> Sb(III) as Sb<sub>2</sub>O<sub>3</sub> (analytical grade), Ni(II), Zn(II) and Al(III) - Sigma-Aldrich Ltd., Dublin, Ireland.
- Sodium Hydroxide (solid) - Ridel de Haën, Germany.
- Sodium Chloride (solid) - Ridel de Haën, Germany.

- Hydrochloric Acid (37%) - LabScan Ltd., Dublin, Ireland.
- Nitric Acid (69%) – Sigma-Aldrich Ltd, Dublin, Ireland.
- Sulfuric Acid (sp. gr. 1.84) - Sigma-Aldrich Ltd, Dublin, Ireland.
- EDTA - Sigma-Aldrich Ltd, Dublin, Ireland.
- Potassium chloride (solid) - Sigma-Aldrich Ltd, Dublin, Ireland.

## 7.4 Results and discussion

### 7.4.1 Screening of potential desorbing solutions

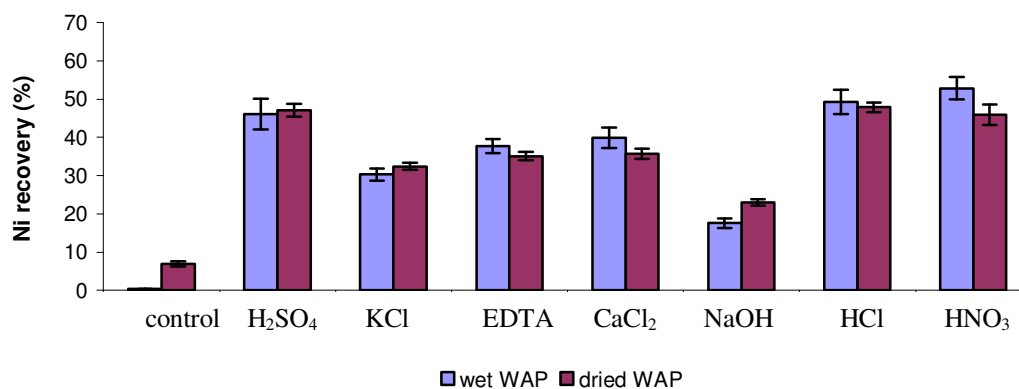


Fig. 7.1 Ni(II) recovery from WAP using various desorbing agents in batch tests. Error bars calculated from four replicates with 95% confidence intervals.

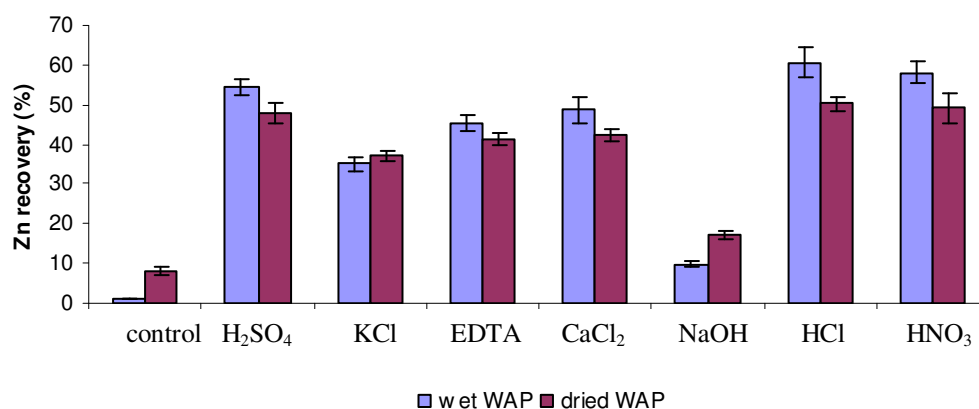


Fig. 7.2 Zn(II) recovery from WAP using various desorbing agents in batch tests. Error bars calculated from four replicates with 95% confidence intervals.

Figs 7.1 & 7.2 show that mineral acids were the most effective for the recovery of Ni(II) and Zn(II) from WAP. Higher Ni(II) recoveries were obtained for HCl and HNO<sub>3</sub>, with 49 and 53% respectively for wet WAP. Similar trends were obtained for Zn(II), with 61 and 58% recovery for HCl and HNO<sub>3</sub>, respectively for wet WAP. The screening of desorbing solutions, for the recovery of Cu and Ni from biomass of *P. aeruginosa*, also showed that mineral acids, in particular HCl and HNO<sub>3</sub>, were very effective in the desorption and regeneration of the biomass (Sar et al., 1999). Another study from Saeed et al. (2005) showed that 0.1 N HCl recovered more than 97% of Cu(II), Cd(II) and Zn(II) after 5 successive metal sorption/desorption cycles utilising papaya wood. HCl is effective for metal recovery and regeneration of the biomass. Furthermore, metal recoveries were higher for wet WAP than dried WAP. This is key operational advantage, as the desorption process will routinely be carried-out on the WAP/agar blocks already fully hydrated.

Other studies have shown that CaCl<sub>2</sub> can also be used as an effective desorbing agent, regenerating the biomass in an effective way (Davis et al., 2000; Vijayaraghavan et al., 2005a). However, in our study CaCl<sub>2</sub> was shown to be less effective for Zn(II) and Ni(II) recovery. As reported by Davis et al (2000), the efficiency of CaCl<sub>2</sub> is pH dependent, performing well at pH 3 in the recovery of Cu(II) from *S. filipendula*. A pH study, at two different concentrations of CaCl<sub>2</sub> (0.1 M and 0.5 M), for the desorption of Zn(II) was performed in this study, with the results shown in Fig. 7.3.

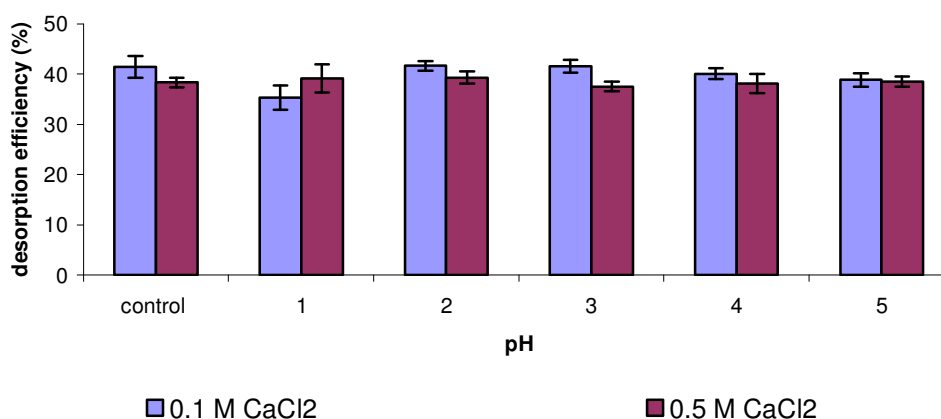


Fig. 7.3 Desorption of Zn(II) from WAP/agar using 0.1 M and 0.5 M CaCl<sub>2</sub> at different pH values. Error bars are calculated from four replicates with 95% confidence intervals.

Fig. 7.3 highlights that  $\text{CaCl}_2$ , at different pHs and at different concentrations, was not effective for the desorption of  $\text{Zn(II)}$  from WAP/agar. A maximum recovery of only 42% was obtained using 0.1M  $\text{CaCl}_2$  at pH 3. As a result, HCl was selected for metal desorption and consequent regeneration of biomass.

#### 7.4.2 Regeneration and re-use of the biomass – Dynamic flow tests

##### 7.4.2.1 Regeneration of WAP/agar blocks after the removal of $\text{Zn(II)}$ in dynamic flow tests using 0.1 M HCl as the desorbing agent.

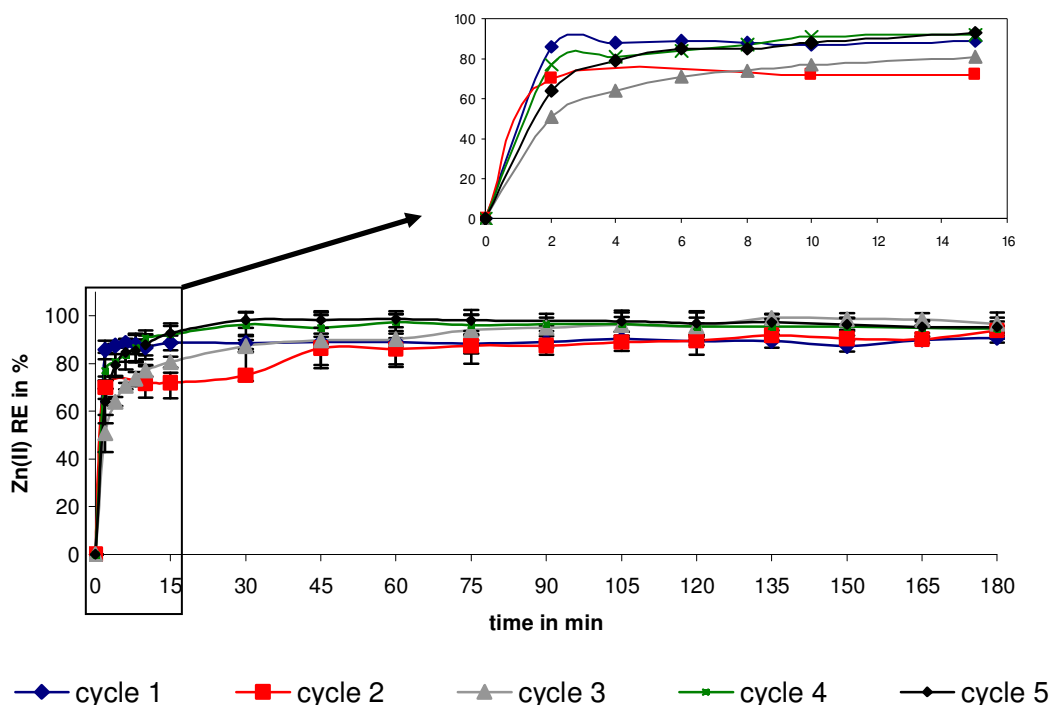


Fig. 7.4 Removal efficiency of  $\text{Zn(II)}$  from WAP/agar blocks in 5 successive regeneration and re-use cycles using 0.1 M HCl as the desorbing. Error bars calculated from four replicates with 95% confidence intervals.

Fig. 7.4 shows that high removal efficiencies were reached within 15 min, with more than 90% of  $\text{Zn(II)}$  removed. For each cycle, equilibrium was reached after 45 min.

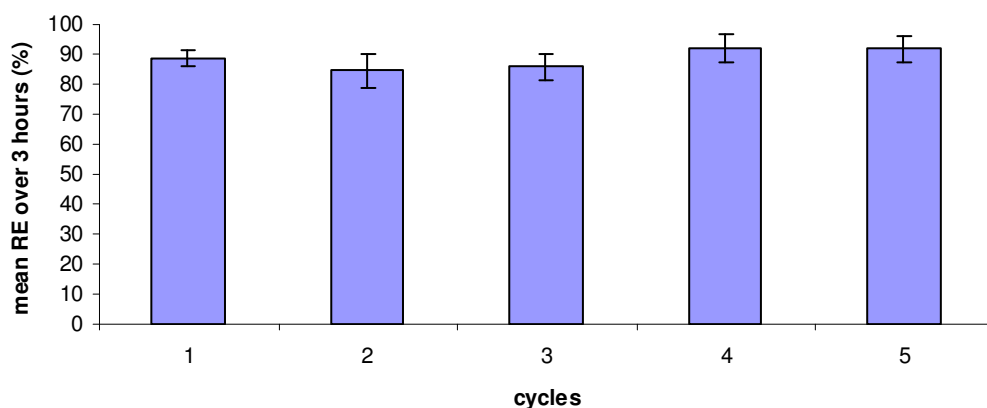


Fig. 7.5 Mean removal efficiency of Zn(II) from WAP/agar blocks over 3 hours from 5 successive regeneration and re-use cycles using 0.1 M HCl as the desorbing agent. Error bars calculated from four replicates with 95% confidence intervals.

Fig. 7.5 shows that the mean RE was very high for the five successive Zn(II) exposure/desorption cycles. No loss of RE for Zn(II) was observed after 4 successive regenerations of the biosorbent.

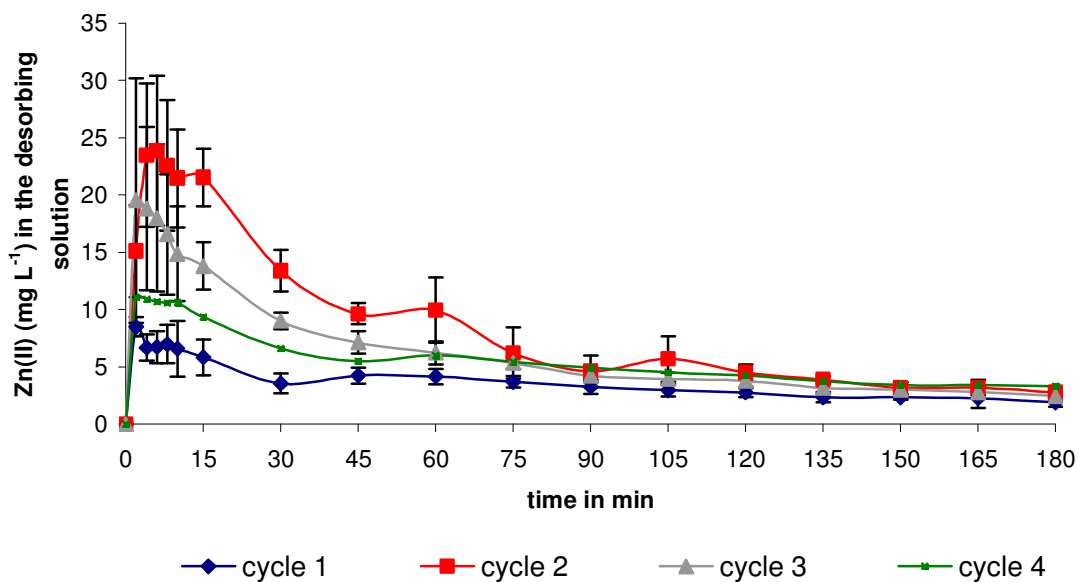


Fig. 7.6 Zn(II) concentrations in effluent during 4 desorption cycles. Error bars calculated from four replicates with 95% confidence intervals.

Fig. 7.6 shows that the majority of Zn(II) recovery occurred within 15 min followed by a sharp decrease in Zn(II) concentrations in the effluent. For the first desorption cycle, out of the 10 mg L<sup>-1</sup> Zn(II) feed, 8.48 mg L<sup>-1</sup> of the metal was recovered within 2 min. For the remaining desorption cycles, Zn(II) concentrations in the effluent generally exceeded 10 mg L<sup>-1</sup> within 60 min, indicating a mechanism of high accumulation of the metal during the metal sorption cycles and a rapid release during the desorption cycles.

#### 7.4.2.2 Regeneration of WAP/agar blocks after the removal of Ni(II) in dynamic flow tests using 0.1 M HCl as the desorbing agent.

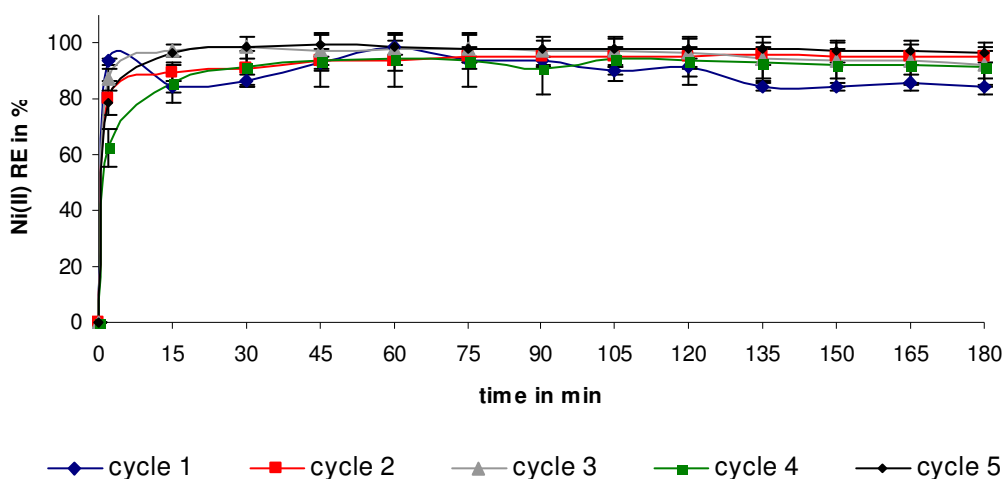


Fig. 7.7 Removal efficiency of Ni(II) from WAP/agar blocks in 5 successive regeneration and re-use cycles using 0.1 M HCl as the desorbing agent. Error bars calculated from four replicates with 95% confidence intervals.

Fig. 7.7 shows that high removal efficiencies were reached within 15 min, with more than 90% of Ni(II) removed. For each cycle, equilibrium was reached after 45 min.

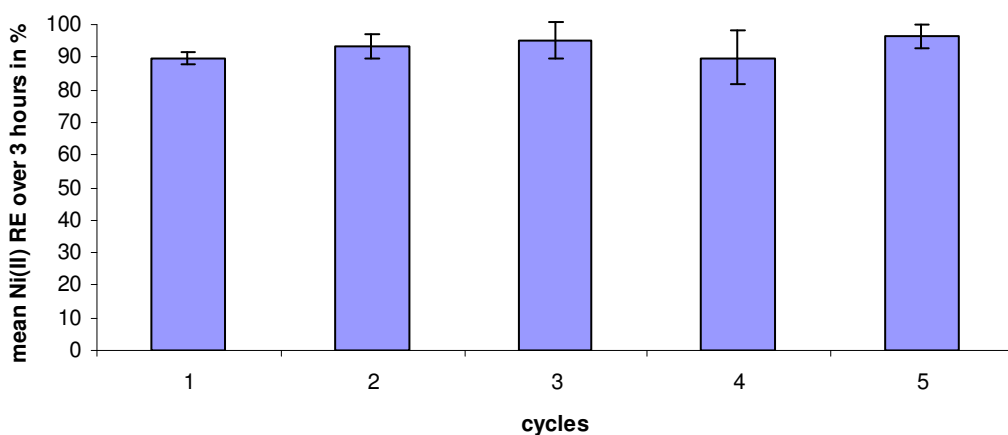


Fig. 7.8 Mean removal efficiency of Ni(II) from WAP/agar blocks over 3 hours from 5 successive regeneration and re-use cycles using 0.1 M HCl as the desorbing agent. Error bars calculated from four replicates with 95% confidence intervals.

Fig. 7.8 shows that the mean RE was greater than 90% for the five successive Ni(II) exposure/desorption cycles. No loss of RE for Ni(II) was observed after 4 successive regenerations of the biosorbent.

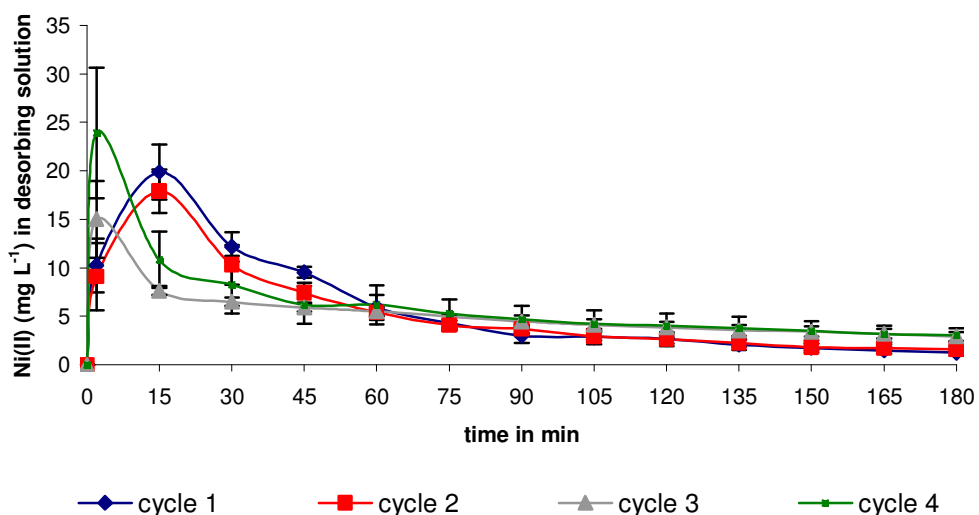


Fig. 7.9 Ni(II) concentrations in effluent during 4 desorption cycles. Error bars calculated from four replicates with 95% confidence intervals.

Fig. 7.9 shows that the majority of Ni(II) recovery occurred within 15 min followed by a sharp decrease in Ni(II) concentrations in the effluent. For the first desorption cycle, out of the 10 mg L<sup>-1</sup> Ni(II) feed, 10 mg L<sup>-1</sup> of the metal was recovered within 2 min. For the other desorption cycles, the Ni(II) concentrations in the effluent exceeded 10 mg L<sup>-1</sup> within 15 min, indicating a mechanism of high accumulation of the metal during the metal sorption cycles and a rapid release during the desorption cycle.

#### 7.4.2.3 Regeneration of WAP/agar blocks after the removal of Al(III) in dynamic flow tests using 0.1 M HCl as the desorbing agent.

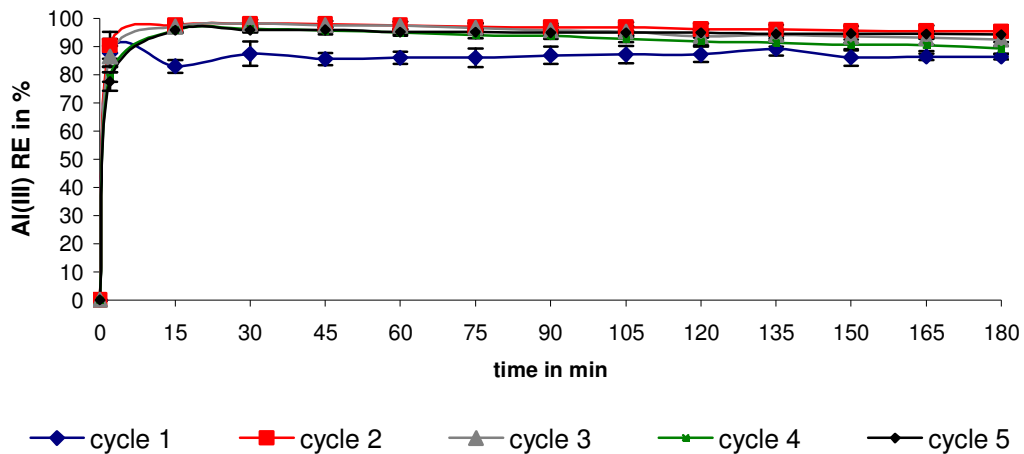


Fig. 7.10 Removal efficiency of Al(III) from WAP/agar blocks in 5 successive regeneration and re-use cycles using 0.1 M HCl as the desorbing agent. Error bars calculated from four replicates with 95% confidence intervals.

Fig. 7.10 shows that high removal efficiencies were reached within 15 min, with more than 90% of Al(III) removed. For each cycle, equilibrium was reached after 15 min.

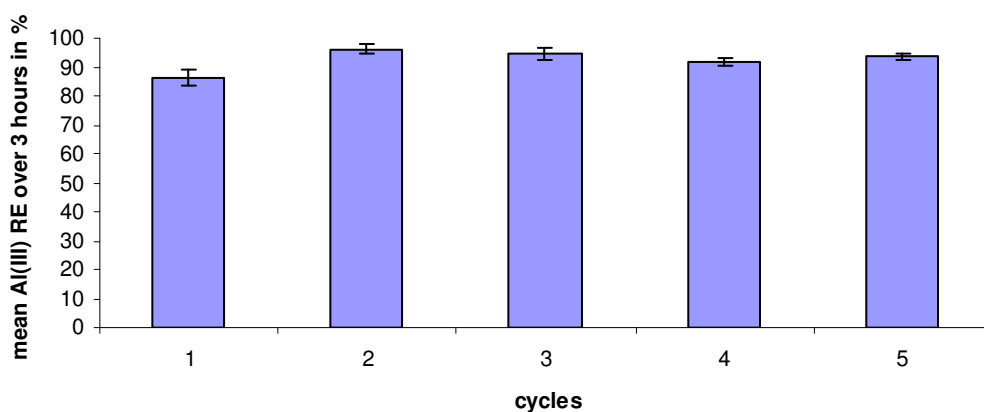


Fig. 7.11 Mean removal efficiency of Al(III) from WAP/agar blocks over 3 hours from 5 successive regeneration and re-use cycles using 0.1 M HCl as the desorbing agent. Error bars calculated from four replicates with 95% confidence intervals.

Fig. 7.11 shows that the mean RE was above 80% for the five successive Al(III) exposure/desorption cycles. No loss of RE for Al(III) was observed after 4 successive regenerations of the sorbent.

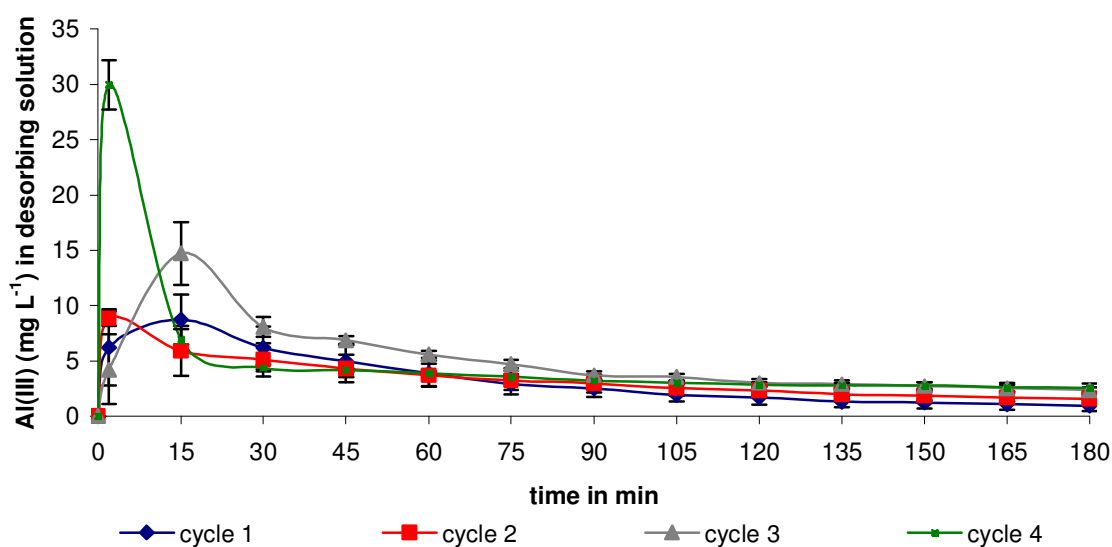


Fig. 7.12 Al(III) concentrations in effluent during 4 desorption cycles. Error bars calculated from four replicates with 95% confidence intervals.

Fig. 7.12 shows that the majority of Al(III) recovery occurred within 15 min, followed by a sharp decrease in Al(III) concentrations in the effluent. For the first desorption cycle, out of the 10 mg L<sup>-1</sup> Al(III) feed, 8.74 mg L<sup>-1</sup> of the metal was recovered within 15 min. For desorption cycles 3 and 4, the Al(III) concentrations in the effluent exceeded 10 mg L<sup>-1</sup> within 15 min, indicating a mechanism of high accumulation of the metal during the metal sorption cycles and a rapid release during the desorption cycles.

#### 7.4.2.4 Regeneration of *P. lanosa*/agar blocks after the removal of Sb(III) in dynamic flow tests using 0.1 M HCl as the desorbing agent.

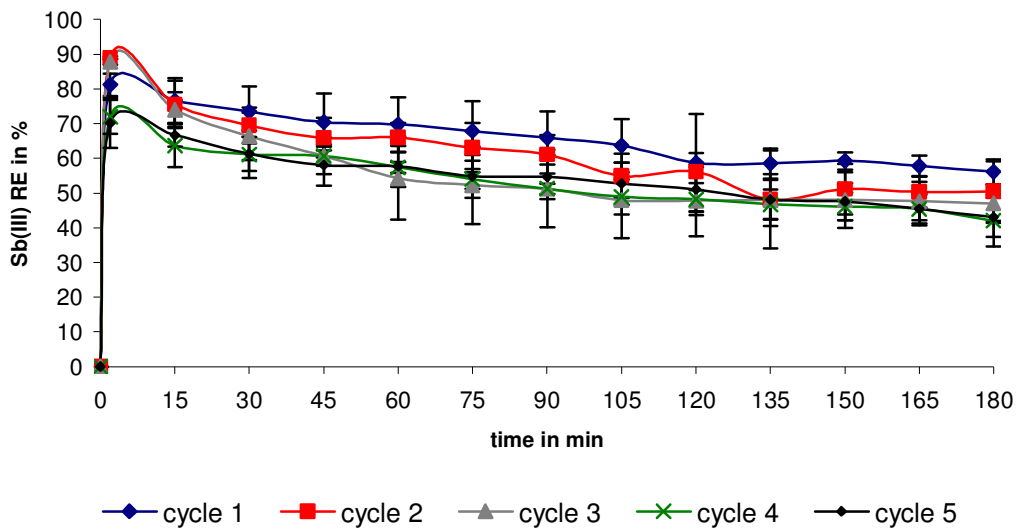


Fig. 7.13 Removal efficiency of Sb(III) from *P. lanosa*/agar blocks 5 successive regeneration and re-use cycles using 0.1 M HCl as the desorbing agent. Error bars calculated from four replicates with 95% confidence intervals.

Fig. 7.13 shows that high REs were achieved for the first three sorption cycles, reaching a maximum within 15 mins of the experiment. Lower REs were observed for cycles 4 & 5, indicating that the biomass has become less efficient in the later cycles.

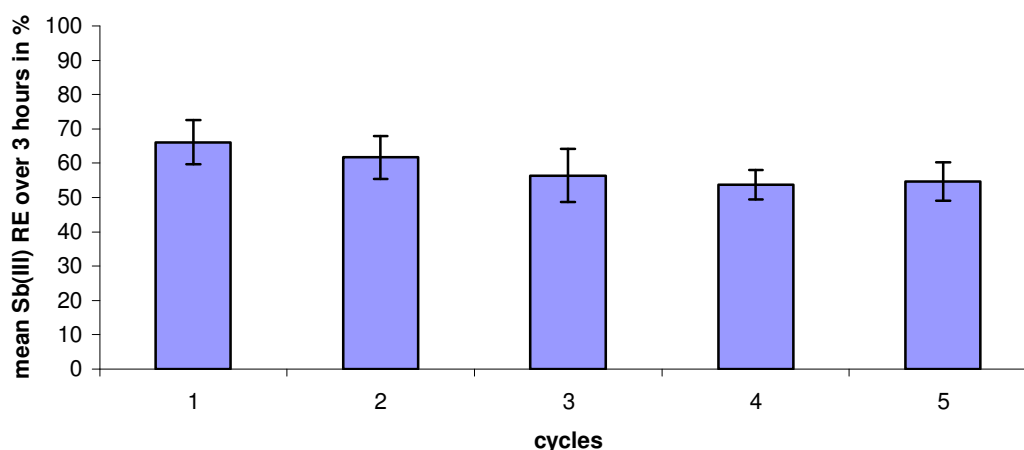


Fig. 7.14 Mean removal efficiency of Sb(III) from *P. lanosa*/agar blocks over 3 hours from 5 successive regeneration and re-use cycles using 0.1 M HCl as the desorbing. Error bars calculated from four replicates with 95% confidence intervals.

Fig. 7.14 shows a gradual decrease in RE during the 4 successive desorption cycles. A maximum RE of 66% was observed for cycle 1, with a minimum for cycle of only 55%.

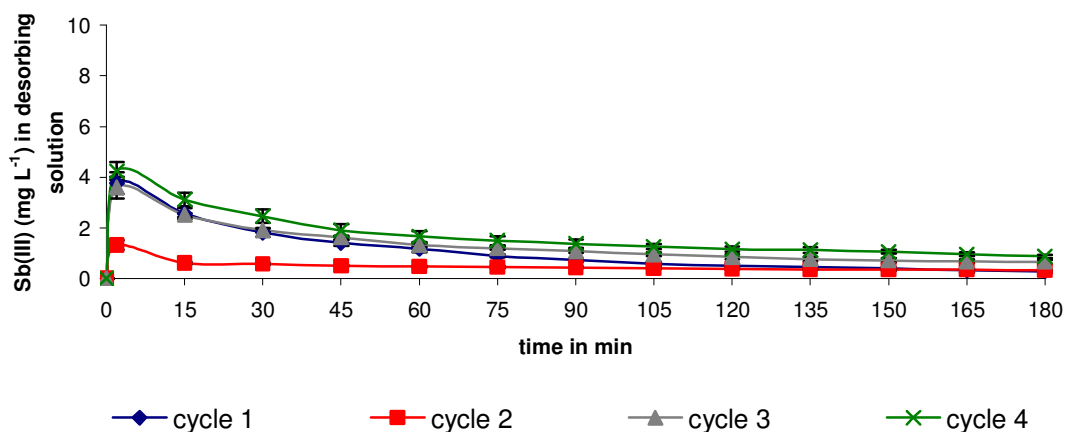


Fig. 7.15 Sb(III) concentrations in effluent during 4 desorption cycles. Error bars calculated from four replicates with 95% confidence intervals.

Fig. 7.15 shows that the recovery of Sb(III) from 7.5% *P. lanosa*/5% agar blocks was lower than the recovery of the other metals, utilising WAP/agar as the sorbent. The majority the of Sb(III) desorption occurred within 15 min, followed by a pronounced

decrease until 60 min. After 60 min, an equilibrium was reached with constant low Sb(III) concentrations in the effluent. Minimum recovery was obtained during cycle 2, with only 1.31 mg L<sup>-1</sup> of Sb(III) detected in the effluent within 15 min.

#### 7.4.2.5 Regeneration of the WAP/agar blocks after the removal of Zn(II), Ni(II) and Al(III) in a multi-metal solution in dynamic flow tests using 0.1 M HCl as the desorbing agent.

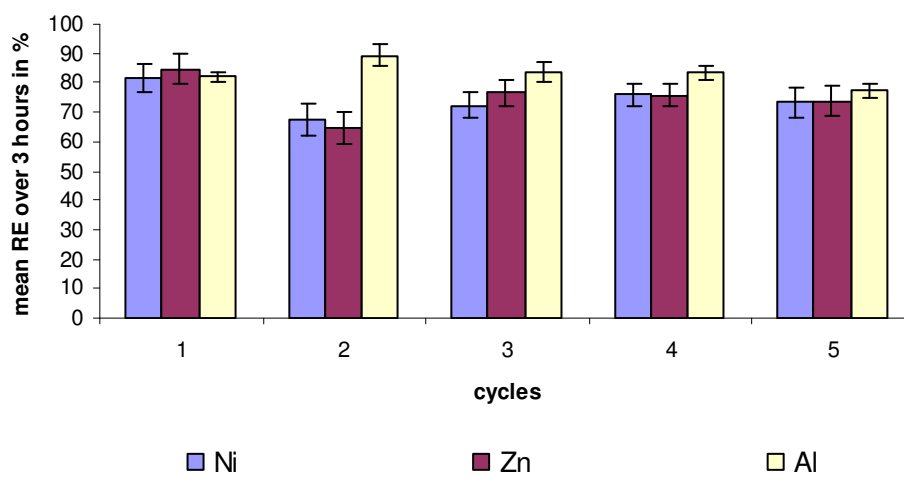


Fig. 7.16 Mean removal efficiency of Ni(II), Zn(II) and Al(III) from WAP/agar over 3 hours in 5 successive regeneration and re-use cycles using 0.1 M HCl as the desorbing agent. Error bars calculated from four replicates with 95% confidence intervals.

Fig. 7.16 shows a variation in mean RE over three hours for the 5 sorption cycles. Cycle 1 displayed similar RE values for the three metals. This was not the case for the remaining cycles. Cycle 2 demonstrated a decrease in RE for both Ni and Zn, while Al increased marginally. This trend was not repeated for the final 3 cycles, with relatively similar RE values for the three metals under investigation.

Nickel:

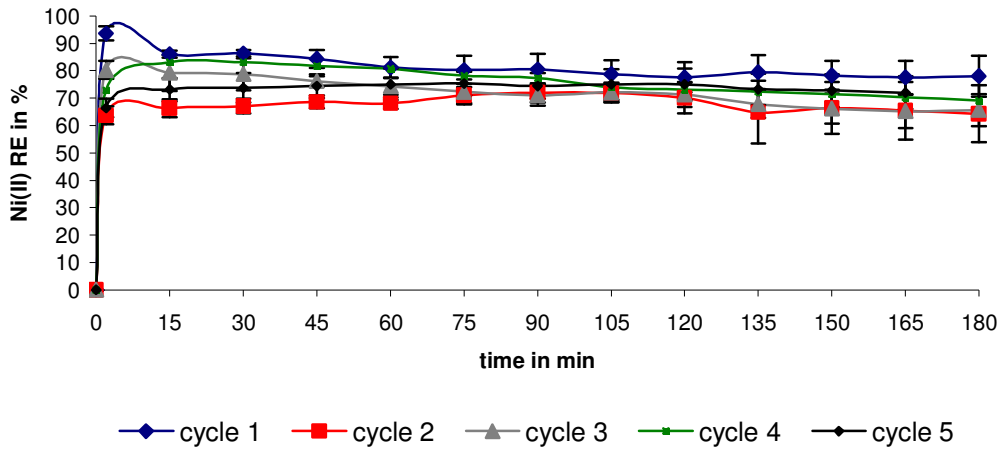


Fig. 7.17 Removal efficiency of Ni(II) from WAP/agar blocks in 5 successive regeneration and re-use cycles using 0.1 M HCl as the desorbing agent, in a multi-metal solution. Error bars calculated from four replicates with 95% confidence intervals.

Fig. 7.17 shows that high REs were obtained for Ni(II) for the 5 sorption cycles. Maximum RE was observed during the first sorption cycle, with a RE of 94% within 2 min. The REs for cycle 2 were generally lower than the other sorption cycles.

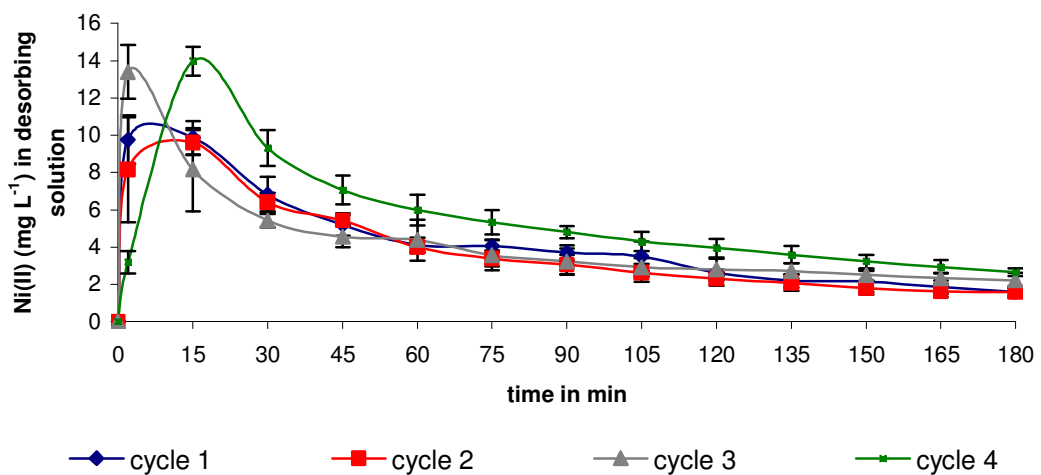


Fig. 7.18 Ni(II) concentrations in effluent during 4 desorption cycles. Error bars calculated from four replicates with 95% confidence intervals.

Fig. 7.18 shows that high Ni(II) concentrations were detected in the effluent within 15 min for all desorption cycles. Maximum observed Ni(II) concentrations were for cycle 4, at  $13.97 \text{ mg L}^{-1}$ . Ni(II) concentrations in the effluent decreased gradually after 15 min to reach minimum values at 180 min.

**Zinc:**

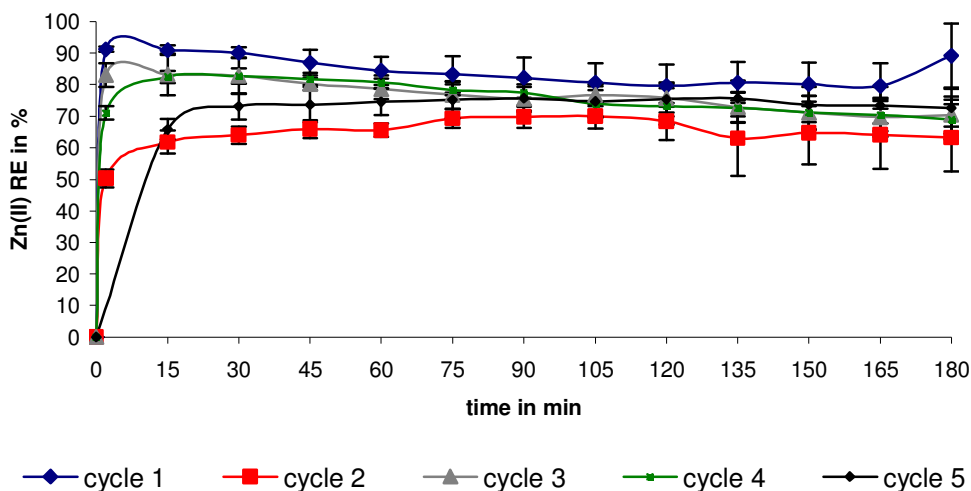


Fig. 7.19 Removal efficiency of Zn(II) from WAP/agar blocks in 5 successive regeneration and re-use cycles using 0.1 M HCl as the desorbing agent, in a multi-metal solution. Error bars calculated from four replicates with 95% confidence intervals.

Fig. 7.19 shows that REs for Zn(II) were relatively high for the 5 sorption cycles. Maximum RE was observed during cycle 1, with 91% of the initial Zn(II) removed. REs for cycle 2 were lower than the other cycles, with values below 70%. However, this did not have any adverse effects on the RE values for the following cycles which were all above 70%.

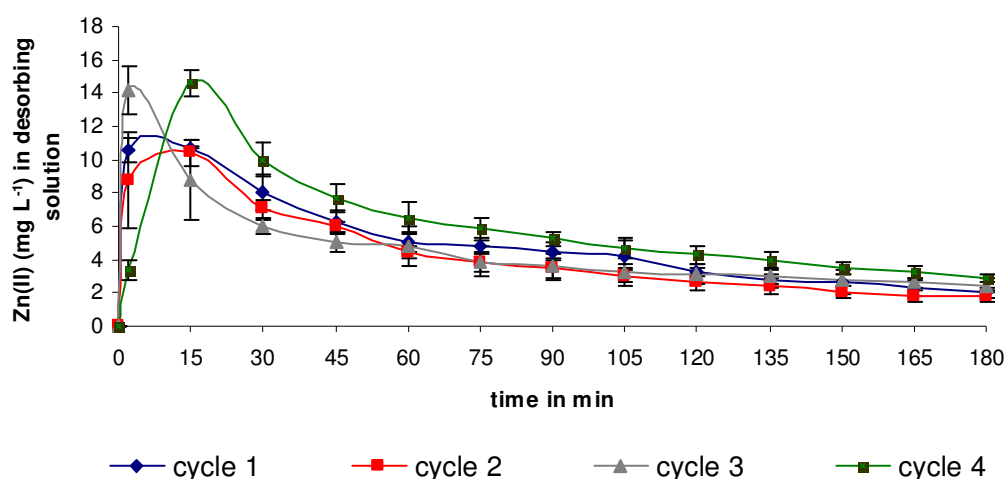


Fig. 7.20 Zn(II) concentrations in effluent during 4 desorption cycles. Error bars calculated from four replicates with 95% confidence intervals.

Fig. 7.20 shows that high Zn(II) concentrations were detected in the effluent within 15 min for all the desorption cycles. Maximum Zn(II) concentrations were observed during cycle 4, at  $14.60 \pm 0.81 \text{ mg L}^{-1}$ . Zn(II) concentrations in the effluent decreased gradually after 15 min to reach minimum values at 180 min.

Aluminium:

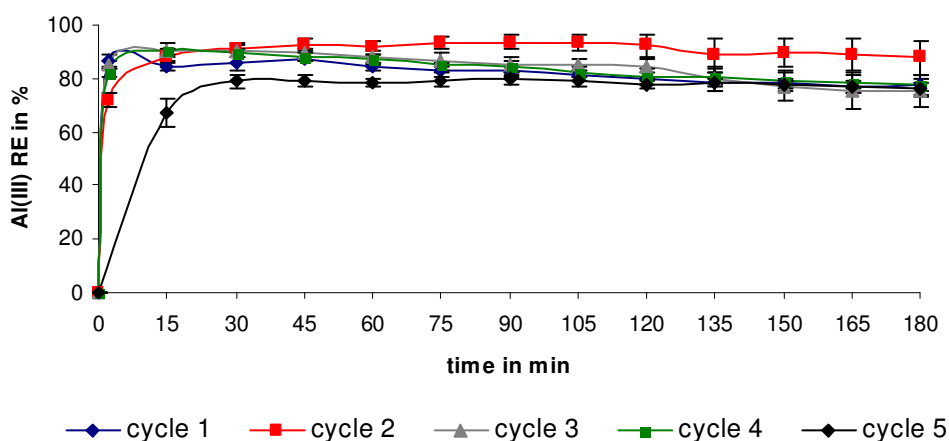


Fig. 7.21 Removal efficiency of Al(III) from WAP/agar blocks in 5 successive regeneration and re-use cycles using 0.1 M HCl as the desorbing agent, in a multi-metal solution. Error bars calculated from four replicates with 95% confidence intervals.

Fig. 7.21 shows that high REs were obtained for all the cycles, with cycle 5 displaying lower values. Maximum REs were obtained for cycles 1, 3 and 4 within 15 min with REs above 90%. For cycle 2, high REs (> 90%) were reached after 30 min. REs obtained for the last sorption cycle were generally lower than for the other cycles.

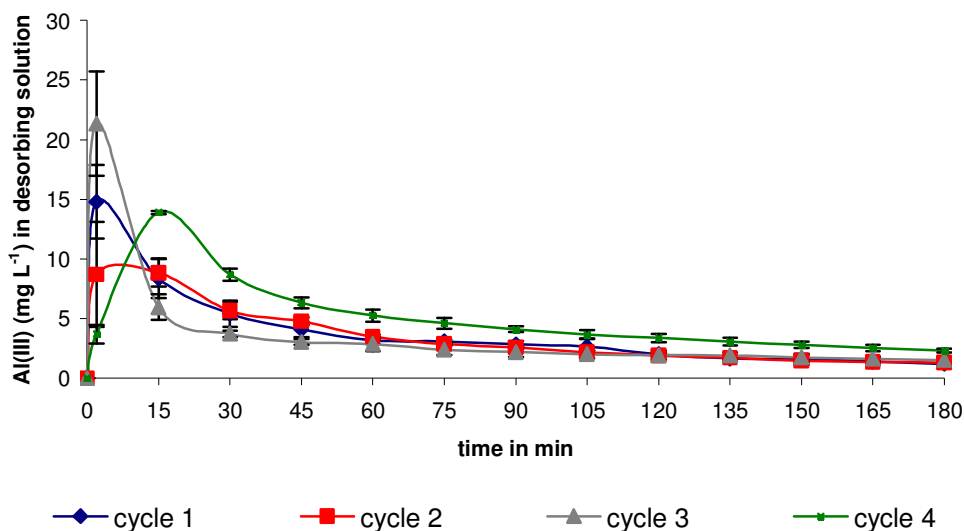


Fig. 7.22 Al(III) concentrations in effluent during 4 desorption cycles. Error bars calculated from four replicates with 95% confidence intervals.

Fig. 7.22 shows that high Al(III) concentrations were detected in the effluent within 15 min for all the desorption cycles. Maximum Al(III) concentrations were observed for cycle 4, at 21.35 mg L<sup>-1</sup>. Al(III) concentrations in the effluent decreased gradually after 15 min to reach minimum values at 180 min.

### Sorption

The sorption of metals, also studied in Chapter 4, was very rapid, and was generally achieved within 15 min. Little or no loss in RE was observed over the 5 metal sorption studies (Figs. 7.5, 7.8, 7.11, 7.14, 7.16). This indicates that WAP metal removal capacity was minimally affected by repeated exposure to the acid. This compares with Senthilkumar et al. (2006), who reported that Zn(II) removal by biomass of *Ulva*

*reticulata* decreased dramatically after 3 sorption/desorption cycles, using 0.1M CaCl<sub>2</sub> in HCl (pH 3.5), from 64.72% RE for cycle 1 down to 55.19% for cycle 3.

REs for Sb(III) using the 7.5% *P. lanosa*/5% agar blocks (Figs. 7.14 & 7.15), were lower than those for the other metals.

### *Desorption*

As seen in Figs. 7.6, 7.9, 7.12, 7.15, 7.18, 7.20 and 7.22, metal desorption, and consequent regeneration of the biomass, is a very rapid process with a maximum recovery achieved within 15 minutes. The desorption rates observed are equivalent to other biosorbents. Saeed et al (2005) showed that the desorption of Cu(II), Cd(II) and Zn(II) from papaya wood using 0.1 N HCl was rapid with maximum metal recovery within 30 min.

Very high metal recovery rates were obtained for Ni(II), Zn(II) and Al(III) in both single and multi-metal systems, with metal concentrations significantly exceeding the initial metal concentrations (Figs. 7.6, 7.9, 7.12, 7.15, 7.18, 7.20 and 7.22). Sawalha et al. (2008) reported similar results for the desorption of Cu(II), Cd(II), Cr(III), Cr(VI), Pb(II) and Zn(II) from silica-immobilised saltbush (*Atriplex canescens*) using 0.1M HCl, with 106.1 % and 113.9% for Cu(II) and Zn(II) respectively recovered in single metal tests.

At the end of each desorption cycles, metal residues from the sorbent were very low, with metal concentrations less than 3 mg L<sup>-1</sup> observed in each case. As a result, little or no negative effect is likely for subsequent metal uptake in the following sorption cycles. This was a limiting factor in the study of Hashim et al. (2000), which showed that residues of Cu(II) after the first desorption cycle negatively influenced the following sorption cycle using immobilised *Sargassum baccaluria*. It was also reported by Lau et al. (2003) that repeated sorption-desorption cycles with *Ulva lactuca* using Cu(II), Ni(II) and Zn(II) led to decreased REs probably due to the destruction or morphological alteration of the binding sites on the biomass surface (Chu et al., 1997). This trend was observed in our study of Sb(III) removal utilising *P. lanosa*/agar blocks, with a pronounced decrease in RE over the 5 sorption cycles. However, this was not the case

when utilising the WAP/ agar blocks for the removal of the other metals, suggesting that WAP/agar blocks are more resistant to acid damage than *P. lanosa*/agar blocks.

A study by Holan et al (1992) showed that the desorption of cadmium from *A. nodosum* increased with increasing molarity of HCl. 95.9% of the initial Cd present in the sorbent was recovered by using a 0.5M HCl solution, compared with only 87.5% for a 0.1M HCl solution. Increasing the molarity of HCl may increase Sb(III) recovery, but may also adversely affect the physical integrity of the sorbent (Walsh, 2008).

## **7.5 Conclusions**

0.1 M HCl was shown to be efficient in the desorption of Ni(II), Zn(II) and Al(III) from 7.5% WAP/5% agar blocks, in both single or multi-metal solutions. High concentrations of metals were recovered within 15 min. Regeneration of the sorbents was achieved with no loss in RE for the 5 sorption/desorption cycles using WAP. However, REs for Sb(III) removal using the 7.5% *P. lanosa*/5% agar decreased significantly over the 5 sorption cycles.

## **Chapter 8**

### **Study of Sb(III) sorption by WAP and *Polysiphonia lanosa*: Antagonistic effects**

## 8.1 Introduction

The use of a laboratory scale fixed-bed sorption column, using an industrial seaweed waste product as biosorbent (WAP), demonstrated high removal efficiencies for a variety of heavy metals, including Ni(II), Zn(II) and Al(III), with 72%, 75% and 87% RE, respectively (see Chapters 2 & 4). The presence of Sb(III) in a combined metal solution suppressed the removal of Ni(II), Zn(II) and Al(III), reducing the RE to 28%, 17% and 24% respectively. Most studies in the past have focused on the adsorption efficiencies and sorption isotherms of different metals combined in aqueous solutions (Holan and Volesky, 1994; Schiewer and Volesky, 1996; Da Costa and De França, 1997; Sag, 2001; Al-Rub et al., 2006; Naja and Volesky, 2006a; Fagundes-Klen et al., 2007). However, a limited amount of work has been carried out on the characterisation of competitive metal biosorption by marine algae, specifically antagonistic and synergistic interactions (Andrade et al., 2006; Al-Rub et al., 2006). When treating multi-metallic effluents, metal ions compete for a limited amount of available binding sites in the biomass. The impact of the presence of co-ions is of particular interest as it can severely reduce the efficiency of the metal removal process (Kratochvil and Volesky, 2000). As reported by (Sag, 2001), when working with non-viable cells as biosorbents for combined metals, three types of responses can be expected:

- The effect of the mixture is greater than that of each of the individual effects of the constituents in the mixture (synergism)
- The effect of the mixture is less than that of each of the individual effects of the constituents in the mixture (antagonism)
- The effect of the mixture is no more or no less than that of each of the individual effects of the constituents in the mixture (non-interaction).

The work of Al-Rub et al (2006) investigated the biosorption of copper, zinc and lead on *Chlorella vulgaris* from single, binary and ternary metal aqueous solutions. Their findings showed that *C. vulgaris* removed copper from single component aqueous solutions at removal efficiencies (RE) close to 100%. However, the presence of Zn and

Pb suppressed the removal of Cu ions. Pb was noted to be the predominant antagonistic agent in the sorption of Cu.

In this chapter, the antagonistic effects of Sb(III) on the sorption of Ni(II), Zn(II) and Al(III) were investigated. Potentiometric and conductimetric titrations, in addition to Fourier Transform Infra-Red (FTIR) and X-ray Photoelectron Spectroscopy (XPS), were carried-out in order to characterise and quantify the key functional groups involved in the binding of Sb(III) by WAP and *Polysiphonia lanosa*.

### **Fourier Transform Infra-Red Spectroscopy (FTIR)**

FTIR spectroscopy has been used to detect vibrational frequency changes in seaweed biomass during metal uptake, and allows identification of the functionalities involved in metal ion binding (Murphy et al., 2008).

### **Potentiometric and Conductimetric Titrations**

Potentiometric and conductimetric titrations have been used for the quantification of acidic groups in seaweed biomass, as well as the quantification of biomass pKa values (Yeoung-Sang, 2004; Murphy et al., 2007).

### **X-ray Photoelectron Spectroscopy (XPS)**

X-ray Photoelectron Spectroscopy, or XPS, allows identification of the sorption sites involved in the binding of metals by a biosorbent, as well as the oxidation state of the metals bound (Dambies et al., 2001). The key advantages of XPS over conventional analytical techniques is the simplification of sample preparation and the generation of accurate and detailed information. XPS is a useful tool for characterising ligand effects in transitional complexes. Electron-donating ligands will lower the binding energy (BE) of the core level electrons, and electron-withdrawing ligands will raise their BE.

XPS analysis has been used by a number of researchers to determine the interactions between the organic functional groups and the metal ions in seaweed/metal binding

(Figueira et al., 1999; Park et al., 2004; Sheng et al., 2004). The functional groups are characterised by the binding energy of carbon.

## 8.2 Aims

- To investigate the competitive sorption of Sb(III) with Ni(II), Zn(II) and Al(III).
- To characterise WAP and *P. lanosa* biomass in terms of the number and type of acidic binding sites present on the surface, and to investigate the effect of Sb(III) binding on the availability of these sites.
- To determine the concentration of each element, as well as their oxidation state during the binding process.

## 8.3 Methods

### Biomass preparation

*Polysiphonia lanosa* was harvested from Fethard-on-Sea, located in the south-east of Ireland (Section 2.3). The seaweed samples were rinsed thoroughly with distilled water in order to remove sand and epiphytes. Samples were oven-dried at 60°C for 12h, and subsequently ground and sieved to a particle size of 500-850 µm. The biomass was stored in airtight polyethylene bottles until required. A seaweed waste product resulting from the industrial processing of *Ascophyllum nodosum* (WAP) was supplied by Oilean Glas Teo (OGT) (Ballymoon Industrial Estate, Kilcar, Co. Donegal, Ireland). The waste was dried at 60°C for 24h, and subsequently ground and sieved to a particle size 500-850 µm.

### 8.3.1 Potentiometric and Conductimetric Titration

#### Chemicals

- 1000mg L<sup>-1</sup> Sb (III) as Sb<sub>2</sub>O<sub>3</sub> (analytical grade) - Sigma-Aldrich Ltd., Dublin, Ireland.
- Sodium Hydroxide (solid) - Ridel de Haën, Germany.
- Sodium Chloride (solid) - Ridel de Haën, Germany.
- Hydrochloric Acid (37%) - LabScan Ltd., Dublin, Ireland.

#### Instrumentation

- Glove Box- Plas Labs Inc. Model number 818-GB/220
- WTW LF 538 Conductivity meter, with WTW TetraCon® 325 probe
- Mettler Toledo MP 220 pH meter with, a Mettler Toledo Inlab® 413 pH electrode

#### Protonation of the biomass

Biomass particles (5 g) were protonated by washing with 250 mL of 0.1M HCl (Fourest and Volesky, 1996). This treatment ensured that any remaining salt ions, e.g. Ca<sup>2+</sup>, Mg<sup>2+</sup>, Na<sup>2+</sup>, K<sup>+</sup>, were removed from the seaweed surface. The suspension was stirred for 6h to ensure that equilibrium had been reached. The biomass was filtered under vacuum and washed with distilled water until a constant conductance was obtained for the filtrate. The protonated biomass was oven-dried at 60°C for 24h and stored in polyethylene bottles until required.

#### Titration of the biomass

For each titration, 200 mg of protonated biomass was dispersed in 100 mL of 1mM NaCl solution. The titration was carried out by a stepwise addition of 0.25 mL of 0.1M NaOH (prepared with boiled distilled water) to the flask, while the suspension was

stirred under a nitrogen atmosphere (Glove Box- Model 818-GB/220, Plas Labs, Inc.). After each addition of titrant, the system was allowed to equilibrate until a stable pH reading was obtained. Conductivity was measured using a WTW LF 538 Conductivity meter with WTW TetraCon® 325 probe while pH measurements were recorded using a Mettler Toledo MP 220 pH meter with a Mettler Toledo Inlab® 413 pH electrode. Potentiometric titrations were carried out in triplicate, with error bars calculated to 95% confidence intervals. Conductimetric titrations were carried out singly to act as verification for potentiometric titration results.

### **Titration of the metal bound biomass**

In order to determine the effects of metal binding on the number of available acidic sites on the biomass surface, 100 mg of protonated WAP and *P. lanosa* were exposed to 50 mL of metal solutions containing 10 mg L<sup>-1</sup> of Sb (III). Experiments were carried out in triplicate. Flasks were shaken at 200 rpm at room temperature (21 ± 1°C). The biomass was then filtered under vacuum and oven dried at 60°C for 24h. Titration of the biomass was carried out as per Section 8.3.1.

### **8.3.2 Fourier Transform Infra-red Spectroscopy (FTIR)**

#### **Chemicals**

- 1000mg L<sup>-1</sup> Sb (III) as Sb<sub>2</sub>O<sub>3</sub> (analytical grade) - Sigma-Aldrich Ltd., Dublin, Ireland.
- Hydrochloric Acid (37%) - LabScan Ltd., Dublin, Ireland.

#### **Instrumentation**

Spectra were obtained using a Digilab Scimitar Series infrared spectrometer (Fig. 8.1a), employing a MIRacle™ Single Reflection HATR accessory (Fig. 8.1b) with up to 815 lbs of pressure available to keep the sample in optical contact with the diamond. Data was processed using Bio-Rad Win-IR Pro 3.1 software.

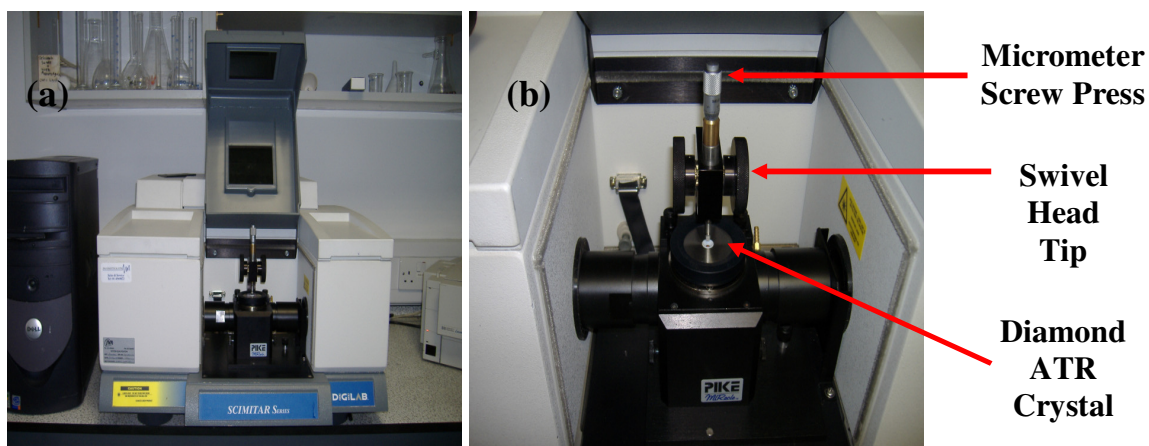


Fig. 8.1 (a) Digilab Scimitar Series Infrared Spectrometer (b) MIRacle™ Single Reflection HATR accessory

Spectra were recorded using a DTGS detector over the wavenumber range  $4000\text{-}600\text{cm}^{-1}$  at a resolution of  $4\text{ cm}^{-1}$ . The average number of scans was 40.

#### Advantages of the method

A key advantage of FTIR is the speed at which samples can be read, resulting from the simultaneous reading of all frequencies. This is sometimes referred to as the Fellgett Advantage. High sensitivity is also critical, in order to obtain well defined shifts between the metal-free and metal-loaded spectra, with minimum background contamination.

### 8.3.3 X-Ray Photoelectron Spectroscopy (XPS)

#### Chemicals

- Sodium Hydroxide (solid) - Ridel de Haën, Germany.
- Hydrochloric Acid (37%) - LabScan Ltd., Dublin, Ireland.
- Analytical grade metal solutions of Sb (III) - Sigma-Aldrich Ltd., Dublin, Ireland.

## Instrumentation



Fig. 8.2 Kratos AXIS 165 X-ray photoelectron spectrometer

**Note: The X-Ray Photoelectron Spectroscopy is located in the Materials and Surface Science Institute (MSSI) in the University of Limerick.**

Samples of raw *P. lanosa* and wet WAP were oven dried at 60°C for 24h, and subsequently exposed to solutions containing 1000 mg L<sup>-1</sup> and 2000 mg L<sup>-1</sup> Sb(III). The use of elevated metal concentrations (relative to previous experiments) ensured detection by the XPS techniques.

The biomass was added at a concentration of 2 mg mL<sup>-1</sup> to each solution. The flasks were agitated at 200 rpm at room temperature (21 ± 1°C) for 6h. The biomass was then filtered under vacuum and washed thoroughly with distilled water. Samples were dried at 60°C for 24h and stored in airtight polyethylene bottles until required.

## 8.4 Results and discussion

### 8.4.1 Potentiometric and Conductimetric titrations

#### 8.4.1.1 Titration of the biomass

Fig. 8.3 shows the potentiometric titration curves for WAP and *P. lanosa*, from the stepwise addition of NaOH.

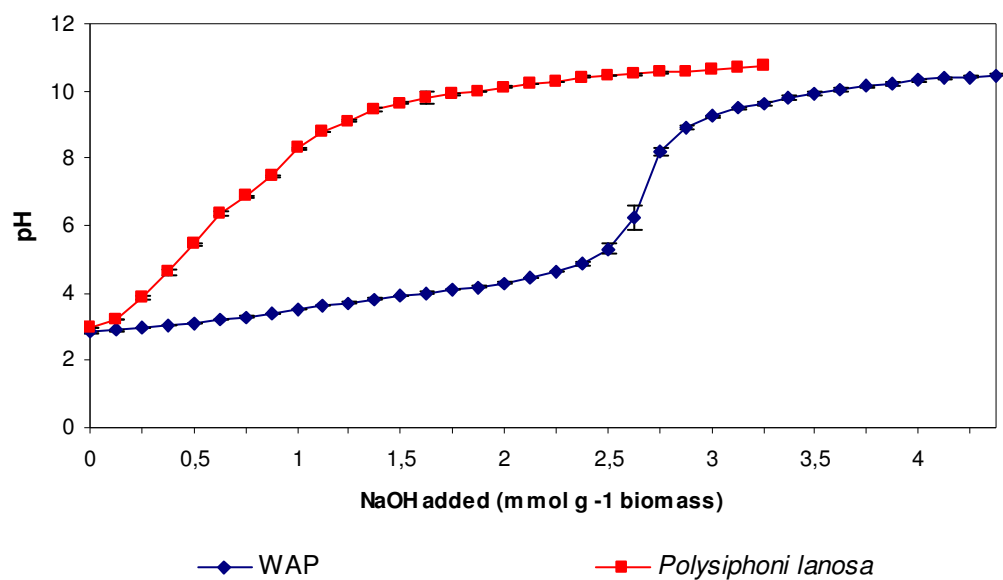


Fig. 8.3 Potentiometric titration curves obtained for protonated WAP and protonated *P. lanosa*. Error bars calculated from triplicate runs with 95% confidence intervals

Fig. 8.4 shows the conductimetric titration curves for protonated biomass of WAP and *P. lanosa*.

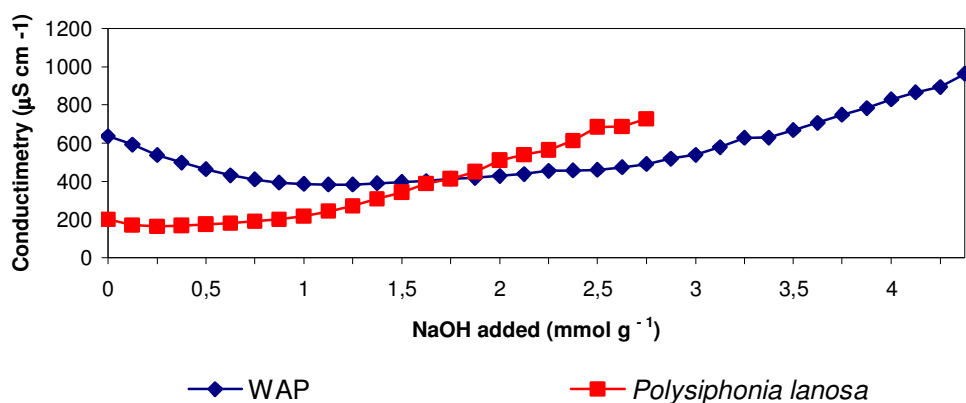


Fig. 8.4 Conductimetric titration for protonated WAP and *P. lanosa* (First derivative plots). Error bars calculated from triplicate runs at 95% confidence intervals

The conductimetric titrations (Fig. 8.4) show that the conductivity initially decreased with the addition of NaOH. When all of the strong acid groups were neutralised, the weaker acidic groups began to dissociate and contribute to the measured conductivity. The neutralisation of weak acids was characterised by a gentle increase in solution conductivity. When all the weak acidic groups were neutralised, the conductivity of the solution increased in proportion with the excess of NaOH added (Murphy, 2007). Potentiometric titrations are employed as indicators of the neutralisation of the free protons from the strong acidic groups.

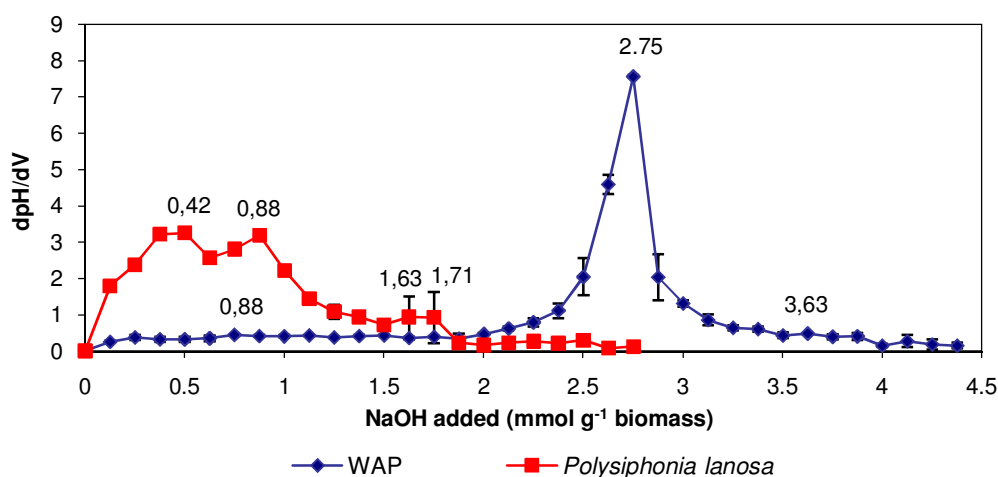


Fig. 8.5 Potentiometric titration of protonated biomass of WAP and *P. lanosa* (First derivative plots). Error bars calculated from triplicate runs at 95% confidence intervals

The number of strong acidic groups was determined from the first peak in Fig. 8.5, while the total number of acidic groups (i.e. strong and weak) was determined from the final peak. The corresponding  $pK_a$  values (Table 8.1) were evaluated by identifying the inflection points of the titration curves (Fig. 8.3). However, this can be quite difficult and a better indication of the position of these inflections was obtained from first derivative plots of average pH titration data (Murphy et al., 2007).

The first derivative plots consist of the midpoint of successive amounts of NaOH added (x-axis) versus  $dpH/dV$  (y-axis). Reading the location of each peak on the x-axis gives the number of acidic groups on the biomass surface.

#### 8.4.1.2 Titration of the metal bound biomass

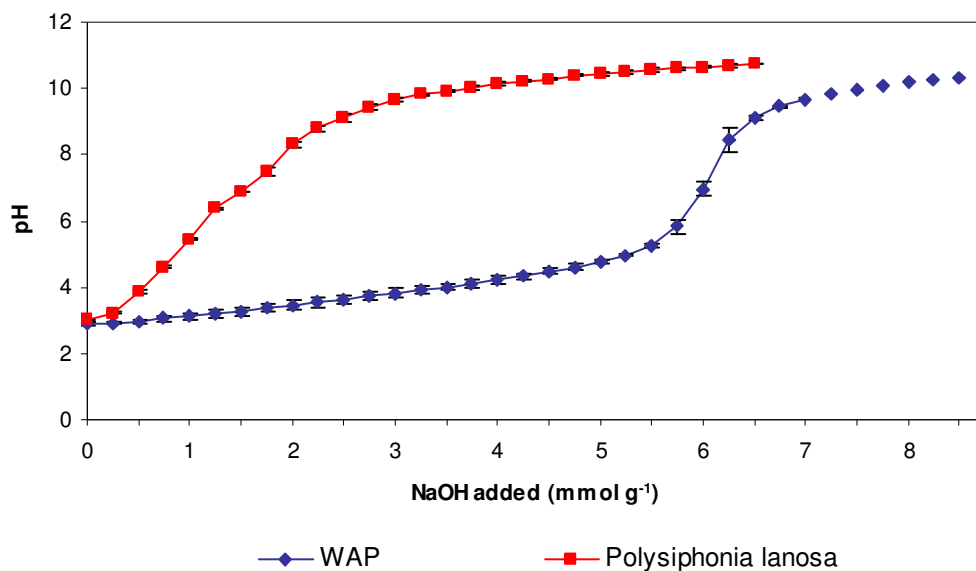


Fig. 8.6 Potentiometric titration curves obtained for Sb(III) exposed WAP and *P. lanosa*. Error bars calculated from triplicate runs with 95% confidence intervals

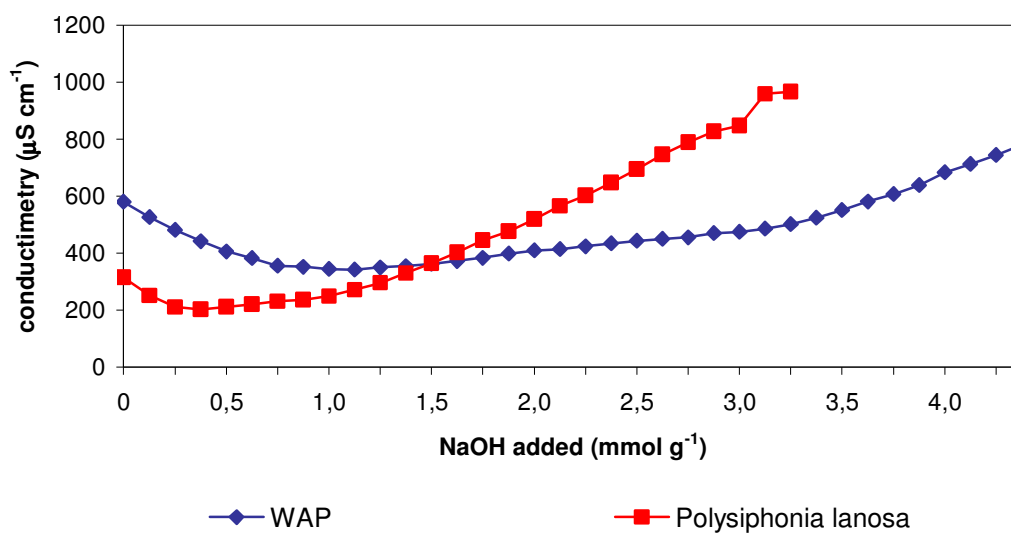


Fig. 8.7 Conductimetric titration curves obtained for Sb(III) exposed WAP and *P. lanosa*

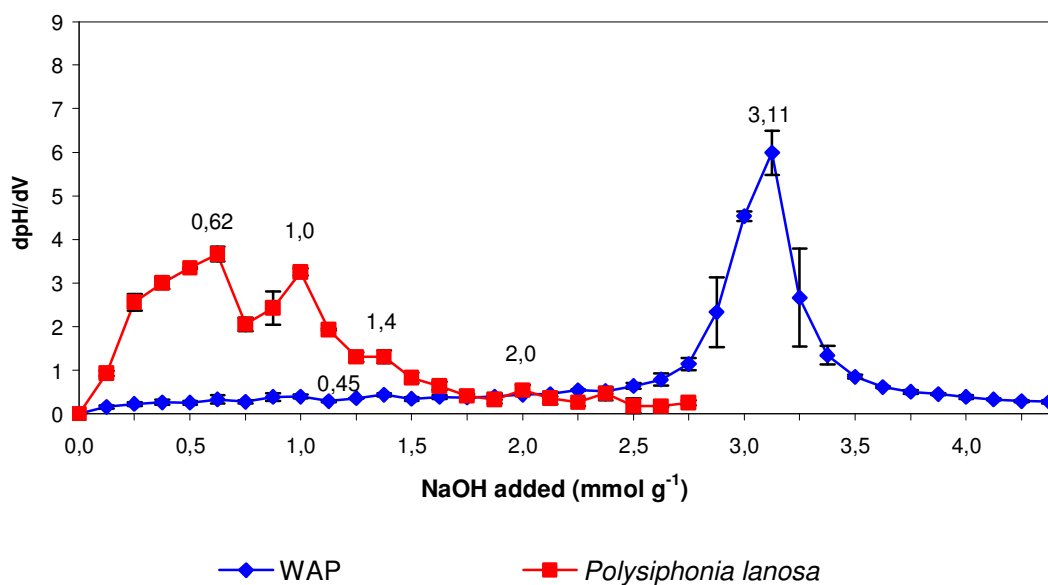


Fig. 8.8 Potentiometric titration of protonated biomass of WAP and *P. lanosa* (First derivative plots). Error bars calculated from triplicate runs at 95% confidence intervals

Table 8.1 pK<sub>a</sub> values and quantity of acidic groups observed during the study. Error bars were calculated based on triplicate runs with 95% confidence intervals.

Biomass	pK <sub>a</sub> values ± 95% CI	Acid Groups (mmol g <sup>-1</sup> biomass)		
		Total	Strong	Weak
Protonated WAP	6.25±0.34	3.63	0.88	2.75
Sb-laden WAP	6.46±0.57	3.11	0.45	2.66
Protonated <i>Polysiphonia</i> <i>lanosa</i>	4.47±0.04	1.71	0.42	1.29
	7.43±0.03			
	9.88±0.06			
	10.36±0.05			
Sb-laden <i>Polysiphonia</i> <i>lanosa</i>	3.63±0.17	0.62	0.28	0.34
	6.36±0.03			
	10.28±0.19			
	10.67±0.04			

First derivative plots for the protonated biomasses are shown in Fig. 8.5. The number of strong acidic groups were determined from the first peaks (0.88 and 0.42 mmol g<sup>-1</sup> for WAP and *P. lanosa*, respectively), whereas the total number of acidic groups were determined from the final peaks (3.63 and 1.71 mmol g<sup>-1</sup> for WAP and *P. lanosa*, respectively).

The corresponding pK<sub>a</sub> values were calculated by identifying the inflection point of the titration curves in Fig. 8.3. However, a more accurate indication of the position of these inflections is obtained from first derivative plots of average pH titration numerical data (Murphy et al., 2008). The pK<sub>a</sub> values and the number of acidic groups on the biomass surface are summarised in Table 8.1.

The first derivative plots consist of the midpoint of successive amounts of NaOH added (x-axis) versus  $\text{dpH/dV}$  (y-axis), permitting a direct reading of the various peaks obtained. Reading the location of each peak on the x-axis gives the number of acidic groups on the seaweed surface (Walsh, 2008). It was shown that protonated WAP, not exposed to a metal, contained a larger amount of total acidic groups ( $3.63 \text{ mmol g}^{-1}$ ) than protonated *P. lanosa* ( $1.71 \text{ mmol g}^{-1}$ ). The large amount of acidic groups is the direct result of the processing of *Ascophyllum nodosum*, with the purification of the sorbing components by elimination of nonsorbing polyphenols (Fourest and Volesky, 1996).

The results for *P. lanosa* were in agreement with Murphy et al. (2007) who obtained a total acidic group content of  $1.81 \text{ mmol g}^{-1}$  for protonated *P. lanosa*. In our study, four distinct  $\text{pK}_a$  peaks were observed for *P. lanosa* as opposed to a single one for WAP. The first  $\text{pK}_a$  observed for Sb(III)-laden *P. lanosa* is very close to the values reported for mannuronic and guluronic acids (3.38 and 3.65, respectively) (Murphy, 2007). For protonated *P. lanosa* the first  $\text{pK}_a$  gave a slightly higher value of 4.47, probably due to configurational differences (Percival and McDowell, 1967). It was also reported that the interaction between cations in solution and algal biomass may be attributed to the carboxyl groups of the alginic molecule at near neutral conditions; alginic acid being the principal structural polysaccharide in brown algae (Percival and McDowell, 1967). This was probably the case for WAP with a single  $\text{pK}_a$  at around 6.25. It was also reported that algal proteins have been known to interact with metal ions, particularly between pH 6-9 (Murphy, 2007).

The large number of acidic groups on WAP, and the  $\text{pK}_a$  values close to neutrality, are the most likely reason for its high metal removal capacity. However, there still remained the anomaly of its low affinity for Sb(III). The titration of the Sb(III)-bound biomasses indicated that weak acidic groups present on the surface of *P. lanosa* had a greater role in Sb(III) binding compared with those on WAP (Table 8.1). A reduction in the number of available acidic sites in metal loaded biomass was recorded for both WAP and *P. lanosa* (Table 8.1). For the Sb(III)-loaded WAP, a reduction from  $3.63$  to  $3.11 \text{ mmol g}^{-1}$  was recorded, of which  $0.43 \text{ mmol g}^{-1}$  was attributed to the strong acidic groups. For the

Sb(III)-loaded *P. lanosa*, a reduction from 1.71 to 0.62 mmol g<sup>-1</sup> was recorded, of which 0.95 mmol g<sup>-1</sup> was attributed to the weak acidic groups.

Decreases in the quantity of strong and weak acidic groups indicate that both sulphonate and carboxyl groups participated in the binding of Sb(III) by the two biomasses (Kratochvil and Volesky, 2000; Murphy et al., 2007). Sulphonate groups dissociate at pH 2, and it has been previously postulated by Figueira et al. (1999) that seaweed sulphonate groups are responsible for the uptake of trivalent metal cations such as Sb(III) in *Sargassum* biomass. This finding was in agreement with the FTIR analysis, (Section 8.4.2) where sulphonates and carboxyl groups were shown to be the principal functionalities involved in the binding of Sb(III) by both WAP and *P. lanosa*.

The difference in the binding mechanism of Sb(III) by the two biomasses appears to result from the relative amounts of weak and strong acidic groups involved. Weak acidic groups were mainly involved in Sb(III) binding by *P. lanosa*, suggesting a more important involvement of the carboxyl groups (Table 8.1). WAP, on the other hand, demonstrated a lesser participation of the carboxyl groups and a greater mobilisation of the strong acidic groups (e.g. sulphonate groups). Such variation in the involvement of carboxyl groups for binding metals by different biomasses has been demonstrated by Fourest et al. (1996) for the uptake of Zn by four macroalgal species. They also concluded that this variation depends on the carrier polymer, the environment of the functionality in which the uptake is occurring as well as the presence of other complexing groups in the biosorbent (Fourest and Volesky, 1996; Murphy, 2007).

#### **8.4.2 Fourier Transform Infra-Red Spectroscopy (FTIR)**

##### **FTIR analysis of biomass**

The assignment of FTIR bands and a summary of wavenumber shifts from protonated to Sb(III)-loaded biomasses (Fig. 8.9) is presented in Table 8.2. Good repeatability was observed for all replicate scans, with all differences less than or equal to three wavenumbers.

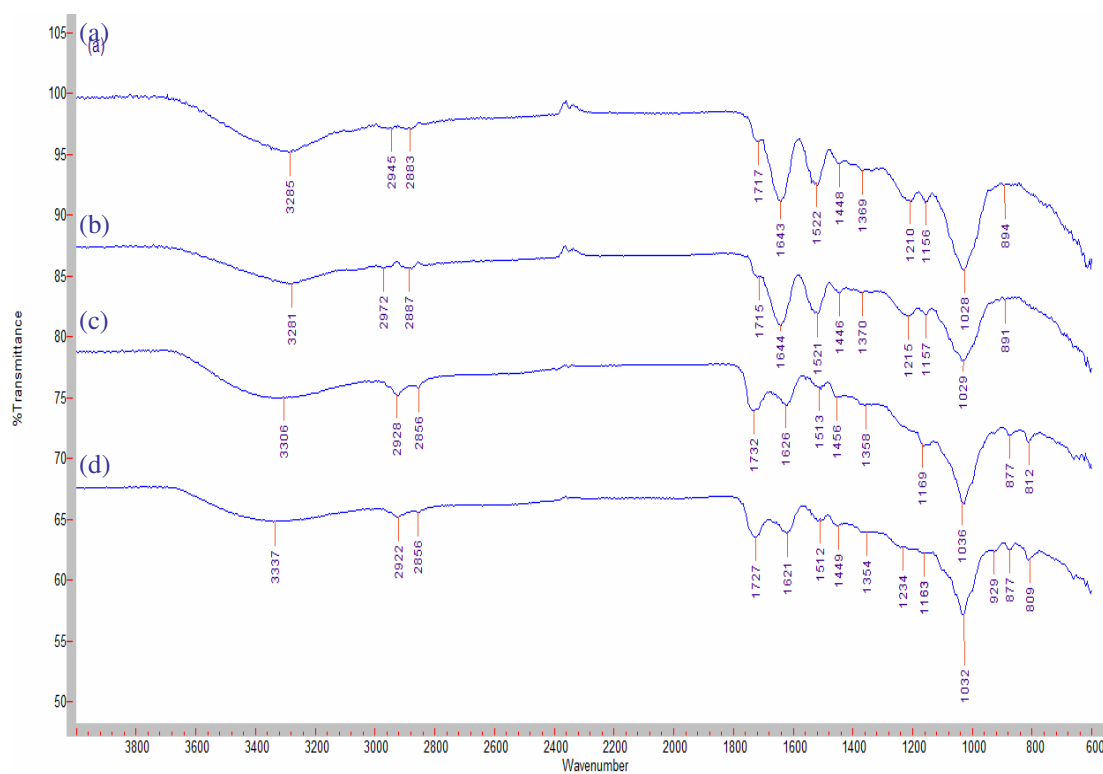


Fig. 8.9. Mid-IR spectra for (a) protonated and (b) Sb(III)-loaded *Polysiphonia lanosa*, (c) protonated and (d) Sb(III)-loaded WAP (number of scans = 40, resolution = 4 cm<sup>-1</sup>). Sample spectra from triplicate runs are shown.

Table 8.2 Stretching frequencies observed for Sb(III) loaded WAP and *P. lanosa*. Wavenumbers obtained for protonated biomass controls are shown in parentheses. Number of scans = 40, resolution = 4 cm<sup>-1</sup>. Average values from triplicate runs are shown.

Group Assignment	Wavenumber (cm <sup>-1</sup> )	
	WAP	<i>Polysiphonia lanosa</i>
-OH (bonded), -NH (stretching)	3337 (3228)	3284 (3293)
-CH (asymmetric)	2921 (2926)	2972 (2943)
Free C=O	1726 (1731)	1714 (1718)
C=O (asymmetric)	1621 (1622)	1642 (1643)
Amide II	1512 (1512)	1521 (1520)
C=O (symmetric)	1450 (1449)	1449 (1447)
-SO <sub>3</sub> (asymmetric)	1354 (1359)	1370 (1365)
C-O (carboxyl)	1203 (1239)	1213 (1217)
-SO <sub>3</sub> (symmetric)	1145 (1160)	1157 (1156)
C-O (alcohol)	1032 (1030)	1028 (1028)

FTIR results (Table 8.2) revealed that sulphonate groups contributed to Sb(III) binding on both WAP and *P. lanosa*. At the working pH of 2.63 ± 0.16 sulphonate groups are dissociated (pKa value of 1-2.5). It was reported by Figueira et al (1999) that sulphonate groups are responsible for the uptake of trivalent metal cations by *Sargassum* biomass. Binding resulted in band shifting for asymmetric -SO<sub>3</sub> in both WAP (1359-1354 cm<sup>-1</sup>) and *P. lanosa* (1370-1365 cm<sup>-1</sup>). A large wavenumber decrease (1160-1145 cm<sup>-1</sup>) was observed for the symmetric -SO<sub>3</sub> in the case of WAP only. No band shift for symmetric -SO<sub>3</sub> was observed for *P. lanosa* exposed to Sb(III). No shifts were observed for the C-

O (alcohol) bands in the  $1030\text{ cm}^{-1}$  region for either WAP or *P. lanosa*. Carboxyl groups were involved in Sb(III) binding as demonstrated by a shift in wavenumbers for both WAP ( $1239\text{-}1203\text{ cm}^{-1}$ ) and *P. lanosa* ( $1217\text{-}1213\text{ cm}^{-1}$ ). A previous study by Murphy et al (2007) reported that the binding of Cu to both *P. lanosa* and *P. palmata* involved the participation of carboxyl and sulphonate functionalities, and this also appears to be the case for Sb(III). No amino interaction was evident for either biomass, with no band shifting in the  $1520\text{ cm}^{-1}$  region.

In this study, the binding of Sb(III) by both WAP and *P. lanosa* included a significant contribution by both carboxyl and sulphonate groups.

### 8.4.3 X-Ray Photoelectron Spectroscopy

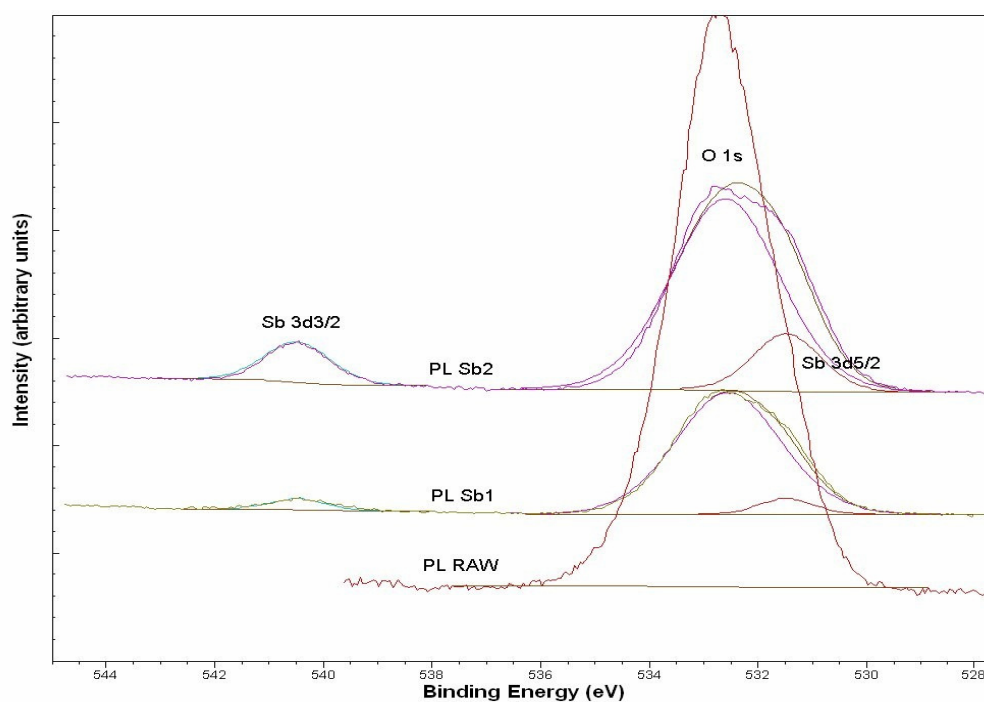


Fig. 8.10 XPS Sb spectra (binding energy against intensity) for raw (PL raw),  $1000\text{ mg L}^{-1}$  (PL Sb1) and  $2000\text{ mg L}^{-1}$  (PL Sb2) Sb (III)-loaded *P. lanosa*.

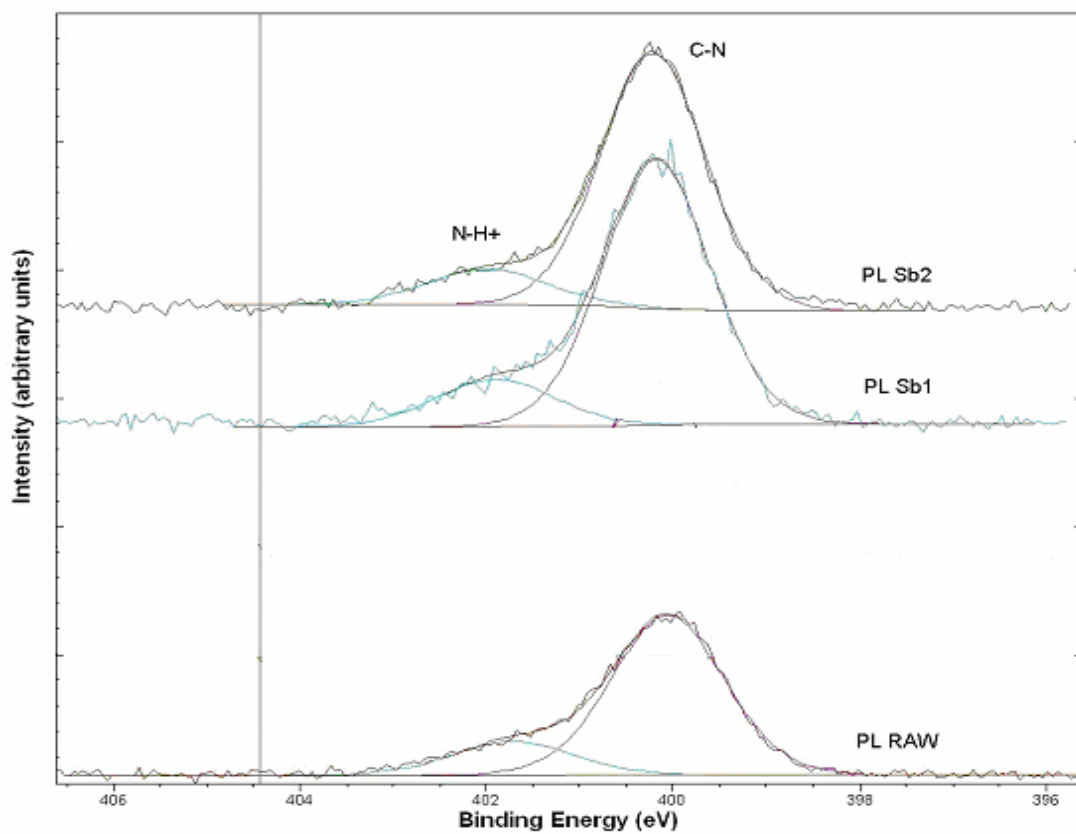


Fig. 8.11 XPS N spectra (binding energy against intensity) for raw *P. lanosa* (PL raw), 1000 (PL Sb1) and 2000 (PL Sb2) mg L<sup>-1</sup> Sb (III)-loaded *P. lanosa*.

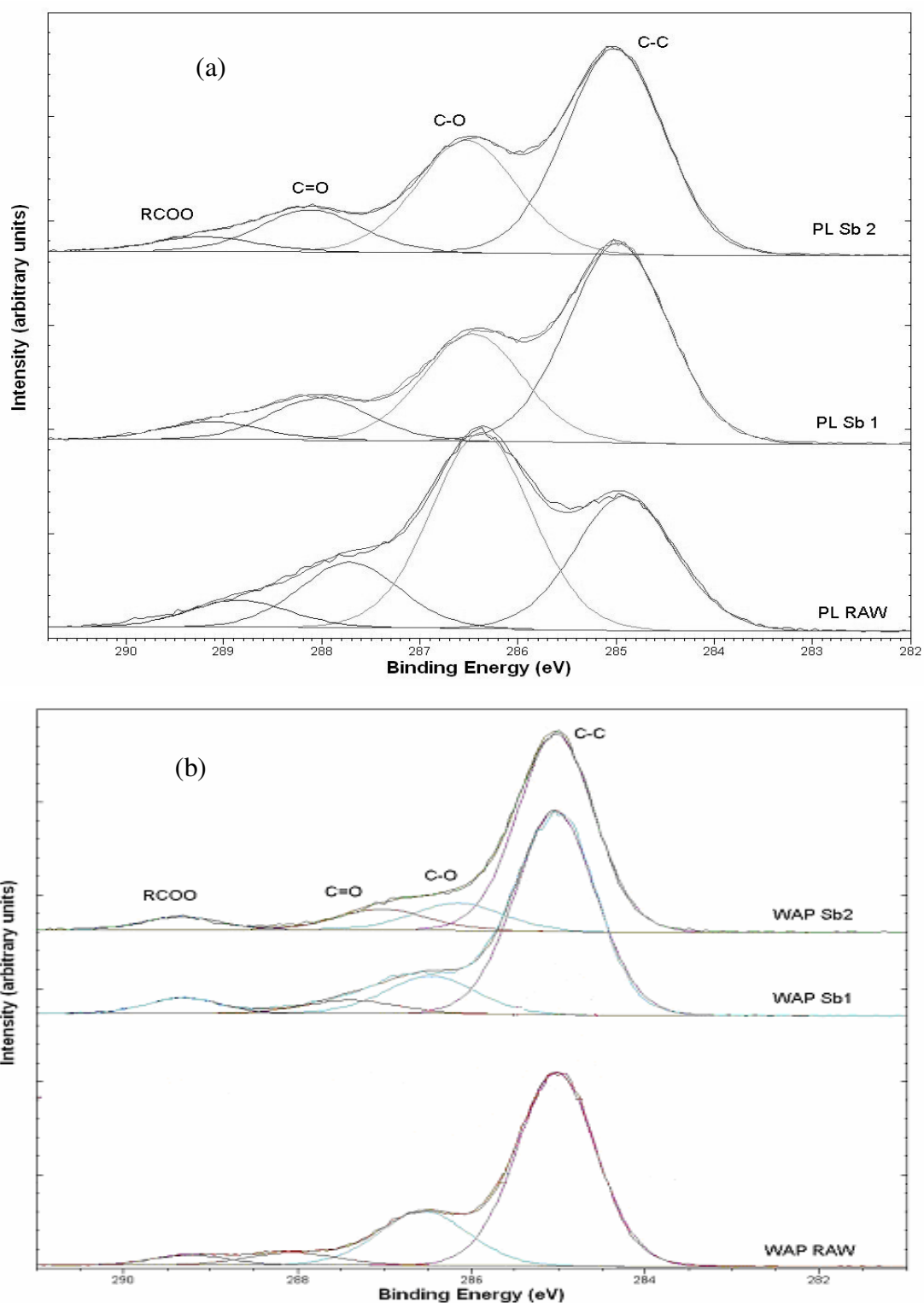


Fig. 8.12 XPS C1s spectra (binding energy against intensity) for (a) Raw *P. lanosa* (PL RAW), 1000 (PL Sb1) and 2000 (PL Sb2) mg L<sup>-1</sup> Sb (III)-loaded *P. lanosa*, (b) Raw WAP (WAP RAW), 1000 (WAP Sb1) and 2000 (WAP Sb2) mg L<sup>-1</sup> Sb (III)-loaded WAP.

Table 8.3 XPS atomic concentrations (in percentage) in WAP and *P. lanosa* before and after exposure to Sb(III) at two different concentrations (1000 and 2000 mg L<sup>-1</sup>).

	Atomic concentration (%)					
	<i>P. lanosa</i> (raw)	<i>P. lanosa</i> 1000 mg L <sup>-1</sup> Sb(III)	<i>P. lanosa</i> 2000 mg L <sup>-1</sup> Sb(III)	WAP (raw)	WAP 1000 mg L <sup>-1</sup> Sb(III)	WAP 2000 mg L <sup>-1</sup> Sb(III)
Element						
C 1s	65.71	70.70	68.10	80.73	84.37	85.19
O 1s	27.44	22.35	25.51	18.28	15.63	14.75
N 1s	4.12	6.67	5.72	ND	ND	ND
S 2p	2.73	ND	ND	0.99	ND	ND
Sb 3d3/2	ND	0.28	0.67	ND	ND	0.06
Cu 2p	ND	ND	ND	ND	ND	ND

ND: not detected

Table 8.4 Carbon 1s binding energies and peak ratios for *Polysiphonia lanosa* and WAP.

Biomass	Assignment of C1s peak	Peak (eV)	Peak Area Ratio (%)		
			Raw	1000 mg L <sup>-1</sup> Sb(III) loaded	2000 mg L <sup>-1</sup> <sup>1</sup> Sb(III) loaded
<i>Polysiphonia lanosa</i>	C-C	284.91	31.72	54.57	54.70
	C-O	286.37	46.44	29.23	30.13
	C=O	287.72	15.45	11.40	11.24
	RCOO	288.85	6.39	4.80	3.94
WAP	C-C	285.02	69.79	74.74	74.43
	C-O	286.55	21.80	15.15	11.83
	C=O	288.05	5.03	5.26	9.04
	RCOO	289.22	3.38	4.85	4.71

A higher proportion of oxygen (O) was found in *P. lanosa* than WAP (Table 8.3), i.e. 27.44% versus 18.28%. This was expected given the large amount of cell polysaccharides present on the seaweed surface. Nitrogen was detected in *P. lanosa* but not in WAP (Fig. 8.11 and Table 8.3). The higher amount of nitrogen in *P. lanosa* was most likely due to surface proteins. Small levels of sulphur were found in both WAP and *P. lanosa*. However, when treated with Sb(III), no sulphur was detected in either biomass. XPS analysis also showed that sulphur was mainly in a bi-polaronic form as the binding energy was similar to SO<sub>4</sub>. As most of the Sb(III) peaks overlapped during analysis of *P. lanosa*, only the Sb 3d<sub>3/2</sub> was suitable for analysis.

It is clear from Table 8.3 that, following exposure, higher concentrations of Sb(III) were present on the surface of *P. lanosa* than WAP. Atomic concentrations increased with increasing Sb(III) solution concentration (i.e. 0.67% for 2000 mg L<sup>-1</sup> Sb versus 0.28% for 1000 mg L<sup>-1</sup> Sb using *P. lanosa*).

Four peaks were identified after deconvolution of the C1s spectra of all samples (Fig. 8.12). The peak with a binding energy of 284.91 eV is attributed to C-C bonding and these hydrocarbon functionalities are used for energy calibration of the instrument. The remaining peaks can be assigned to alcohol (C-O), ether (C=O) and carboxylic (RCOO) groups, with BEs of 286.37, 287.72 and 288.85 eV, respectively (Chen et al., 2002). The area distribution of the four peaks indicated that alcohol groups are dominant in the two biomasses (Table 8.4). The area of the carboxyl peak decreased after Sb(III) binding to *P. lanosa*, indicating that the formation of carboxyl-metal complexes had taken place. The formation of carboxyl-metal complexes was, however, not seen when exposing WAP to Sb(III), and the slight increases observed may have been due to potential surface contamination during exposure (Dambies et al., 2001).

For *P. lanosa* exposed to Sb(III), the formation of alcohol and ether-metal complexes was also observed. For WAP, the formation of only alcohol-metal complexes was observed. This confirms that more diverse functional groups were involved in Sb(III) binding by *P. lanosa* (carboxyl, alcohol and ether) than WAP (ether groups only), as demonstrated in Section 8.4.2 by FTIR. Atomic concentrations also showed that a greater number of carboxyl groups were involved in Sb(III) binding by *P. lanosa* as opposed to WAP, as previously demonstrated with the potentiometric and conductimetric titrations.

### ***Summary of results***

The high affinity of Sb(III) for *P. lanosa* was found to be a direct result of the diversity and quantity of functional groups present on the surface of the biomass. Sb(III) was found to bind mainly on the surface of *P. lanosa* primarily through the involvement of sulphonate, carboxyl, alcohol and ether groups. The antagonistic effect of Sb(III) on the sorption of Zn(II), Ni(II) and Al(III) may be due to the fact that Sb(III) has a greater affinity for these binding sites, reducing the number of sites available for the other metals. It was also noted by Wase et al (1997) that carboxylate polysaccharides exhibit preferential binding of cations with large ionic radii (Wase and Forster, 1997). As *P. lanosa* was shown to contain a larger amount of carboxyl groups, by potentiometric titration and XPS analysis, the large ionic radius of Sb(III) (0.90 Å) may be a contributory factor in the high affinity between the metal and biomass. The similar extent of inhibition for Ni(II) and Zn(II) may be due to the similarity of their ionic radii (0.88 and 0.83 Å respectively).

### **8.5 Conclusions**

A seaweed (*Polysiphonia lanosa*) and an industrial seaweed waste product (WAP) were investigated for the removal of Zn(II), Ni(II), Al(III) and Sb(III) from single and combined metal solutions (Chapters 2 & 4). WAP was shown to be very efficient for the removal of Zn(II), Ni(II) and Al(III), in both single and combined solutions. However, *P. lanosa* was found to be more efficient for the removal of Sb(III). When combined with other metals, Sb(III) reduced their removal efficiencies by WAP. The antagonistic effect of Sb(III) on the sorption of Ni(II), Zn(II) and Al(III) was investigated further using FTIR, potentiometric titrations and XPS analysis.

FTIR analysis indicated that both carboxyl and sulphonate groups were involved in Sb(III) binding by both *P. lanosa* and WAP. Quantification of biomass surface acidic groups by potentiometric titrations showed that a greater amount of acidic groups (mostly carboxylic functionalities) were utilised in Sb binding by *P. lanosa* than by WAP. WAP, on the other hand, demonstrated a greater involvement of sulphonate groups. These results were confirmed by XPS analysis, which highlighted the

participation of carboxyl, alcohol and ether groups in Sb(III) binding by *P. lanosa* as opposed to only carboxyl and sulphonate groups by WAP. A possible explanation for the antagonistic effect of Sb(III) on the sorption of the other metal species is the impact of atomic sizes. Sb(III) was also found to bind to a larger and more diversified number of binding sites, preventing the uptake of Zn(II), Ni(II) and Al(III) by both *P. lanosa* and WAP. Finally, this study showed that the complementary use of FTIR, XPS and potentiometric titrations is a highly effective tool for the study of metal sorption behaviour onto biomass.

## **Chapter 9**

### **Mathematical modelling of sorption in a fixed-bed column**

## 9.1 Introduction

### The Yoon-Nelson model

Yoon and Nelson (1984) developed a simple model for describing the adsorption and breakthrough of sorbates (e.g. metal) with respect to activated carbon (Quintelas et al., 2008). This model (Eq. [9]) is based on the assumption that the rate of decrease in the probability of sorption for each sorbate molecule is proportional to the probability of sorbate sorption and the probability of sorbate breakthrough on the sorbent. (Tabakci and Yilmaz, 2008).

The Yoon and Nelson equation for a single component system is expressed as follows (Tabakci and Yilmaz, 2008):

$$\frac{C_e}{C_0} = \frac{1}{1 + \exp[k(\tau - t)]} \quad \text{Eq. [9]}$$

where  $C_0$  is the initial concentration ( $\text{mg L}^{-1}$ ),  $C_e$  is the concentration at equilibrium ( $\text{mg L}^{-1}$ ),  $k$  is the rate constant ( $\text{min}^{-1}$ ),  $\tau$  is the time required for 50% sorbate breakthrough (min), and  $t$  is the breakthrough (sampling) time (min).

The linear expression of the Yoon-Nelson model (Eq. [10]) can be written as follows (Tabakci and Yilmaz, 2008):

$$t = \tau + \frac{1}{k} \ln \frac{C_e}{C_0 - C_e} \quad \text{Eq. [10]}$$

## 9.2 Aims

- To develop a mathematical model for the prediction of metal removal behaviour in a fixed bed sorption column.

### 9.3 Methods

t (time in min) is plotted against  $\ln [C_e/(C_0-C_e)]$ . A linear regression line is then fitted to the experimental data (data generated in Chapter 4), and the generated equation yields both k and  $\tau$ .  $\tau$  may also be obtained at the sorption time when  $\ln [C_e/(C_0-C_e)]$  is zero ( $\tau$  is the sorption time when  $C_e$  is half of  $C_0$ ). However, as the dynamic flow tests in this study were only carried out over 3 hours, half the initial concentration was not reached. As a result  $\tau$  was calculated graphically.

### 9.4 Results and discussion

#### 9.4.1 Zn(II) removal by WAP/agar

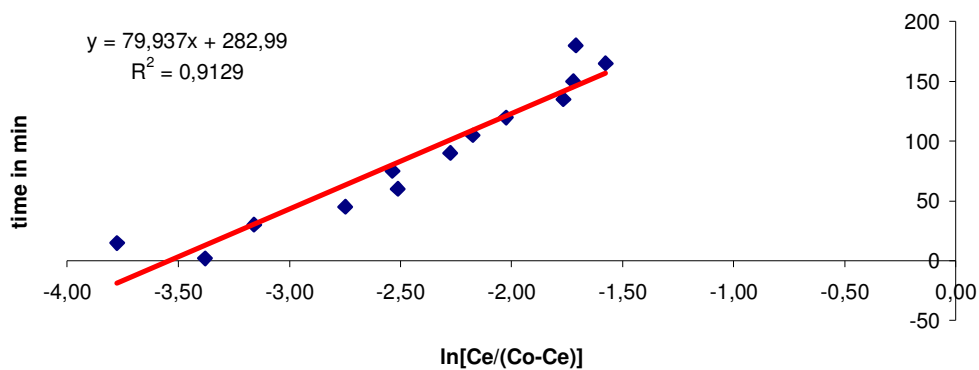


Fig. 9.1 Linear plot of the Yoon-Nelson model for Zn(II) removal by WAP/agar.

Fig. 9.1 shows good linearity, with a correlation coefficient of 0.9129.

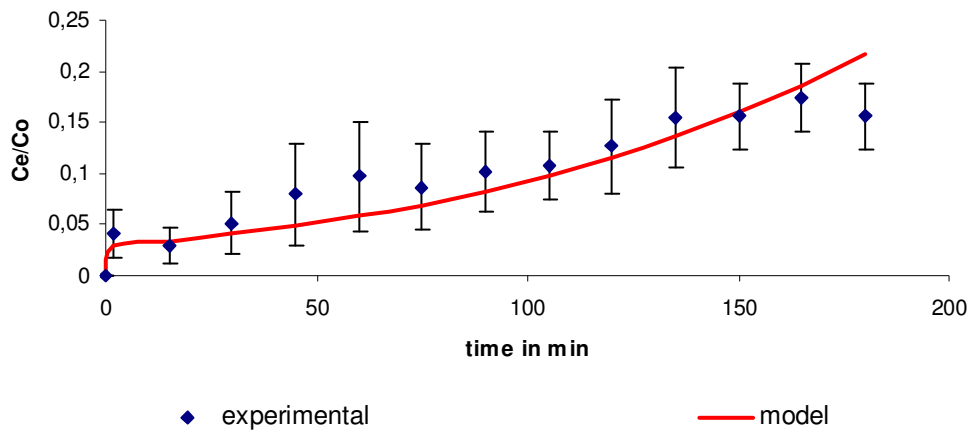


Fig. 9.2 Model fitting to the experimental data for Zn(II) removal by WAP/agar. Error bars are calculated based on four replicates with 95% Confidence Intervals.

#### 9.4.2 Ni(II) removal by WAP/agar

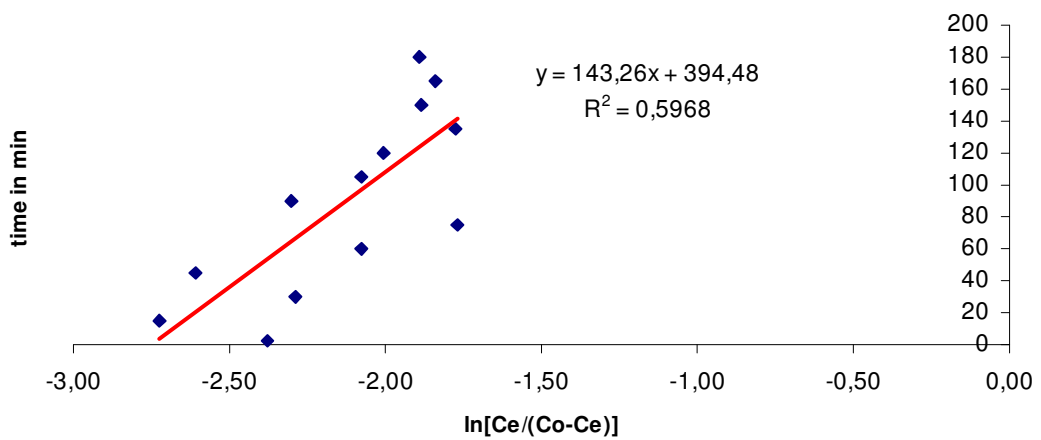


Fig. 9.3 Linear plot of the Yoon-Nelson model for Ni(II) removal by WAP/agar.

Fig. 9.3 shows linearity, with a correlation coefficient of 0.5968.

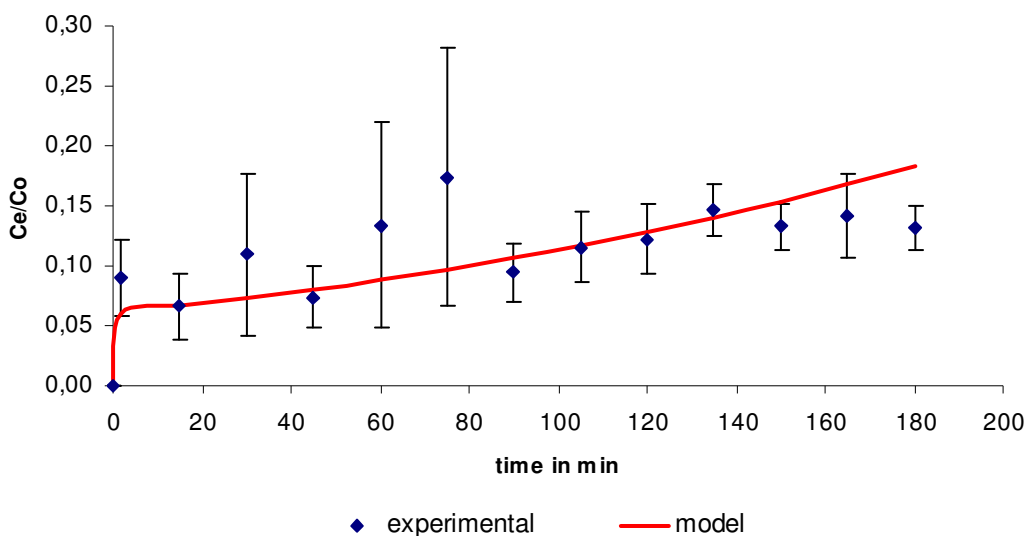


Fig. 9.4 Model fitting to the experimental data for Ni(II) removal by WAP/agar. Error bars are calculated based on four replicates with 95% Confidence Intervals.

### 9.4.3 Al(III) removal by WAP/agar

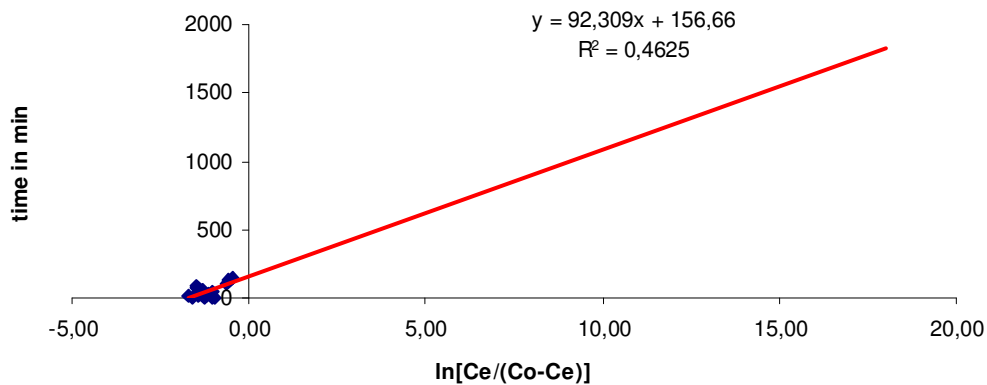


Fig. 9.5 Linear plot of the Yoon-Nelson model for Al(III) removal by WAP/agar.

Fig. 9.5 shows poor linearity, with a correlation coefficient of 0.4625.

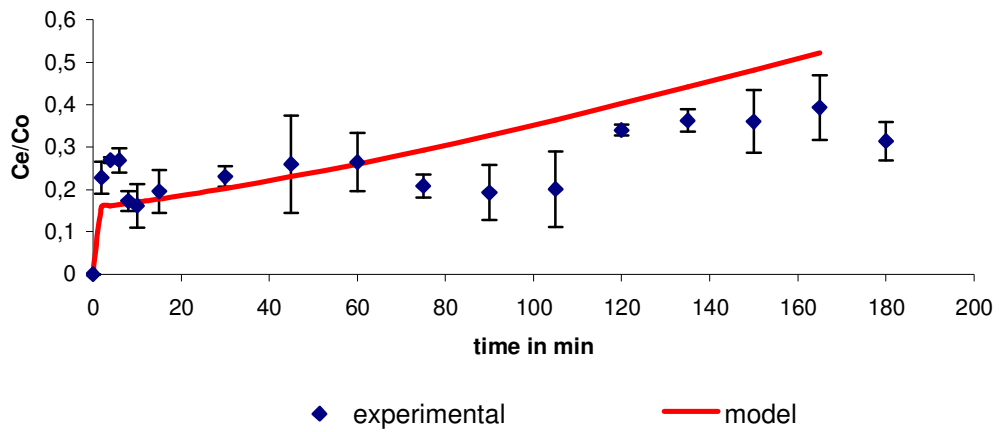


Fig. 9.6 Model fitting to the experimental data for Al(III) removal by WAP/agar. Error bars are calculated based on four replicates with 95% Confidence Intervals.

#### 9.4.4 Sb(III) removal by WAP/agar

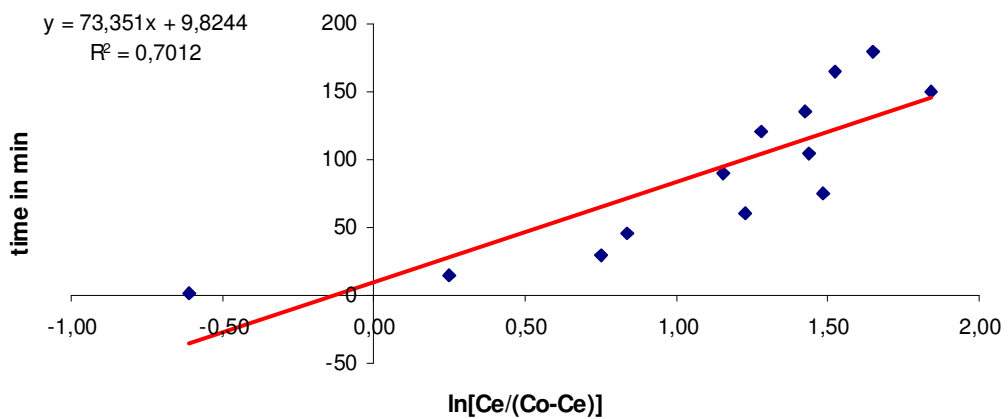


Fig. 9.7 Linear plot of the Yoon-Nelson model for Sb(III) removal by WAP/agar.

Fig. 9.7 shows linearity, with a correlation coefficient of 0.7012.

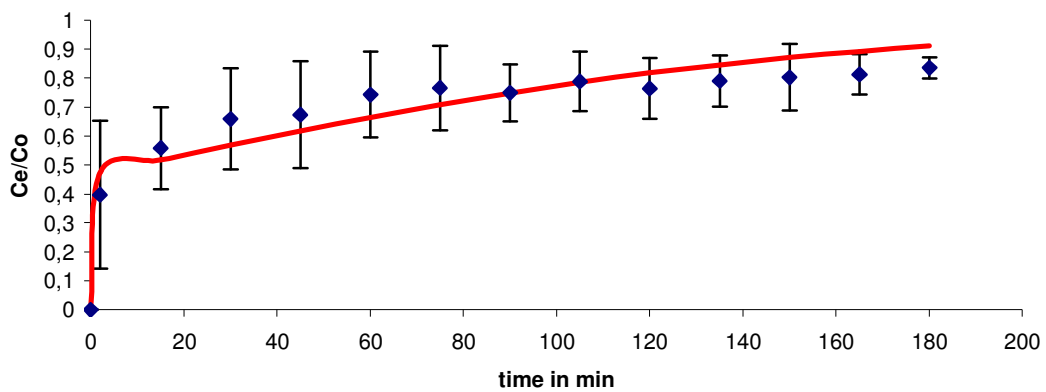


Fig. 9.8 Model fitting to the experimental data of Sb(III) removal by WAP/agar. Error bars are calculated based on four replicates with 95% Confidence Intervals.

#### 9.4.5 Sb(III) removal by *P. lanosa*/agar

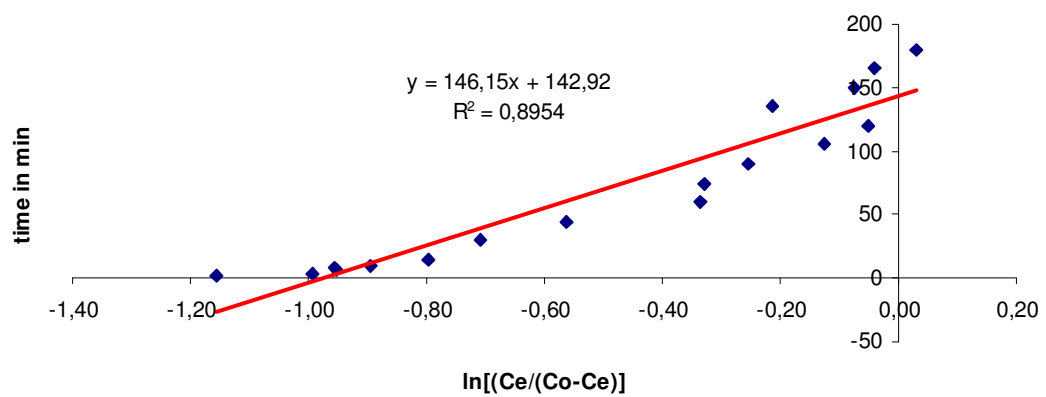


Fig. 9.9 Linear plot of the Yoon-Nelson model for Sb(III) removal by *P. lanosa*/agar.

Fig. 9.9 shows good linearity, with a correlation coefficient of 0.8954.

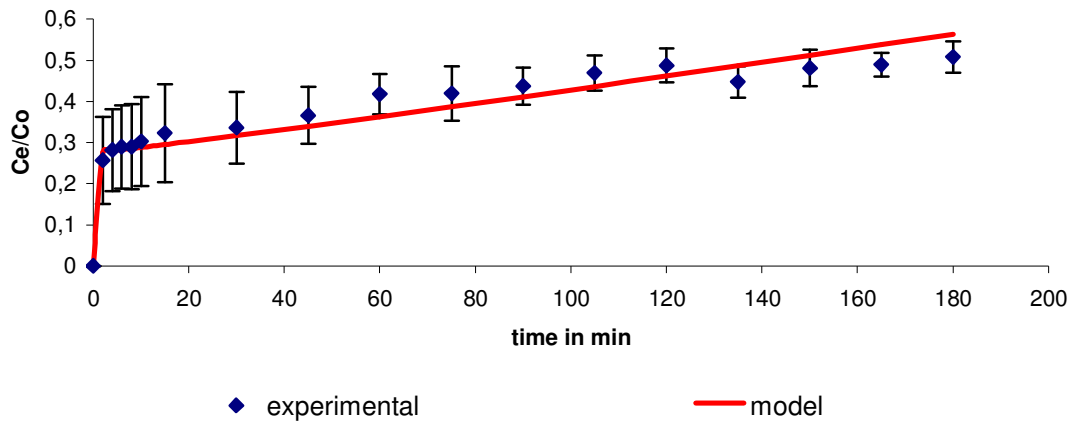


Fig. 9.10 Model fitting to the experimental data for Sb(III) removal by *P. lanosalagar*. Error bars are calculated based on four replicates with 95% Confidence Intervals.

#### 9.4.6 Zn(II), Ni(II) and Al(III) removal by WAP/agar

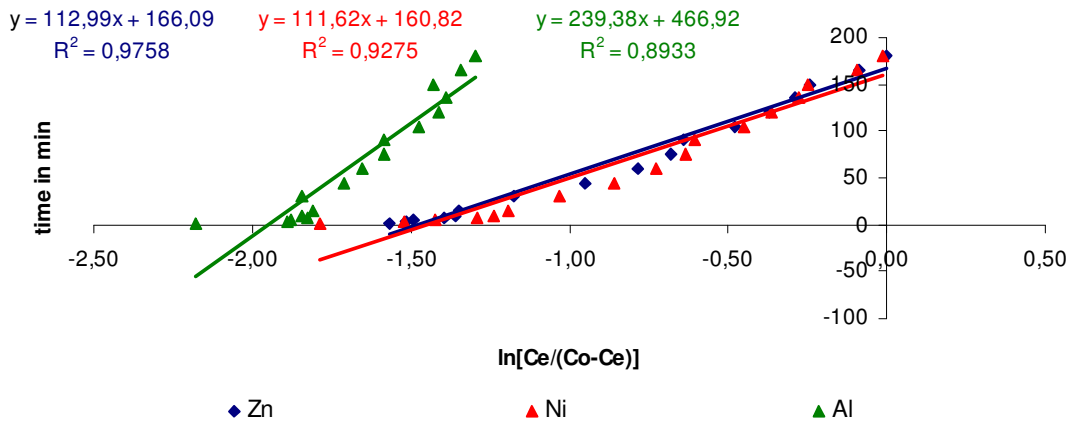


Fig. 9.11 Linear plot of the Yoon-Nelson model for Zn(II), Ni(II) and Al(III) removal by WAP/agar.

Fig. 9.11 shows good linearity for all metals, with correlation coefficients of 0.9758, 0.9275 and 0.8933 for Zn, Ni and Al, respectively.

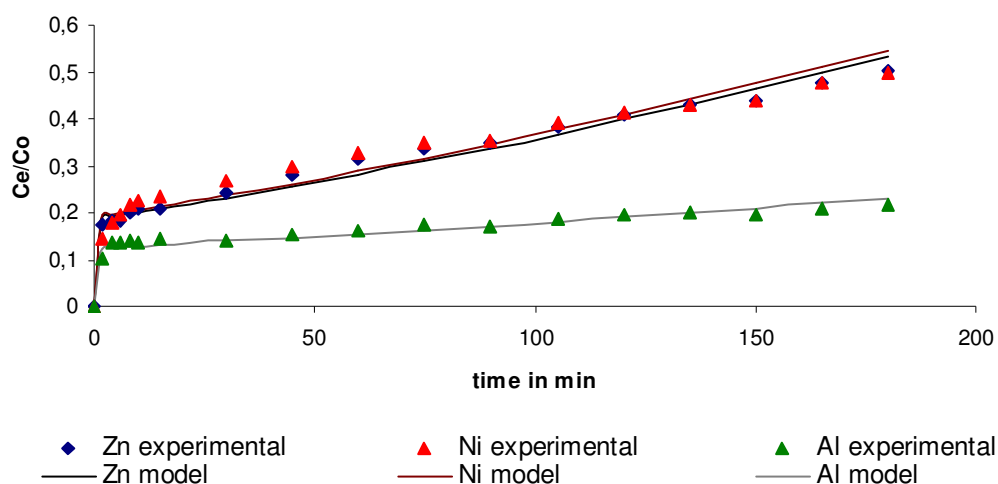


Fig. 9.12 Model fitting to the experimental data. Average results from four replicates are shown. Error bars have been omitted for clarity.

#### 9.4.7 Zn(II), Ni(II), Al(III) and Sb(III) removal by WAP/agar

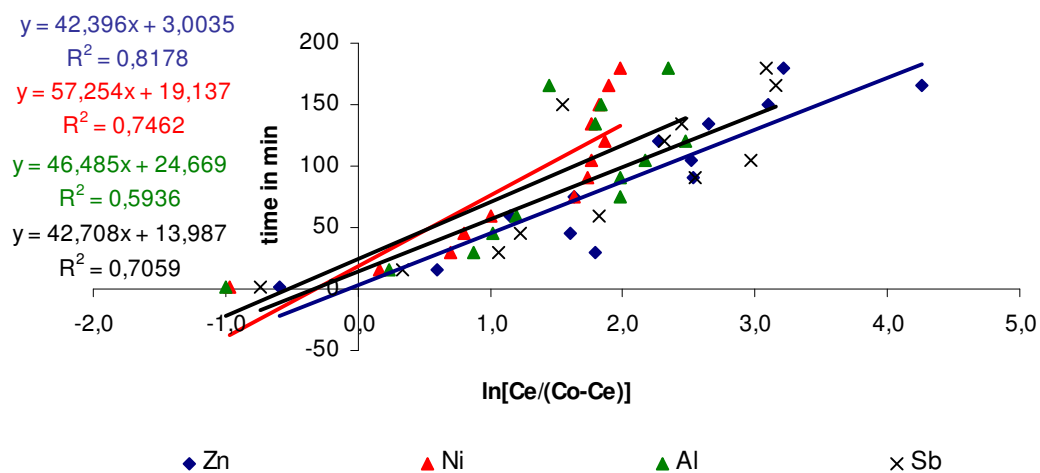


Fig. 9.13 Linear plot of the Yoon-Nelson model for Zn(II), Ni(II), Al(III) and Sb(III) removal by WAP/agar.

Fig. 9.13 shows linearity for each metal, with correlation coefficients of 0.8178, 0.7462, 0.5936 and 0.7059 for Zn, Ni, Al and Sb respectively.

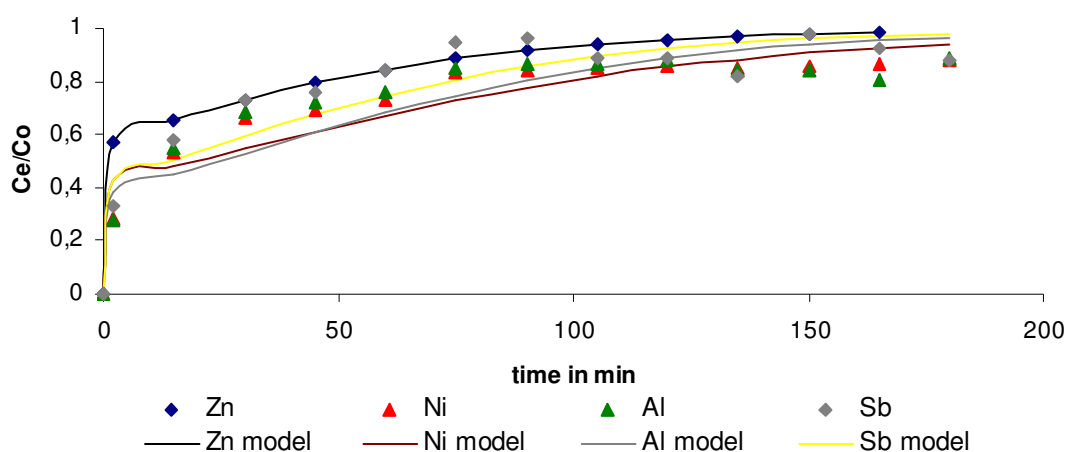


Fig. 9.14 Model fitting to the experimental data. Average results from four replicates are shown. Error bars have been omitted for clarity.

### Summary of results

Table 9.1: Summary of parameters and correlation coefficients ( $K$  = Yoon-Nelson model rate constant,  $\tau$  = time required for 50% sorbate breakthrough).

Metals		biomass	$r^2$	$K$	$\tau$
Zn(II)		WAP	0.9129	0.012	282.99
Ni(II)		WAP	0.5968	0.007	394.48
Al(III)		WAP	0.4625	0.011	156.66
Sb(III)		WAP	0.7012	0.014	9.8244
Sb(III)		<i>P. lanosa</i>	0.8954	0.007	142.92
Zn(II)/Ni(II)/Al(III)	Zn(II)	WAP	0.9758	0.009	166.09
	Ni(II)		0.9275	0.009	160.82
	Al(III)		0.8933	0.004	466.92
Zn(II)/Ni(II)/Al(III)/Sb(III)	Zn(II)	WAP	0.8178	0.023	3.01
	Ni(II)		0.7462	0.017	19.14
	Al(III)		0.5936	0.02	24.67
	Sb(III)		0.7059	0.02	13.99

### 9.4.8 Predictions

Prediction of breakthrough curves was performed out using the Yoon-Nelson model. The model was extended until  $C_e = C_o$ .

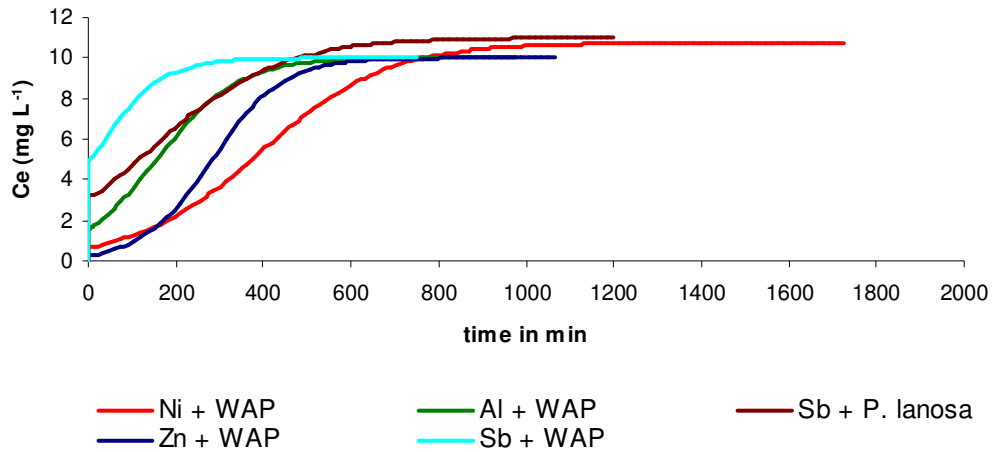


Fig. 9.15 Breakthrough curve predictions using Yoon-Nelson model for metals in single component solutions with WAP/agar.

Fig. 9.15 shows that the breakthrough curve for Ni(II) removal by WAP is the longest, with a breakthrough point at 1725 min. The shortest breakthrough time was seen for Sb(III) removal by WAP, with a time of 750 min.

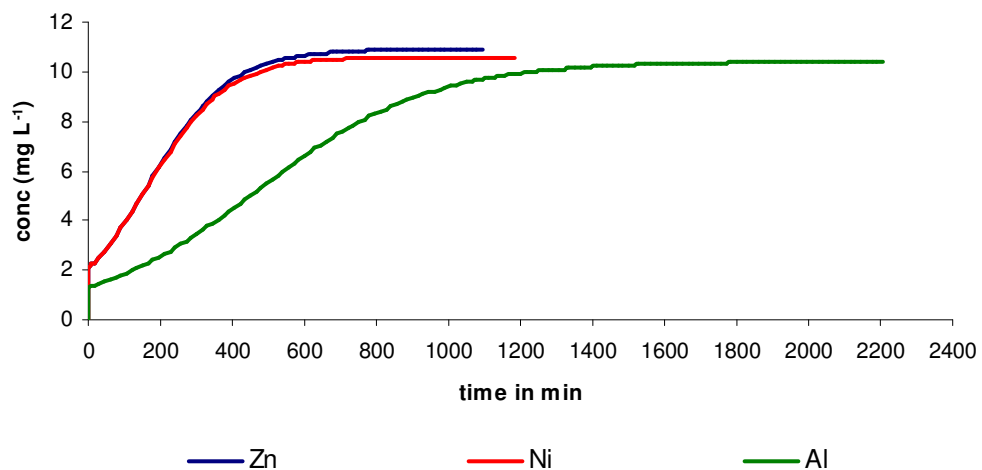


Fig. 9.16 Breakthrough curve predictions using Yoon-Nelson model for Zn(II), Ni(II) and Al(III) in a combined metal solution with WAP/agar.

Fig. 9.16 shows that breakthrough curves for Zn(II) and Ni(II) were very similar. Al(III) demonstrated a far longer breakthrough curve, indicating a slower saturation of the sorbent, corresponding to a lower removal efficiency.

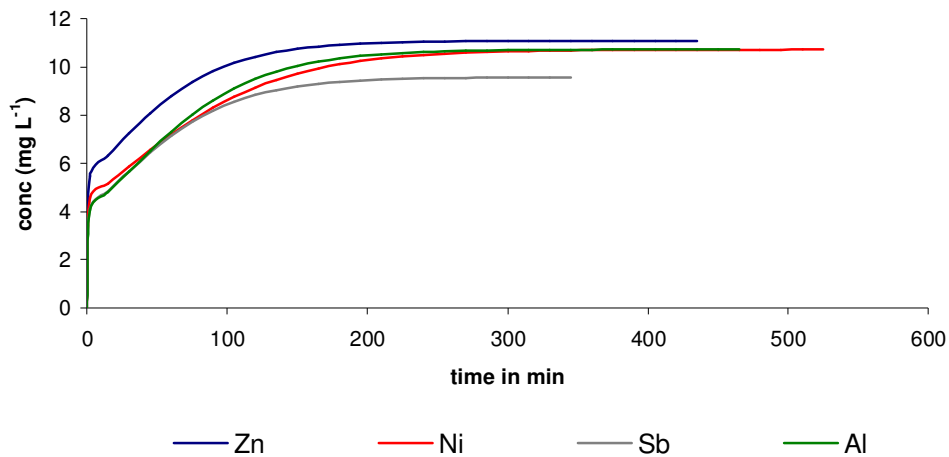


Fig. 9.17 Breakthrough curve predictions using Yoon-Nelson model for Zn(II), Ni(II), Al(III) and Sb(III) in a combined metal solution with WAP/agar.

Fig. 9.17 shows that the breakthrough curves are significantly shorter when all the metals are combined in a single aqueous solution.

## 9.5 Conclusions

A mathematical model, with regression parameters, was developed for all the different fixed-bed sorption column studies. Predictions were derived accurately within the time scale of the experiment (i.e. 3 hours). Forecasts were also carried-out with an extended time scale. However, such extrapolation from the models must be performed in a stepwise approach, and the values obtained compared to experimental data. For each study, extrapolations generally underestimated experimental values, highlighting the need for more complex and accurate models such as the COMSOL model discussed in Chapter 10.

## **Chapter 10**

### **COMSOL modelling**

## 10.1 Introduction

Predicting metal biosorption performance is an important step for any industrial application. In industry, time is a crucial factor and it is important to know quickly when the sorbent is saturated and needs to be regenerated. The mathematical modelling presented in Chapter 9 is a useful tool in predicting concentration breakthroughs. However, this kind of modelling is limited by operational settings, such as dimensions of the columns, and experimental results, which could include errors. Other studies have shown that a series of variables have to be taken into account, such as the fluid velocity along the bed, the flow rate, the bed height, the inlet concentration as well as the sorbent size and porosity (Gupta and Babu, 2005).

As a result, more complex modelling tools, such as COMSOL (formerly known as FEMLAB software), may be used to develop efficient and flexible biosorption models. Naja et al (2005) succeeded in predicting metal biosorption performance under various conditions, including for different flow rates, inlet concentrations, column sizes, bed porosity and ionic forms of the biosorbent. They stated that the main disadvantage of using COMSOL was that all the parameters of the fixed-bed column, especially the mass-transfer coefficients for all the ionic species in the system, must be known. The values of these coefficients must be calculated, derived or determined by fitting the model to experimental data. However, it was also shown that models generated from COMSOL are valuable for potential industrial applications by selecting the operational conditions prior to pilot tests and then selecting a final column design and predicting its performance based on these results (Kratochvil and Volesky, 2000; Naja et al., 2005).

The main focus of this chapter was to provide an introduction into the use of COMSOL to describe metal biosorption behaviour. Only single metal systems were considered in this chapter, with the simulation of biosorption for multi-metal systems described in Chapter 12.

### 10.1.1 The Mass Transfer Column Model (MTCM)

The Mass Transfer Column Model (MTCM) was used by Kratochvil in his PhD thesis (Kratochvil, 1997), and in subsequent work by Kratochvil's supervisor, Prof. Bohumil Volesky (Kratochvil and Volesky, 2000; Naja and Volesky, 2006a). The notation employed here is similar to that used in the work by Kratochvil and Volesky (2000).

#### Theoretical model

The MTCM was developed to describe the sorption and transport of ionic species inside and between the two phases present in the fixed bed sorption column, namely the stationary solid phase and the mobile liquid phase. The mobile liquid phase,  $x_M(t,z)$ , and the stationary solid phase,  $y_M(t,z)$ , can be expressed by the following scaled equations (Kratochvil, 1997; Naja et al., 2005):

$$\text{Mobile liquid phase: } \frac{\partial x_M}{\partial z} - \frac{1}{P_e} \frac{\partial^2 x_M}{\partial z^2} + \frac{\partial x_M}{\partial t} + D_s \frac{\partial y_M}{\partial t} = 0 \quad \text{Eq. [11]}$$

$$\text{Stationary solid phase } \frac{\partial y_M}{\partial t} = Sh_M (y_M^* - y_M) \quad \text{Eq. [12]}$$

Here the equilibrium relation is assumed to be

$$y_M^* = \frac{K_{N,M}}{C_0 + x_M (K_{N,M} - C_0)} \quad \text{Eq. [13]}$$

With scaling:

$$y_M = \frac{q_M}{Q}; \quad x_M = \frac{C_M}{C_0}; \quad z = \frac{l}{L_0}; \quad t = \frac{\tau v}{L_0}$$

- $x_M$  and  $y_M$  represent the metal concentration in the liquid and solid phase respectively. (Note: In the COMSOL implementation, the  $z$  coordinate is represented by the  $x$  coordinate).
- $C_M$  is the concentration of metal M in the liquid (meq L<sup>-1</sup>)
- $C_0$  is the normality of a metal bearing solution used as column feed (meq L<sup>-1</sup>)
- $Q$  is the concentration of binding sites in the biosorbent (meq g<sup>-1</sup>)
- $l$  is the unscaled vertical distance from the top of the column (cm)
- $L_0$  is the length of the column (cm)
- $Pe$  is the Peclet number (-) and  $Pe = \frac{L_0 v}{D_z}$
- $v$  is the interstitial velocity of the liquid in the fixed-bed sorption column (cm min<sup>-1</sup>)
- $D_z$  is the axial dispersion coefficient (cm<sup>2</sup> s<sup>-1</sup>)
- $D_g$  is the solute distribution parameter (-) and  $D_g = \frac{\rho_b Q}{C_0 \varepsilon}$
- $\rho_b$  is the packing density of dry biomass in the fixed-bed sorption column (g L<sup>-1</sup>)
- $\varepsilon$  is the column void fraction (-)
- $\tau$  is the unscaled time since start of experiment (min)
- $Sh_M$  is the rate constant for ion exchange (min<sup>-1</sup>) and  $Sh_M = \frac{K_{fm} L_0}{v}$
- $Y_M^*$  is the equilibrium equivalent fraction of species M in solid phase when the equivalent fraction of species M in the liquid is  $x_M$ .
- $K_{N,M}$  is the equilibrium binding constant
- $K_{fM}$  is the overall mass transfer coefficient of the metal M (min<sup>-1</sup>)

and,

- $t > 0$  is scaled time (-)
- $0 < z < 1$  is the scaled length along the column measure from the top and end of the column

The individual terms in Eq. [11] represent the concentration of the metal M in the liquid due to (from the left): the convection, the axial dispersion, the accumulation in the interstices of the packing, and the sorption onto the solid biosorbent (Kratochvil, 1997). The right-hand side of Eq. [12], representing the rate of diffusion of the metal M, is expressed using an overall mass transfer coefficient,  $K_{fM}$ , and the corresponding overall driving force. The value of  $K_{fM}$  reflects the magnitude of the combined mass transfer resistance due to the intraparticle and the external film diffusion (Kratochvil, 1997). It is also the case for the value of  $Sh_M$ , which depends on the value of  $K_{fM}$ . The overall driving force for the diffusion of M from the aqueous solution to the binding sites in the sorbent is assumed to be equal to the difference between the equilibrium uptake  $y_M^*$  (Eq. 13), corresponding to the instantaneous value of the concentration  $C_M$  in the aqueous solution, and the actual average uptake of  $q_M$  at the same position in the column. The initial and boundary conditions for the differential equations (Eqs. 11 & 12) are defined as follows (Naja et al., 2005):

- initially ( $t = 0$ ) the concentration is zero, i.e.

$$t = 0 \qquad 0 < z < 1 \qquad x_M = 0, y_M = 0$$

- the concentration at the inlet is  $C_M$ , i.e.

$$t > 0 \qquad z = 0 \qquad x_M = 1 + \frac{1}{Pe} \frac{\partial x_M}{\partial z}$$

- at the outlet the flux is zero, i.e.

$$t > 0 \qquad z = 1 \qquad \frac{\partial x_M}{\partial z} = 0$$

#### The role of dimensionless groups

According to Kratochvil (1997), the use of dimensionless groups, e.g.  $Pe$  or  $Sh_M$ , simplifies the description of biosorption in columns as it reduces the number of variables and allows for comparisons of the results obtained under different experimental conditions.

### Column Peclet number, $Pe$

The Peclet number describes the degree of deviation between ideal pug-flow and the actual liquid flow pattern developing in the column. Assuming that  $Pe = \infty$  means that all elements of liquid entering the column travel through the fixed bed sorption column with the same speed (Kratochvil, 1997). In reality, this is not the case as the liquid entering the column is following different pathways, some longer than others leading to a differential liquid repartition inside the column.

$$Pe = \frac{\text{rate of transport by convection}}{\text{rate of transport by axial dispersion}}$$

### Mass Transfer/column length parameter for a species $M$ , $Sh_M$

$Sh_M$  represents the ratio of the rate of sorption and the residence time of liquid in an empty column. The greater the value of  $Sh_M$ , the longer is the retention time of the metal ions in the column, and thus better removal efficiencies (Kratochvil, 1997). Kratochvil (1997) also stated that, as the rate of the sorption and the residence time of the liquid are related to the mass transfer resistance and to the column size, the  $Sh_M$  can be used for scale up of the fixed bed sorption column. However, as  $Sh_M$  depends on the value of the diffusivity of  $M$ , different values for  $Sh_M$  can be obtained for different ions and we may need to adapt the model for different metals (Kratochvil, 1997).

$$Sh_M = \frac{\text{rate of sorption of } M}{\text{rate of transport of } M \text{ by convection}}$$

### Solute distribution parameter, $Dg$

$Dg_M$  relates to the capacity of the column to the total concentration of ions in the feed. At fixed values of  $Sh_M$  and  $Pe$ , decreasing  $Dg_M$  leads to broader ion exchange zones of species  $M$ . Furthermore, the lower the  $Dg_M$ , the greater the chance that the sorption rate is controlled by intraparticle diffusion (Vermeulen et al., 1973; Kratochvil, 1997).

$$D_g = \frac{\text{concentration of ions in solid phase at saturation}}{\text{concentration of ions in liquid phase at saturation}}$$

## 10.2 Aims

- To develop a computer model, using COMSOL modelling package, for single metal systems.
- To compare the model and experimental data

## 10.3 Methods

### 10.3.1 Using COMSOL Multiphysics

COMSOL Multiphysics™, version 3.4, was provided by COMSOL Ltd., UK (UH Innovation Centre, College Lane, Hatfield, UK). While the standard COMSOL package contains a large number of predefined models, none appeared applicable to MTCM. Hence a new model was developed using the Coefficient Form PDE Model which deals with equations of the form (using COMSOL notation):

$$e_a \frac{\partial^2 u}{\partial t^2} + d_a \frac{\partial u}{\partial t} - \nabla \cdot (c \nabla u + \alpha u - \gamma) + \beta \cdot \nabla u + au = f \quad \text{in } \Omega \quad \text{Eq. [14]}$$

$$\vec{n} \cdot (c \nabla u + \alpha u - \gamma) + qu = g - h^T \mu \quad \text{on } \delta\Omega \quad \text{Eq. [15]}$$

$$hu = r \quad \text{on } \delta\Omega \quad \text{Eq. [16]}$$

This template also support systems of equations. Using COMSOL, steps 1-7 were performed.

### Step 1 Create Model.

- From the model Navigator select 1D in Space dimension, COMSOL Multiphysics>PDE Modes, PDE, Coefficient Form in Application Modes, and Time-dependent analysis.
- Set the dependent geometry and mesh

### Step 2 Construct geometry and mesh.

The column is represented by a one dimensional structure (0,0) to (1,0), as represented in Fig. 10.1.

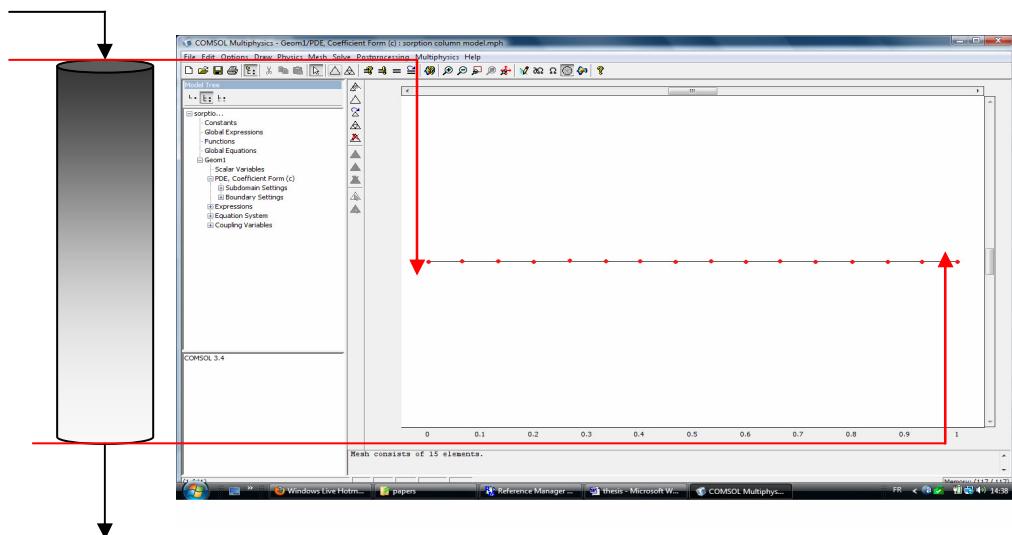


Fig. 10.1 Mesh representation in COMSOL.

### Step 3 Specify problem parameters.

- Select Menu **Options** → **Constants...** and enter the data as shown.

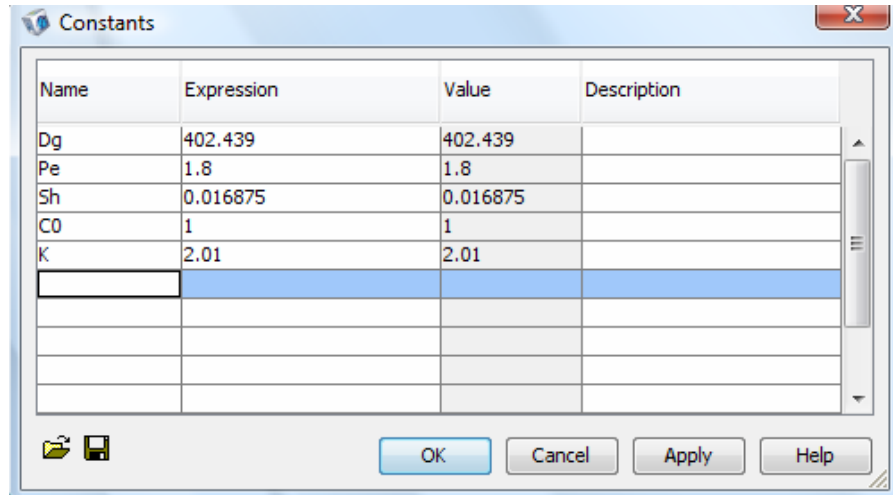


Fig. 10.2 Constant values in COMSOL.

**Step 4** Specify sub-domain equation parameters.

- Select Menu **Physics** → **Subdomain Settings...** In sub-domain 1 (only one) set coefficients as follows

○ The diffusion coefficient: 
$$c = \begin{pmatrix} 1/Pe & 0 \\ 0 & 0 \end{pmatrix}$$

○ The absorption coefficient: 
$$a = \begin{pmatrix} 0 & 0 \\ 0 & Sh_M \end{pmatrix}$$

○ The source term: 
$$f = \begin{pmatrix} 0 \\ Sh_M \cdot K_{N,M} \cdot x_M / (C_0 + x_M (K - C_0)) \end{pmatrix}$$

○ The mass coefficient: 
$$e_a = \begin{pmatrix} 0 & 0 \\ 0 & 0 \end{pmatrix}$$

○ The damping coefficient or a mass coefficient: 
$$d_a = \begin{pmatrix} 1 & D_s \\ 0 & 1 \end{pmatrix}$$

○ The conservative flux convection coefficient: 
$$\alpha = \begin{pmatrix} -1 & 0 \\ 0 & 0 \end{pmatrix}$$

○ The convection coefficient: 
$$\beta = \begin{pmatrix} 0 & 0 \\ 0 & 0 \end{pmatrix}$$

○ The conservative flux source term: 
$$\gamma = \begin{pmatrix} 0 \\ 0 \end{pmatrix}$$

**Step 5** Specify boundary condition parameters.

- Select Menu **Physics** → **Subdomain Settings...**

For boundary 1 (inlet end of the column) set constraint to be of Dirichlet type and set coefficients as follows:

$$q = \begin{pmatrix} 0 & 0 \\ 0 & 0 \end{pmatrix} \quad g = \begin{pmatrix} 1 \\ 0 \end{pmatrix} \quad h = \begin{pmatrix} 1 & 0 \\ 0 & 0 \end{pmatrix} \quad r = \begin{pmatrix} 1 \\ 0 \end{pmatrix}$$

For boundary 2 (outlet end of column) set constraints to be of Neumann type and set coefficients as follows:

$$q = \begin{pmatrix} 1 & 0 \\ 0 & 0 \end{pmatrix} \quad g = \begin{pmatrix} 0 \\ 0 \end{pmatrix}$$

**Step 6** Solve problem.

- Select Menu **Solve** → **Solver Parameters...**

Change **Time Stepping** → **Times** to 0:0.1:800.

**Step 7** Draw breakthrough curve.

- Select Menu **Postprocessing** → **Cross-section Plot Parameters...**

Select **Point** and in **Coordinates** txt box enter 1.

As stated Section 10.1, in order to obtain accurate models all the parameters of the fixed-bed sorption column must be known. In order to estimate the key parameters, such as the axial dispersion coefficient ( $Dz$ ) or the overall mass transfer coefficient of the metal ( $K_M$ ), a COMSOL script was created as described in Section 10.3.2.

## 10.3.2 Using COMSOL Script

### MTCM scripts

In order to simplify tasks when developing and testing the MTCM implementation, the following set of commands were defined (see Appendix D):

- **mtcm\_animate (f)**  
Animate the behaviour of  $f$  over time  $t$ .  
Typically  $f$  is  $x_M$  or  $y_M$  to plot the equivalent fraction of species  $M$  in liquid or in solid respectively.
- **mtcm\_breakthrough**  
Plots the breakthrough curve.  
This is just a wrapper function that calls `mtcm_crossplot ('xM')`
- **mtcm\_crossdata (f)**  
Evaluate the expression in  $f$  at  $x = 1$  over time  $t$ .  
Typically  $f$  is  $x_M$  or  $y_M$  to plot the equivalent fraction of species  $M$  in liquid or in solid respectively.
- **mtcm\_crossplot (f)**  
Plot the expression in  $f$  at  $x = 1$  over time  $t$ .  
Typically  $f$  is  $x_M$  or  $y_M$  to plot the equivalent fraction of species  $M$  in liquid or in solid respectively.
- **mtcm\_fit**  
Fit the expected MTCM breakthrough curve to the observed data.  
Use the unconstrained non-linear optimisation Nelder-Mead algorithm to minimise the sum of squares errors between the observed breakthrough curve and the (expected) breakthrough curve generated by solving the PDE system representing the theoretical MTCM.
- **mtcm\_load**  
Load from a .CSV file the observed breakthrough curve.

- **mtcm\_objective**

Function used in optimisation to calculate the SSE between the observed breakthrough curve and that generated by MTCM implementation.

- **mtcm\_plot(f)**

Plot the expression in f over the interval  $0 \leq x \leq 1$ .

Typically f is 'xM' or 'yM' to plot the equivalent fraction of species M in liquid or in solid respectively. By default the end time is used but to plot behaviour at other points is possible as in

```
C> mtcm_plot('xM', 'T', 1.5)
```

which plots  $x_M$  at time  $t = 1.5$  for  $0 \leq x \leq 1$ .

- **mtcm\_solve**

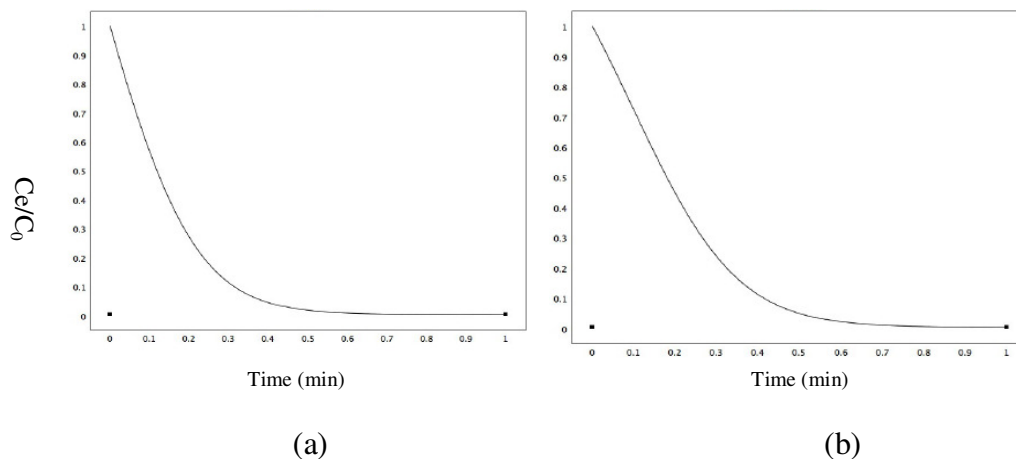
Solve the PDE system using current parameter values.

More information on each of these commands is available through the `help` command and their use is demonstrated in the Appendix D.

## 10.4 Results and discussion

The first approach was to repeat the model simulations of Naja and Volesky (2008), in order to ensure that the MTCM model was effective at describing metal sorption behaviour for the case of Cu(II).

### 10.4.1 Time dependent analysis (from naja.m script)



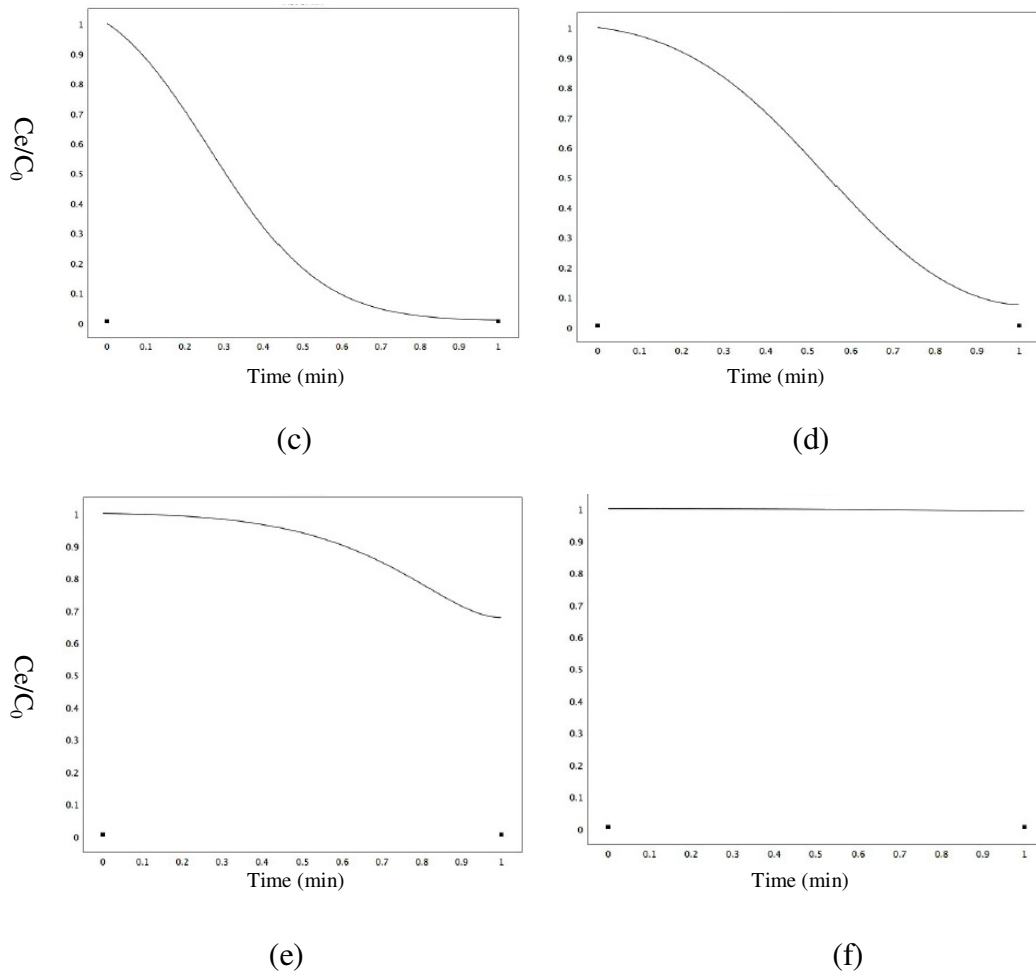


Fig. 10.3 Breakthrough concentration curves versus time in min, (a)  $t=25$ , (b)  $t=50$ , (c)  $t=100$ , (d)  $t=200$ , (e)  $t=400$ , (f)  $t=800$ .

Fig. 10.3 shows that at the beginning of the experiment ( $t_0$ ), the initial concentration of the metal solution is equal to 1 (Fig.10.3a). With time, the concentration in the column gradually increases (Fig. 10.3b-10.3e), to reach a final concentration equal to the initial concentration ( $C_e = C_0$ ), representing a complete saturation of the column (Fig. 10.3f). Fig. 10.3 shows that the MTCM model is effective at representing biosorption behaviour over time.

The next stage was to illustrate the importance of some key parameters such as the mass transfer coefficient ( $K_{fM}$ ), the axial dispersion coefficient ( $Dz$ ) and the void fraction ( $\epsilon$ ). Although most of the parameters are known experimentally, e.g. the void fraction, a number were determined by COMSOL script, e.g.  $K_{fM}$  and  $Dz$ .

## 10.4.2 Parametric analysis

Figs. 10.4-10.6 present the reproduced breakthrough curves for Cu(II) sorption by Ca-loaded *S. fluitans* using COMSOL script, obtained for varying values of  $K_{fm}$ ,  $D_z$  and  $\mathcal{E}$  according to the work of Naja and Volesky, 2008.

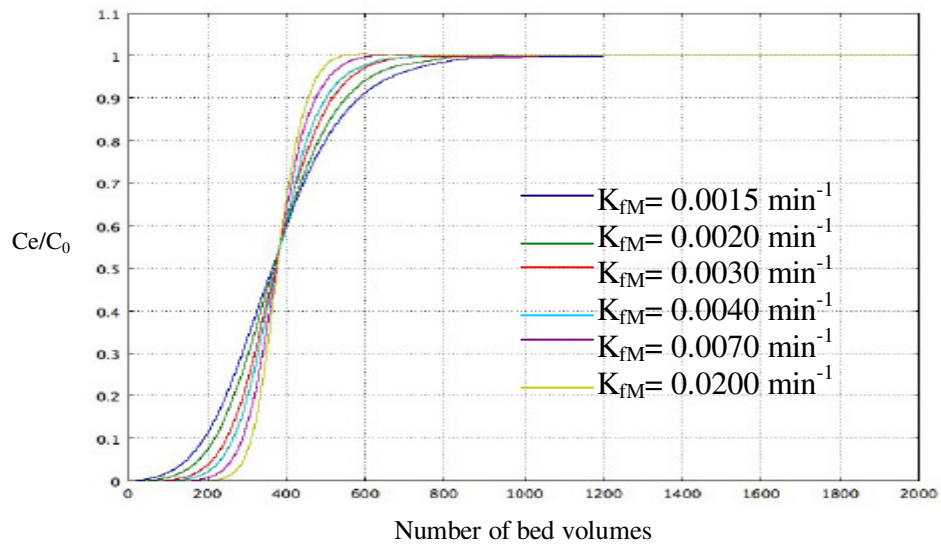


Fig. 10.4 Breakthrough curves for different mass transfer coefficients ( $K_{fm}$ )

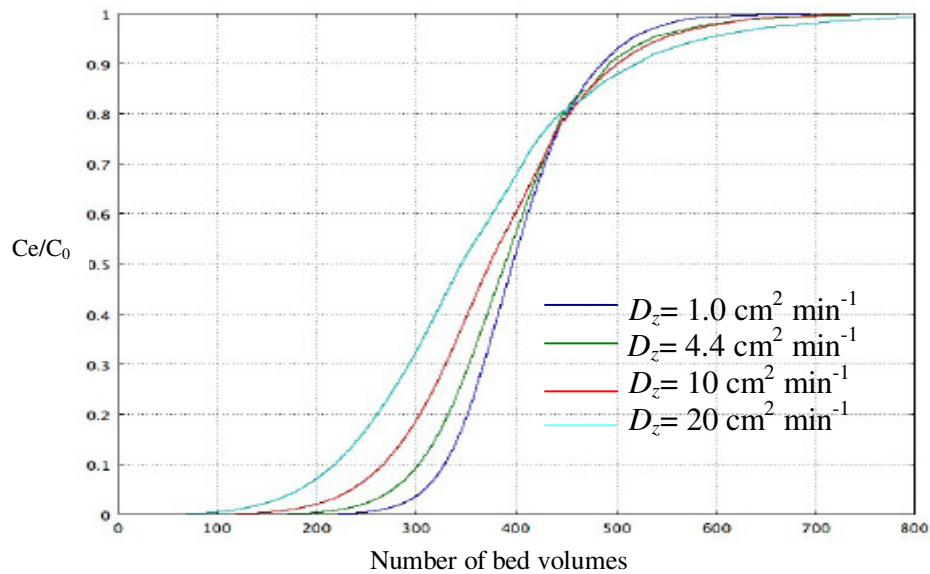


Fig. 10.5 Breakthrough curves for different axial dispersion coefficients ( $D_z$ )

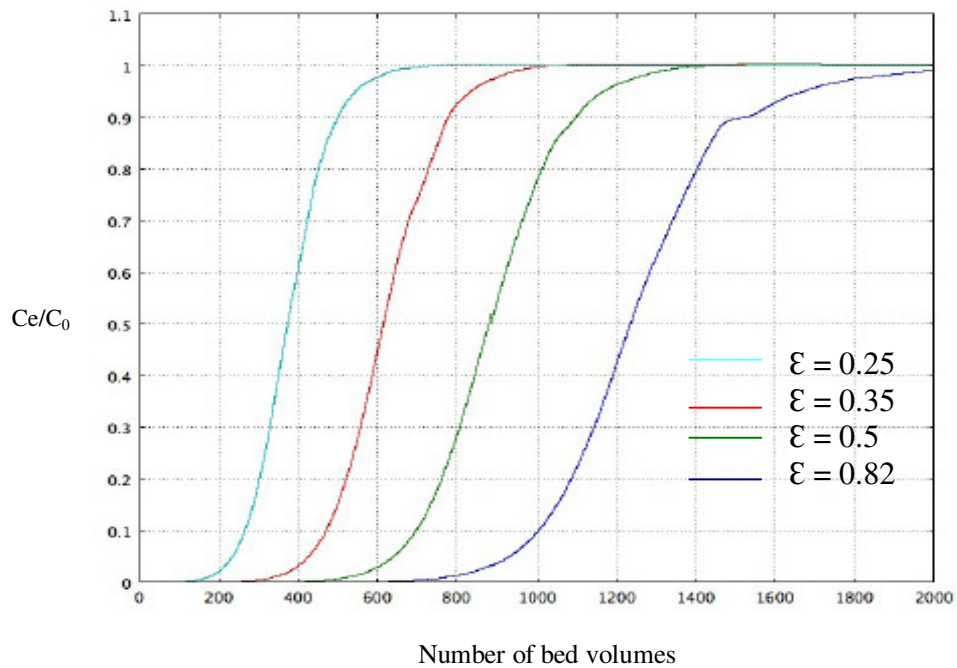


Fig. 10.6 Breakthrough curves for different void fractions ( $\epsilon$ )

There are several parameters related to the design and operation of a fixed-bed sorption column. The operating parameters (also called process input variables) can be readily manipulated, e.g. the flow rate ( $F_0$ ) or the initial metal feed concentration ( $C_0$ ). Other parameters are directly influenced by process input variables. For example, the liquid flow through the column has a direct impact on the axial dispersion of the flow through the fixed-bed, reflected mainly in  $Dz$  (axial dispersion coefficient) as shown in Fig. 10.5 (Naja and Volesky, 2008). In the same way the mass transfer coefficient ( $K_{FM}$ ), representing the intraparticle mass transfer, is based on sorbent properties and is, in most cases, the main rate-limiting step (Naja and Volesky, 2008).

#### 10.4.3 COMSOL model for zinc removal by WAP/agar blocks

The COMSOL scripts presented in Appendices D.2.2-D.2.6 permitted the generation of the models (Figs. 10.7-10.11).

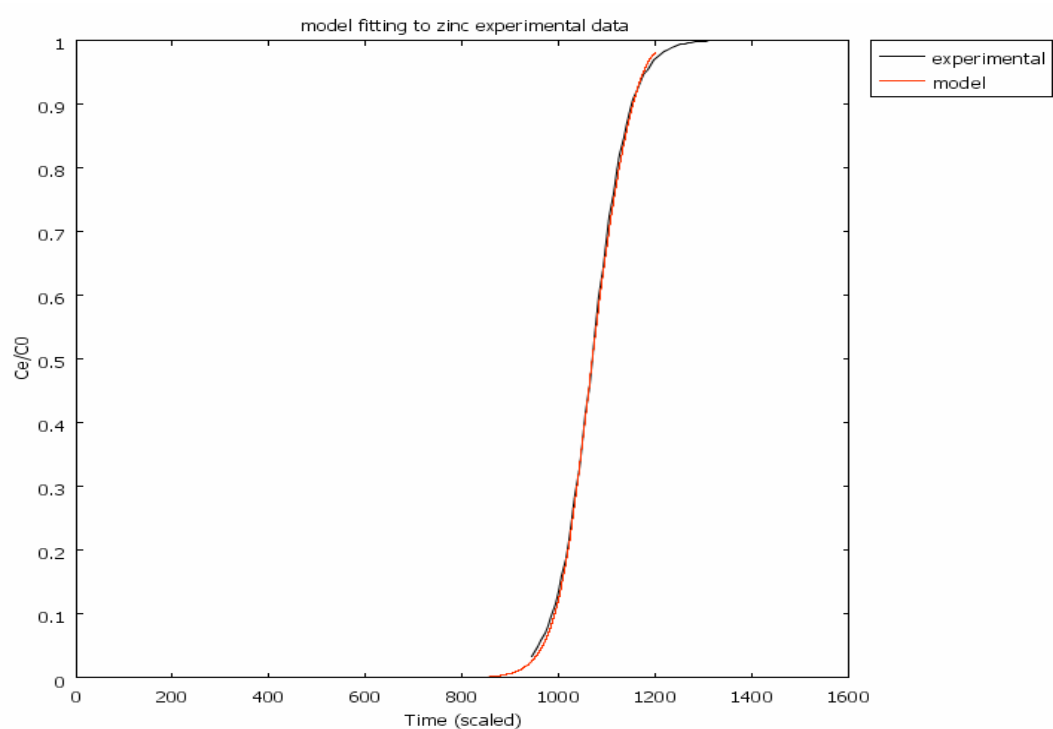


Fig. 10.7 Model generated from COMSOL script for Zn(II) removal by WAP/agar.

The COMSOL script for Zn(II) removal by WAP/agar blocks is shown in Appendix D.2.2.

Table 10.1 Operational settings for Zn(II) removal by WAP/agar blocks.

<b>Settings</b>		
Initial metal concentration	$C_0$ (mg/L)	10
Column length	$L_0$ (cm)	17
Packing density of dry biomass in the column	$\rho_b$ (g/L)	137.1
Concentration of binding sites in biosorbent	$Q$ (mmol/g)	3.63
Axial dispersion coefficient	$D_z$ (cm <sup>2</sup> /min)	3.72
Overall mass transfer coefficient	$K_{fM}$ (min <sup>-1</sup> )	1.33

#### 10.4.4 COMSOL model for nickel removal by WAP/agar blocks

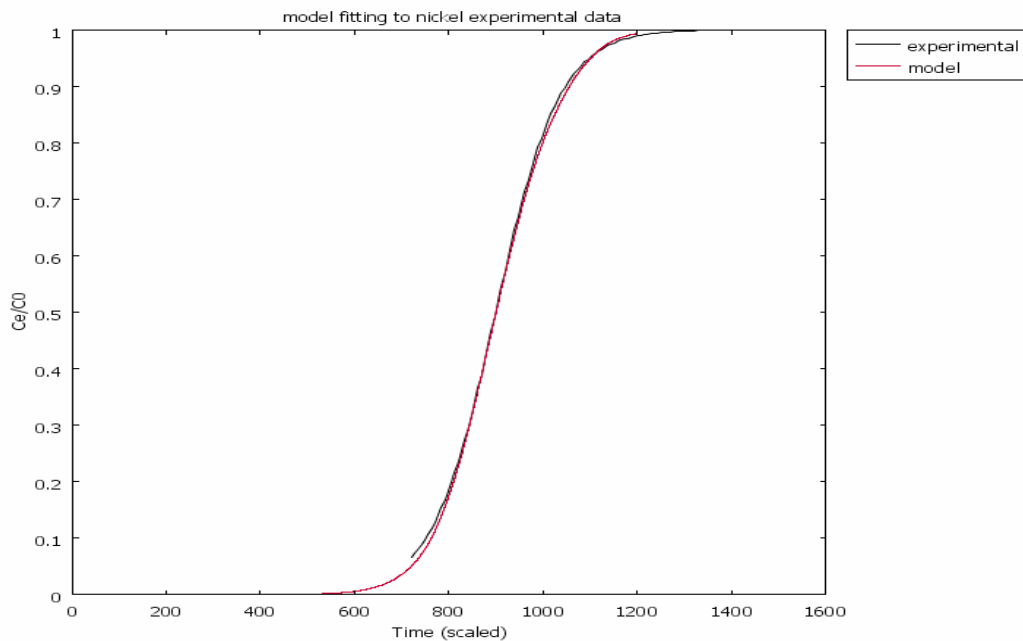


Fig. 10.8 Model generated from COMSOL script for Ni(II) removal by WAP/agar.

The COMSOL script for Ni(II) removal by WAP/agar blocks is shown in Appendix D.2.3.

Table 10.2 Operational settings for Ni(II) removal by WAP/agar blocks.

Settings		
Initial metal concentration	$C_0$ (mg/L)	10.734
Column length	$L_0$ (cm)	17
Packing density of dry biomass in the column	$\rho_b$ (g/L)	125.5
Concentration of binding sites in biosorbent	$Q$ (mmol/g)	3.63
Axial dispersion coefficient	$D_z$ (cm <sup>2</sup> /min)	2.44
Overall mass transfer coefficient	$K_{fM}$ (min <sup>-1</sup> )	0.014

### 10.4.5 COMSOL model for aluminium removal by WAP/agar blocks

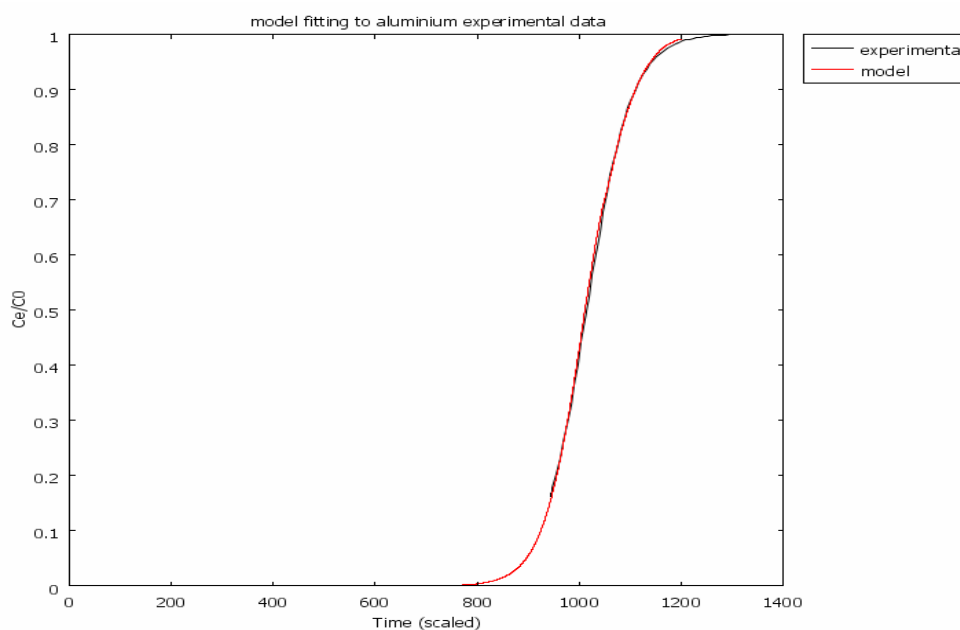


Fig. 10.9 Model generated from COMSOL script for Al(III) removal by WAP/agar.

The COMSOL script for Al(III) removal by WAP/agar blocks is shown in Appendix D.2.4.

Table 10.3 Operational settings for Al(III) removal by WAP/agar blocks.

Settings		
Initial metal concentration	$C_0$ (mg/L)	10
Column length	$L_0$ (cm)	17
Packing density of dry biomass in the column	$\rho_b$ (g/L)	130.3
Concentration of binding sites in biosorbent	$Q$ (mmol/g)	3.63
Axial dispersion coefficient	$D_z$ (cm <sup>2</sup> /min)	1.78
Overall mass transfer coefficient	$K_{fM}$ (min <sup>-1</sup> )	0.028

#### 10.4.6 COMSOL model for antimony removal by WAP/agar blocks

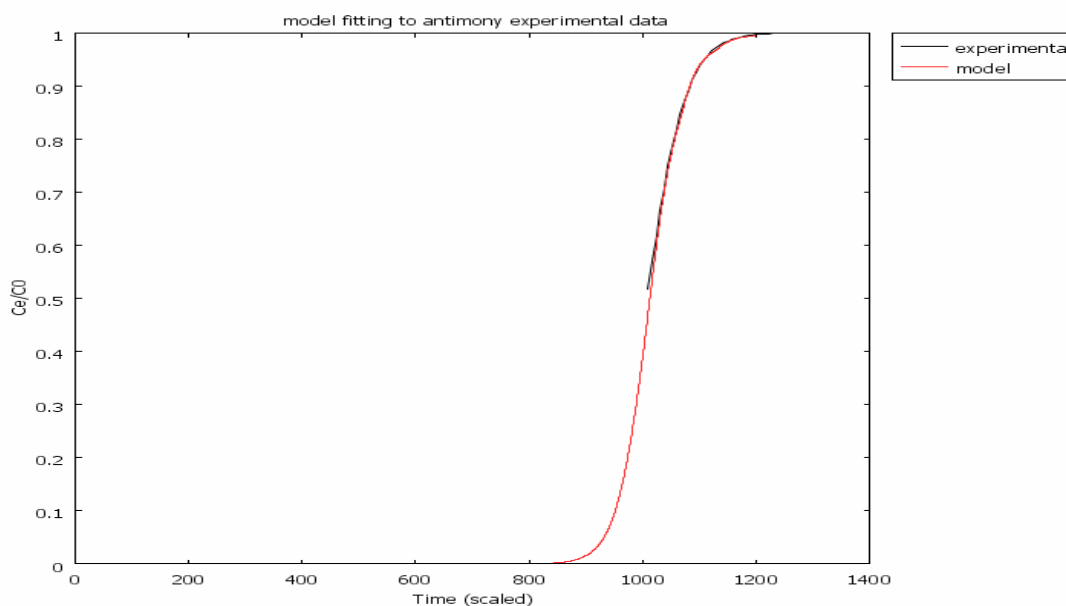


Fig. 10.10 Model generated from COMSOL script for Sb(III) removal by WAP/agar.

The COMSOL script for Sb(III) removal by WAP/agar blocks is shown in Appendix D.2.5.

Table 10.4 Operational settings for Sb(III) removal by WAP/agar blocks.

Settings		
Initial metal concentration	$C_0$ (mg/L)	10
Column length	$L_0$ (cm)	17
Packing density of dry biomass in the column	$\rho_b$ (g/L)	129.9
Concentration of binding sites in biosorbent	$Q$ (mmol/g)	3.63
Axial dispersion coefficient	$D_z$ (cm <sup>2</sup> /min)	1.42
Overall mass transfer coefficient	$K_{FM}$ (min <sup>-1</sup> )	0.04

### 10.4.7 COMSOL model for antimony removal by *P. lanosa*/agar blocks

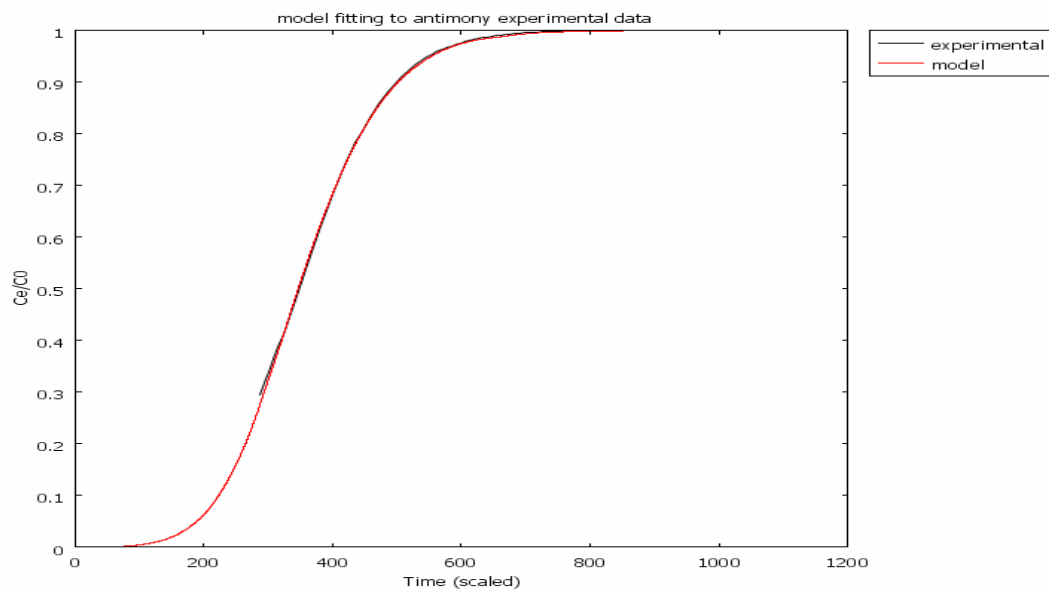


Fig. 10.11 Model generated from COMSOL script for Sb(III) removal by *P. lanosa*/agar.

The COMSOL script for Sb(III) removal by *P. lanosa*/agar blocks is shown in Appendix D.2.6.

Table 10.5 Operational settings for Sb(III) removal by *P. lanosa*/agar blocks.

Settings		
Initial metal concentration	$C_0$ (mg/L)	11
Column length	$L_0$ (cm)	17
Packing density of dry biomass in the column	$\rho_b$ (g/L)	109
Concentration of binding sites in biosorbent	$Q$ (mmol/g)	1.71
Axial dispersion coefficient	$D_z$ (cm <sup>2</sup> /min)	3.89
Overall mass transfer coefficient	$K_{FM}$ (min <sup>-1</sup> )	0.01

Figs. 10.7-10.11 highlight that COMSOL was a very effective tool in generating models to describe metal biosorption for both WAP/agar and *P. lanosa*/agar. The models fitted well with experimental data. COMSOL script determined fitting parameters, as shown in Appendices D2.2-D.2.6. Changing the operating settings in COMSOL script, such as the initial metal concentration or the column length, simulated metal biosorption under different conditions; thereby potentially reducing significantly the number of costly experimental procedures during column development. This would be a major advantage for the scale-up of the fixed bed sorption column prior to any industrial pilot test.

## 10.5 Conclusions

COMSOL script represented very closely Zn(II), Ni(II), Al(III) and Sb(III) sorption by WAP/agar blocks and Sb(III) removal by *P. lanosa*/agar blocks. COMSOL scripts also determined all the fitting parameters, such as mass transfer coefficients ( $K_M$ ) and axial dispersion coefficients ( $D_z$ ), of the columns. COMSOL was shown to be an effective tool for describing sorption behaviour in a fixed bed column.

## **Chapter 11**

### **Scale-up of fixed-bed sorption column**

## 11.1 Introduction

Scale-up of the laboratory prototype to an industrial scale, with no loss in removal efficiencies (Fig. 4.3) is critical. A study of state-of-the-art column design was necessary to identify an effective and cost efficient design. A key advantage of using a fixed-bed column is that the scale-up of a laboratory prototype is achieved by simply increasing the working volume (Volesky, 2004). The scale-up was achieved by choosing low-cost materials and optimising some important criteria such as the biomass preparation, the bed height and the flow rate of the effluent (BV Sorbex, 2008a; BV Sorbex, 2008b).

As the scaled-up system requires a much larger amount of immobilised biomass, a production line for the manufacture of WAP and *P. lanosa* blocks was designed (Fig. 11.1).

## 11.2 Aims

- To design and develop a production line for the efficient manufacture of WAP/agar and *P. lanosa*/agar blocks.
- To design and construct a scaled-up version of the laboratory fixed-bed sorption column.
- To optimise the scaled-up prototype, with different flow rates and different sorbent bed heights.

## 11.3 Method

### Manufacture of the WAP/Agar and *P. lanosa*/agar (7.5:5 w:w) blocks

Due to the large quantity of blocks required for the scaled-up version of the fixed-bed sorption column, a production line was necessary (Fig. 11.1). The production line for the manufacture of WAP/agar and *P. lanosa*/agar is divided into three main stages:

- Processing of the raw WAP and raw *P. lanosa*, drying and sizing ( $\leq 850 \mu\text{m}$ )
- Manufacture of the blocks using a mixing tank, autoclave and trays for the cooling and cutting stage
- Packaging and storage of the dried blocks.

150 g of dried WAP or *P. lanosa* ( $\leq 850 \mu\text{m}$ ) and 100 g of agar were placed into a large bowl mixer (i.e. mixing tank). 2 L of distilled water was added and the mix was homogenised using the bowl mixer. 4.5 L of the WAP/agar mix or the *P. lanosa*/agar mix was then placed into a 1L conical flask, and autoclaved at 121°C for 15 min. The mix was then poured into a large tray and left to solidify at room temperature for approximately 20 min. A cutting mesh was then used to cut blocks of homogeneous size (20x20x15 mm). The blocks were then placed into an oven at 60°C for 24 hours. The total time period involved for the full procedure, including drying, was approximately 27 hours. Prior to utilisation, the dried blocks were left to expand in distilled water for 2 hours.

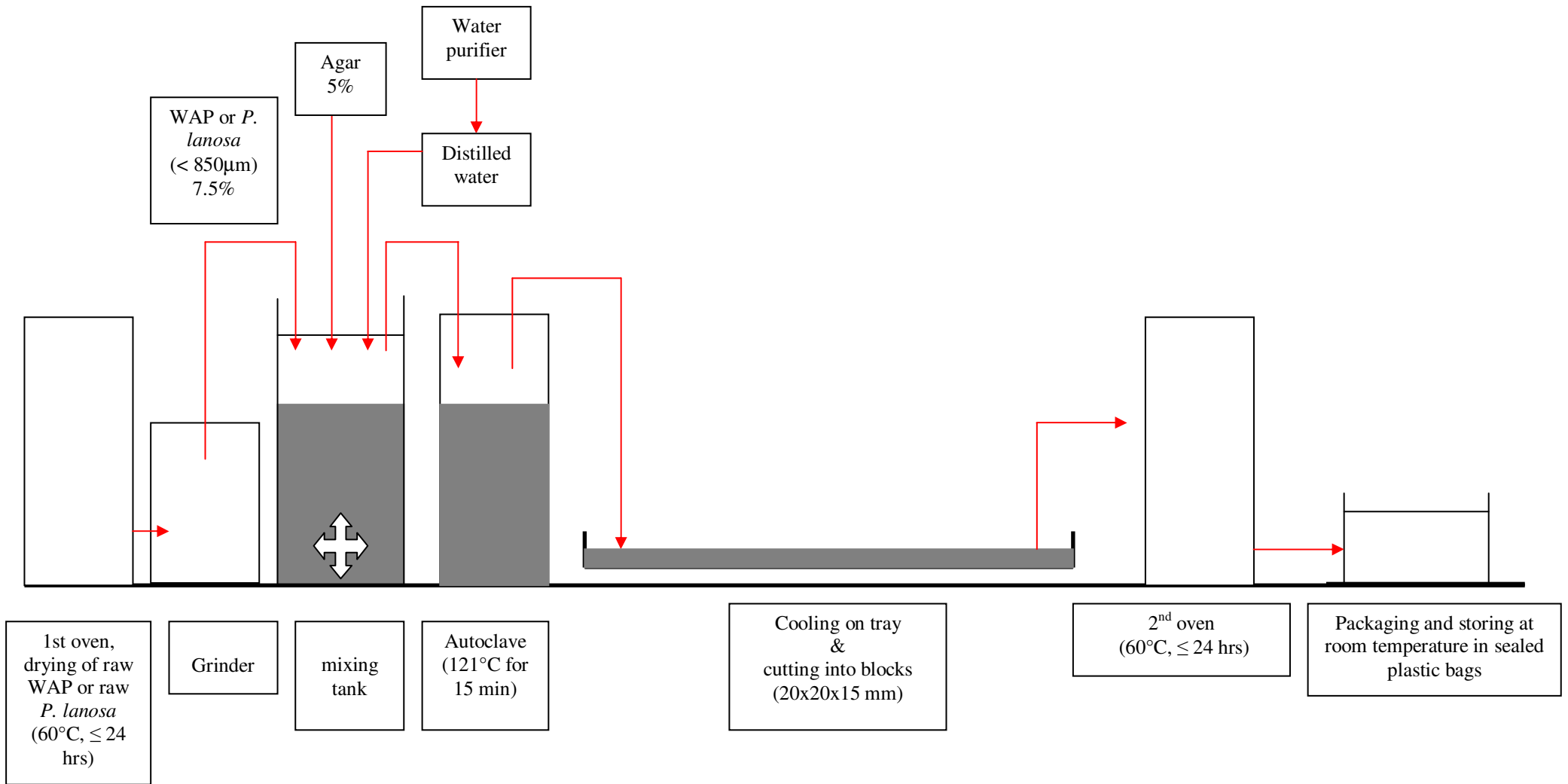


Fig. 11.1 Production line for the processing of 5% agar/7.5% WAP or *P. lanosa* blocks

## Chemicals

- 1000mg L<sup>-1</sup> Sb(III) as Sb<sub>2</sub>O<sub>3</sub> (analytical grade), Ni(II), Zn(II) and Al(III) - Sigma-Aldrich Ltd., Dublin, Ireland.
- Agar (OXOID LP0011 agar bacteriological No. 1).

## Design of the fixed bed sorption column

Design of the scaled up sorption column (Figs. 11.2-11.5) was based on four main criteria as listed below:

- Not chemically reactive
- Portable and robust
- Flexibility in design (easy to scale-up or scale-down)
- Cost-effective

### *Not chemically reactive*

Any source of metal was avoided in order to eliminate any metal contamination. A polycarbonate tubing was selected for the main column, due to its low-chemical reactivity and its high resistance to diluted acids.

### *Portable and robust*

The equipment size (960 mm length by 310 mm wide) allows the column to be transported easily. Also, the configuration of the whole system (Fig. 11.3) is highly flexible and allows rapid setup of the column.

### *Flexibility in design*

The scaled-up version of the fixed-bed column is highly flexible in design. Depending on the amount of wastewater to be treated and the velocity of the discharge a larger version can be manufactured by simply multiplying the dimensions of the column.

*Cost-effective*

The prototype was manufactured using relatively low-cost materials and the whole system was assembled in the laboratory. The 1 metre length polycarbonate tube (200 mm I.D.) was purchased from Murphy Engineers Limited (Units 75/77 Westside Business Park, Old Kilmeaden Road, Waterford).

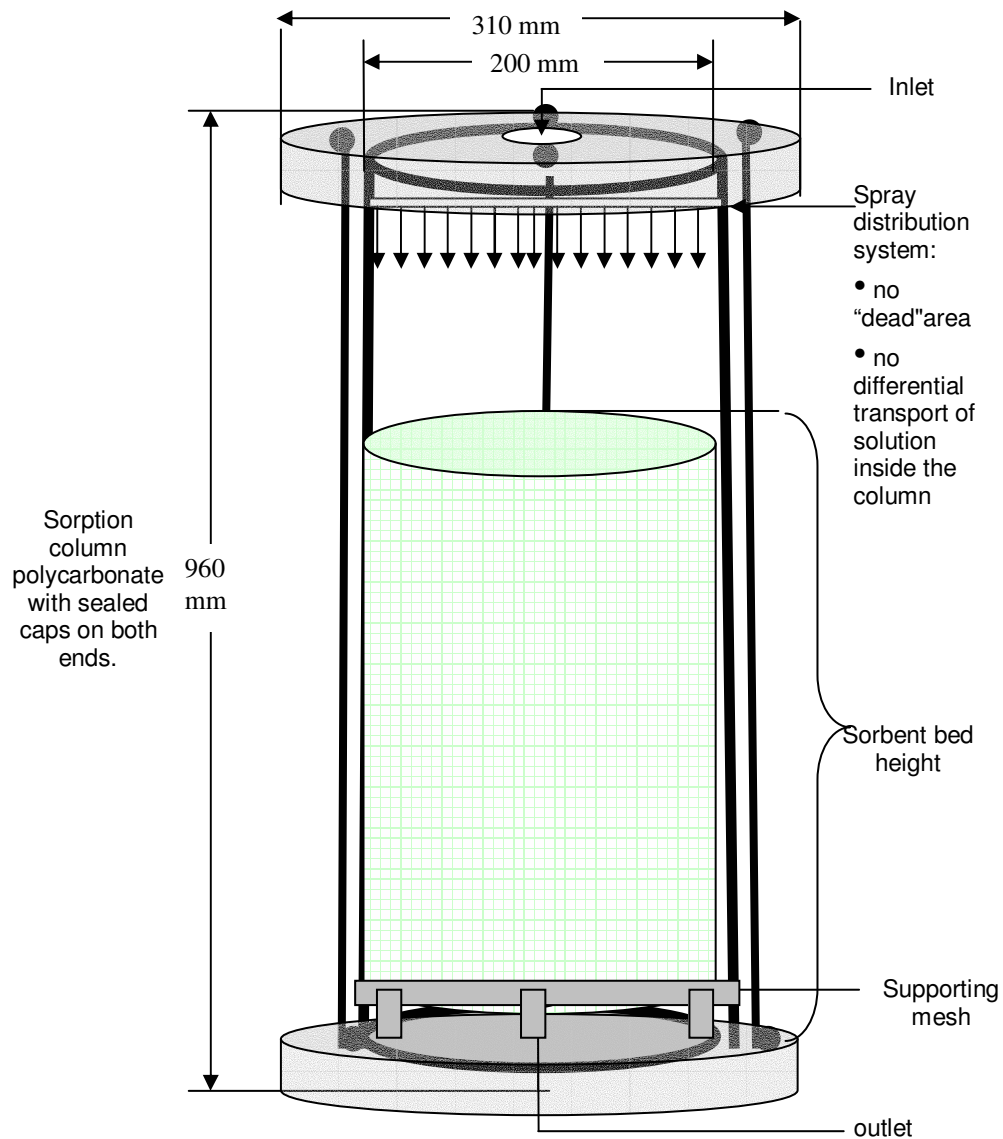


Fig. 11.2 Schematic representation of the scaled-up fixed bed sorption column

Fig. 11.2 shows that the prototype is composed of a single polycarbonate tube (200 mm internal diameter (I.D.), 960 mm length) sealed at both ends by caps tightened together with four screw rods. The total working volume was 30 159 cm<sup>3</sup>, corresponding to a 47 times increase in the working volume of the laboratory-scale column.

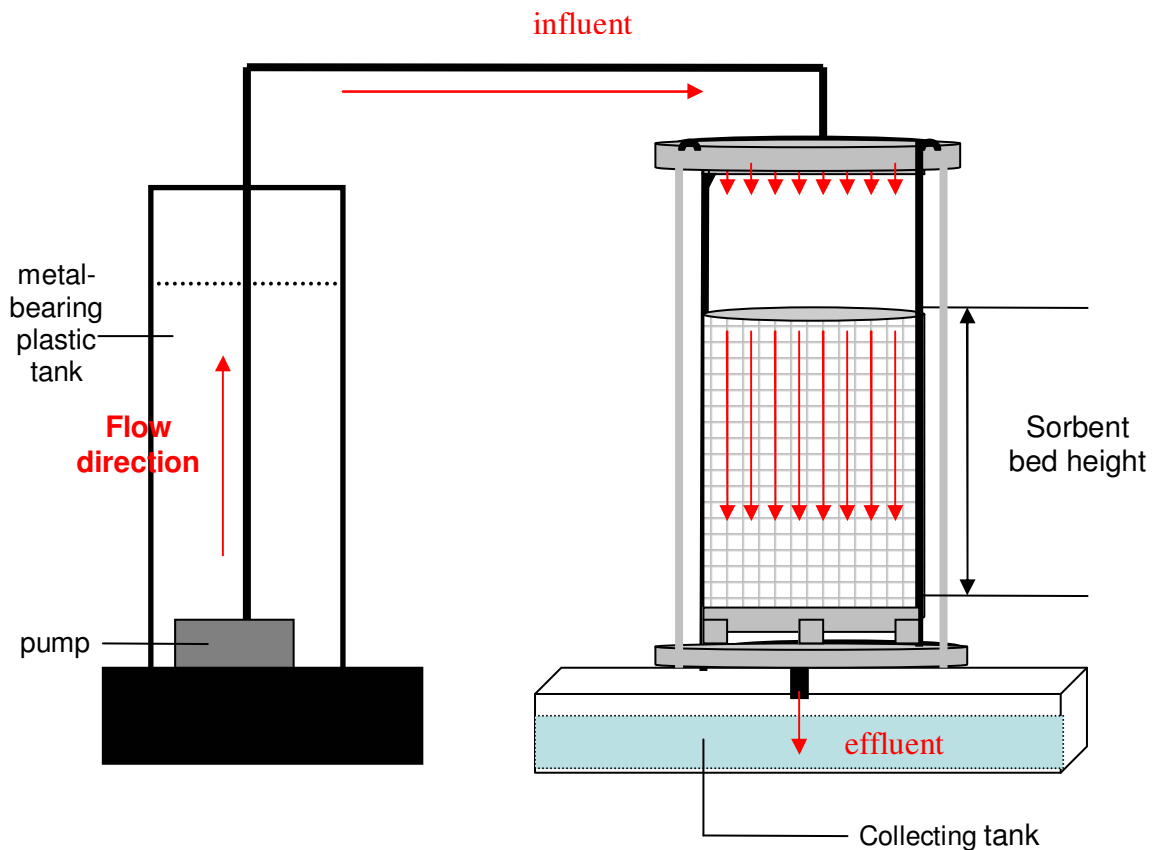


Fig. 11.3 Laboratory configuration and set-up of the scaled-up fixed bed sorption column

Fig. 11.3 shows that the metal-bearing solution (influent) was transported from a plastic tank to the column through plastic tubing using a pump. The metal solution was introduced inside the column through a spray system and the effluent was collected into a collecting tank.

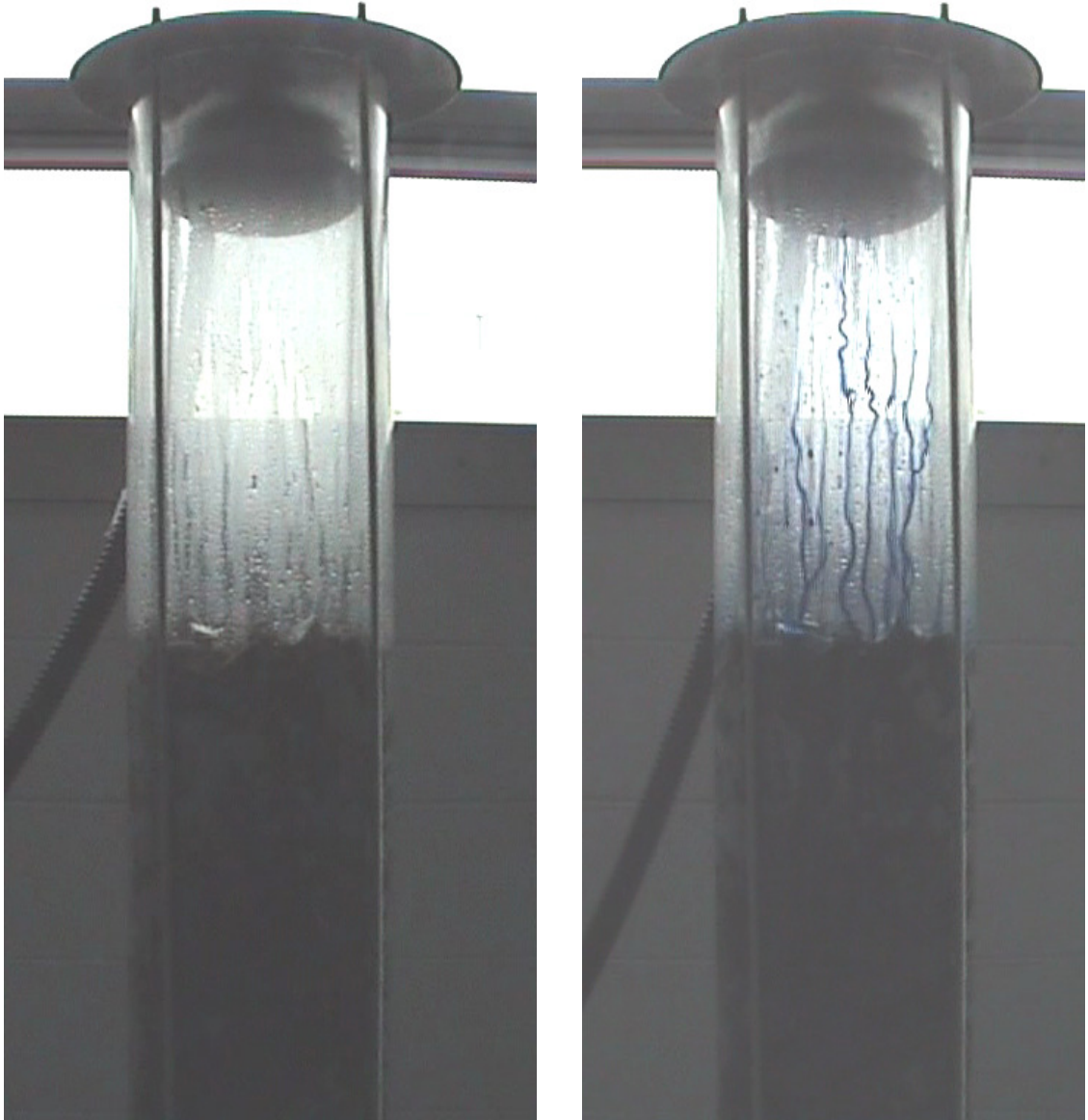


Fig. 11.4 Spray system for the introduction of the metal bearing solution

Fig. 11.4 illustrates the utilisation of a spray system for the introduction of the metal-bearing solution into the sorption column. This ensured that the influent was sprayed evenly over the column avoiding any “dead areas” within the sorbents.



Scale: X 0.5

X 1

Fig. 11.5 WAP/agar blocks packed into the scaled-up fixed bed column. A blue dye was added to highlight any void fractions between the blocks

Fig. 11.5 shows that the blocks were randomly positioned inside the column, forming a range of free spaces (void fraction), allowing the metal solution to percolate through the sorbent bed.

### **Flow rate requirements**

The flow-rate is a key factor in column design as the velocity of the metal-bearing solution within the column must be slow enough to ensure an efficient contact time but

rapid enough to ensure a large quantity of metal solution is treated. A pump with a maximum flow-rate of  $50 \text{ L min}^{-1}$  was selected (Neptune Eco 3000 pump, Oase GmbH, Germany). However, for all experiments the flow-rate was measured coming from the outlet, as it may vary depending on the distribution of blocks inside the column.

### **Metal-bearing solutions**

The influent was  $10 \text{ mg L}^{-1}$  solutions of Zn(II), Ni(II), Al(III) and Sb(III), prepared from  $1000 \text{ mg L}^{-1}$  analytical grade standard solutions (Sigma-Aldrich Dublin, Ireland), in distilled water.

### **Optimisation of the bed height**

An optimisation of the sorbent bed height was performed for WAP/agar blocks using Zn(II). Three different bed heights (30, 50 and 60 cm) were tested, at constant flow rates ( $3.99 \pm 0.28 \text{ L min}^{-1}$  at the outlet), for the removal of Zn(II) in an aqueous solution. The corresponding volume of metal solution treated over 15 min was  $59.84 \pm 4.13 \text{ L}$ . The most efficient sorbent bed length was used for the subsequent dynamic flow tests with other metals.

### **Dynamic flow tests**

Dynamic flow tests were carried out for the removal of Zn(II), Ni(II) and Al(III) by WAP/agar blocks in both single and multi-metallic solutions, and Sb(III) by *P. lanosa*/agar blocks. The sorbent bed height was kept constant after the optimisation with Zn(II). The flow rate was  $3.06 \pm 0.38 \text{ L min}^{-1}$  and the time period for the experiment was 60 min. The corresponding volume of metal solutions treated was 183.6 L over 60 min. All experiments were carried out singly due to the large amount of metal influent needed and to reduce the operational costs (e.g. metal solutions preparation, immobilisation of the biomass using agar).

## 11.4 Results and discussion

### 11.4.1 Manufacture of WAP/agar and *Polysiphonia lanosa*/agar blocks

The process (see Fig. 11.1) is suitable for the manufacture of both WAP/agar blocks and *P. lanosa*/agar blocks. The automatic mixing and heating of large quantities of biomass/immobiliser (WAP or *P. lanosa* and agar), in addition to the use of the cutting mesh, permitted a significant increase in the rate of production of the blocks.

### 11.4.2 Dynamic flow tests

#### 11.4.2.1 Optimisation of the bed height

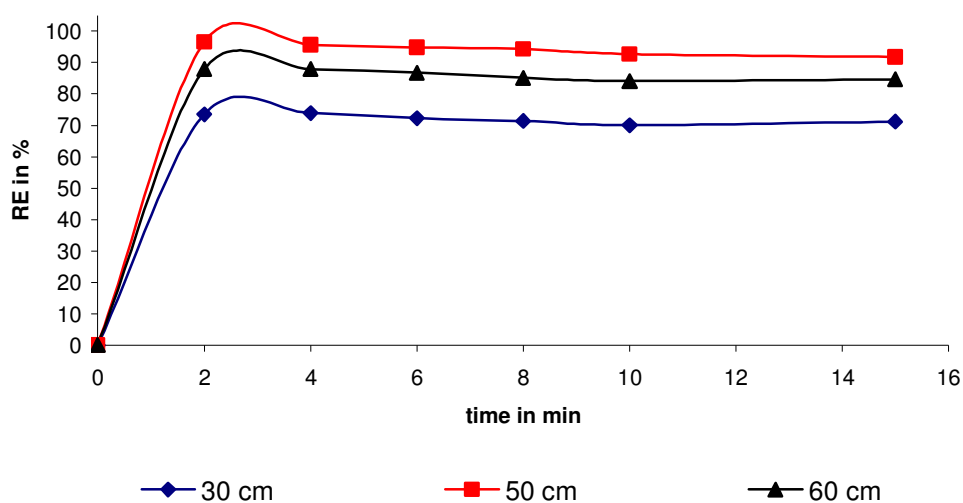


Fig. 11.6 Zn(II) RE (%) by 7.5% WAP/5% agar blocks over 15 min for different bed heights.

Fig. 11.6 shows that maximum REs were obtained for a bed length of 50 cm with RE values of more than 90% within 15 min. A maximum RE of 97% was obtained within 2 min and this was almost maintained throughout the 15 min of the experiment.

With a bed length of 60 cm, the metal solution accumulated on the top of the column, indicating an excess of liquid pressure on the blocks at the bottom of the column and a decrease in the void fraction between the blocks. As a result, the pathway between the blocks appeared to be reduced, inhibiting effective flow transport. This phenomenon can be described as the “over-packing” of the column. A bed length of 50 cm was therefore selected for the dynamic flow tests. The corresponding working volume of the column was  $30\,159\text{ cm}^3$ , 47 times the working volume of the laboratory scale columns ( $638\text{ cm}^3$ ).

#### 11.4.2.2 Dynamic flow test for Zn(II) removal in a single metal solution using WAP/agar blocks

Table 11.1 Operational settings for Zn(II) dynamic flow test

Settings	
Sorbent bed height (cm)	$50.67 \pm 1.41$
Flow rate at the outlet ( $\text{L min}^{-1}$ )	$2.32 \pm 0.06$
Spraying system position above sorbent bed (cm)	$33 \pm 0.53$
Bed volume ( $\text{dm}^3$ )	$30.58 \pm 0.66$
Volume of metal solution treated in 60 min (L)	$139.2 \pm 3.84$

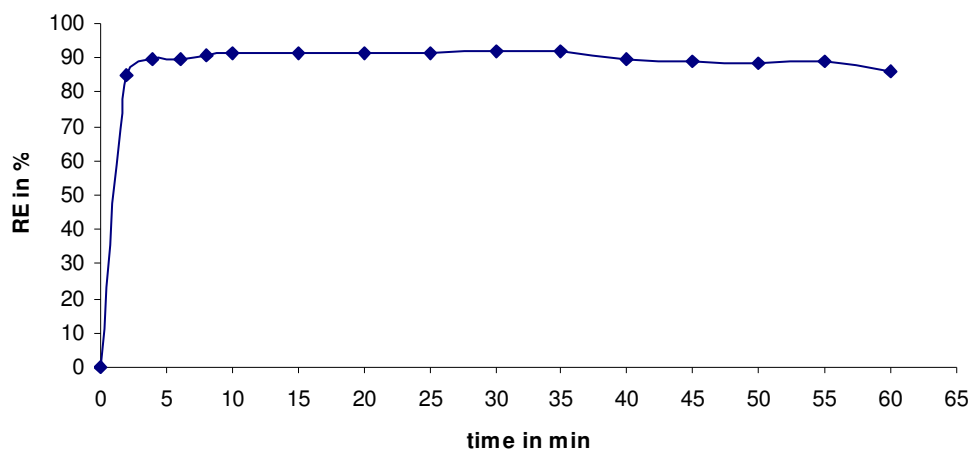


Fig. 11.7 RE in % for Zn(II) by 7.5% WAP/5% agar blocks in a single metal system.

Fig. 11.7 shows that high REs were achieved for Zn(II), with a maximum RE of 92% within 10 min. RE subsequently decreased slowly over time to reach a final RE of 86% at the 60 min time point. Due to the large volume of metal solution required, the metal bearing tank had to be refilled after 35 min.

#### 11.4.2.3 Dynamic flow test for Ni(II) removal in a single metal solution using WAP/agar blocks

Table 11.2 Operational settings for Ni(II) dynamic flow test

Settings	
Sorbent bed height (cm)	50.88 ± 0.71
Flow rate at the outlet (L min <sup>-1</sup> )	2.99 ± 0.10
Spraying system position above sorbent bed (cm)	33 ± 0.48
Bed volume (dm <sup>3</sup> )	31.3 ± 0.44
Volume of metal solution treated in 60 min (L)	179.4 ± 5.84

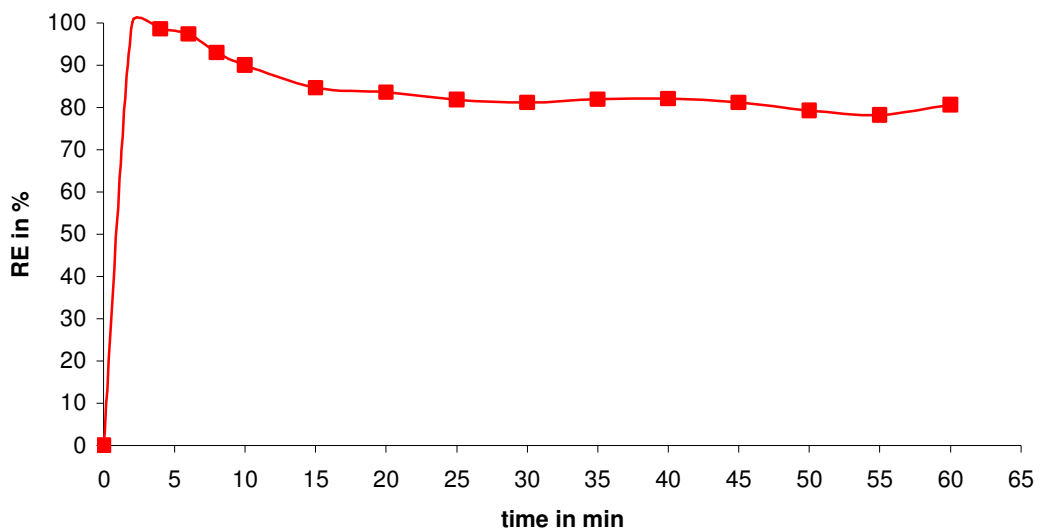


Fig. 11.8 RE in % for Ni(II) by 7.5% WAP/5% agar blocks in a single metal system.

Fig. 11.8 shows that high REs were achieved for Ni(II), with a maximum RE of 100% within 2 min. RE subsequently decreased slowly over time to find minimum RE of 81%

after 60 min. Due to the large volume of metal solution required, the metal bearing tank had to be refilled after 35 min.

#### 11.4.2.4 Dynamic flow test for Al(III) removal in a single metal solution using WAP/agar blocks

Table 11.3 Operational settings for Al(III) dynamic flow test

Settings	
Sorbent bed height (cm)	50.88 ± 0.71
Flow rate at the outlet (L min <sup>-1</sup> )	2.99 ± 0.10
Spraying system position above sorbent bed (cm)	33 ± 0.48
Bed volume (dm <sup>3</sup> )	30.69 ± 0.60
Volume of metal solution treated in 60 min (L)	179.4 ± 5.84

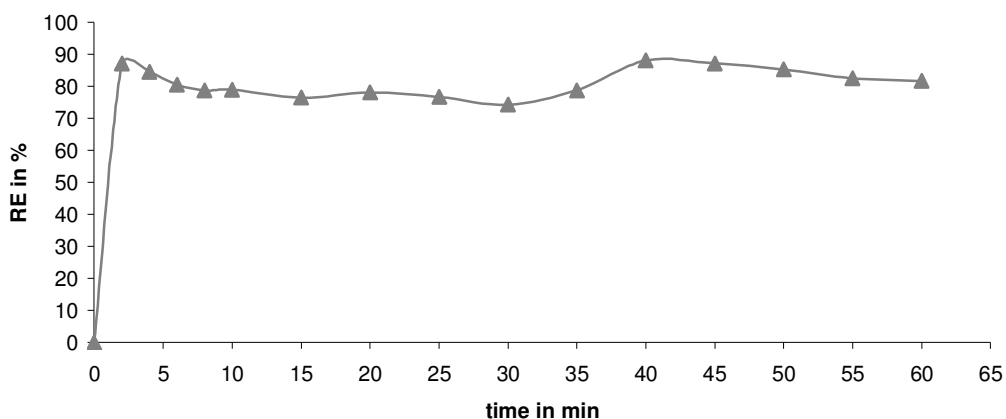


Fig. 11.9 RE in % for Al(III) by 7.5% WAP/5% agar blocks in a single metal system.

Fig. 11.9 shows that relatively high REs were achieved for Al(III), with a maximum RE of 87% within 2 min. RE subsequently decreased slowly over time to reach a final RE of 82% after 60 min. Due to the large volume of metal solution required, the metal bearing tank had to be refilled after 40 min, explaining the sudden change in shape of the curve. As the pump was stopped for a few minutes the sorbents inside the column may have started to dry, and consequently could retain more liquid on start up of the pump.

### 11.4.2.5 Dynamic flow test for Sb(III) removal in a single metal solution using *P. lanosa*/agar blocks

Table 11.4 Operational settings for Sb(III) dynamic flow test

Settings	
Sorbent bed height (cm)	41.33 ± 1.41
Flow rate at the outlet (L min <sup>-1</sup> )	3.52 ± 0.28
Bed volume (dm <sup>3</sup> )	25.45 ± 0.87
Spraying system position above sorbent bed (cm)	43 ± 0.71
Volume of metal solution treated in 60 min (L)	211.2 ± 16.74

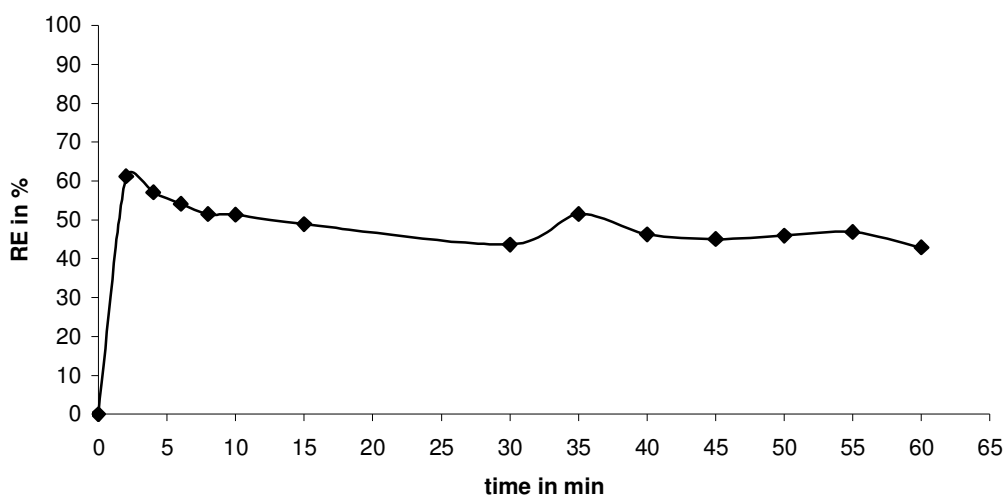


Fig. 11.10 RE in % for Sb(III) by 7.5% *P. lanosa*/5% agar blocks in a single metal system.

Fig. 11.10 shows that a maximum RE of 61% was reached within 2 min. RE subsequently decreased slowly over time to reach a final RE of 43% after 60 min. Due to the large volume of metal solution required, the metal bearing tank had to be refilled after 35 min, explaining the sudden change in shape of the curve. As the pump was stopped for a few minutes the sorbents inside the column may have started to dry, and consequently could retain more liquid on restarting the pump.

### 11.4.2.6 Dynamic flow test for Zn(II), Ni(II) and Al(III) in a multi-metal solution using WAP/agar blocks

Table 11.5 Operational settings for Zn(II), Ni(II) and Al(III) dynamic flow test (multi-metal system)

Settings	
Sorbent bed height (cm)	50.88 ± 0.71
Flow rate at the outlet (L min <sup>-1</sup> )	3.46 ± 0.27
Spraying system position above sorbent bed (cm)	33 ± 0.48
Bed volume (dm <sup>3</sup> )	30.79 ± 0.28
Volume of metal solution treated in 60 min (L)	207.6 ± 16.41

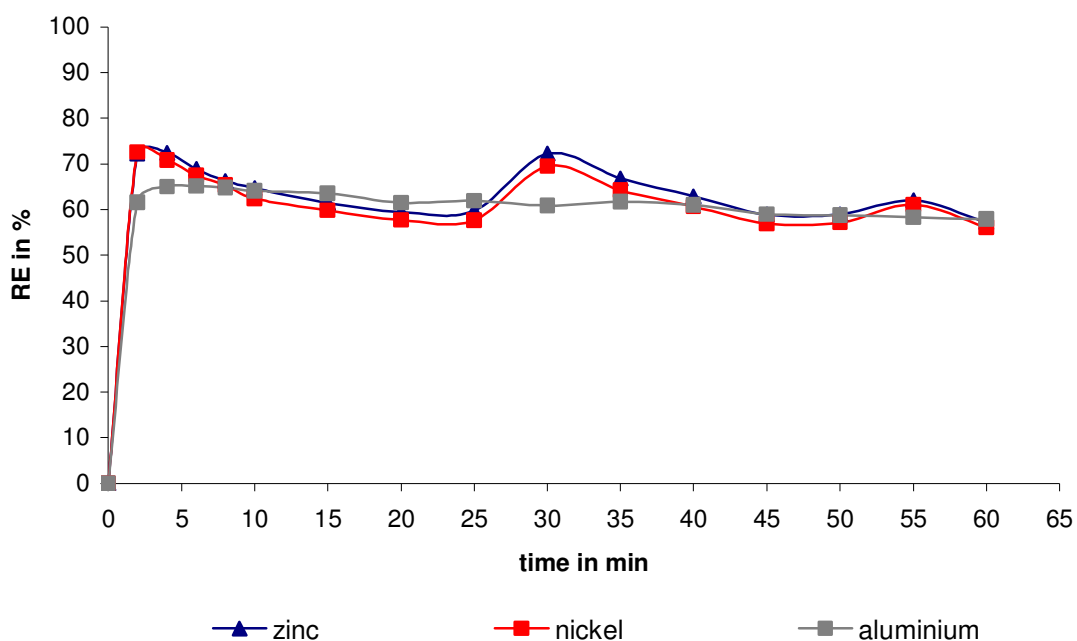


Fig. 11.11 RE in % for Zn(II), Ni(II) and Al(II) by 7.5% WAP/5% agar blocks in a multi metal system.

Fig. 11.11 shows that relatively high REs were obtained for all metals. Maximum observed REs of 72% and 73% were seen for Zn and Ni, respectively. A maximum of 65% RE was achieved for Al within 4 min. Minimum REs of 58, 57 and 56% were

observed for Al, Zn and Ni, respectively. Due to the large volume of metal solution required, the metal bearing tank had to be refilled after 30 min, explaining the sudden change in shape of the curve. As the pump was stopped for a few minutes the sorbents inside the column may have started to dry, and consequently could retain more liquid on restarting the pump. However, this phenomenon was less pronounced for in the case of Al(III).

### **Summary of results**

Table 11.6 Mean RE (%) over 60 min for Zn(II), Ni(II) and Al(III) in single and multi-metal systems by WAP/agar, and Sb(III) removal by *P. lanosa*/agar.

<b>Metals</b>	<b>Sorbent</b>	<b>Mean RE in % over 60 min</b>		
Zn(II)	WAP/agar	94 ± 1.30		
Ni(II)	WAP/agar	86 ± 3.67		
Al(III)	WAP/agar	81 ± 2.12		
Sb(III)	<i>P. lanosa</i> /agar	50 ± 2.83		
Zn(II)/Ni(II)/Al(III)	WAP/agar	64 ± 2.58	63 ± 2.66	62 ± 1.20

Table 11.6 highlights that the scaled-up column was very effective at removing Zn(II), Ni(II) and Al(III) from single metal solutions. Furthermore, the system performed satisfactorily for multi-metal systems. The decrease in RE in multi-metal systems may be explained by metal ion competition for the binding sites available (Bakir et al., 2009). The loss in RE can be controlled by decreasing the flow rate, which will increase the exposure time of the metal solution with the sorbent bed. A lower RE, of only 50% was observed for Sb(III) removal using *P. lanosa*/agar. In the same way, RE may be increased either by lowering the flow rate or by increasing the bed height without “over-packing” the column (section 11.4.2.1).

The large increase in the working volume of the column, corresponding to 47 times the working volume of the laboratory scale column, permitted the treatment of larger volumes of influents, as show in Tables 11.1-11.5. Furthermore, the utilisation of a spray system allowed an even distribution of the metal solution across the sorbent bed.

The scaled-up system is highly flexible and could easily be scaled-up further. For industrial use, metal identification, as well as a quantitative determination of the metals present in the effluent may be required. The column would need to be optimised, ensuring that final effluent concentrations comply with legal requirements.

## 11.5 Conclusions

The scale up of the laboratory fixed bed sorption column was achieved, with a 47 times increase in the working volume of the small scale column. The scaled-up version removed 94, 86 and 81% of Zn(II), Ni(II) and Al(III) respectively using 7.5%WAP/5% agar blocks in single metal systems. In a multi-metal solution, the REs decreased to 64, 63 and 62 for the same metals, due to ion competition for the limited number of binding sites. *P. lanosa*/agar blocks underperformed, with a maximum RE of only 61% for Sb(III) removal. A series of steps have been proposed to increase this RE, such as decreasing the flow rate and/or increasing the sorbent bed height, but avoiding “over-packing” of the column.

## **Chapter 12**

**Summary and**

**Future Work**

## 12.1 Summary

*Fucus vesiculosus*, *Polysiphonia lanosa*, *Ulva lactuca* and a seaweed waste material resulting from the industrial processing of *Ascophyllum nodosum* (WAP), in dried form, were screened for Zn(II), Ni(II), Al(III) and Sb(III) in both single and multi-metal systems. WAP and *P. lanosa* were found to be more effective at removing metal ions compared with the other seaweed biomasses. Metal uptake by WAP was shown to be efficient at removing Zn(II), Ni(II) and Al(III) in both single and multi-metal systems. *Polysiphonia lanosa* was found to be more effective at removing Sb(III) than WAP. WAP and *P. lanosa* were subsequently selected for metal sorption using a laboratory fixed-bed sorption column. Particles of WAP and *P. lanosa* were immobilised in agar to form blocks of homogenous form and size. Immobilisation of biomass allowed the production of a robust sorbent while avoiding any blockage of the column.

Fixed-bed column studies using WAP and *P. lanosa* immobilised in agar resulted in high removal efficiencies (RE) for Zn(II), Ni(II) and Al(III) respectively for WAP/agar, and Sb(III) removal by *P. lanosa*/agar, over 3 hours. Agar alone was found to contribute to the RE of the metals.

In multi-metal systems, Sb(III) was found to adversely affect the sorption of Zn(II), Ni(II) and Al(III) by WAP, while *P. lanosa* removed Sb(III) in multi-metal systems. The antagonistic effect of Sb(III) on the sorption of the other metals by WAP was investigated using FTIR, XPS and conductimetric titrations. The results demonstrated that Sb(III) was able to bind on to a larger and more diversified number of binding sites on *P. lanosa*, preventing the uptake of Zn(II), Ni(II) and Al(III). WAP also displayed a low affinity for Sb(III) due to its difference in composition than *P. lanosa* (Bakir et al., 2009).

Maximum uptake capacity values ( $q_{\max}$ ) were calculated using the Langmuir, Freundlich and the combined Langmuir-Freundlich sorption isotherms. The Langmuir model was found to be generally more efficient at representing metal sorption than the other models.  $q_{\max}$  values, calculated from the Langmuir model, were very high in the case of WAP for the sorption of Zn(II), Ni(II) and Al(III). The  $q_{\max}$  value for *P. lanosa* and Sb(III) was significantly lower.  $q_{\max}$  values for WAP were found to be as efficient as chemically enhanced biomasses for Zn(II), Ni(II) and Al(III) (Lee and Suh, 2001;

Lau et al., 2003; Sheng et al., 2004). The maximum column capacity showed that the column continued to be operational over a large period of time before reaching saturation. Comparing the mass transfer zones (MTZ) for the different metals, which indicated how efficiently the column was being used, showed that the column was efficient for the removal of all metals with the exception of Ni(II) which displayed a large MTZ. In practice, this could be overcome by changing some key operational settings such as decreasing the flow rate or increasing the sorbent bed height inside the column allowing a faster removal and consequently a shorter MTZ.

Different desorbing solutions were screened for desorption and reuse of WAP and *P. lanosa*. Mineral acids, and especially HCl, were found to be more efficient at desorbing metals from both biomasses. The regeneration and reuse of the biosorbents were achieved using 0.1M HCl with very little loss in metal reuptake efficiency over five sorption cycles. WAP/agar was found to be robust and did not show any loss in physical integrity following repeated acid washes. This was not the case for *P. lanosa*/agar which displayed a loss in RE following repeated acid washes (Bakir et al., 2010).

Scale-up of the laboratory column was carried out, and a high RE was observed for all metals under investigation. Scale-up was achieved by increasing the sorbent bed height and the working volume of the scaled-up column corresponding to a 47 times increase in the working volume of the laboratory scale column. A mathematical model (Yoon-Nelson Model) was shown to accurately represent metal sorption over the experiment time period (3 hours). However, when attempting predictions over a longer period of time, the Yoon-Nelson model significantly underestimated the experimental data. As a result, a more complex simulation tool was needed. COMSOL Multiphysics™ is an effective tool at simulating metal sorption behaviour. The experimental data fitted very closely to an existing column simulating model (MTCM) (Kratochvil, 1997). It was possible to derive some valuable operating settings such as overall mass transfer and the axial dispersion coefficient. COMSOL is a valuable tool for industrial applications. The software is easily applicable for predicting breakthrough curves for various industrial processes (e.g. different waste stream compositions, column size, flow rate) prior to any pilot trial. COMSOL could be very valuable at bridging the research phase and the industrial pilot trial process.

## 12.2 Future work

This chapter outlines areas in which further work could progress the research outlined in this project. These are:

- Further characterisation of the WAP biosorbent,
- Development of an industrial-scale sorption system,
- Further COMSOL modelling for multi-metal solutions and for different operating settings,
- Detailed examination of costings and market potential.

### 12.2.1 Further characterisation of WAP

Despite having gathered substantial data on metal removal by WAP, little is known about its production and composition. Indeed, as outlined in Chapter 11, the large metal removal capacity by WAP appears to result from the cold extraction processing of *Ascophyllum nodosum* by Oilean Glas Teo (OGT) (Ballymoon Industrial Estate, Kilcar, Co. Donegal, Ireland), with the purification of the binding sites on the surface. FTIR, potentiometric and conductimetric titrations, as well as XPS analysis, carried out in this work, gave detailed information on the structure and behaviour of the sorbent for metal uptake. However, some characteristics remain to be investigated, such as surface morphology before and after metal exposure. The use of Scanning Electron Microscopy (SEM) could provide useful information on the surface morphology as well as the distribution of metal ions about the surface after metal sorption (Murphy, 2007).

### **12.2.2 Industrial-scale fixed bed sorption column**

As stated in previous chapters, the main advantage of a fixed-bed sorption column is its flexibility in design. Scale-up is commonly achieved by simply increasing the bed height, according to the length and internal diameter of the column (Volesky, 2004). In this project, a medium-scale column was designed and tested for a limited range of metals (Zn(II), Ni(II), Al(III) and Sb(III)). However, a larger column could be designed and tested under actual industrial conditions. In this case, the manufacturing process of the WAP/Agar and *P. lanosa*/Agar blocks would have to be scaled-up proportionately.

### **12.2.3 Further COMSOL modelling**

As seen in Chapter 10, COMSOL was an effective tool for generating models accurately, describing metal biosorption onto biomass for single metal systems. The next step would be to simulate metal sorption in multi-metal systems, as would be expected in most industrial effluents. Predicting breakthrough concentrations for different operating settings, such as the initial metal concentration, column size or flow rate, would also give valuable information on fixed bed sorption effectiveness under industrial conditions.

### **12.2.4 Costing and market assessment**

A detailed assessment of costing for the biosorption system, compared with alternative systems, needs to be carried out. An investigation of the potential global market would also be required prior to commercial exploitation.

# References

Aderhold, D., Williams, C.J. and Edyvean, R.G. 1996, "The removal of heavy metal ions by seaweed and their derivatives", *Bioresource technology*, vol. 58, pp. 1-6.

Ahner, B.A., Kong, S. and Morel, F.M.M., 1995, "Phytochelatin Production in Marine Algae. 1-An interspecies Comparison", *Limnology and Oceanography*, vol. 40, pp. 649-657.

Aksu, Z., Açikel, U. and Kutsal, T. 1997, "Applications of Multicomponent Adsorption Isotherms to Simultaneous Biosorption of Iron (III) and Chromium (VI) on *C. vulgaris*", *Journals of Chemical Technology & Biotechnology*, vol. 41, pp. 368-378.

Al-Rub, F.A.A., 2006, "Biosorption of zinc on palm tree leaves: equilibrium, kinetics, and thermodynamics studies", *Separation and Purification Technology*, pp. 3499-3515.

Al-Rub, F.A.A., El-Naas, M.H., Ashour, I. and Al-Marzouqi, M., 2006, "Biosorption of copper on *Chlorella vulgaris* from single, binary and ternary metal aqueous solutions", *Process Biochemistry*, vol. 41, pp. 457-464.

Alexopoulos, E., McCrohan, E., Powell, C.R., Jugdaohsingh, R. and White, K.N., 2004, "Bioavailability and Toxicity of Freshly Neutralized Aluminium to the Freshwater Crayfish *Pacifastacus leniusculus*", *Archives of Environmental Contamination and Toxicology*, vol. 45, pp. 509-514.

Algaebase. *Fucus vesiculosus* Linnaeus. [www.algaebase.org](http://www.algaebase.org) . 2008a.

Algaebase. *Polysiphonia lanosa* (Linnaeus) Tandy. [www.algaebase.org](http://www.algaebase.org) . 2008b.

Andrade, S., Medina, M.H., Moffet, J.W. and Correa, J.A., 2006, "Cadmium-Copper Antagonism in Seaweed Inhabiting Coastal Areas Affected by Copper Mine waste Disposals", *Environmental Science & Technology*, vol. 40, pp. 4382-4387.

Andresen, I.L., Skipnes, O., Smidrod, O., Ostgarrd, K. and Hemmer, P., 1977, "Some biological functions of matrix components in benthic algae in relation to their chemistry and the composition of seawater", *ACS Symposium*, vol. 48, pp. 361-381.

Bakir, A., McLoughlin, P., Tofail, S.A.M. and Fitzgerald, E., 2009, "Competitive sorption of antimony with zinc, nickel and aluminium in a seaweed based fixed-bed sorption column", *Clean – Soil, Air, Water*, vol. 37, pp. 712-719.

Bakir, A., McLoughlin, P. and Fitzgerald, E., 2010, "Regeneration and reuse of a seaweed-based biosorbent in single and multi-metal systems", *Clean – Soil, Air, Water*, vol. 38, pp. 257-262.

Birchall, J.D. and Chappel, J.S., 1998, "The chemistry of Aluminium and Silicon within the Biological Environment", *Aluminium in Biology and Medicine*, Wiley-Inter-science, pp. 50-54.

Brierley, J.A., Brierley, C.L. and Goyak, G.M., 1986, "AMT-BIOCLAIM: A new wastewater treatment and metal recovery technology", in Lawrence, R.W, Branion, R.M.R. and H.G. Ebne (eds.), *Fundamental and Applied Biohydrometallurgy*, Elsevier, Amsterdam, pp. 291-304.

Brower, J.B., Ryan, R.L. and Pazirandeh, M., 1997, "Comparison of Ion-exchange resins and biosorbents for the removal of heavy metals from plating factory wastewater", *Environmental Science & Technology*. vol. 31, pp. 2910-2914.

BV Sorbex. Technology description. [www.bvsorbex.com](http://www.bvsorbex.com) . 2008a.

BV Sorbex. The Biosorption process. [www.bvsorbex.com](http://www.bvsorbex.com) . 2008b.

Campbell, A., 2002, "The Potential role of Aluminium in Alzheimer's disease", *Nephrology Dialysis Transplantation*, vol. 17, pp. 17-20.

Chen, J.P., Hong, L.A., Wang, S.N. and Wang, L., 2002, "Elucidation of interactions between metal ions and Ca alginate-based ion-exchange resin by spectroscopic analysis and modeling simulation", *Langmuir*, vol.18, pp. 9413-9421.

Chen, L.C.M., McLachlan, J., Neish, A.C. and Shacklock, P.F., 1973, "The ratio of kappa- to lambda-carrageenan in nuclear phases of the *rhodophycean* algae, *Chondrus crispus* and *Gigartina stellata*", *Marine Biological Association of the United Kingdom*, vol. 53, pp. 11-16.

Chu, K.H., Hashim, M.A., Phang, S.M. and Samuel, V.B., 1997, "Biosorption of cadmium by algae biomass: adsorption and desorption characteristics", *Water Science and Technology*, vol. 35, pp. 115-122.

Clenaghan, C., O'Neill, N., and Page, D., 2005, "Dangerous substances regulations", 129-138. 2005, *Environmental Protection Agency*, pp. 129-138.

Cossich, E.S., 2004, "Biosorption of Chromium(III) by biomass of Seaweed *Sargassum sp.* in a fixed-bed column", *Chemical Engineering Journal*, vol. 10, pp. 129-138.

Cotton, F.A., Wilkinson, G. and Gaus, P.L., 1995, *Basic Inorganic Chemistry*, John Wiley & Sons, Inc.

Crist, R., Martin, J.R., Gutpill, P.W. and Eslinger, J.M., 1990, "Interaction of metals and protons with Algae 2. Ion exchange in adsorption and metal displacement by protons", *Environmental Science & Technology*, vol. 24, pp. 337-342.

Crist, R.H., Martin, J.R., Carr, D., Watson, J.R. and Clarke, J., 1994, "Interaction of metals and protons with algae. 4. Ion exchange vs. Adsorption models and a reassessment of Scatchard Plots; Ion-exchange rates and equilibria compared with calcium alginate", *Environmental Science & Technology*, vol. 28, pp. 1859-1866.

Crist, R.H., Oberholser, K. and McGarrity, J., 1992, "Interaction of Metals and Protons with Algae 3. Marine algae with emphasis on lead and aluminium", *Environmental Science & Technology*, vol. 26, pp. 496-502.

Cybercolloids. Agar structure. [www.cybercolloids.net](http://www.cybercolloids.net) . 2004.

Da Costa, A.C.A. and De França, F.P., 1997, "Biosorption of Zinc, Cadmium and Copper by a brown seaweed (*Sargassum sp.*) in a continuous fixed-bed laboratory reactor", *Bioseparation*, vol. 6, pp. 335-341.

Dambies, L., Guiman, C., Yiacoumi, S. and Guibal, E., 2001, "Characterisation of metal ion interactions with chitosan by X-ray photoelectron spectroscopy.", *Colloids and Surfaces A: Physicochemical and Engineering Aspects*, vol. 177, pp. 203-214.

Darnall, D. W. and Hosea, J. M., 1990, "Site-Emerging technologies: Removal and Recovery of metal ions from groundwater".

Davis, T.A., Volesky, B. and Mucci, A., 2003, "A review of the biochemistry of heavy metal biosorption by brown algae", *Water Research*, vol. 37, pp. 4311-4330.

Davis, T.A., Volesky, B. and Vieira, R.H.S.F., 2000, "Sargassum seaweed as biosorbent for heavy metals", *Water Research*, vol. 34, pp. 4270-4278.

De França, F.P., Tavares, A.P. and Da Costa, A.C.A., 2002, "Calcium interference with continuous biosorption of zinc by *Sargassum sp.* (Phaeophyceae) in tubular laboratory reactors", *Bioresource technology*, vol. 83, pp. 159-163.

Department of the Environment and Water Resources, "Antimony & compounds fact sheet", <http://www.npi.gov.au/database/substance-info/profiles/10.html>. 2008.

Draget, K.I., Smidsrød, O. and Skjåk-Bræk, G., 2005, "Alginates from Algae in Polysaccharides and Polyamides in the Food Industry. Properties, Production, and Patents", *Wiley-VCH Verlag & Co, Weinheim*.

Duffield, J.R. and Williams, D.R., 1998, "Aluminium in Food and the Environment. In The Proceedings of a Symposium organised by the Environment and Food chemistry Groups of the Industrial Division of the Royal Society of Chemistry", *Royal Society of Chemistry, special Publication*, vol. 73.

Dupont, D., Bouanda, J. and Dumonceau, J., 2005, "Biosorption of Cu(II) and Zn(II) onto a lignocellulosic substrate extracted from wheat bran", *Environmental Chemistry Letters*, pp. 165-168.

Environmental Protection Agency. ENVision. 2008.

Fagundes-Klen, M.R., Ferri, P., Martins, T.D., Tavares, A.P. and Silva, E.A., 2007, "Equilibrium of the binary mixture of cadmium-zinc ions biosorption by the *Sargassum filipendula* species using adsorption isotherms models and neural network", *Biochemical Engineering Journal*, vol. 34, pp. 136-146.

Feng, D. and Aldrich, C., 2004, "Adsorption of heavy metals by biomaterials derived from the marine algae *Ecklonia maxima*", *Hydrometallurgy*, vol. 73, pp. 1-10.

Figueira, M.M., Volesky, B. and Mathieu, H.J., 1999, "Instrumental analysis study of iron species biosorption by *Sargassum* biomass", *Environmental science & Technology*, vol. 33, pp. 1840-1846.

Fitzgerald, E., 2002, "Metal concentrations in the Suir estuary as indicated by analysis of biota, sediments and water", The Open University.

Fosmire, G.J., 2008, 'Zinc toxicity', *The American Journal of Clinical nutrition*.

Fourest, E., Serre, A. and Roux, J.C., 1996, "Contribution of carboxyl groups to heavy metal binding sites in fungal wall", *Toxicology and Environmental Chemistry*, vol. 54, pp. 1-10.

Fourest, E. and Volesky, B., 1996, "Contribution of sulphonate groups and alginate to heavy metal biosorption by the dry biomass of *Sargassum fluitans*", *Environmental Science & Technology*, vol. 30, pp. 49-58.

García-Calzón, J.A. and Díaz-García, M.E., 2007, "Characterisation of binding sites in molecular imprinted polymers", *Sensors and Actuators*, vol. B, pp. 1180-1194.

Greenwood, N.N. and Earnshaw, A., 1994, "*Chemistry of the elements*", Pergamon Press, London.

Guiry, M. *Fucus*. [www.seaweed.ie](http://www.seaweed.ie) . 2008.

Gupta, B., Begum I,Z. and Rajput, G., 2008, "Equilibrium and kinetic studies for the adsorption of Mn(II) and Co(II) from aqueous medium using Agar-Agar as sorbent", *Chemical Engineering Communications* , vol. 195, pp. 1200-1212.

Gupta, S. and Babu, B.V., 2005, "Modeling and Simulation of Fixed Bed Adsorption Column: Effect of Operating Variables", pp. 391-394.

Gupta, S. and Rastogi, A., 2008, "Equilibrium and kinetic modelling of cadmium(II) biosorption by nonliving algal biomass *Oedogonium* sp. from aqueous phase.", *Journal of Hazardous Materials*, vol. 153, pp. 759-766.

Guyen, K.C. and Akyuz, K., 1995, "Selectivity of heavy metal binding by algal polysaccharides", *Toxicological and Environmental Chemistry*, vol. 47, pp. 65-70.

Hamdy, A.A., 2000, "Biosorption of Heavy metals by marine algae", *Current Microbiology*, vol. 41, pp. 232-238.

Hanif, M.A., Nadeema, R., Bhatti, H.N., Ahmada, N.R. and Ansari, T.M., 2007, "Ni(II) biosorption by *Cassia fistula* (golden shower) biomass", *Journal of Hazardous Materials*, vol. B, pp. 345-355.

Harland, C.E., 1994, "Discovery and Structure of Solid Inorganic Ion Exchange Materials", *Ion exchange: Theory and Practice*, Royal Society of Chemistry, pp. 1-19.

Hashim, M.A., Tan, H.N. and Chu, K.H.: 2000, "Immobilized marine algal biomass for multiple cycles of copper adsorption and desorption", *Separation and Purification methods*, vol. 19, pp. 39-42.

Haug, A., "The affinity of some divalent metals to different types of alginates.", *Acta Chemica Scandinavica*, vol. 15, pp. 1794-1795.

Haug, A., Myklestad, S. and Smidrod, O., 1967, "Correlation between chemical structure and physical properties of alginates", *Acta Chemica Scandinavica*, vol. 21, pp. 768-778.

Helfferich, F.G., 1995, *Ion exchange*, Dove Publications.

Hilliou, L., Larotonda, F.D.S., Abreu, P., Ramos, A.M., Sereno, A.M. and Gonçalves, M.P., 2006, "Effect of extraction parameters on the chemical structure and gel properties of k/i-hybrid carrageenans obtained from *Mastocarpus stellatus* " , *Biomolecular Engineering*, vol. 23, pp. 201-208.

Holan,Z .R. and Volesky, B., 1994, "Biosorption of lead and nickel by biomass of marine algae", *Biotechnology and Bioengineering*, vol. 43, pp. 1001-1009.

Hou, H.B. and Narasaki, H., 1998, "Differential Determination of Antimony (III) and Antimony (V) by Inductively Coupled Plasma Atomic Emission Spectroscopy with Hybride Generation", *Analytical sciences*, vol. 14, pp. 1161-1164.

International Agency for Research on Cancer (IARC). [www.IARC.fr](http://www.IARC.fr) . 2009

International Aluminium Institute, "Aluminium sustainability", <http://www.world-aluminium.org/> . 2000.

Jeffers, T. H., Ferguson, C. R., and Bennett, P. G., 1991, "Biosorption of metal contaminants using immobilized biomass-A laboratory study", Bureau of Mines. 9340, pp. 1-9, United States Department of the Interior, Report of Investigations, 2009.

Ko, D.C.K., Porter, J.F. and McKay, G., 2000, "Optimised correlations for the fixed bed adsorption of metal ions on bone char", *Chemical Engineering Science*, vol. 55, pp. 5819-5829.

Kratochvil, D., 1997, "A study of the metal biosorption process utilizing *Sargassum* seaweed biomass", *PhD thesis*, McGill University, Quebec, Canada.

Kratochvil, D. and Volesky, B.: 2000, "Multicomponent biosorption in fixed beds", *Water Research*, vol. 34, pp. 3186-3196.

Lau, T.C., Ang, P.O. and Wong, P.K., 2003, "Development of seaweed biomass as a biosorbent for metal ions", *Water Science and Technology*, vol. 47, pp. 49-54.

Lee, H.S. and Suh, J.H., 2001, "Interference of aluminium in heavy metal biosorption by a seaweed biosorbent", *Korean Journal of Chemical Engineering*, vol. 18, pp. 692-697.

Lee, H.S. and Volesky, B., 1997, "Interaction of light metals and protons with seaweed biosorbents", *Water Research*, vol. 31, pp. 3082-3088.

Lee, H.S. and Volesky, B., 1999, "Interference of aluminium in copper biosorption by an algal biosorbent", *Water Quality Research Journal of Canada*, vol. 34, pp. 519-531.

Lee, T.F., 1977, "*The Seaweed Handbook-An illustrated guide to seaweeds from North Carolina to the Arctic*", Dover Publications, Inc., New York.

Lesmana, S.O., Febriana, N., Soetaredjo, F.E., Sunarso, J. and Ismadji, S., 2008, "Studies on potential applications of biomass for the separation of heavy metals from water and wastewater", *Biochemical Engineering Journal*. vol. 44, pp. 19-41.

- Leusch, A., Holan, Z.R. and Volesky, B., 1995, "Biosorption of Heavy Metals (Cd, Cu, Ni, Pb, Zn) by Chemically-Reinforced Biomass of Marine Algae", *Journal of Chemical Technology & Biotechnology*, vol. 62, pp. 279-288.
- Lewis, T.E., 1990, "*Environmental Chemistry and Toxicology of Aluminium*", Lewis Publishers, Inc.
- Lodeiro, P., Herrero, R. and Sastre de Vicente, M.E., 2006, "The use of protonated *Sargassum muticum* as biosorbent for cadmium removal in a fixed-bed column", *Journal of Hazardous Materials*, vol. B137, pp. 244-253.
- MarLIN. *Polysiphonia lanosa*, The Marine Life Information Network from Britain & Ireland, 2008b.
- MarLIN. *Fucus vesiculosus*, The Marine Life Information Network from Britain & Ireland, 2008a.
- MarLIN. Sea lettuce-*Ulva lactuca*, The Marine Life Information Network from Britain & Ireland, 2008c.
- Mohan, S. and Sreelakshmi, G., 2008, "Fixed bed column study for heavy metal removal using phosphate treated rice husk", *Journal of Hazardous Materials*, pp. 75-82.
- Murphy, V., 2007, "An investigation into the uptake and mechanism of heavy metal binding in selected seaweed species", *PhD thesis*, Waterford Institute of Technology, Ireland.
- Murphy, V., Hugues, H. and McLoughlin, P., 2007, "Cu(II) binding by dried biomass of red, green and brown macroalgae", *Water Research*, vol. 41, pp. 731-740.
- Murphy, V., Hugues, H. and McLoughlin, P., 2008, "Comparative study of chromium biosorption by red, green and brown macroalgae", *Chemosphere*, vol. 70, 1128-1134.
- Naja, G., Diniz, V. and Volesky, B., 2005, "Predicting metal biosorption performance", in Harrison, S.T.L., Rawlings, D.E. and J.Petersen, J. (eds.), 2005, pp. 553-562.
- Naja, G. and Volesky, B., 2006b, "Multi-metal biosorption in a fixed-bed flow-through column", *Colloids and Surfaces A: Physicochemical and Engineering Aspects*, vol. 281, pp. 194-201.
- Naja, G. and Volesky, B., 2008, "Optimization of a biosorption column performance", *Environmental Science & Technology*, vol. 42, pp. 5622-5629.

- Naja, G. and Volesky, B., 2006a, "Behavior of the Mass Transfer Zone in biosorption column", *Environmental Science & Technology*, vol. 40, pp. 3996-4003.
- Nigro, S., Stirk, W.A. and Staden, J.V., 2002, "Optimising heavy metal adsorbance by dried seaweed", *South African journal of Botany*, vol. 68, pp. 333-341.
- Oilean Glas Teo. "Cold Process Seaweed Extract", [www.OGT.ie](http://www.OGT.ie) . 2008.
- Olguin, E.J., Sanchez, G. and Hernandez, E., 2000, "*Environmental Biotechnology and cleaner bioprocesses*", Taylor & Francis Limited, Cornwall.
- Park, D., Yun, Y.S. and Park, J.M., 2004, "Reduction of hexavalent chromium with the brown seaweed *Ecklonia* biomass", *Environmental Science Technology*, vol. 38, pp. 4860-4864.
- Parmentier, J. "*Polysiphonia*, a red algae". Microscopy-UK, 1999.
- Pawlik-Skowronska, B., 2001, "Phytochelatin production in freshwater algae *Stigeoclonium* in response to heavy metal contained in mining water; effects of some environmental factors", *Aquatic Toxicology*, vol. 52, pp. 241-249.
- Percival, E. and McDowell, R.H., 1967, "*Chemistry and enzymology of marine algal polysaccharides*", Academic Press, London, UK.
- Quintelas, C., Fernandes, B. and Castro, J., 2008, "Biosorption of Cr(VI) by three different bacterial species supported on granular activated carbon-A comparative study", *Journal of Hazardous Materials*, vol. 153, pp. 799-809.
- Ray, H.C., Oberholser, K., Shank, N. and Nguyen, M., 1981, "Nature of Bonding between Metallic Ions and Algal Cell Walls", *Environmental Science & Technology*, pp. 1212.
- Renault, F., Sancey, B., Badot, P.-M. and Crini, G., 2008, "Chitosan for coagulation/flocculation processes-An eco-friendly approach", *European Polymer Journal*. vol. 45, pp. 1337-1348.
- Romera, E., Gonzáles, F., Ballester, A., Blázquez, M.L. and Muñoz, J.A., 2006, "Biosorption with Algae: A statistical review", *Critical Reviews in Biotechnology*, vol. 26, pp. 223-235.
- Romera, E., Gonzáles, F., A., Blázquez, M.L. and Muñoz, J.A., 2007, "Comparative study of biosorption of heavy metals using different types of algae.", *Bioresource Technology*, vol. 98, pp. 3344-3353.

Ruthven, D.M., 1984, “*Principles of adsorption and adsorption processes*”, Wiley, New York.

Sag, Y., 2001, “Biosorption of heavy metals by fungal biomass and modeling of fungal biosorption: A review”, *Separation and Purification methods*, vol. 30, pp. 1-48.

Sag, Y. and Kutsal, T., 1998, “The simultaneous biosorption of Cr (VI), Fe(III) and Cu (II) on *Rhizopus arrhizus*”, *Process Biochemistry*, vol. 33, pp. 571-579.

Schiewer, S. and Volesky, B., 1996, “Modeling Multi-metal ion exchange in biosorption”, *Environmental Science & Technology*, vol. 30, pp. 2921-2927.

Senthilkumar, R., Vijayaraghavan, K., Thilakavathi, M., Iyer, P.V.R. and Velan, M.: 2006, “Seaweeds for the remediation of wastewaters contaminated with zinc(II) ions”, *Journal of Hazardous Materials*, vol. B136, pp. 791-799.

Shay, N.F. and Mangian, H.F., 2000, “Neurobiology of Zinc-Influenced Eating Behavior”, *Journal of nutrition*, vol. 130, pp. 1493-1499.

Sheindorf, C.H. and Rebhun, M., 1980, “A Freundlich-Type Multicomponent Isotherm”, *Journal of Colloid and Interface Science*, vol. 79, pp. 136-142.

Sheng, P.X., Ting, Y.P., Chen, J.P. and Hong, L., 2004, “Sorption of lead, copper, cadmium, zinc and nickel by marine algal biomass: characterization of biosorptive capacity and investigation of mechanisms”, *Journal of Colloid and Interface Science*, vol. 275, pp. 131-141.

Stanley, M., 2006, “Production, Properties and Uses of carrageenan”, Food and Agriculture organization of the United Nations.

Stirk, W.A. and Van Staden, J., 2000, 'Removal of Heavy Metals from solution using dried brown seaweed material', *Botanica Marina*, vol. 43, pp. 467-473.

Tabakci, M. and Yilmaz, M., 2008, “Sorption characteristics of Cu(II) ions onto silica gel-immobilized calix[4]arene polymer in aqueous solutions: Batch and column studies”, *Journal of Hazardous Materials*, vol. 151, pp. 331-338.

Umpleby, R.J., Baxter, S.C., Chen, Y., Shah, R.N. and Shimzu, K.D., 2001, “Characterization of molecularly imprinted polymers with the Langmuir-Freundlich isotherm”, *Analytical Chemistry*, vol. 73, pp. 4584-4591.

United Nations Environmental Programme, 1997, “Aluminium-International Health Criteria”, International Labour Organisation. World Health Organisation.

United States Environmental Protection Agency, 2008, "Resource Management & Recovery".

US Geological Surveys, 2008, "Statistics and Information".

Uzun, I. and Guzel, F. (2000) "Adsorption of some heavy metal ions from aqueous solution by activated carbon and comparison of percent adsorption results of activated carbon with those of some other adsorbents", *Turkish Journal of Chemistry*, vol. 24, pp. 291-297.

Vermeulen, T., Klein, G. and Heister, N.K., 1973, "Adsorption and ion exchange", *Chemical engineer's Handbook*, Mc Graw-Hill, New-York.

Vijayaraghavan, K., Jegan, J., Palanivelu, K. and Velan, M., 2005a, "Batch and column removal of copper from aqueous solution using a brown marine alga *Turbinaria ornate*", *Chemical Engineering Journal*, vol. 106, pp. 177-184.

Vijayaraghavan, K., Jegan, J., Palanivelu, K. and Velan, M.: 2005b, "Biosorption of cobalt(II) and nickel(II) by seaweeds: batch and column studies", *Separation and Purification methods*, vol. 44, pp. 53-59.

Vijayaraghavan, K., Palanivelu, K. and Velan, M., 2006, "Treatment of nickel containing electroplating effluents with *sargassum wightii* biomass", *Process Biochemistry*, pp. 853-859.

Volesky, B., 1990, "Biosorption of Heavy Metals", CRC Press.

Volesky, B., 2001a, "Detoxification of metal-bearing effluents: biosorption for the next century", *Hydrometallurgy*, vol. 59, pp. 203-216.

Volesky, B., 2004, "Sorptions and Biosorption", BV Sorbex, Inc., Montreal.

Volesky, B., 2001b, "Detoxification of metal-bearing effluents: biosorption for the next century", *Hydrometallurgy*, pp. 203-216.

Volesky, B. and Naja, G., 2007, "Biosorption technology: starting up an enterprise", *International Journal of Technology Transfer and Commercialisation*, vol. 6, pp. 196-211.

Volesky, B., Weber, J. and Park, J.M., 2003, "Continuous-flow metal biosorption in a regenerable *Sargassum* column", *Water Research*, vol. 37, pp. 297-306.

Walsh, R., 2008, "Development of a biosorption column utilising seaweed based biosorbents for the removal of metals from industrial waste streams", *PhD thesis*, Waterford Institute of Technology, Ireland.

Wang, X.S., Qin, Y. and Li, Z.F., 2006, "Biosorption of zinc from aqueous solutions by rice bran: kinetics and equilibrium studies", *Separation and Purification Science Technology*, pp. 747-756.

Wase, J. and Forster, C., 1997, "*Biosorbents for metal ions*", Taylor & Francis.

Yeoung-Sang, Y., 2004, "Characterization of functional groups of protonated *Sargassum polycystum* biomass capable of binding protons and metal ions", *Journal of Microbiology and Biotechnology*, vol. 14, pp. 29-34.

Yu, Q., Matheickal, J.T., Yin, P. and Kaewsarn, P., 1999, "Heavy metal uptake capacities of common marine macro algal biomass", *Water Research*, vol. 33, pp. 1534-1537.

Zeroyal, Y., Moutaouakkil, A., Dzairi, F.Z., Talbi, M., Chung, P.U., Lee, K. and Blaghen, M.: 2003, 'Biosorption of mercury from aqueous solution by *Ulva lactuca* biomass', *Bioresource technology*. **90**, 349-351.

Zhao, M., Duncan, J.R. and Van Hille, R.P., 1999, "Removal and recovery of Zinc from solution and electroplating effluent using *Azolla Filiculoides*", *Water Research*, vol. 33, pp. 1516-1522.

# **Appendix A**

**A. Bakir, P. McLoughlin, S.A.M. Tofail, E.  
Fitzgerald,**

*“Competitive sorption of antimony with zinc, nickel  
and aluminium in a seaweed-based fixed-bed  
sorption column”,*

**CLEAN 37 (9) (2009) 712-719**

Adil Bakir<sup>1</sup>  
Peter McLoughlin<sup>1</sup>  
Syed A. M. Tofail<sup>2</sup>  
Eddy Fitzgerald<sup>1</sup>

<sup>1</sup>Estuarine Research Group, Eco-Innovation Research Centre, Department of Chemical and Life Sciences, Waterford Institute of Technology, Waterford, Ireland.

<sup>2</sup>Materials and Surface Science Institute, University of Limerick, Limerick, Ireland.

## Research Article

# Competitive Sorption of Antimony with Zinc, Nickel, and Aluminum in a Seaweed Based Fixed-bed Sorption Column

The removal of heavy metals such as Ni(II), Zn(II), Al(III), and Sb(III) from aqueous metal solutions was investigated using novel, cost effective, seaweed derived sorbents. Studies with a laboratory scale fixed-bed sorption column, using a seaweed waste material (referred to as waste *Ascophyllum* product (WAP)) from the processing of *Ascophyllum nodosum* as biosorbent, demonstrated high removal efficiencies (RE) for a variety of heavy metals including Ni(II), Zn(II) and Al(III), with 90, 90 and 74% RE achieved from initial 10 mg/L metal solutions, respectively. The presence of Sb(III) in multi component metal solutions suppressed the removal of Ni(II), Zn(II) and Al(III), reducing the RE to 28, 17 and 24%, respectively. The use of *Polysiphonia lanosa* as a biosorbent showed a 67% RE for Sb(III), both alone and in combination with other metals. Potentiometric and conductometric titrations, X-ray photoelectron and mid-infrared spectroscopic analysis demonstrated that carboxyl, alcohol, sulfonate and ether groups were heavily involved in Sb(III) binding by *P. lanosa*. Only carboxyl and sulfonate groups were involved in Sb(III) binding by WAP. Furthermore, a greater amount of weak acidic groups (mainly carboxylic functions) were involved in Sb(III) binding by *P. lanosa*, compared to WAP which involved a greater concentration of strong acidic groups (mainly sulfonates).

**Keywords:** Antagonism; Antimony; Biosorption; Heavy metals; Seaweed

**Received:** July 29, 2009; **revised:** August 14, 2009; **accepted:** August 16, 2009

**DOI:** 10.1002/clean.200900164

## 1 Introduction

Contamination of water by heavy metals is a worldwide problem resulting from their widespread use in a wide range of industrial processes. There is a requirement to adopt environmentally friendly processes for metal removal from industrial effluents. Effective removal of metals known to be toxic, such as nickel, zinc, and aluminum from industrial effluents is of particular interest. The most important sources of these metals are from the electroplating, alloy manufacturing, and glass and crystal industries.

The accelerating depletion of natural metal ores has also increased the need for sequestering and recycling metals from industrial effluents. Biosorbents must display good regeneration properties and the potential for selective metal recovery for recycling purposes [1]. Among the wide choice of biomass types available, seaweed biosorbents have been shown to be among the most promising for heavy metal recovery [2, 3]. The utilization of sorbents in industrial fixed-bed sorption columns for the removal of a wide range of metals has been shown to be practically and economically viable due to its cost efficiency and high metal removal capacity [3].

In this study, a seaweed waste material from the industrial processing of *Ascophyllum nodosum* was investigated for metal removal efficiency using a pilot scale fixed-bed sorption column. The reuse of the waste material for the development of a novel biosorbent could be integrated into a new waste management scheme for the seaweed processing industry.

Most studies in the past have focused on the adsorption efficiencies and sorption isotherms of different metals combined in aqueous solutions [4–10]. However, only a limited amount of work has been carried out on the characterization of competitive metal biosorption by marine algae, specifically antagonistic and synergistic interactions [9, 11]. FTIR and XPS analysis have been used by a number of authors to gain an insight into biosorption phenomena, and to help in the development of potential biosorbents possessing high metal removal capacities [12]. Potentiometric and conductometric titrations have also been used in past studies for the quantification of the amount of binding sites on the surface of different biomasses, specifically seaweeds [12, 13].

The metal removal capacity of seaweeds has been mainly attributed to their fiber like structure, and the amorphous embedding matrix of various polysaccharides in their cell walls [12]. Several chemical groups, present on the surface of seaweeds, have been identified as contributing to metal binding. Such functional groups include hydroxyl, carboxyl, carbonyl, sulfonate, amide, and phosphonate groups [1–3], and their relative contribution to metal binding depends on many different factors such as the quantity of sites,

**Correspondence:** A. Bakir, Estuarine Research Group, Eco-Innovation Research Centre, Department of Chemical and Life Sciences, Waterford Institute of Technology, Cork Road, Waterford, Ireland.  
E-mail: abakir@wit.ie

**Abbreviations:** RE, Removal efficiency; WAP, Waste *Ascophyllum* product

their accessibility and the affinity between the site and the metal [14].

A key objective of this study was to investigate the efficiency of a seaweed waste material (WAP) and *P. lanosa* in the removal of Zn(II), Ni(II), Al(III), and Sb(III) in batch tests and also by utilizing a continuous flow fixed-bed sorption column. The antagonistic effects of Sb(III) on the removal efficiency of Zn(II), Ni(II), and Al(III) from combined metal aqueous solutions was also investigated, along with the identification of the binding functional groups present in both WAP and *P. lanosa*. The relative contribution of these functional groups to the binding of Sb(III) was also investigated using FTIR, potentiometric titrations and XPS analysis.

## 2 Materials and Methods

### 2.1 Biomass

*Polysiphonia lanosa* was harvested at Fethard on Sea, Co. Wexford, Ireland (52° 11' 53.68" N 6° 49' 34.64" W). The *P. lanosa* samples were rinsed thoroughly with distilled water, oven dried at 60°C for 12 h, and subsequently ground and sieved to a particle size of 500–850 µm. A seaweed waste material, resulting from the industrial processing of *Ascophyllum nodosum* (referred to as waste *Ascophyllum* product or WAP), was also investigated. This was supplied by Oilean Glas Teo (OGT) (Ballymoon Industrial Estate, Kilcar, Co. Donegal, Ireland). The waste material was dried at 60°C for 24 h, and subsequently ground and sieved to a particle size of 500–850 µm.

### 2.2 Metal Solutions

Standard metal solutions (analytical grade) containing 1000 mg/L Ni(II), Zn(II), Sb(III) and Al(III) (Sigma-Aldrich) were used. The pH of all prepared metal solutions was  $2.63 \pm 0.16$ . Metal concentrations were determined using an Inductively Coupled Plasma-Optical Emission Spectrometer equipped with an autosampler (Varian 710-ES ICP Optical Emission Spectrometer, ICP Expert II Software).

### 2.3 Metal Sorption Studies

#### 2.3.1 Batch Sorption Experiments

2 g of dried and ground *P. lanosa* and WAP were exposed separately to 200 mL of 10 mg/L single and combined (10 mg/L each) solutions of Ni(II), Zn(II), Sb(III), and Al(III). The suspension was agitated for 12 h at 180 rpm [13]. The biomass was removed by filtration under vacuum and the solution was analyzed using ICP-OES. Biomass free solutions and metal free solutions were used as controls.

#### 2.3.2 Fixed Bed Column Sorption Studies

##### 2.3.2.1 Biosorbent Preparation

Prior to utilization, the dried and ground biomass (WAP or *P. lanosa*) was immobilized in agar to produce blocks of homogeneous size ( $6 \times 10 \times 15$  mm). 10 g of agar was mixed with 15 g of biomass in a conical flask and 200 mL of distilled water was added. The mixture was homogenized and the flask was autoclaved for 20 min. The mixture was transferred into small trays and left to cool and solidify for 15 min. The solid blocks were then dried at 60°C for 24 h. The dried blocks were then soaked in distilled water for 2 h for expansion. The fixed-bed sorption columns (refer to Section 2.3.2.2) were then filled

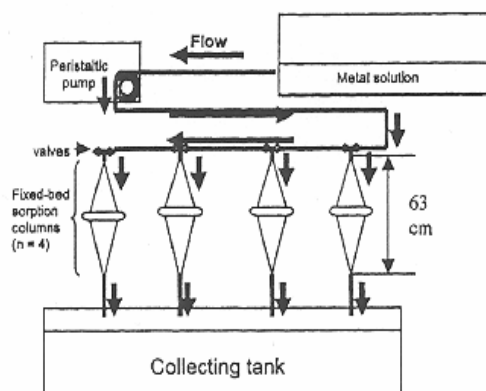


Figure 1. Setup of laboratory scale fixed-bed sorption columns.

with the agar/biomass blocks. During runs, a flow rate of 25 mL/min through the columns was employed. The effluent was sampled every 2 min for the first 10 min, during which most of the sorption takes place [15]; and thereafter every 15 min until the end of the experiment (3 h). For each experiment, four fixed-bed sorption columns were run in parallel (see Fig. 1).

##### 2.3.2.2 Column Design

A laboratory scale biosorption system was set up as shown in Fig. 1 [15]. For each column the total bed length was  $22.9 \pm 0.3$  cm, with an inner diameter (ID) of 7.2 cm and a working volume of 638 mL. The metal solution was transported by a peristaltic pump through silicon tubing to each column using upper valves to regulate the flow rate. The metal solution was loaded onto each column and treated samples of the single and combined metal solutions were collected and analyzed for metal concentration using ICP-OES.

### 2.4 Fourier Transform Infra Red Spectroscopy (FTIR)

#### 2.4.1 FTIR Analysis of Biomass

Protonated biomass was used as the biosorbent control during FTIR analysis. Protonated biomass (at a concentration of 1.0 g/L) was exposed to a 10 mg/L solution of Sb(III) over a 6 h period. Exposed biomass was removed from the metal solution by filtration under vacuum and analyzed directly using a Digilab Scimitar Series infra-red spectrometer (MIRacle™ Single Reflection HATR diamond accessory). A background scan was run before each analysis. Triplicate samples were analyzed over 40 scans at a resolution of  $4 \text{ cm}^{-1}$  [13].

### 2.5 Potentiometric and Conductometric Titrations

#### 2.5.1 Titration of Protonated Biomass

For each titration, 200 mg of protonated biomass was dispersed in 100 mL of 1 mM NaCl solution. The titration was carried out by the stepwise addition of 0.25 mL of 0.1 M NaOH (prepared with boiled distilled water) to the flask while the suspension was stirred under a nitrogen atmosphere (Glove Box Model 818-GB/220, Plas Labs, Inc.). Conductivity was measured using a WTW LF 538 Conductivity Meter with a WTW TetraCon1 325 probe. pH measurements were recorded

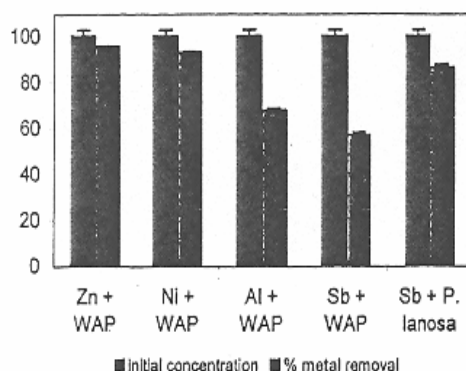


Figure 2. Mean removal efficiencies (RE) in% for Zn(II), Ni(II), Al(III), and Sb(III) by WAP and *P. lanosa* from 10 mg/L single metal solutions in batch sorption experiments. Error bars were calculated based on four replicates with 95% confidence intervals.

using a Mettler Toledo Inlab1 413 pH electrode. Potentiometric titrations were carried out in triplicate while conductometric titrations were carried out singly to act as verification for the potentiometric titration results [13].

### 2.5.2 Titration of Metal Bound Biomass

100 mg of protonated WAP and *P. lanosa* were exposed to 50 mL of 10 mg/L Sb(III). Experiments were carried out in triplicate. Flasks were shaken at 180 rpm for 12 h at room temperature ( $21 \pm 1^\circ\text{C}$ ). The biomass was then filtered under vacuum and oven dried for 24 h. Titration of the biomass was carried out as described in Section 2.5.1.

## 2.6 X-ray Photoelectron Spectroscopy (XPS)

Raw *P. lanosa* samples and wet WAP were oven dried at  $60^\circ\text{C}$  for 24 h and subsequently exposed to solutions containing 1000 and 2000 mg/L Sb(III). The use of elevated metal concentrations ensured detection by the XPS techniques. The biomass was added at a concentration of 2 mg/mL to each solution. The flasks were agitated at 180 rpm at room temperature ( $21 \pm 1^\circ\text{C}$ ) for 6 h. The biomass was then filtered under vacuum and washed thoroughly with distilled water. Samples were dried at  $60^\circ\text{C}$  for 24 h and analyzed using X-ray photoelectron spectroscopy (Kratos Axis 165).

The functional groups present were identified by the binding energy of C, and the relative abundance of elements (C, O, N, S, Sb) was determined before and after exposure to metals [12].

## 3 Results and Discussion

### 3.1 Batch Sorption Experiments

The removal efficiency (RE in %) of metals by WAP is shown in Fig. 2 and was calculated according to the following equation:

$$\text{RE} = 10 (C_i - C_f) \quad (1)$$

where  $C_i$  and  $C_f$  are the initial and final metal concentrations (mg/L). The REs were 96, 93, 68 and 57% for Zn(II), Ni(II), Al(III), and Sb(III), respectively.

Table 1. Uptake capacities ( $q$ ) in mg/g by WAP and *P. lanosa* for Zn, Ni, Al, and Sb.

Metal	$q$ (mg/g)	
	WAP	<i>Polysiphonia lanosa</i>
Zn	$1.92 \pm 0.01$	$0.96 \pm 0.01$
Ni	$1.86 \pm 0.01$	$1.30 \pm 0.02$
Al	$1.35 \pm 0.03$	$1.11 \pm 0.04$
Sb	$1.14 \pm 0.02$	$1.73 \pm 0.01$

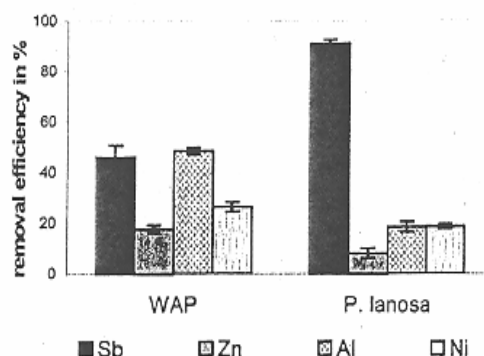


Figure 3. Mean removal efficiencies (RE) in% for Sb(III), Al(III), Ni(II), and Zn(II) by WAP and *P. lanosa* starting with 10 mg/L combined metal solutions (10 mg/L each). Error bars were calculated based on four replicates with 95% confidence intervals.

### 3.2 Metal Uptake ( $q$ ) Values

Metal uptake  $q$  (mg/g) was calculated according to the following equation [1, 3]:

$$q = (V(C_i - C_f))/S \quad (2)$$

where  $V$  is the volume of the metal solution (mL),  $C_i$  and  $C_f$  are the initial and final metal concentrations (mg/L) and  $S$  is the mass of the biomass (g).

Table 1 shows the uptake capacities ( $q$ ) for Zn(II), Ni(II), Al(III), and Sb(III) by WAP. The highest  $q$  values resulted from the uptake of Zn(II) and Ni(II), whilst the lowest  $q$  value was for Sb(III) uptake. In contrast, the highest  $q$  value for *P. lanosa* was for Sb(III) uptake. The high metal uptake values obtained for WAP are a direct result of the industrial extraction process, with the purification of the sorbing components by elimination of the nonsorbing polyphenols [16].

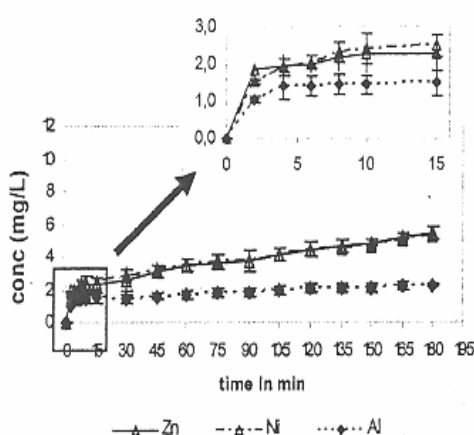
As shown in Tab. 2 and Fig. 3, Sb(III), when combined with Ni(II), Zn(II), and Al(III), reduced the capacity of WAP for binding other metals. This suggests an antagonistic effect of Sb(III) on the sorption of Ni(II), Zn(II) and Al(III) by the WAP biomass.

### 3.3 Fixed-bed Sorption Column Studies for Mixed Metals

Figure 4 shows the resulting concentrations of Ni(II), Zn(II), and Al(III) after treatment using the fixed-bed sorption column over 3 h. The mean removal efficiencies over 3 h are shown in Tab. 3 and were calculated using Eq. (1). Very high RE values were recorded in

**Table 2.** Uptake capacities ( $q$ ) in mg/g for WAP and *P. lanosa* for Zn, Ni, Al, and Sb in combined metal solutions.

Combined metals	$q$ (mg/g)							
	WAP				<i>Polysiphonia lanosa</i>			
Zn/Ni	Zn		Ni		Zn		Ni	
	1.77 ± 0.04		1.74 ± 0.01		0.82 ± 0.02		0.91 ± 0.01	
Zn/Sb	Zn		Sb		Zn		Sb	
	0.61 ± 0.02		0.85 ± 0.02		0.32 ± 0.03		1.80 ± 0.01	
Ni/Sb	Ni		Sb		Ni		Sb	
	0.71 ± 0.02		0.67 ± 0.01		0.49 ± 0.02		1.76 ± 0.02	
Ni/Zn/Al/Sb	Ni	Zn	Al	Sb	Ni	Zn	Al	Sb
	0.53 ± 0.04	0.35 ± 0.03	0.97 ± 0.03	0.92 ± 0.09	0.37 ± 0.02	0.16 ± 0.04	0.37 ± 0.04	1.82 ± 0.03

**Figure 4.** Mean concentrations of Al(III), Ni(II), and Zn(II) in the effluent over 3 h from a fixed-bed sorption column containing WAP, starting with 10 mg/L combined metal solutions (10 mg/L each). Error bars were calculated based on four replicates with 95% confidence intervals.

the case of WAP for Ni(II), Zn(II), and Al(III) in single metal solutions of 90% for both Ni and Zn, and 74% for Al. The mean RE was 72, 75, and 87% for Ni(II), Zn(II), and Al(III), respectively, when combined in the same metal solution (see Fig. 5). The WAP/agar blocks demonstrated poor removal of Sb(III) at only 28% RE. However, *P. lanosa* immobilized in agar removed 67% of the Sb(III) over a 3 h period (see Tab. 3 and Fig. 6). When Sb(III) was combined with the other metals, the RE was reduced to 28, 17 and 24% for Ni(II), Zn(II), and Al(III), respectively (see Tab. 3 and Fig. 5). This indicates an antagonistic effect. Metal antagonism has been observed by a number of authors for other metals [9, 11], but not for Sb(III).

### 3.4 Fourier Transform Infra Red Spectroscopy

#### 3.4.1 FTIR Analysis of Biomass

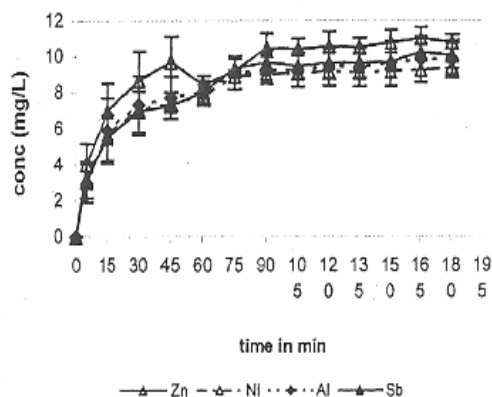
The assignment of FTIR bands and wavenumber shifts of the protonated biomass and Sb(III) loaded biomasses are summarized in Tab. 4. Good repeatability was observed for all replicate scans, with any differences seen being three wavenumbers or less.

FTIR results revealed that sulfonate groups contributed to Sb(III) binding on both WAP and *P. lanosa*. At the working pH of  $2.63 \pm 0.16$ , sulfonate groups are dissociated (pK<sub>a</sub> value of 1–2.5). It was reported by Figueira et al. [17] that sulfonate groups are responsible for the uptake of trivalent metal cations by *Sargassum* biomass. Binding

**Table 3.** Mean % removal efficiencies (RE) over 3 h after treatment using the fixed-bed sorption column.

Metal	Mean % RE	
	WAP/Agar	<i>P. lanosa</i> /Agar
Ni	90	na <sup>a)</sup>
Zn	90	na <sup>a)</sup>
Al	74	na <sup>a)</sup>
Sb	28	67
Ni/Zn/Al	72/75/87	na <sup>a)</sup>
Ni/Zn/Al/Sb	28/17/24/16	na <sup>a)</sup>

<sup>a)</sup> na = not assessed

**Figure 5.** Mean concentrations of Al(III), Ni(II), Zn(II), and Sb(III) in the effluent over 3 h from a fixed-bed sorption column containing WAP, starting with 10 mg/L combined metal solutions (10 mg/L each). Error bars were calculated based on four replicates with 95% confidence intervals.

resulted in a small band shift for asymmetric  $\text{-SO}_2$  in the case of both WAP ( $1359\text{--}1354\text{ cm}^{-1}$ ) and *P. lanosa* ( $1370\text{--}1365\text{ cm}^{-1}$ ). A large wavenumber decrease ( $1160\text{--}1145\text{ cm}^{-1}$ ) was observed for the symmetric  $\text{-SO}_2$  bond in the case of WAP only. No band shift for symmetric  $\text{-SO}_2$  was observed for *P. lanosa* exposed to Sb(III). No shifts were observed for the C-O (alcohol) bands in the  $1033\text{ cm}^{-1}$  region for either WAP or *P. lanosa*. Carboxyl groups were also involved in Sb(III) binding as demonstrated by a decrease in wavenumbers for both WAP ( $1239\text{--}1203\text{ cm}^{-1}$ ) and *P. lanosa* ( $1217\text{--}1213\text{ cm}^{-1}$ ). Murphy et al. [18] reported that the binding of Cu to both *P. lanosa* and *P. palmata* involved the participation of carboxyl and sulfonate functionalities, and this appears to be the case for Sb(III). No amino interac-

**Table 4.** Stretching frequencies for Sb(III) loaded WAP and *P. lanosa*. Wavenumbers obtained for protonated biomass controls are shown in parentheses. Number of scans = 40, resolution = 4 cm<sup>-1</sup>. Average values from triplicate runs are shown.

	Wavenumber (cm <sup>-1</sup> )	
	WAP	<i>Polysiphonia lanosa</i>
-OH (bonded), -NH (stretching)	3337 (3228)	3284 (3293)
-CH (asymmetric)	2921 (2926)	2972 (2943)
Free C=O	1726 (1731)	1714 (1718)
C=O (asymmetric)	1621 (1622)	1642 (1643)
Amide II	1512 (1512)	1521 (1520)
C=O (symmetric)	1450 (1449)	1449 (1447)
-SO <sub>3</sub> (asymmetric)	1354 (1359)	1370 (1365)
C-O (carboxyl)	1203 (1239)	1213 (1217)
-SO <sub>3</sub> (symmetric)	1145 (1160)	1157 (1156)
C-O (ether)	<sup>a)</sup>	<sup>a)</sup>
C-O (alcohol)	1032 (1030)	1028 (1028)

<sup>a)</sup> Band not observed.

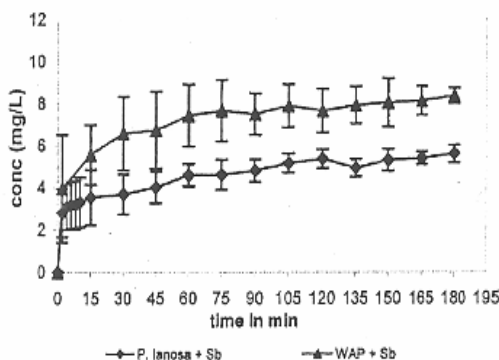


**Figure 6.** Mean concentrations of Sb(III) in the effluent over 3 h from a fixed-bed sorption column containing *P. lanosa* or WAP, starting with a 10 mg/L Sb(III) solution. Error bars were calculated based on four replicates with 95% confidence intervals.

tion was evident for either biomass with no band shifting apparent in the 1530 cm<sup>-1</sup> area.

In this study, the binding of Sb(III) by both WAP and *P. lanosa* indicated a significant contribution by both carboxyl and sulfonate groups.

### 3.5 Potentiometric and Conductometric Titrations

First derivative plots resulting from the addition of NaOH are shown in Figs. 7a and 7b. The number of strong acidic groups was determined from the first peaks in Figs. 7a (0.88 and 0.42 mmol/g for WAP and *P. lanosa*, respectively), while the total number of acidic groups was determined from the final peaks (3.63 and 1.71 mmol/g for WAP and *P. lanosa*, respectively).

The corresponding pK<sub>a</sub> values were calculated by identifying the inflection point of the titration curves. However, a more accurate indication of the position of these inflections is obtained from first derivative plots of average pH titration numerical data [13]. The pK<sub>a</sub> values and the number of acidic groups on the biomass surface are summarized in Tab. 5.

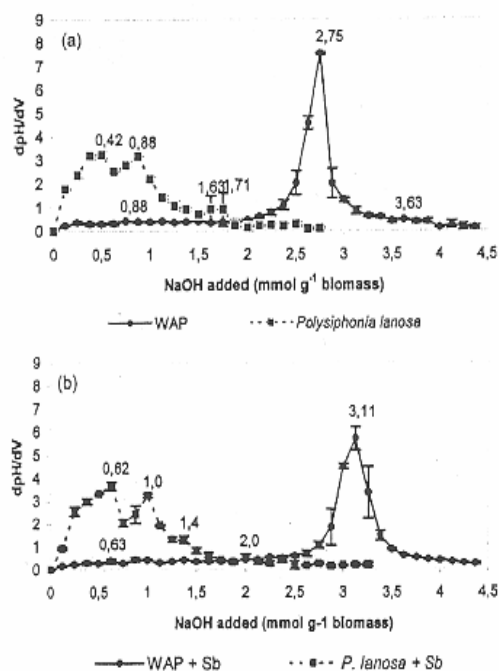


**Figure 7.** First derivative plots of average pH titration data for, (a) protonated WAP and *P. lanosa*, and (b) Sb(III) exposed WAP and *P. lanosa*. Error bars were calculated based on triplicate runs with 95% confidence intervals.

The first derivative plots consist of the midpoint of successive amounts of NaOH added (x axis) versus dPH/dV (y axis), permitting a direct reading of the various peaks obtained. Reading the location of each peak on the x axis gives the number of acidic groups on the seaweed surface [15]. It was shown that protonated WAP, not exposed to a metal (see Fig. 7a), contained a larger amount of total acidic groups (3.63 mmol/g) compared to *P. lanosa* (1.71 mmol/g). The large amount of acidic groups is the direct result of the processing of *Ascophyllum nodosum* with the purification of the sorbing components by elimination of nonsorbing polyphenols [16].

The results for *P. lanosa* were in agreement with Murphy et al. [18] who obtained a total acidic group content of 1.81 mmol/g for *P. lanosa*. Four distinct pK<sub>a</sub> peaks were recorded for *P. lanosa* as opposed to a single one for WAP. The first pK<sub>a</sub> recorded for Sb(III) laden *P. lanosa* was very close to the values reported for mannuronic and guluronic acids with values of 3.38 and 3.65, respectively [19]. For protonated *P. lanosa* the first pK<sub>a</sub> gave a slightly higher value of 4.47, probably due to configurational differences [19]. It was also reported that the interaction between cations in solution and algal biomass may be attributed to the carboxyl groups of the alginic molecule at near neutral conditions; alginic acid being the principal structural polysaccharide in brown algae [19]. This was probably the case for WAP with a single pK<sub>a</sub> peak at around 6.25–6.46. It was also reported that algal proteins have been known to interact with metal ions, particularly between pH 6–9 [20].

The large amount of acidic groups on WAP and the pK<sub>a</sub> values close to neutrality are the most likely reason for its high metal removal capacity. However, there still remains the anomaly of the low affinity for Sb(III). The titration of the Sb(III) bound biomass (see

**Table 5.**  $pK_a$  values and quantity of acidic groups. Error bars were calculated based on triplicate runs with 95% confidence intervals.

Biomass	$pK_a$ values $\pm$ 95% CI	No. of acidic groups on the biomass surface (mmol/g)		
		Total	Strong	Weak
Protonated WAP	6.25 $\pm$ 0.34	3.63	0.88	2.75
Sb(III) laden WAP	6.46 $\pm$ 0.57	3.11	0.45	2.66
Protonated <i>Polysiphonia lanosa</i>	4.47 $\pm$ 0.04	1.71	0.42	1.29
	7.43 $\pm$ 0.03			
	9.88 $\pm$ 0.06			
	10.36 $\pm$ 0.05			
Sb(III) laden <i>Polysiphonia lanosa</i>	3.63 $\pm$ 0.17	0.62	0.28	0.34
	6.36 $\pm$ 0.03			
	10.28 $\pm$ 0.19			
	10.67 $\pm$ 0.04			

Fig. 7b)) indicated that weak acidic groups present on the surface of *P. lanosa* had a greater role in Sb(III) binding compared with WAP (see Tab. 5). A reduction in the number of available acidic sites in metal loaded biomass was recorded for both WAP and *P. lanosa* (see Tab. 5). For the Sb(III) loaded WAP, a reduction from 3.63 to 3.11 mmol/g was recorded, of which 0.43 mmol/g was attributed to the strong acidic groups. For the Sb(III) loaded *P. lanosa*, a reduction from 1.71 to 0.62 mmol/g was recorded, of which 0.95 mmol/g was attributed to the weak acidic groups.

Decreases in the quantity of strong and weak acidic groups indicate that both sulfonate and carboxyl groups participated in the binding of Sb(III) by the two biomasses [20, 21]. This results from the dissociation of sulfonate groups at pH 2, and it has been previously postulated by Figueira et al. [17] that seaweed sulfonate groups are responsible for the uptake of trivalent metal cations such as Sb(III). This finding was in agreement with the FTIR analysis where sulfonates and carboxyl groups were shown to be the principal functionalities involved in the binding of Sb(III) by both WAP and *P. lanosa*.

The difference in the binding mechanism of Sb(III) by the two biomasses appears to be due to the relative amounts of weak and strong acidic groups involved. Weak acidic groups were mainly involved in Sb(III) binding by *P. lanosa*, suggesting more important involvement of the carboxyl groups (see Tab. 5). WAP, on the other hand, demonstrated lesser participation of the carboxyl groups and greater utilization of the strong acidic groups (corresponding to the sulfonate groups). Such variation in the involvement of carboxyl groups for binding metals by different biomasses has been demonstrated by Fourest et al. [16] for the uptake of Zn using four macroalgal species. They also concluded that this variation depends on the carrier polymer, the environment of the function as well as the presence of other complexing groups in the biosorbent.

### 3.6 X-ray Photoelectron Spectroscopy

X-ray photoelectron spectroscopy (XPS) has been widely used to characterize the sorption sites involved in the accumulation of metals, as well as the chemical speciation of the metals sorbed by a biosorbent [16]. In this study, XPS was employed to investigate the changes in binding energy (BE) of the coordination atoms (C-C, C-O, C=O, RCOO) in the biomass of both WAP and *P. lanosa* before and after exposure to Sb(III) [20]. XPS analysis was also employed as a verification of the results obtained in the potentiometric titrations and FTIR analysis. Furthermore, XPS provides superior surface composition results due to the greater surface sensitivity of the technique

**Table 6.** XPS atomic concentration (in percentage) of the relevant chemical elements in (a) *P. lanosa* and (b) WAP before and after exposure to Sb(III) ions at two different concentrations (1000 and 2000 mg/L).

(a)	Atomic concentration (%)		
	<i>P. lanosa</i> (raw)	<i>P. lanosa</i> 1000 mg/L Sb(III)	<i>P. lanosa</i> 2000 mg/L Sb(III)
Element			
C 1s	65.71	70.70	68.10
O 1s	27.44	22.35	25.51
N 1s	4.12	6.67	5.72
S 2p	2.73	ND <sup>1</sup>	ND <sup>1</sup>
Sb 3d <sub>3/2</sub>	ND <sup>1</sup>	0.28	0.67

(b)	Atomic concentration (%)		
	WAP (raw)	WAP 1000 mg/L Sb(III)	WAP 2000 mg/L Sb(III)
Element			
C 1s	80.73	84.37	85.19
O 1s	18.28	15.63	14.75
N 1s	ND <sup>1</sup>	ND <sup>1</sup>	ND <sup>1</sup>
S 2p	0.99	ND <sup>1</sup>	ND <sup>1</sup>
Sb 3d <sub>3/2</sub>	ND <sup>1</sup>	ND <sup>1</sup>	0.06

<sup>1</sup> ND = not detected

[22]. XPS results are presented in Tabs. 6 and 7 and spectra are summarized in Fig. 8.

A higher proportion of the element oxygen (O) was found for *P. lanosa* compared to WAP (see Tabs. 6a and 6b). This was expected given the large amount of cell polysaccharides present on the seaweed cell surface. Nitrogen was detected in the case of *P. lanosa* but not for WAP. The higher amount of nitrogen in *P. lanosa* was due to surface proteins in *P. lanosa*. Sulfur was observed in for both raw WAP and *P. lanosa*. However, when treated with Sb(III), no sulfur was detected for either biomass at both metal concentrations. XPS analysis also showed that sulfur was mainly in a bi-polaronic form as the binding energy was similar to  $SO_4$  binding energy. As most of the Sb(III) peaks overlapped during analysis of *P. lanosa*, only the Sb 3d<sub>3/2</sub> was suitable for analysis.

It is clear from Tab. 6 that higher concentrations of Sb(III) were associated with the surface of *P. lanosa* after exposure to the metal compared with WAP. The atomic concentrations detected for *P. lanosa* were also higher for higher Sb(III) concentrations used (0.67 versus 0.28%).

**Table 7.** Carbon 1s binding energies and peak ratios for *Polysiphonia lanosa* and WAP.

Biomass	Assignment of C1s peak	Peak (eV)	Peak Area Ratio (%)		
			Raw	1000 mg/L Sb (III) loaded	2000 mg/L Sb (III) loaded
<i>Polysiphonia lanosa</i>	C-C	284.91	31.72	54.57	54.70
	C-O	286.37	46.44	29.23	30.13
	C=O	287.72	15.45	11.40	11.24
	RCOO	288.85	6.39	4.80	3.94
WAP	C-C	285.02	69.79	74.74	74.43
	C-O	286.55	21.80	15.15	11.83
	C=O	288.05	5.03	5.26	9.04
	RCOO	289.22	3.38	4.85	4.71

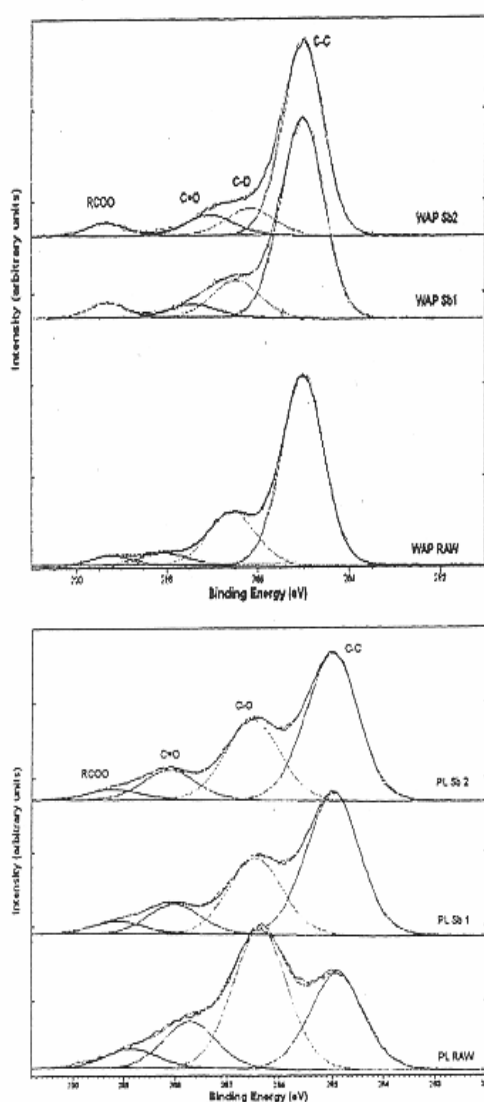


**Figure 8.** XPS C 1s spectra (intensity against binding energy). (a) Raw WAP and Sb(III) loaded WAP (WAP Sb1 = 1000 mg/L; WAP Sb2 = 2000 mg/L). (b) Raw *P. lanosa* and Sb(III) loaded *P. lanosa* (PL Sb1 = 1000 mg/L; PL Sb2 = 2000 mg/L).

Four peaks were identified after deconvolution of the C 1s spectra of all samples (see Fig. 8). The peak with the binding energy of 284.91 eV is attributed to C-C bonding and these hydrocarbon functionalities are used for energy calibration of the instrument. The remaining peaks can be assigned to the alcohol (C-O), ether (C=O), and carboxylic (RCOO) groups with BE of 286.37, 287.72 and 288.85 eV, respectively [23]. The area distribution of the four peaks indicated that alcohol groups are dominant in the two different biomasses (see Tab. 7). The area of the carboxyl peak decreased after Sb(III) binding to *P. lanosa* indicating that the formation of carboxyl-metal complexes had taken place (see Fig. 8). The formation of carboxyl-metal complexes, however, was not seen when exposing WAP to Sb(III) and the slight increases may have been due to potential surface contamination during exposure [24].

For *P. lanosa* exposed to Sb(III), the formation of alcohol and ether-metal complexes was also observed. For WAP, a slight reduction in one of the peak area ratios for alcohol alone was observed. This confirms that more diverse functional groups were involved in Sb(III) binding by *P. lanosa* (carboxyl, alcohol and ether) compared to WAP (alcohol groups only) as demonstrated by FTIR. XPS data also showed that a greater amount of carboxyl groups were involved in Sb(III) binding by *P. lanosa* as opposed to WAP as previously demonstrated with the potentiometric and conductometric titrations.

The high affinity of Sb(III) for *P. lanosa* was found to be a direct result of the diversity and quantity of the functional groups present on the surface of the biomass. Sb(III) bound mainly on the surface of *P. lanosa* through the involvement of sulfonate, carboxyl, alcohol, and ether groups. The antagonistic effect of Sb(III) for the sorption of Zn(II), Ni(II), and Al(III) was due to the fact that Sb(III) has a greater affinity for those binding sites, reducing the number of binding sites available to the other metals. It was noted by Wase and Foster [25] that carboxylate polysaccharides exhibit preferential binding of cations with large ionic radii. As *P. lanosa* was shown to contain a larger amount of carboxyl groups by potentiometric titration and XPS analysis, the large ionic radius of Sb(III) (0.90 Å) may be a contributory factor to the high affinity between the metal and the biomass. The extent of inhibition of Ni(II) and Zn(II) sorption may be due to their smaller ionic radii (0.88 and 0.83 Å, respectively) [26, 27].

#### 4 Conclusions

A seaweed (*Polysiphonia lanosa*) and an industrial seaweed waste material from the processing of *Ascophyllum nodosum* (WAP) were investigated for the removal of Zn(II), Ni(II), Al(III), and Sb(III) from single

and combined metal solutions. WAP was shown to be very efficient in the removal of Zn(II), Ni(II), and Al(III) in both single and combined solutions. However, *P. lanosa* was found to be more efficient for the removal of Sb(III). When combined with other metals, Sb(III) reduced the removal capacity of these other metals by WAP. The antagonistic effect of Sb(III) on the sorption of Ni(II), Zn(II), and Al(III) was investigated further using FTIR, potentiometric titrations and XPS analysis.

FTIR analysis strongly suggested that both carboxyl and sulfonate groups were involved in Sb(III) binding by both *P. lanosa* and WAP. Quantification of the acidic groups by potentiometric titrations further showed that a greater amount of weak acidic groups (mostly carboxylic functions) were utilized in metal binding by *P. lanosa* when compared with WAP, which demonstrated greater involvement of the sulfonate groups. These results were confirmed by XPS analysis, with the participation of carboxyl, alcohol, and ether groups in Sb(III) binding by *P. lanosa*, as opposed to WAP which displayed only carboxyl and sulfonate group involvement. A possible explanation for the antagonistic effect of Sb(III) on the sorption of the other metal species is the impact of atomic size. Sb(III) was also found to bind to a larger and more diversified number of binding sites, disrupting the uptake of Zn(II), Ni(II), and Al(III) onto both *P. lanosa* and WAP.

Finally, this study showed that the complementary use of FTIR, XPS, and potentiometric titrations is a highly effective tool for the investigation of metal sorption behavior onto biomass.

The authors gratefully acknowledge the support of the Irish Environmental Protection Agency for funding the project under the Masters and Doctoral Scholarship Scheme 2006. The authors also wish to acknowledge Oilean Glas Teo (OGT) for supplying the Waste Ascophyllum Product.

The authors have declared no conflict of interest.

## References

- [1] B. Volesky, *Biosorption of Heavy Metals*, CRC Press, Boca Raton, FL 1990.
- [2] E. Fourest, A. Serre, J. C. Roux, Contribution of Carboxyl Groups to Heavy Metal Binding Sites in Fungal Wall, *Toxicol. Environ. Chem.* 1996, 54, 1–10.
- [3] B. Volesky, *Sorption and Biosorption*, BV Sorbex Inc., Montreal, Canada 2003.
- [4] G. Naja, B. Volesky, Multi-metal Biosorption in a Fixed-bed Flow-through Column, *Colloids Surf., A* 2006, 281, 194–201.
- [5] A. C. A. Da Costa, F. P. De França, Biosorption of Zinc, Cadmium and Copper by a Brown Seaweed (*Sargassum* sp.) in a Continuous Fixed-bed Laboratory Reactor, *Bioseparation* 1997, 6, 335–341.
- [6] Z. R. Holan, B. Volesky, Biosorption of Lead and Nickel by Biomass of Marine Algae, *Biotechnol. Bioeng.* 1994, 43, 1001–1009.
- [7] Y. Sag, Biosorption of Heavy Metals by Fungal Biomass and Modeling of Fungal Biosorption: A Review, *Sep. Purif. Rev.* 2001, 30, 1–48.
- [8] M. R. Fagundes-Klen et al., Equilibrium of the Binary Mixture of Cadmium-zinc Ions Biosorption by the *Sargassum filipendula* Species Using Adsorption Isotherms Models and Neural Network, *Biochem. Eng. J.* 2007, 34, 136–146.
- [9] F. A. A. Al-Rub, M. H. El-Naas, I. Ashour, M. Al-Marzouqi, Biosorption of Copper on *Chlorella vulgaris* from Single, Binary and Ternary Metal Aqueous Solutions, *Process Biochem.* 2006, 41, 457–464.
- [10] S. Schiewer, B. Volesky, Modeling Multi-metal Ion Exchange in Biosorption, *Environ. Sci. Technol.* 1996, 30, 2921–2927.
- [11] S. Andrade, M. H. Medina, J. W. Moffet, J. A. Correa, Cadmium-copper Antagonism in Seaweed Inhabiting Coastal Areas Affected by Copper Mine waste Disposals, *Environ. Sci. Technol.* 2006, 40, 4382–4387.
- [12] P. X. Sheng, Y. P. Ting, J. P. Chen, L. Hong, Sorption of Lead, Copper, Cadmium, Zinc and Nickel by Marine Algal Biomass: Characterization of Biosorptive Capacity and Investigation of Mechanisms, *J. Colloid Interface Sci.* 2004, 275, 131–141.
- [13] V. Murphy, H. Hughes, P. McLoughlin, Comparative Study of Chromium Sorption by Red, Green and Brown Macroalgae, *Chemosphere* 2008, 70, 1128–1134.
- [14] K. I. Draget, O. Smidsrød, G. Skjåk-Bræk, in *Alginates from Algae in Polysaccharides and Polyamides in the Food Industry: Properties, Production, and Patents* (Eds.: A. Steinbüchel, S. K. Rhee), Wiley-VCH, Weinheim 2005.
- [15] R. Walsh, Development of a Biosorption Column Utilizing Seaweed Based Biosorbents for the Removal of Metals from Industrial Waste Streams, *PhD Thesis*, Waterford Institute of Technology, Ireland 2008.
- [16] E. Fourest, B. Volesky, Contribution of Sulfonate Groups and Alginate to Heavy Metal Biosorption by the Dry Biomass of *Sargassum fluitans*, *Environ. Sci. Tech.* 1996, 30, 49–58.
- [17] M. M. Figueira, B. Volesky, H. J. Mathieu, Instrumental Analysis Study of Iron Species Biosorption by *Sargassum* Biomass, *Environ. Sci. Tech.* 1999, 33, 1840–1846.
- [18] V. Murphy, H. Hughes, P. McLoughlin, Cu(II) Binding by Dried Biomass of Red, Green and Brown Macroalgae, *Water Res.* 2007, 41, 731–740.
- [19] E. Percival, R. H. McDowell, *Chemistry and Enzymology of Marine Algal Polysaccharides*, Academic Press, London 1967.
- [20] V. Murphy, An Investigation into the Uptake and Mechanism of Heavy Metal Binding in Selected Seaweed Species, *PhD Thesis*, Waterford Institute of Technology, Ireland 2007.
- [21] D. Kratochvil, B. Volesky, Multicomponent Biosorption in Fixed Beds, *Water Res.* 2000, 34, 3186–3196.
- [22] A. S. Sarac et al., Surface Characterization of Electrografted Random Poly[Carbazole-co-3-methylthiophene] Copolymers on Carbon Fiber: XPS, AFM and Raman Spectroscopy, *Appl. Surf. Sci.* 2004, 222, 148–165.
- [23] J. P. Chen, L. A. Hong, S. N. Wang, L. Wang, Elucidation of Interactions Between Metal Ions and Ca Alginate-based Ion-exchange Resin By Spectroscopic Analysis and Modeling Simulation, *Langmuir* 2002, 18, 9413–9421.
- [24] L. Dambies, C. Guilmon, S. Yiacoumi, B. Guibal, Characterization of Metal Ions Interactions with Chitosan by X-ray Photoelectron Spectroscopy, *Colloids Surf., A* 2001, 203–214.
- [25] J. Wase, C. F. Foster, *Biosorbents for Metal Ions*, CRC Press, Boca Raton, FL 1997.
- [26] F. A. Cotton, G. Wilkinson, P. L. Gaus, *Basic Inorganic Chemistry*, 3rd ed., John Wiley & Sons, New York 1995.
- [27] P. Sar, S. K. Kazy, R. K. Asthana, S. P. Singh, Metal Adsorption and Desorption by Lyophilized *Pseudomonas aeruginosa*, *Int. Biodeterior. Biodegrad.* 1999, 44, 101–110.

# **Appendix B**

**A. Bakir, P. McLoughlin, E. Fitzgerald,**  
*“Regeneration and reuse of a seaweed-based  
biosorbent in single and multi-metal systems”*,  
**CLEAN 38 (3) (2010) 257-262**

Adli Bakir<sup>1</sup>  
Peter McLoughlin<sup>1</sup>  
Eddy Fitzgerald<sup>1</sup>

<sup>1</sup>Estuarine Research Group, Eco-Innovation Research Centre, Department of Chemical and Life Sciences, Waterford Institute of Technology, Ireland.

## Research Article

# Regeneration and Reuse of a Seaweed-Based Biosorbent in Single and Multi-Metal Systems

A seaweed-waste material resulting from the processing of *Ascophyllum nodosum* was previously shown to be very efficient at removing Zn(II), Ni(II) and Al(III) both in single and multi-metal waste streams. In this study, the regeneration of the biosorbent using an acid wash resulted in the release of high metal concentrations during multiple desorption cycles. Maximum desorption efficiencies (DE) of 183, 122 and 91% were achieved for Zn(II), Ni(II) and Al(III), respectively, for subsequent metal loading cycles, significantly exceeding the desorption rates observed for conventional sorbents. The regeneration of the sorbent was accomplished with very little loss in metal removal efficiency (RE) for both single and multi-metal systems. Values of 92, 96 and 94% RE were achieved for Zn(II), Ni(II) and Al(III), respectively, for the 5<sup>th</sup> sorption cycle in single metal aqueous solutions. A slight decrease was observed for the same metals in multi-metal systems with maximum REs of 85, 82 and 82% for Zn(II), Ni(II) and Al(III), respectively. This study showed that the novel sorbent derived from a seaweed industrial waste would be suitable for multiple metal sorption cycles without any significant loss in RE.

**Keywords:** Biosorption; Heavy metals; Recovery; Regeneration; Seaweed-waste material

**Received:** November 9, 2009; **revised:** December 16, 2009; **accepted:** December 24, 2009

**DOI:** 10.1002/clean.200900250

## 1 Introduction

Contamination of water by heavy metals is a worldwide problem resulting from their widespread use in a wide range of industrial processes. The effective removal of metals known to be toxic, such as nickel, zinc and aluminum from industrial effluents is of particular interest. The most important sources of these metals are from the electroplating, alloy manufacturing, and glass and crystal industries.

The metal removal properties of a large variety of marine macroalgae have been widely investigated [1–7]. Using seaweed-based sorbents in fixed-bed columns present numerous advantages over conventional wastewater treatment systems, such as an efficient utilization of the biosorbent, low metal concentrations in effluents and the regeneration of the sorbent with metal recovery at low cost [8]. Several studies have concentrated on the screening of suitable desorbing agents for metal recovery [9–11]. An effective desorbing agent should accomplish complete metal recovery with an unchanged capacity of the sorbent for metal removal [12]. Jalali et al. [13] showed that mineral acids were very efficient for metal recovery with little or no loss in removal efficiency (RE).

In this study, a seaweed waste material from the industrial processing of *Ascophyllum nodosum* was investigated for multiple sorption-desorption cycles using a pilot scale fixed-bed sorption col-

umn. The reuse of the waste material for the development of a novel biosorbent could be integrated into a new waste management system for the seaweed processing industry. The utilization of 0.1 M HCl was investigated for the recovery of Zn(II), Ni(II) and Al(III) in both single and multi-metal systems. The regeneration of the sorbent was investigated over 5 consecutive sorption-desorption cycles using a fixed-bed sorption column [12]. The main objectives of this study were to investigate the removal capacity of the seaweed waste material for multiple sorption cycles after regeneration using 0.1 M HCl and to assess the physical integrity (robustness) of the biosorbent for multiple reuses.

## 2 Materials and Methods

### 2.1 Biomass Preparation

A seaweed waste material, resulting from the industrial processing of *Ascophyllum nodosum* (referred to as Waste *Ascophyllum* Product or WAP) supplied by Olean Glas Teo (CGT, Ballymoon Industrial Estate, Kilar, Co. Donegal, Ireland) was investigated. The waste material was dried at 60°C for 24 h, and subsequently ground and sieved to a particle size of 500–850 µm.

### 2.2 Metal Solutions

Standard metal solutions (analytical grade) containing 1000 mg L<sup>-1</sup> Ni(NO<sub>3</sub>)<sub>2</sub>, Zn(NO<sub>3</sub>)<sub>2</sub> and Al(NO<sub>3</sub>)<sub>3</sub> (Sigma-Aldrich) were used to prepare 10 mg L<sup>-1</sup> metal solutions (initial concentrations or C<sub>0</sub>). Multi-metal

Correspondence: A. Bakir, Estuarine Research Group, Eco-Innovation Research Centre, Department of Chemical and Life Sciences, Waterford Institute of Technology, Cork Road, Waterford, Ireland.  
E-mail: abakir@wit.ie

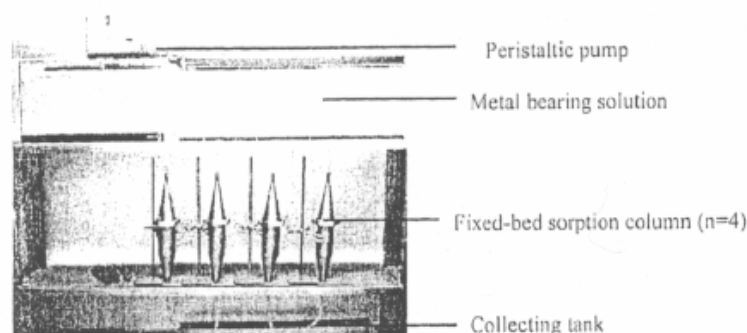


Figure 1. Setup of laboratory scale fixed-bed sorption columns.

solutions were prepared by combining  $10 \text{ mg L}^{-1}$  of each metal under investigation. The pH of all metal solutions was  $2.63 \pm 0.16$ . Metal concentrations were determined using an Inductively Coupled Plasma Optical Emission Spectrometer with auto-sampler (Varian 710-ES ICP Optical Emission Spectrometer, ICP Expert II Software).

## 2.3 Metal Sorption Studies

### 2.3.1 Fixed-Bed Column Sorption Studies

Prior to utilisation, the dried and ground waste *Ascophyllum nodosum* product (WAP) was immobilised in agar to produce blocks of homogeneous sizes ( $6 \times 10 \times 15 \text{ mm}$ ). A previous study comparing the metal removal of WAP immobilized in agar, carrageenan and sodium alginate showed that agar presented higher metal removal capacity [14]. 10 g of agar was mixed with 15 g of biomass in a conical flask and 200 mL of distilled water was added. The mix was homogenised and the flask was autoclaved for 20 min. The mix was then transferred into small trays and left to cool and solidify for 15 min. The solid blocks were then dried at  $60^\circ\text{C}$  for 24 h. The dried blocks were then soaked in distilled water for 2 h to allow expansion. The fixed-bed sorption columns (see Fig. 1) were then filled with the agar/biomass blocks. During runs, flow rates of  $25 \text{ mL min}^{-1}$  were employed through the columns. The effluent was sampled every 2 min for the first 10 min, during which most of the sorption takes place [14], and thereafter, every 15 min until the end of each sorption run (180 min).

For each experiment, four fixed-bed sorption columns were run in parallel. For each column the bed height was  $22.9 \pm 0.3 \text{ cm}$ , with an inner diameter (ID) of 7.2 cm and a working volume of 638 mL. The metal solution was transported by a peristaltic pump through silicon tubing to each column using upper valves to regulate the flow rate. The metal solutions flowed through each column and sorbed samples of the single and combined metal solutions were collected and analysed for metal concentration using the ICP-OES.

For desorption experiments, the metal loaded biomass was exposed to a continuous feed of a 0.1 M HCl solution at  $25 \text{ mL min}^{-1}$  for 180 min. 0.1 M HCl was selected due to its high metal desorption properties and its lower cost of operation [9–11, 13, 15]. All the settings for the fixed-bed sorption columns were kept constant throughout the 5 successive sorption-desorption cycles.

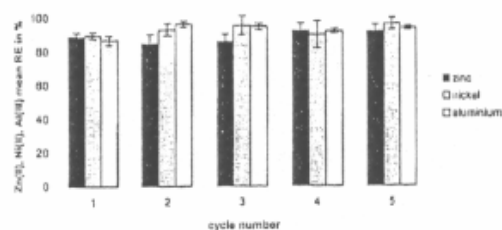


Figure 2. Zn(II), Ni(II) and Al(III) mean RE over 3 h in single-metal systems. Error bars calculated with 95% CI from four replicates.

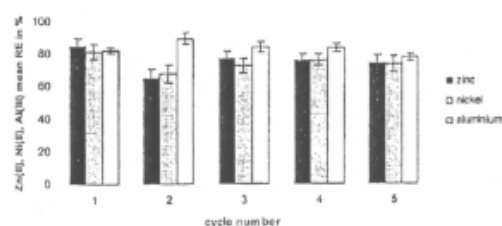


Figure 3. Zn(II), Ni(II) and Al(III) mean RE over 3 h in multi-metal systems. Error bars calculated with 95% CI from four replicates.

## 3 Results and Discussion

### 3.1 Regeneration of the Sorbent and Metal Re-uptake

The removal efficiency (RE) was investigated for both single and multi-metal systems (Figs. 2 and 3) as industrial effluents are expected to contain a variety of mixed heavy metals. The RE was calculated using Eq. (1) and the results are shown in Figs. 2 and 3.

$$RE = (C_i - C_f) \times 10 \quad (1)$$

where  $C_i$  is the initial concentration in  $\text{mg L}^{-1}$  ( $10 \text{ mg L}^{-1}$ ) and  $C_f$  the final concentration in  $\text{mg L}^{-1}$ .

High metal removal was observed for the first sorption cycle with 89, 89 and 87% RE for Zn(II), Ni(II) and Al(III), respectively, in single

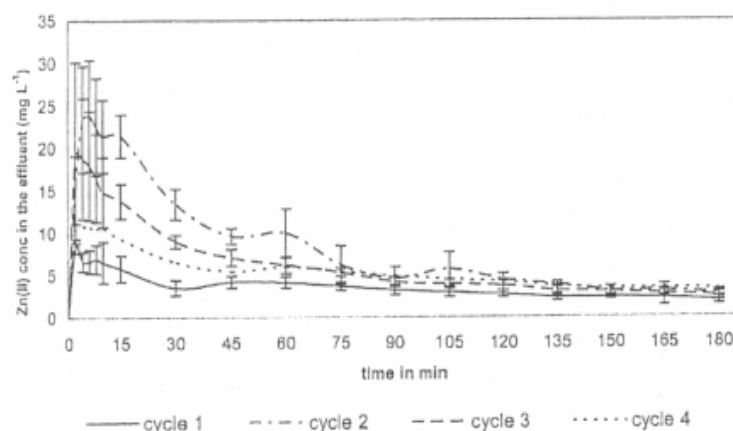


Figure 4. Zn(II) concentration in the effluent in a single-metal system after desorption of Zn(II) loaded WAP/agar for 4 desorption cycles. Error bars calculated with 95% CI from four replicates.

Table 1. Zn(II), Ni(II) and Al(III) removal efficiency (RE in%) and desorption efficiency (DE in%) within 60 min in single metal systems.

Cycle	RE, (%)			DE, (%)		
	Zn(II)	Ni(II)	Al(III)	Zn(II)	Ni(II)	Al(III)
1	89 ± 3	89 ± 2	87 ± 3	68 ± 15	108 ± 18	58 ± 19
2	84 ± 6	93 ± 4	96 ± 2	183 ± 38	95 ± 20	45 ± 10
3	86 ± 5	95 ± 6	95 ± 2	84 ± 15	72 ± 10	64 ± 13
4	92 ± 5	90 ± 8	92 ± 1	102 ± 23	122 ± 35	91 ± 6
5	92 ± 4	96 ± 3	94 ± 1	na <sup>a</sup>	na <sup>a</sup>	na <sup>a</sup>

<sup>a</sup> na: not assessed.

metal systems. The high metal sorption by WAP was previously shown to be related to the nature and amount of functional groups present on its surface. FTIR, XPS and potentiometric titrations showed that carboxylic and sulfonate groups were especially involved. It was also shown that WAP contained a large number of acidic groups (3.63 mmol/g) with pK<sub>a</sub> values close to neutrality [16]. It was reported that the interaction between cations in solution and algal biomass may be attributed to the carboxyl groups of the alginic acid, being the principal structural polysaccharide in brown algae [17]. Very little loss in RE was observed over the 5 metal sorption studies (Fig. 2 and Tab. 1) for single metal systems. The RE values were generally lower for metals in multi-metal systems with 85, 82 and 82% seen for Zn(II), Ni(II) and Al(III), respectively, which is probably due to metal ion competition for a limited number of binding sites (Fig. 3 and Tab. 2) [16].

The agar/WAP metal removal capacity was not affected by the repeated exposure to 0.1 M HCl. Regeneration without damaging the metal removal capacity of the sorbent is a very important factor in developing novel biosorbents. Senthilkumar et al. [8] reported that Zn(II) removal by *Utricularia reticulata* using a packed column decreased after 3 sorption-desorption cycles using CaCl<sub>2</sub> from 64.72% RE for cycle 1 down to 55.19% for cycle 3, probably due to the destruction or morphological alteration of the binding sites on the surface of the biomass [18]. It was also reported by Lau et al. [11]

Table 2. Zn(II), Ni(II) and Al(III) removal efficiency (RE in%) and desorption efficiency (DE in%) within 60 min in multi-metal systems.

Cycle	RE, (%)			DE, (%)		
	Zn(II)	Ni(II)	Al(III)	Zn(II)	Ni(II)	Al(III)
1	85 ± 5	82 ± 5	82 ± 2	76 ± 6	68 ± 6	70 ± 14
2	65 ± 6	68 ± 5	89 ± 4	102 ± 16	92 ± 13	64 ± 15
3	77 ± 5	72 ± 5	84 ± 3	79 ± 12	76 ± 12	71 ± 13
4	76 ± 4	76 ± 4	83 ± 2	86 ± 10	81 ± 9	71 ± 5
5	74 ± 5	73 ± 5	77 ± 2	na <sup>a</sup>	na <sup>a</sup>	na <sup>a</sup>

<sup>a</sup> na: not assessed.

that repeated sorption-desorption cycles using H<sub>2</sub>SO<sub>4</sub> on *Ulva lactuca* in batch tests decreased its removal potential for Cu(II), Ni(II) and Zn(II).

### 3.2 Desorption Kinetic Studies in Single- and Multi-Metal Systems

Figs. 4–6 show the Zn(II), Ni(II) and Al(III) concentrations in the effluent during 4 desorption cycles following 5 sorption cycles in single metal solutions with an initial metal concentration of 10 mg L<sup>-1</sup>. Figs. 7–9 show the metal concentrations in the effluent in a multi-metal system. The desorption of each metal in single or multi-metal systems was a rapid process with very high metal concentrations detected in the effluent within 15 min (Figs. 1–6). For all metals, concentrations greatly exceeded the metal concentration feed of 10 mg L<sup>-1</sup> indicating that the sorbent is constantly accumulating metals over the 3 h sorption period followed by rapid release during the desorption stage.

The desorption efficiency (DE) was calculated using the following expression, Eq. (2), [12] and the results are also listed in Tabs. 1 and 2:

$$DE = \frac{\text{Amount of metal desorbed in one cycle}}{\text{Amount of metal loaded in one cycle}} \times 100 \quad (2)$$

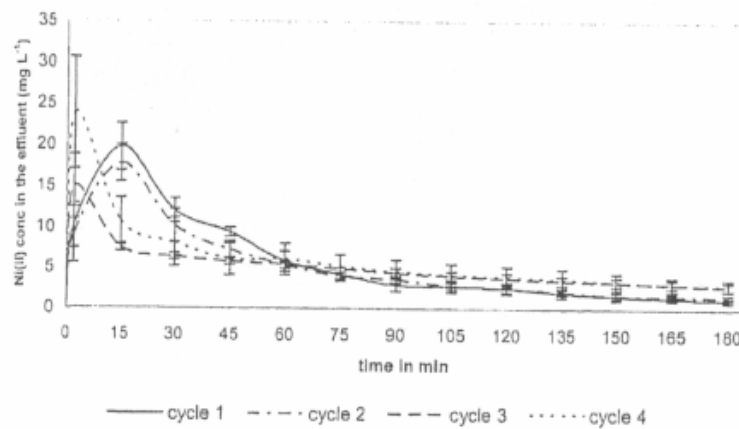


Figure 5. Ni(II) concentration in the effluent in a single-metal system after desorption of Ni(II) for 4 desorption cycles. Error bars calculated with 95% CI from four replicates.

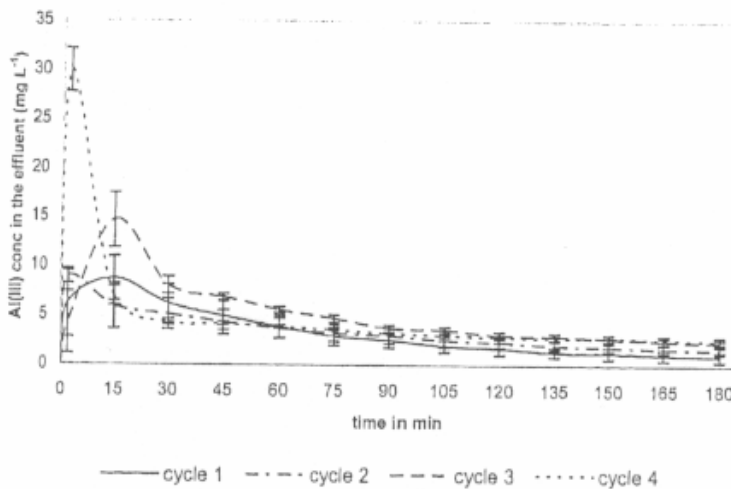


Figure 6. Al(III) concentration in the effluent in a single-metal system after desorption of Al(III) for 4 desorption cycles. Error bars calculated with 95% CI from four replicates.

As stated earlier, metal concentrations in the effluent for subsequent metal loadings within 15 min exceeded the initial metal concentration feed of  $10 \text{ mg L}^{-1}$ . As a result DEs over 60 min (Tabs. 1 and 2) appear higher than 100% in a few cases. This could also be explained by the relatively high 95% confidence intervals due to the experimental variations between the replicates. In all cases, the DEs are within error range of 100% indicating a complete desorption efficiency.

The desorption continued at a high rate for up to 60 min after initiation of the experiment for all the metals. At the end of the experiment less than  $3 \text{ mg L}^{-1}$  of all metals after 5 desorption cycles remained in the effluent in single and multi-metal systems. A study carried out by Saeed et al. [14] showed that the desorption of Cu(II), Cd(II) and Zn(II) from papaya wood, loaded with  $10 \text{ mg L}^{-1}$  of the

metals under investigation, using 0.1 N HCl was also rapid and a maximum metal recovery reached within 30 min and an equilibrium reached within 60 min [19]. Rapid desorption was an advantage in this study as the volume of effluent to dispose over 60 min (1.5 L) was minimal compared to the volume of metal solution treated over 180 min (4.5 L) making the whole sorption system highly efficient for industrial applications.

Very high metal recovery rates were obtained for Ni(II), Zn(II) and Al(III) in both single and multi-metal systems (Tabs. 1 and 2), with metal concentrations significantly exceeding the initial metal concentrations. These results compared favorably with Sawalha et al. [20] for the desorption of a range of metals from silica-immobilized saltbush (*Atriplex canescens*) using 0.1 M HCl. Values of 106.1% and 113.9% of Cu(II) and Zn(II), respectively, were recovered in single

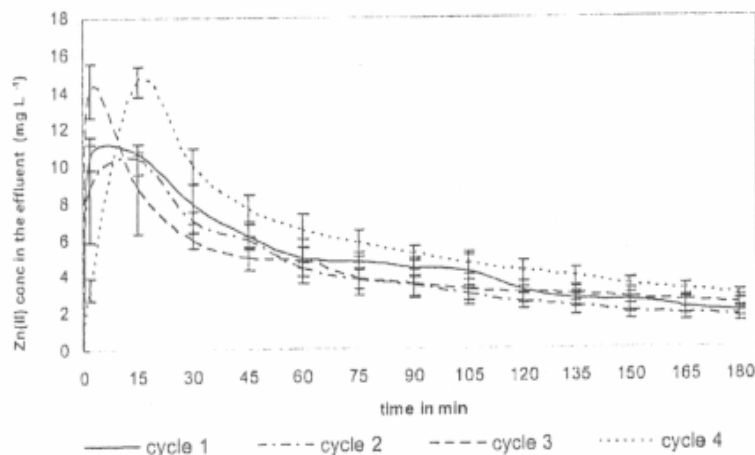


Figure 7. Zn(II) concentration in the effluent in a multi-metal system after desorption of the Zn(II), Ni(II) Al(III) loaded WAP/agar. Error bars calculated with 95% CI from four replicates.

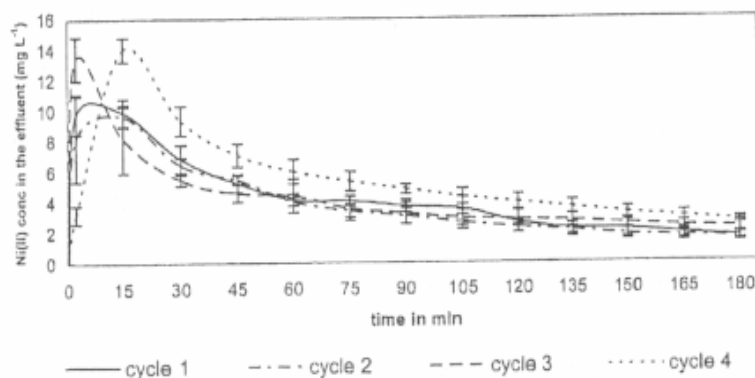


Figure 8. Ni(II) concentration in the effluent in a multi-metal system after desorption of the Zn(II), Ni(II) Al(III) loaded WAP/agar blocks for 4 desorption cycles. Error bars calculated with 95% CI from four replicates.

metal tests while 113.3% of Cu(II) was recovered from a multi-metal solution [20].

At the end of each desorption cycle, metal concentrations in the effluent were very low with metal concentrations below  $3 \text{ mg L}^{-1}$  in each case. As a result, no negative effect was caused for subsequent metal uptake in the different sorption cycles (Figs. 7 and 8). This was a limiting factor in the study by Hashim et al. [12], which showed that residues of Cu(II) after the first desorption cycle negatively influenced the following sorption cycle using immobilized *Sargassum baccularia*. They also reported that the utilization of HCl at pH 1.0 and 2 mM EDTA physically damaged the biosorbent with a possible destruction of the binding sites on its surface [12]. This was not the case in this study as the waste *Ascophyllum* product achieved high removal efficiencies over the multiple sorption cycles. This indicates that the seaweed waste material was highly resistant to repeated acid washes.

Lowering the pH with 0.1 M HCl was very effective at regenerating the sorbent, and therefore, demonstrated the influence of pH on

metal sorption. Lowering the pH is facilitating the replacement of metal ions by  $\text{H}^+$  ions with the diminution of negatively charged groups presenting less affinity for metal binding [21].

#### 4 Conclusions

An industrial waste material generated by the seaweed industry (WAP) was shown to be suitable for reuse as a novel biosorbent for the removal of heavy metals from waste streams. WAP was found to be an effective sorbent for the removal of Zn(II), Ni(II) and Al(III) in waste streams and could consequently be integrated into a waste treatment scheme. 0.1 M HCl, as a desorbing agent, was shown to be highly efficient for the desorption of the same metals from WAP/agar blocks in a fixed-bed sorption column for single metal systems but less so in the case of multi-metal systems. The rapid regeneration of the biosorbent as well as the high metal removal efficiencies over multiple sorption cycles also showed that the WAP/agar mate-

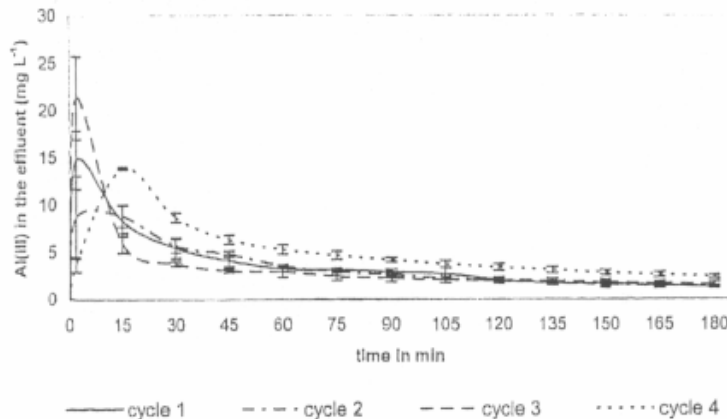


Figure 9. Al(III) concentration in the effluent in a multi-metal system after desorption of the Zn(II), Ni(II) Al(III) loaded WAP/agar blocks for 4 desorption cycles. Error bars calculated with 95% CI from four replicates.

rial is a robust and promising sorbent for an environmental-friendly industrial wastewater treatment for heavy metals. Future research will include the efficiency of metal removal under different waste stream conditions such as metal composition, pH and the impact of the presence of organic materials in the wastewater.

#### Acknowledgements

The authors gratefully acknowledge the support of the Irish Environmental Protection Agency for funding the project under the Masters and Doctoral Scholarship Scheme 2006. The authors also wish to acknowledge Oilean Glas Teo (OGT) for supplying the Waste *Asophyllum* material.

The authors have declared no conflict of interest.

#### References

- [1] Z. R. Holan, B. Volesky, Biosorption of Lead and Nickel by Biomass of Marine Algae, *Biotechnol. Bioeng.* 1994, 43, 1001–1009.
- [2] S. Schiewer, B. Volesky, Modeling Multi-metal Ion Exchange in Biosorption, *Environ. Sci. Technol.* 1996, 30, 2921–2927.
- [3] A. C. A. Da Costa, F. P. De França, Biosorption of Zinc, Cadmium and Copper by a Brown Seaweed (*Sargassum* sp.) in a Continuous Fixed-bed Laboratory Reactor, *Bioseparation* 1997, 6, 335–341.
- [4] Y. Sag, Biosorption of Heavy Metals by Fungal Biomass and Modeling of Fungal Biosorption: A Review, *Sep. Purif. Rev.* 2001, 30, 1–48.
- [5] G. Najm, B. Volesky, Multi-metal Biosorption in a Fixed-bed Flow-through Column, *Colloid Surf. A* 2006, 281, 194–201.
- [6] F. A. A. Al-Rub, M. H. El-Naas, I. Ashour, M. Al-Marzouqi, Biosorption of Copper on *Chlorella vulgaris* from Single, Binary and Ternary Metal Aqueous Solutions, *Process Biochem.* 2006, 41, 457–464.
- [7] M. R. Fagundes-Klen, P. Ferri, T. D. Martins, A. P. Tavares, E. A. Silva, Equilibrium of the binary mixture of cadmium-zinc ions biosorption by the *Sargassum filipendula* species using adsorption isotherms models and neural network, *Biochem. Eng. J.* 2007, 34, 136–146.
- [8] R. Senthilkumar, V. Vijayaraghavan, M. Thalakavathi, P. V. R. Iyer, M. Velan, Seaweeds for the remediation of wastewaters contaminated with zinc(II) ions, *J. Hazard. Mater.* 2006, 81 36, 791–799.
- [9] Z. R. Holan, B. Volesky, I. Prasetyo, Biosorption of cadmium by biomass of marine algae, *Biotechnol. Bioeng.* 1992, 41, 819–825.
- [10] P. Sar, S. K. Kazy, R. K. Asthana, S. P. Singh, Metal Adsorption and Desorption by Lyophilized *Pseudomonas aeruginosa*, *Int. Biodeterior. Biodegrad.* 1999, 44, 101–110.
- [11] T. C. Lau, P. O. Ang, P. X. Wong, Development of seaweed biomass as a biosorbent for metal ions, *Water Sci. Technol.* 2003, 47 (10), 49–54.
- [12] M. A. Hashim, N. H. Tan, K. H. Chu, Immobilized marine algal biomass for multiple cycles of copper adsorption and desorption, *Sep. Purif. Technol.* 2000, 19, 39–42.
- [13] R. Jalali, H. Ghafourian, Y. Asef, S. J. Davarpanah, S. Sepehr, Removal and recovery of lead using nonliving biomass of marine algae, *J. Hazard. Mater.* 2002, B92, 253–262.
- [14] R. Walsh, Development of a Biosorption Column Utilizing Seaweed Based Biosorbents for the Removal of Metals from Industrial Waste Streams, PhD Thesis, Waterford Institute of Technology, Ireland 2008.
- [15] V. K. Gupta, A. Rastogi, Biosorption of lead(II) from aqueous solutions by non-living algal biomass *Oedogonium* sp. and *Nostoc* sp. – A comparative study, *Colloid Surface B* 2008, 64, 170–178.
- [16] A. Bakir, P. McLoughlin, S. A. M. Tofail, E. Fitzgerald, Competitive sorption of antimony with zinc, nickel, and aluminium in a seaweed based fixed-bed sorption column, *Clean – Soil, Air, Water* 2009, 37 (9), 712–719.
- [17] E. Percival, R. H. McDowell, *Chemistry and Enzymology of Marine Algal Polysaccharides*, Academic Press, London 1967.
- [18] K. H. Chu, M. A. Hashim, S. M. Phang, V. B. Samuel, Biosorption of cadmium by algae biomass: adsorption and desorption characteristics, *Water Sci. Technol.* 1997, 35 (7), 115–122.
- [19] A. Sneed, M. W. Akhter, M. Iqbal, Removal and recovery of heavy metals from aqueous solution using papaya wood as a new biosorbent, *Sep. Purif. Technol.* 2005, 45, 25–31.
- [20] M. F. Sawalha, J. R. Peralta-Videa, B. Sanchez-Salcedo, J. L. Gardea-Torresday, Sorption of hazardous metals from single and multi-element solutions by saltbush biomass in batch and continuous mode: Interference of calcium and magnesium in batch mode, *J. Environ. Manage.* 2008, 1–6.
- [21] E. Luef, T. Prey, C. P. Kubicek, Biosorption of zinc by fungal mycelial wastes, *Appl. Microbiol. Biotechnol.* 1991, 688–692.

# Appendix C

*Langmuir and Freundlich  
binding isotherms*

## C.1 Freundlich sorption isotherms

*Zinc removal by WAP/agar blocks*

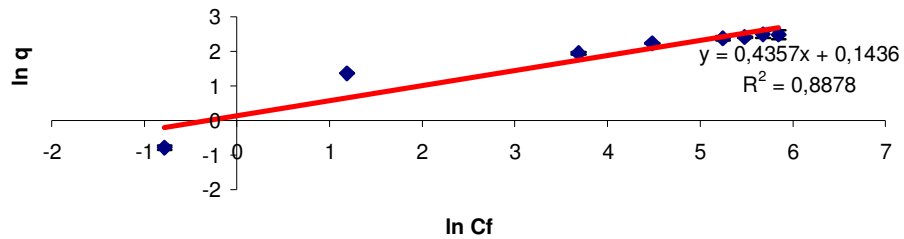


Fig. C.1 Linearised plot of the Freundlich relationship ( $\ln q$  vs.  $\ln C_f$ ) between  $q$  and  $C_f$  of WAP biosorption isotherm for Zn(II). Regression value displayed ( $\pm 95\%$  confidence intervals,  $n = 4$ ).

*Nickel removal by WAP/agar blocks*

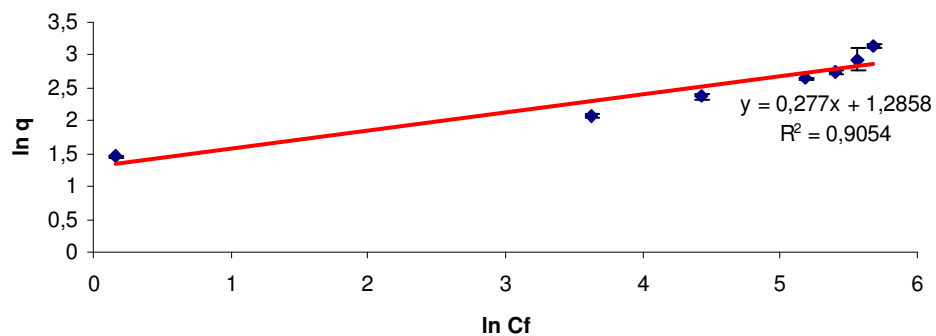


Fig. C.2 Linearised plot of the Freundlich relationship ( $\ln q$  vs.  $\ln C_f$ ) between  $q$  and  $C_f$  of WAP biosorption isotherm. Regression value displayed ( $\pm 95\%$  confidence intervals,  $n = 4$ ).

*Aluminium removal by WAP/agar blocks*

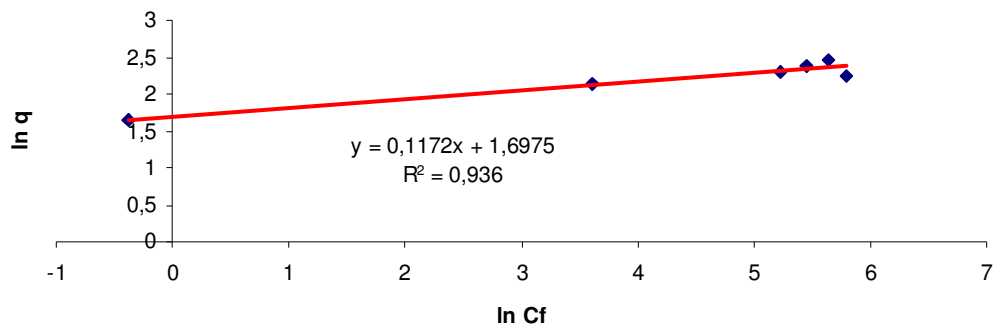


Fig. C.3 Linearised plot of the Freundlich relationship ( $\ln q$  vs.  $\ln C_f$ ) between  $q$  and  $C_f$  of WAP biosorption isotherm. Equation of the line and regression value displayed ( $\pm 95\%$  confidence intervals,  $n = 4$ ).

*Antimony removal by WAP/agar blocks*

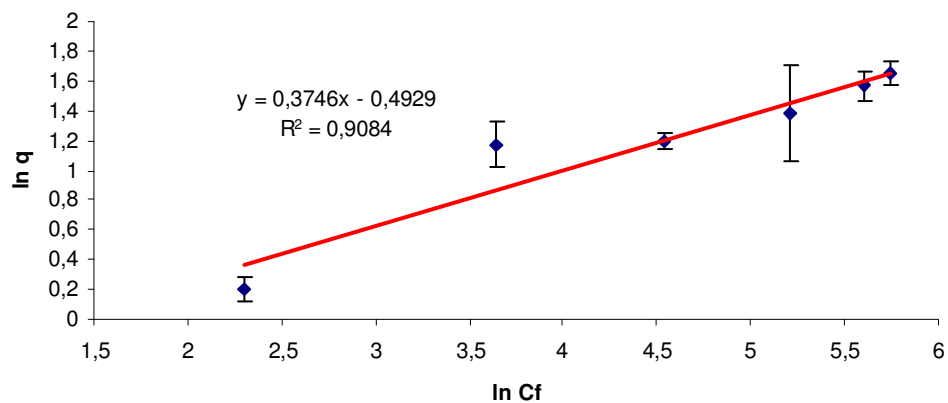


Fig. C4 Linearised plot of the Freundlich relationship ( $\ln q$  vs.  $\ln C_f$ ) between  $q$  and  $C_f$  of WAP biosorption isotherm. Equation of the line and regression value displayed ( $\pm 95\%$  confidence intervals,  $n = 4$ ).

*Antimony removal by P. lanosa/agar blocks*

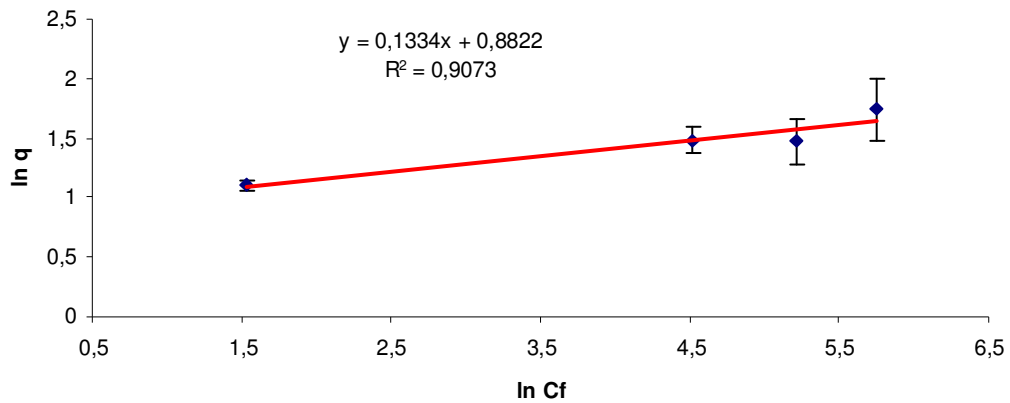


Fig. C.5 Linearised plot of the Freundlich relationship ( $\ln q$  vs.  $\ln C_f$ ) between  $q$  and  $C_f$  of WAP biosorption isotherm. Equation of the line and regression value displayed ( $\pm 95\%$  confidence intervals,  $n = 4$ ).

*Zinc, nickel and aluminium removal by WAP/agar blocks in a multi-metal system*

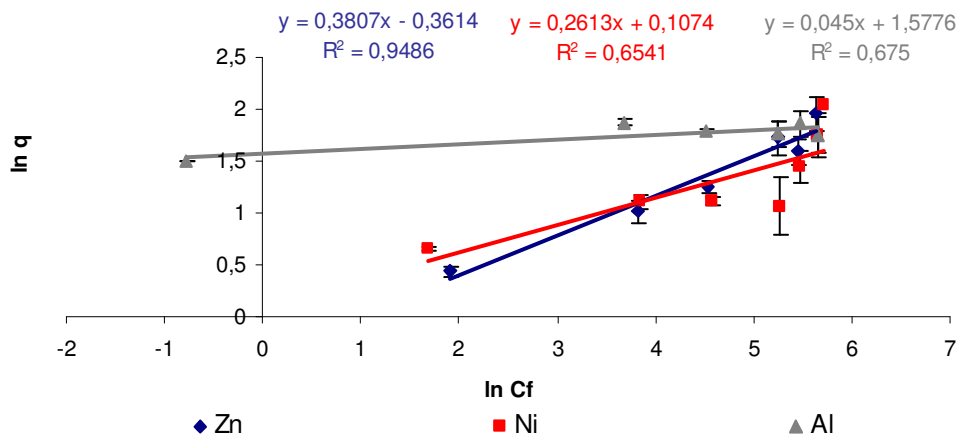


Fig. C.6 Linearised plot of the Freundlich relationship ( $\ln q$  vs.  $\ln C_f$ ) between  $q$  and  $C_f$  of WAP biosorption isotherm. Equation of the line and regression value displayed ( $\pm 95\%$  confidence intervals,  $n = 4$ ).

Zinc, nickel, aluminium and antimony removal by WAP/agar blocks in a multi-metal system

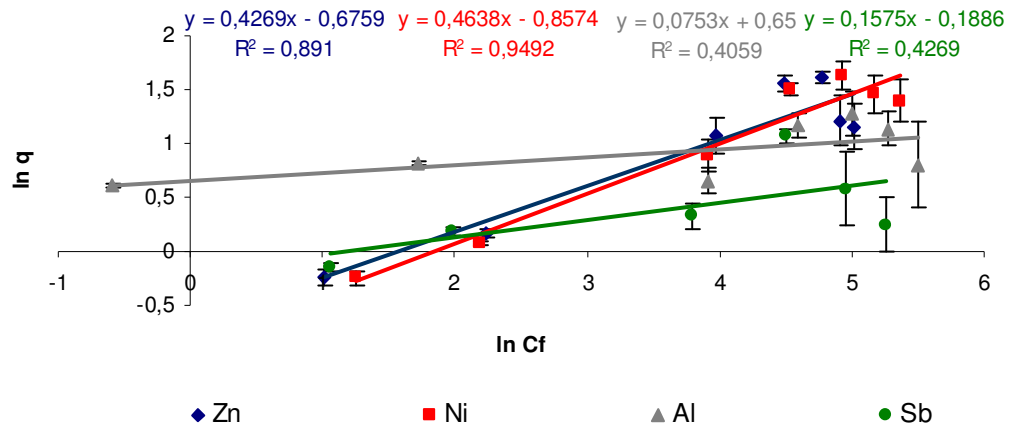


Fig. C.7 Linearised plot of the Freundlich relationship ( $\ln q$  vs.  $\ln C_f$ ) between  $q$  and  $C_f$  of WAP biosorption isotherm. Equation of the line and regression value displayed ( $\pm 95\%$  confidence intervals,  $n = 4$ ).

Table C.1 Freundlich parameters.

biomass	metals	k (mmol/g)	k (mg/g)	n	r <sup>2</sup>
WAP	Zn	1.76 ± 0.20	115.44 ± 12.89	2.32 ± 0.07	0.888
WAP	Ni	6.16 ± 0.31	361.76 ± 18.33	3.57 ± 0.24	0.842
WAP	Al	2.02 ± 0.03	54.60 ± 0.78	8.33 ± 0.03	0.936
WAP	Sb	0.17 ± 0.02	20.29 ± 2.86	2.70 ± 0.51	0.908
<i>P. lanosa</i>	Sb	0.20 ± 0.01	24.16 ± 1.44	7.69 ± 0.48	0.907
WAP (combined metals)	Zn	2.19 ± 0.20	143.53 ± 13.19	2.63 ± 0.13	0.949
	Ni	1.90 ± 0.11	111.34 ± 6.42	3.85 ± 0.11	0.654
	Al	1.79 ± 0.02	48.43 ± 2.28	2.5 ± 0.52	0.675
WAP (combined metals)	Zn	0.3 ± 0.04	19.66 ± 2.42	2.32 ± 0.20	0.891
	Ni	0.22 ± 0.03	12.92 ± 1.61	2.17 ± 0.10	0.949
	Al	0.71 ± 0.13	19.15 ± 3.61	14.28 ± 3.48	0.406
	Sb	0.1 ± 0.01	12.07 ± 0.87	6.25 ± 1.39	0.427

## C.2 Combined Langmuir-Freundlich sorption isotherms

*Zinc removal by WAP/agar blocks*

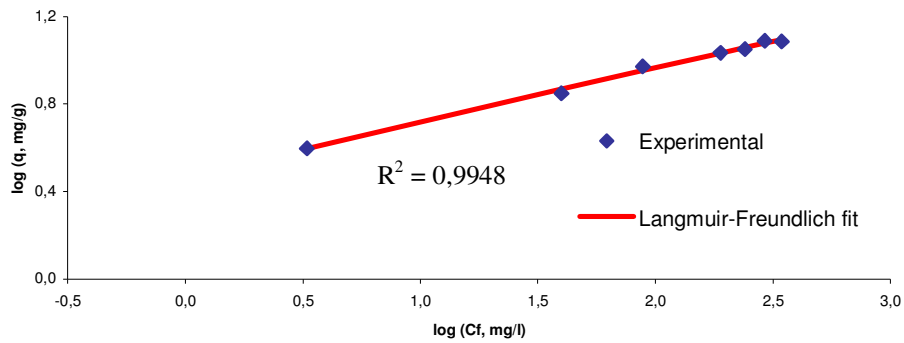


Fig. C.8 Linearised plot of the Langmuir-Freundlich relationship ( $\log(q_e)$  vs.  $\log(C_f)$ ) between  $q$  and  $C_f$  of WAP biosorption isotherm. Regression value displayed.

*Nickel removal by WAP/agar blocks*

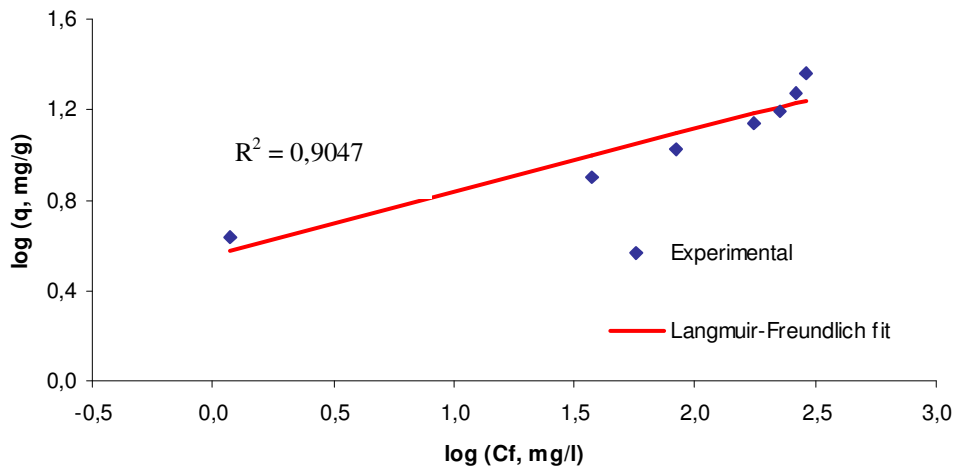


Fig. C.9 Linearised plot of the Langmuir-Freundlich relationship ( $\log(q_e)$  vs.  $\log(C_f)$ ) between  $q$  and  $C_f$  of WAP biosorption isotherm. Regression value displayed.

*Aluminium removal by WAP/agar blocks*

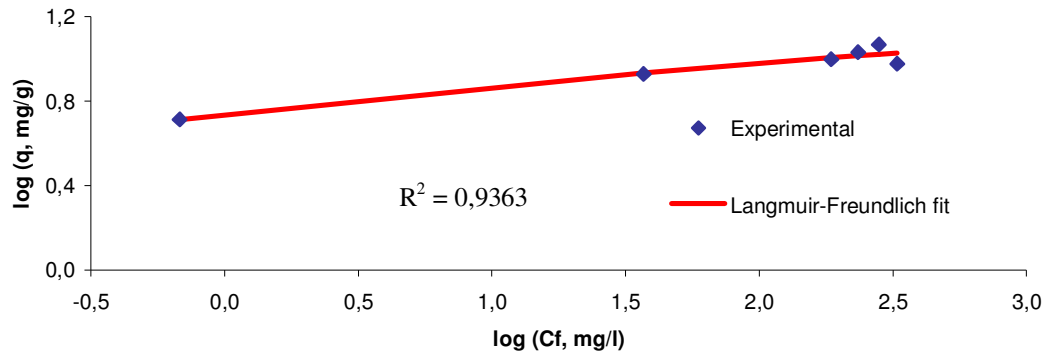


Fig. C.10 Linearised plot of the Langmuir-Freundlich relationship ( $\log(q_e)$  vs.  $\log(C_f)$ ) between  $q$  and  $C_f$  of WAP biosorption isotherm. Regression value displayed.

*Antimony removal by WAP/agar blocks*

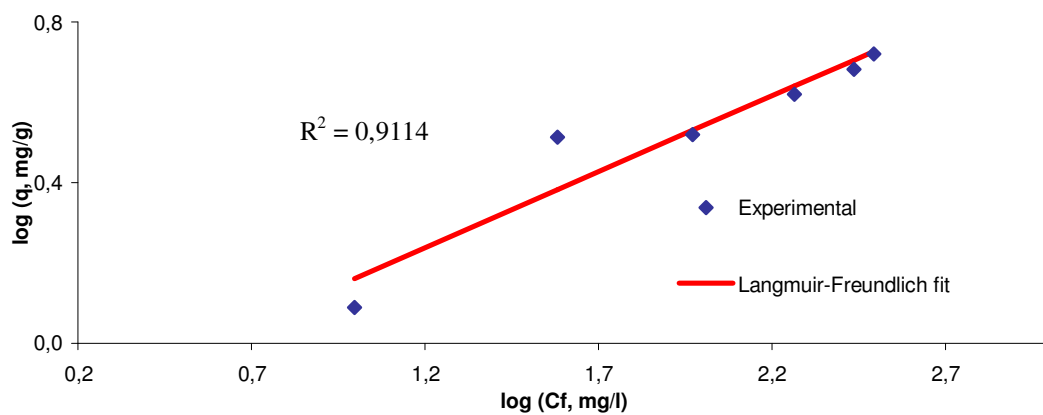


Fig. C.11 Linearised plot of the Langmuir-Freundlich relationship ( $\log(q_e)$  vs.  $\log(C_f)$ ) between  $q$  and  $C_f$  of WAP biosorption isotherm. Regression value displayed.

*Antimony removal by P. lanosa/agar blocks*

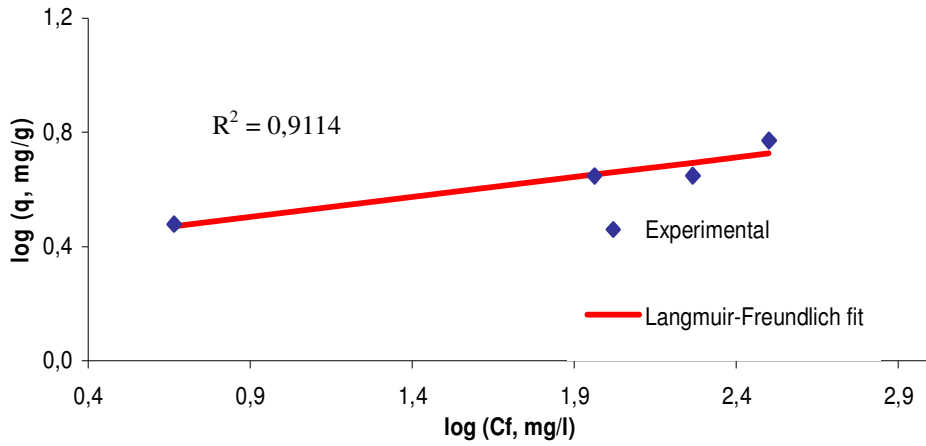


Fig. C.12 Linearised plot of the Langmuir-Freundlich relationship ( $\log(q_e)$  vs.  $\log(C_f)$ ) between  $q$  and  $C_f$  of WAP biosorption isotherm. Regression value displayed.

*Zinc, nickel and aluminium removal by WAP/agar blocks in a multi-metal system*

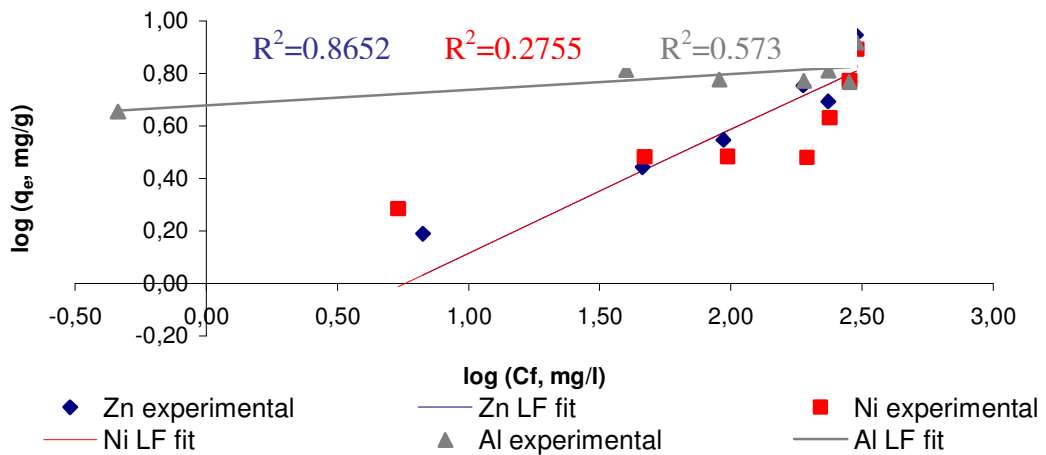


Fig. C.13 Linearised plot of the Langmuir-Freundlich relationship ( $\log(q_e)$  vs.  $\log(C_f)$ ) between  $q$  and  $C_f$  of WAP biosorption isotherm. Regression value displayed.

*Zinc, nickel, aluminium and antimony removal by WAP/agar blocks in a multi-metal system*

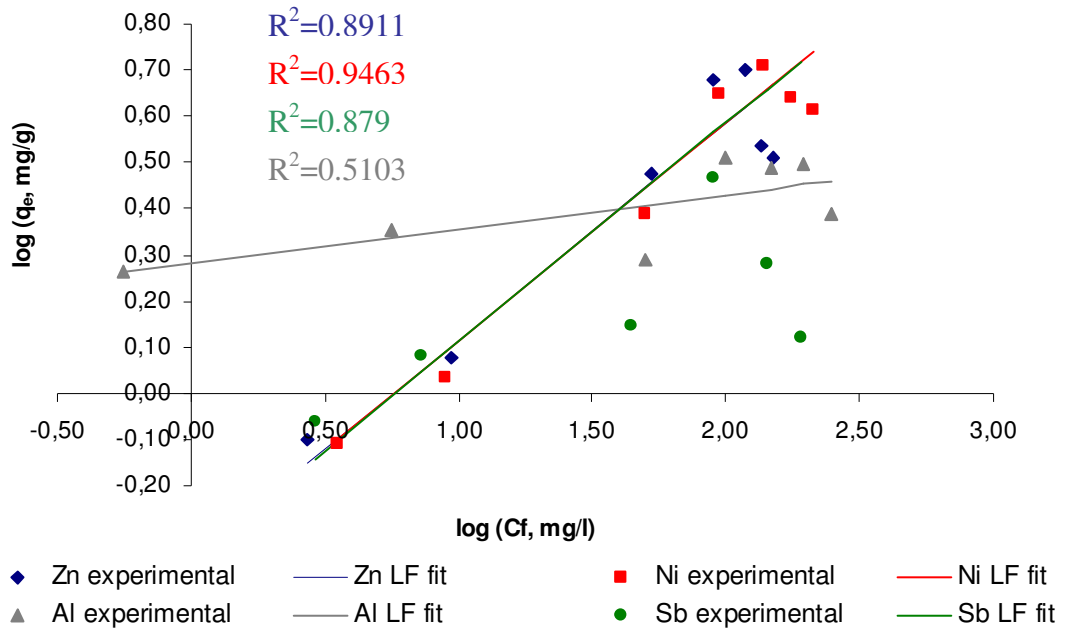


Fig. C.14 Linearised plot of the Langmuir-Freundlich relationship ( $\log(q_e)$  vs.  $\log(C_f)$ ) between  $q$  and  $C_f$  of WAP biosorption isotherm. Regression value displayed.

Table C.2 Fitting parameters and summary statistics of the combined Langmuir-Freundlich isotherm.

biomass	metals	Fitting Parameters and Summary statistics					
		$N_t$ ( $\mu\text{mol/g}$ )	$a$	$m$	RSS	TSS	$R^2$
WAP	Zn	131.461	0.023	0.262	0.001	0.190	0.995
WAP	Ni	398.953	0.001	0.279	0.035	0.371	0.905
WAP	Al	131.946	0.043	0.125	0.005	0.080	0.934
WAP	Sb	130.840	0.005	0.387	0.023	0.262	0.911
<i>P. lanosa</i>	Sb	131.144	0.019	0.144	0.004	0.043	0.903
WAP (combined metals)	Zn	130.832	0.003	0.481	0.055	0.406	0.865
	Ni	130.832	0.003	0.481	0.184	0.253	0.276
	Al	134.94	0.037	0.062	0.016	0.037	0.573
WAP (combined metals)	Zn	130.83	0.003	0.481	0.061	0.561	0.891
	Ni	130.832	0.003	0.481	0.035	0.653	0.946
	Al	131.489	0.015	0.076	0.031	0.063	0.510
	Sb	130.83	0.003	0.481	0.07	0.054	0.879

# Appendix D

*COMSOL scripts*

The scripts in this section are organised as utility scripts which perform a particular task and run scripts which use a number of the utility scripts to test the MTCM implementation or to `_t` the MTCM to experimental data.

## D.1 Utility Scripts

### D.1.1 mtcM plot.m

---

```

1 function mtcM_plot(f,varargin)
2 %MTCMPLOT Plot experssion f at a particular time point
3 %
4 %           Typically the experssion in f is 'xM' or 'yM'.
5
6 % extract required data from global mtcM structure
7 global mtcM
8
9 % Animate solution
10 postplot(mtcM.fem, ...
11         'liny',{f,'cont','internal'}, ...
12         'lincolor',[0.0,0.0,0.0], ...
13         'title',['Plot of ',f], ...
14         'axis',[-0.34999999999999964,1.6500000000000006], varargin{:});

```

---

## D.2 Run Scripts

### D.2.1 naja.m

The following script was used to generate the results given in the work of Naja & Volesky (2008) and shown in section .

---

```

1 % naja.m
2 % Experiment = comparision with the results of Naja & Voleksy
3
4 clear
5 global mtcM
6
7 disp('Processing model parameters...');
8 % START - experiment specific parameters
9
10 mtcM.CO = 1;           % normality of the solution [meq/L]
11 mtcM.L0 = 45;         % length of column [cm]
12 mtcM.K = 2.01;        % Equilibrium coefficient [-]
13 mtcM.Q = 2.2;         % concentration of binding sites in the biosorbent [mmol/g]
14 mtcM.r = 1.25;        % radius of column [cm]
15 mtcM.v = 4;           % interstitial fluid velocity [cm/min]
16
17 mtcM.eps = 0.82;      % column void fraction [-]
18 mtcM.rho_b = 150.0;   % packing density of dry biomass in the packed-bed [g/L]
19
20 % time settings
21 mtcM.tDelta = 0.1;    % time step used in solving PDE system
22 mtcM.tMax = 800;     % end time for simulation
23
24 % initial estimate for fit parameters
25 % mtcM.Pe = 100;      % initial estimate for Pe
26 % mtcM.Sh = 1;        % initial estimate for Sh
27
28 mtcM.Dz = 10;         % Axial dispersion coefficient [cm^2/min]

```

```

29 mtcM.K_fm = 0.0040;          % Overall mass transfer coefficient [/min]
30
31 mtcM.root='naja';          % root name for all input/output files
32
33 % END - experiment specific parameters
34
35 mtcM_setup;
36
37 % Demonstrate dependence on K_fm
38 %
39 disp('Calculate dependence on K_fm graph');
40 %
41 mtcM.K_fm = 0.0015;    mtcM_solve;    e_0015 = mtcM_crossdata('xM');
42 mtcM.K_fm = 0.0020;    mtcM_solve;    e_0020 = mtcM_crossdata('xM');
43 mtcM.K_fm = 0.0030;    mtcM_solve;    e_0030 = mtcM_crossdata('xM');
44 mtcM.K_fm = 0.0040;    mtcM_solve;    e_0040 = mtcM_crossdata('xM');
45 mtcM.K_fm = 0.0070;    mtcM_solve;    e_0070 = mtcM_crossdata('xM');
46 mtcM.K_fm = 0.0200;    mtcM_solve;    e_0200 = mtcM_crossdata('xM');
47 t = mtcM_crossdata('t');
48 plot(t,e_0015, t,e_0020, t,e_0030, t,e_0040, t,e_0070, t,e_0200);
49 mtcM_saveimage('K_fm-dependence');
50
51 % Demonstrate dependence on eps
52 %
53 disp('Calculate dependence on eps graph');
54 %
55 mtcM.tMax = 2000;
56 mtcM.K_fm = 0.0200;
57 mtcM.eps = 0.25;    mtcM_solve;    e_25 = mtcM_crossdata('xM');
58 mtcM.eps = 0.35;    mtcM_solve;    e_35 = mtcM_crossdata('xM');
59 mtcM.eps = 0.50;    mtcM_solve;    e_50 = mtcM_crossdata('xM');
60 mtcM.eps = 0.82;    mtcM_solve;    e_82 = mtcM_crossdata('xM');
61 t = mtcM_crossdata('t');
62 plot(t,e_25, t,e_35, t,e_50, t,e_82);
63 mtcM_saveimage('eps-dependence');
64
65 % Demonstrate dependence on Dz
66 %
67 disp('Calculate dependence on Dz graph');
68 %
69 mtcM.tMax = 800;
70 mtcM.eps = 0.82;
71 mtcM.Dz = 1.0;    mtcM_solve;    e_010 = mtcM_crossdata('xM');
72 mtcM.Dz = 4.4;    mtcM_solve;    e_044 = mtcM_crossdata('xM');
73 mtcM.Dz = 10.0;    mtcM_solve;    e_100 = mtcM_crossdata('xM');
74 mtcM.Dz = 20.0;    mtcM_solve;    e_200 = mtcM_crossdata('xM');
75 t = mtcM_crossdata('t');
76 plot(t,e_010, t,e_044, t,e_100, t,e_200);
77 mtcM_saveimage('Dz-dependence');
78
79 % Generate snapshots of xM over time
80 %
81 disp('Generate snapshots of xM over time');
82 %
83 mtcM.tMax = 800;
84 mtcM.eps = 0.82;
85 mtcM.Dz = 20.0;    mtcM_solve;
86 t = mtcM_crossdata('t');
87 mtcM_plot('xM', 'T', 25);    mtcM_saveimage('T_025');
88 mtcM_plot('xM', 'T', 50);    mtcM_saveimage('T_050');
89 mtcM_plot('xM', 'T', 100);    mtcM_saveimage('T_100');
90 mtcM_plot('xM', 'T', 200);    mtcM_saveimage('T_200');

```

```

91 mtcM_plot('xM', 'T', 400);    mtcM_saveimage('T_400');
92 mtcM_plot('xM', 'T', 800);    mtcM_saveimage('T_800');
93
94
95 % Demonstrate dependence on Dz
96 %

```

---

## D.2.2 Zinc fitting to model, output log of script zinc\_s1.m

---

```

1 % zinc_s1.m
2 % Experiment = zinc into sorbant 1
3
4 clear
5 global mtcM
6
7 disp('Processing_model_parameters...');
8
9 % START - experiment specific parameters
10
11 mtcM.CO = 10;           % normality of the solution [meq/L]
12 mtcM.L0 = 17;          % length of column [cm]
13 mtcM.K = 2.01;         % Equilibrium coefficient [-]
14 mtcM.Q = 3.63;         % concentration of binding sites in the biosorbent [mmol/g]
15 mtcM.r = 1.25;         % radius of column [cm]
16 mtcM.v = 8;            % interstitial fluid velocity [cm/min]
17
18 mtcM.eps = 0.046;      % column void fraction [-]
19 mtcM.rho_b = 137.1;    % packing density of dry biomass in the packed-bed [g/L]
20
21 % time settings
22 mtcM.tDelta = 0.5;     % time step used in solving PDE system
23 mtcM.tMax = 1200;     % end time for simulation
24
25 % initial estimate for fit parameters
26 mtcM.Dz = 1;           % Axial dispersion coefficient [cm^2/min]
27 mtcM.K_fm = 1;         % Overall mass transfer coefficient [/min]
28 % optimal = mtcM.Dz = 3.7206;    mtcM.K_fm = 1.3344;    mtcM.sse = 0.0078182;
29
30 mtcM.root='zinc_s1';   % root name for all input/output files
31
32 % END - experiment specific parameters
33
34 % input and output files
35 mtcM.infile = [mtcM.root, '.csv'];
36 mtcM.outfile = [mtcM.root, '.out'];
37
38 % Create geometry and initialize mesh
39 disp('Creating_mesh...');
40 fem.geom = geomcsg({solid1([0 1])});
41 fem.mesh = meshinit(fem, 'hmax', 0.01, 'hmaxvtx', [1; 0.1]);
42
43 % store multiphysics fem structure for later use
44 mtcM.fem = fem;
45
46 % load observed experimental breakthrough curve
47 mtcM.load;
48
49 % fit model (expected) to observed
50 % mtcM_fit;

```

```

Processing model parameters ...
Loading observed experimental data from file zinc_s1.csv ...
Fitting mtcM to observed breakthrough curve ...
Solving PDE system ...
  Q/eps = 78.913   =>   Dg = 1081.8978
  Dz     = 1       =>   Pe = 136
  K_fm   = 1       =>   Sh = 2.125
Fit parameters: Dz = 1   K_fm = 1   SSE = 0.91219
Solving PDE system ...
  Q/eps = 78.913   =>   Dg = 1081.8978
  Dz     = 2       =>   Pe = 68
  K_fm   = 1       =>   Sh = 2.125
Fit parameters: Dz = 2   K_fm = 1   SSE = 0.32361
.
.
.
Solving PDE system ...
  Q/eps = 78.913   =>   Dg = 1081.8978
  Dz     = 3.7206  =>   Pe = 36.5536
  K_fm   = 1.3344  =>   Sh = 2.8356
Fit parameters: Dz = 3.7206   K_fm = 1.3344   SSE = 0.0078182

```

---

### D.2.3 Nickel fitting to model, output log of script nickel\_s1.m

---

```

% nickel_s1.m
% Experiment = nickel into sorbent 1(WAP)

clear
global mtcM

disp('Processing model parameters ...');

% START - experiment specific parameters

mtcM.C0 = 10.734;           % normality of the solution [meq/L]
mtcM.L0 = 17;              % length of column [cm]
mtcM.K = 2.01;             % Equilibrium coefficient [-]
mtcM.Q = 3.63;             % concentration of binding sites in the
biosorbent [mmol/g]
mtcM.r = 1.25;             % radius of column [cm]
mtcM.v = 8;                % interstitial fluid velocity [cm/min]
mtcM.eps = 0.046;         % column void fraction [-]
mtcM.rho_b = 125.5;       % packing density of dry biomass in the
packed-bed [g/L]

                                % time settings
mtcM.tDelta = 0.5;        % time step used in solving PDE system
mtcM.tMax = 1200;        % end time for simulation
                                % initial estimate for fit parameters
mtcM.Dz = 1.25;          % Axial dispersion coefficient [cm^2/min]
mtcM.K_fm = 0.03;        % Overall mass transfer coefficient [/min]
mtcM.root='nickel_s1';   % root name for all input/output files

% END - experiment specific parameters
% input and output files

```

```

mtcm.infile = [mtcm.root, '.csv'];
mtcm.outfile = [mtcm.root, '.out'];

% Create geometry
fem.geom = geomcsg({solid1([0 1])});

% Initialize mesh
fem.mesh = meshinit(fem, 'hmax', 0.01, 'hmaxvtx', [1; 0.1]);

% store multiphysics fem structure for later use
mtcm.fem = fem;

% load observed experimental breakthrough curve
mtcm_load;

% fit model (expected) to observed
% mtc_fit;

Processing model parameters ...
Loading observed experimental data from file nickel_s1.csv ...
C> mtc_fit
Fitting mtc to observed breakthrough curve ...
Solving PDE system ...
    Q/eps = 78.913    =>    Dg = 922.6371
    Dz      = 1.25    =>    Pe = 108.8
    K_fm    = 0.03    =>    Sh = 0.06375
Fit parameters: Dz = 1.25    K_fm = 0.03    SSE = 0.65401
Solving PDE system ...
    Q/eps = 78.913    =>    Dg = 922.6371
    Dz      = 2.25    =>    Pe = 60.4444
    K_fm    = 0.03    =>    Sh = 0.06375
•
•
•
Solving PDE system ...
    Q/eps = 78.913    =>    Dg = 922.6371
    Dz      = 2.4403  =>    Pe = 55.73
    K_fm    = 0.014492 =>    Sh = 0.030797
Fit parameters: Dz = 2.4403    K_fm = 0.014492    SSE = 0.0084423

```

---

### D.2.4 Aluminium fitting to model, output log of script aluminium\_s1.m

---

```

% aluminium_s1.m
% Experiment = aluminium into sorbent 1(WAP)

clear
global mtc

disp('Processing model parameters ...');

% START - experiment specific parameters

mtcm.CO = 10;           % normality of the solution [meq/L]
mtcm.L0 = 17;          % length of column [cm]
mtcm.K = 2.01;         % Equilibrium coefficient [-]

```

```

mtcm.Q = 3.63; % concentration of binding sites in
the biosorbent [mmol/g]
mtcm.r = 1.25; % radius of column [cm]
mtcm.v = 8; % interstitial fluid velocity
[cm/min]

mtcm.eps = 0.046; % column void fraction [-]
mtcm.rho_b = 130.3; % packing density of dry biomass in
the packed-bed [g/L]

% time settings
mtcm.tDelta = 0.5; % time step used in solving PDE
system
mtcm.tMax = 1200; % end time for simulation

% initial estimate for fit parameters
mtcm.Dz = 1.25; % Axial dispersion coefficient
[cm^2/min]
mtcm.K_fM = 0.03; % Overall mass transfer coefficient
[/min]

mtcm.root='aluminium_s1'; % root name for all input/output
files

% END - experiment specific parameters

% input and output files
mtcm.infile = [mtcm.root, '.csv'];
mtcm.outfile = [mtcm.root, '.out'];

% Create geometry
fem.geom = geomcsg({solid1([0 1])});

% Initialize mesh
fem.mesh = meshinit(fem, 'hmax', 0.01, 'hmaxvtx', [1; 0.1]);

% store multiphysics fem structure for later use
mtcm.fem = fem;

% load observed experimental breakthrough curve
mtcm_load;

% fit model (expected) to observed
mtcm_fit;

Processing model parameters ...
Loading observed experimental data from file aluminium_s1.csv ...
Fitting mtcm to observed breakthrough curve ...
Solving PDE system ...
    Q/eps = 78.913    =>    Dg = 1028.237
    Dz      = 1.25    =>    Pe = 108.8
    K_fM    = 0.03    =>    Sh = 0.06375
Fit parameters: Dz = 1.25    K_fM = 0.03    SSE = 0.047165
Solving PDE system ...
    Q/eps = 78.913    =>    Dg = 1028.237
    Dz      = 2.25    =>    Pe = 60.4444
    K_fM    = 0.03    =>    Sh = 0.06375aluminium_s1

```

•

- 
- 

Solving PDE system ...

Q/eps = 78.913 => Dg = 1028.237  
Dz = 1.7838 => Pe = 76.242  
K\_fM = 0.027502 => Sh = 0.058441

Fit parameters: Dz = 1.7838      K\_fM = 0.027502      SSE = 0.0050769

---

### D.2.5 Antimony (with WAP) fitting to model, output log of script antimony\_s1.m

---

```
% antimony_s1.m
% Experiment = antimony into sorbent 1(WAP)

clear
global mtcM

disp('Processing model parameters ...');

% START - experiment specific parameters

mtcM.CO = 10;           % normality of the solution [meq/L]
mtcM.L0 = 17;          % length of column [cm]
mtcM.K = 2.01;         % Equilibrium coefficient [-]
mtcM.Q = 3.63;         % concentration of binding sites in
the biosorbent [mmol/g]
mtcM.r = 1.25;         % radius of column [cm]
mtcM.v = 8;            % interstitial fluid velocity
[cm/min]

mtcM.eps = 0.046;     % column void fraction [-]
mtcM.rho_b = 129.9;   % packing density of dry biomass in
the packed-bed [g/L]

% time settings
mtcM.tDelta = 0.5;    % time step used in solving PDE
system
mtcM.tMax = 1200;     % end time for simulation

% initial estimate for fit parameters
mtcM.Dz = 1.25;       % Axial dispersion coefficient
[cm^2/min]
mtcM.K_fM = 0.03;     % Overall mass transfer coefficient
[/min]

mtcM.root='antimony_s1'; % root name for all input/output
files

% END - experiment specific parameters

% input and output files
mtcM.infile = [mtcM.root, '.csv'];
mtcM.outfile = [mtcM.root, '.out'];

% Create geometry
fem.geom = geomcsg({solid1([0 1])});
```

```

% Initialize mesh
fem.mesh = meshinit(fem, 'hmax', 0.01, 'hmaxvtx', [1; 0.1]);

% store multiphysics fem structure for later use
mtcm.fem = fem;

% load observed experimental breakthrough curve
mtcm_load;

% fit model (expected) to observed
mtcm_fit;

Processing model parameters ...
Loading observed experimental data from file antimony_s1.csv ...
Fitting mtc to observed breakthrough curve ...
Solving PDE system ...
    Q/eps = 78.913    =>    Dg = 1025.0804
    Dz      = 1.25    =>    Pe = 108.8
    K_fM    = 0.03    =>    Sh = 0.06375
Fit parameters: Dz = 1.25    K_fM = 0.03    SSE = 0.026653
•
•
•
Fit parameters: Dz = 1.4229    K_fM = 0.043643    SSE = 0.0059532
Solving PDE system ...
    Q/eps = 78.913    =>    Dg = 1025.0804
    Dz      = 1.4227    =>    Pe = 95.5898
    K_fM    = 0.043625    =>    Sh = 0.092704
Fit parameters: Dz = 1.4227    K_fM = 0.043625    SSE = 0.0052913

```

---

### D.2.6 Antimony (with *P. Lanosa*) fitting to model, output log of script antimony\_s2.m

---

```

% antimony_s2.m
% Experiment = antimony into sorbent 2(P. lanosa)

clear
global mtc

disp('Processing model parameters ...');

% START - experiment specific parameters

mtcm.C0 = 11;           % normality of the solution [meq/L]
mtcm.L0 = 17;          % length of column [cm]
mtcm.K = 2.01;         % Equilibrium coefficient [-]
mtcm.Q = 1.71;         % concentration of binding sites in
the biosorbent [mmol/g]
mtcm.r = 1.25;         % radius of column [cm]
mtcm.v = 8;            % interstitial fluid velocity
[cm/min]

mtcm.eps = 0.046;     % column void fraction [-]

```

```

mtcm.rho_b = 109;                % packing density of dry biomass in the
packed-bed [g/L]

% time settings
mtcm.tDelta = 0.5;              % time step used in solving PDE system
mtcm.tMax = 1200;              % end time for simulation

% initial estimate for fit parameters
mtcm.Dz = 1.25;                % Axial dispersion coefficient [cm^2/min]
mtcm.K_fM = 0.03;             % Overall mass transfer coefficient [/min]

mtcm.root='antimony_s2';      % root name for all input/output files

% END - experiment specific parameters

% input and output files
mtcm.infile = [mtcm.root, '.csv'];
mtcm.outfile = [mtcm.root, '.out'];

% Create geometry
fem.geom = geomcsg({solid1([0 1])});

% Initialize mesh
fem.mesh = meshinit(fem, 'hmax', 0.01, 'hmaxvtx', [1; 0.1]);

% store multiphysics fem structure for later use
mtcm.fem = fem;

% load observed experimental breakthrough curve
mtcm_load;

% fit model (expected) to observed
mtcm_fit;

Processing model parameters ...
Loading observed experimental data from file antimony_s2.csv ...
Fitting mtcm to observed breakthrough curve ...
Solving PDE system ...
    Q/eps = 37.1739    =>    Dg = 368.3597
    Dz      = 1.25      =>    Pe = 108.8
    K_fM    = 0.03     =>    Sh = 0.06375
Fit parameters: Dz = 1.25    K_fM = 0.03    SSE = 0.68748
•
•
•
Solving PDE system ...
    Q/eps = 37.1739    =>    Dg = 368.3597
    Dz      = 3.8904    =>    Pe = 34.9578
    K_fM    = 0.011241  =>    Sh = 0.023887
Fit parameters: Dz = 3.8904    K_fM = 0.011241    SSE = 0.0013368

```